

AES/RE/12-34

**Modelling of material flow and size distribution
of ore in a stockpile at Tara Mines, Ireland**

21/09/2012

E.J. Dolman

Title : Modelling of material flow and size distribution of ore
in a stockpile at Tara Mines, Ireland

Author(s) : E.J. Dolman

Date : 21 September 2012

Professor(s) : Dr. M.W.N. Buxton
Dr. ir. D.L. Schott

TA Report number : AES/RE/12-34

Postal Address : Section for Resource Engineering
Department of Applied Earth Sciences
Delft University of Technology
P.O. Box 5028
The Netherlands

Telephone : (31) 15 2781328 (secretary)

Telefax : (31) 15 2781189

Copyright ©2012 Section for Resource Engineering

*All rights reserved.
No parts of this publication may be reproduced,
Stored in a retrieval system, or transmitted,
In any form or by any means, electronic,
Mechanical, photocopying, recording, or otherwise,
Without the prior written permission of the
Section for Resource Engineering*

Abstract

This study aims to understand the material behaviour of ore inside a coarse ore stockpile by using discrete element modelling. The underground zinc/lead mine of Boliden Tara Mines is located in Ireland. The broken ore is brought to surface where it is stored in the stockpile called the Tepee. From the Tepee the coarse ore is fed to a recently installed autogenous grinding (AG) mill. The AG mill grinds the ore to below 75 microns, in order to extract the metals in the flotation circuit. AG grinding requires a minimum amount of 20% coarse material to be effective in power consumption and throughput.

The size distribution feeding the stockpile is important since the stockpile is the last stage to control the size distribution of ore in the ore handling system before feeding the grinding circuit. An optimal size distribution is required for efficient grinding in an autogenous grinding (AG) mill. The Tepee discharge determines the feed of the mill by the mode of material flow. However, at present it is largely unknown how the material in the stockpile flows.

Therefore, the aim of this project is to obtain understanding of the behaviour of the material inside the stockpile by using discrete element modelling. The individual particle characteristics are important to apply in the modelling; hence the discrete element method is very well suited for this type of modelling due to its distinct particle character. In this work the discrete element package used is EDEM, which is a discrete element modelling package developed by the commercial company DEM Solutions.

In order to study this aim, several measures in the modelling were taken. The size distribution was divided into the three important sizes, as they are determined by the AG mill. Fines are sized 30mm, pebbles are 80mm and coarse particles are 130mm. A calibration of the parameters of these particles was carried out in order to acquire the correct bulk density, angle of repose and static wall friction of the material in the simulations. Furthermore, an effective simulation model was found by the application of two measures. Firstly, the use of a 3D slice instead of a full 3D simulation showed good results. The second measure was to simulate only coarse sized material to represent each of the particles sizes, which also proved to be very well applicable.

Based on observations at Tara Mines two different methods to fill the stockpile were determined; batch and mixed filling. The influence of these filling methods was simulated for different flow modes in order to review the impact on the discharged size distribution.

It was found that the best suitable mill feed was obtained by batch filled stockpiles, especially since core flow was the expected flow mode. Furthermore, it was found that the ratio between input and output rate has a significant impact on the size distribution at the discharge, since this ratio determines whether there is a 'last-in, first-out' system. High input rates result in heap formation, which leads to segregation of coarse sized material. Therefore at a high input rate it is advised to feed finer material. Feeding of coarser material at moments with a low input rate result in a more optimal size discharge, then when this is done at moments with high input rate.

Acknowledgement

The final part of my study at Delft University of Technology is this thesis. I would like to express my gratitude to many people who helped me during my work on this thesis towards finishing my Masters degree for Resource Engineering.

First of all, I am very grateful to my supervisors Mike Buxton and Dingena Schott for all their support and guidance. I really appreciate their time for quick chats and extensive discussions on technical issues and their advice in writing this thesis. In particular, I like to thank Mike for his thrust in my decision to change the focus of the project. My thanks to Dingena, for giving me the opportunity to use the software package and for her advice and insights to my models.

My special thanks to several people at Boliden Tara Mines for their help during my practical work on-site in Ireland. I would like to thank Benson Plunkett for the organisation of this project and creating the opportunity for me to work together with Tara Mines. My great appreciation for Paddy Mc Connell, who was a great technical help during the two months on-site and for the very pleasant lunch meetings we had together with Tom Moore. Furthermore, I like to thank my housemates Tom and Simon for the many great evenings.

I would like to thank the other graduating students; Nanne, Pieter, Dorien, Louise, Andrina, Rutger, Chris, Joelle, Stephanie, Ko and Mathijs for the great working environment on the 'afstudeerzolder' and the very pleasant coffee and lunch conversations. My special thanks to Andrina for her feedback and help in finalising this thesis. Last, but not least I like to thank my parents for making my entire study and related activities possible.

Contents

Abstract.....	i
Acknowledgement.....	ii
Contents.....	iii
List of figures	vii
List of tables	xi
Nomenclature.....	xii
1 Introduction	1
1.1 General locality.....	1
1.2 Problem statement.....	3
1.3 Aim and objectives.....	4
1.3.1 Original aim and objectives.....	4
1.3.2 Final aim and objectives.....	4
1.4 Research question	6
1.5 Report outline.....	7
1.6 Research scope and limitations.....	9
2 Review of background information	11
2.1 Autogenous grinding mill	12
2.1.1 Grinding	12
2.1.2 Requirements for AG milling	13
2.2 Particle fundamentals	17
2.2.1 Particle characterisation	17
2.2.2 Size analysis.....	22
2.3 Bulk material	24
2.3.1 Particle size and size distribution	24
2.3.2 Bulk density.....	24
2.3.3 The angle of repose	25
2.3.4 Moisture content.....	26
2.3.5 Bulk stresses and friction angles.....	26
2.4 Flow in stockpiles.....	28
2.4.1 Flow regions	28
2.4.2 Mass and core flow.....	29
2.4.3 Advantages and disadvantages of mass and core flow	31
2.4.4 Arching and ratholing.....	32

2.4.5	Gravity reclaim stockpile	37
2.5	Segregation	38
2.5.1	Heap segregation.....	38
2.5.2	Percolation	39
2.5.3	Trajectory segregation	39
2.5.4	Segregation by impact	39
2.5.5	Optimisation of the filling process.....	40
3	Discrete element modelling and material calibration	43
3.1	Discrete element method.....	44
3.1.1	Principles	44
3.1.2	Contact model	46
3.1.3	Calculation of new particle position	48
3.1.4	Rayleigh time step	49
3.2	EDEM parameters.....	50
3.2.1	Creator	50
3.2.2	Simulator	52
3.2.3	Analyst	52
3.3	Material calibration tests	53
3.3.1	Bulk density.....	54
3.3.2	Angle of repose	56
3.3.3	Repeatability test	62
3.3.4	Static wall friction	63
4	Simulation setup and methodology	65
4.1	Simulation methodology	66
4.1.1	Design of the Tepee stockpile	66
4.1.2	Particle dimensions.....	69
4.1.3	Filling of the Tepee.....	71
4.1.4	Reduction of calculation time	74
4.2	Experimental plan and simulation settings	76
4.3	Display of results.....	79
4.3.1	Screen captures.....	79
4.3.2	Size distribution graph	80
4.3.3	Angle of repose and withdrawal angle.....	85
5	Simulation results	87
5.1	Overview of simulations	87
5.2	Basic results.....	89

5.2.1	3D simulation approach by using a 3D slice	89
5.2.2	Using a single particle size	95
5.3	Primary results	97
5.3.1	Impact of different filling methods.....	97
5.3.2	Impact of the ratio between input rate and output rate on the discharge	99
5.3.3	Impact of the wall angle.....	103
5.4	Secondary results.....	107
5.4.1	Outlet splitter.....	107
5.4.2	Asymmetric input.....	110
5.4.3	Interrupted discharge	111
5.4.4	Fill level of the Tepee at 100%	112
6	Discussion	113
6.1	Reflection on the validity of the simulations	113
6.2	The optimal way of operating the Tepee	114
6.2.1	Simulations without input.....	114
6.2.2	Simulations with input	115
7	Conclusion.....	117
8	Recommendations.....	119
	References.....	121
	Appendix A: Paper.....	127
	Appendix B: Tara Mines	139
	Introduction.....	139
	Geology	140
	Mining cycle.....	145
	Stockpile	149
	Processing	150
	Fragmentation project.....	151
	Appendix C: Simulation results.....	159

List of figures

Figure 1: Geographic location of Tara mines (OpenStreetMaps, 2012).....	1
Figure 2: Flow chart of the ore handling system at Tara Mines with the stockpile in the red box..	2
Figure 3: Aim and objectives	5
Figure 4: Research questions and objectives.....	6
Figure 5: Objectives in the report structure	7
Figure 6: Mechanisms of breakage (Napier-Munn et al., 1996).....	12
Figure 7: Motions of charge in a tumbling mill (Wills and Napier-Munn, 2006).....	12
Figure 8: AG mill breakage and classification mechanisms (Napier-Munn et al., 1996)	13
Figure 9: Breakage rate as a function of particle size (Napier-Munn et al., 1996)	13
Figure 10: Impact on breakage rate of: a) ball load increase, b) mill load increase, c) mill speed increase and d) ball size increase (Morrell, 2004)	16
Figure 11: Particle dimensions: (A) Feret's diameter, (B) Martin's diameter, (C) projected area diameter (Filterworld, 2005)	17
Figure 12: Histogram and distribution curve for same data set (Holdich, 2002).....	19
Figure 13: Cumulative size distributions; same data set, different functions (Holdich, 2002).....	19
Figure 14: Examples of shape descriptors (Merkus, 2010).....	20
Figure 15: Particle examples with their roundness and sphericity (Santamarina and Cho, 2004)..	21
Figure 16: Difference between accuracy and precision in a bull's eye target (Maerz, 2001)	23
Figure 17: Measurement of repose angle; (a) poured angle of repose, (b) drained angle of repose and (c) dynamic angle of repose (Schulze, 2008)	25
Figure 18: Measurement of unconfined yield strength, shown in Mohr's stress circles (Schulze, 2008)	26
Figure 19: Classification of flow behaviour (Schulze, 2008)	27
Figure 20: Areas of flow after Brown and Hawksley (as quoted in Swedes, 1998)	28
Figure 21: Ellipsoids of motion in bulk materials as proposed by Kvapil (as quoted in Janelid and Kvapil, 1966).....	29
Figure 22: Flow profile: (a) mass flow, (b) funnel flow with stagnant zones to the top of filling (piping), (c) combination of mass and funnel flow (low stagnant zones) after Schulze (2008).....	29
Figure 23: Design chart after Jenike (1961); flow mode in a conical hopper (Schulze, 2008)	30
Figure 24: Design chart after Jenike (1961); flow mode in a wedge-shaped hopper (Schulze, 2008)	30
Figure 25: (a) Arching due to interlocking and wedging, (b) Arching due to cohesive strength of bulk material, (c) ratholing (Schulze, 2008)	32
Figure 26: Determination of the minimum outlet size (d_{crit}) to avoid arching (Schulze, 2008).....	33
Figure 27: Flow factor diagram for conical hopper (Schulze, 2008).....	34
Figure 28: Flow factor diagram for wedge-shaped hopper (Schulze, 2008)	34
Figure 29: Function $H(\Theta)$ for hopper geometry (Schulze, 2008).....	35
Figure 30: Stable rathole and circumferential stress (Schulze, 2008)	36
Figure 31: Function $f(\varphi_i)$ (Schulze, 2008).....	36
Figure 32: Example of a gravity reclaim stockpile (Roberts, 2009).....	37
Figure 33: Heap segregation, due to: (a) repose angle and particle shape, (b) repose angle and particle size dominant, (c) particle size and sifting effect (Schulze, 2008)	38
Figure 34: Segregation caused by percolation (a) and the mechanism; fines entering the open voids (Schulze, 2008)	39
Figure 35: Trajectory segregation on a conveyor belt.....	39
Figure 36: The same silo fill (a) discharged in: (b) funnel flow produces fines followed by coarse and (c) mass flow produces a remixed bulk material (Enstad and Mosby, 1998).....	40

Figure 37: Methods for distributed fill (Schulze, 2008).....	40
Figure 38: Silo with two outlets: (a) unsymmetrical filling, symmetric discharge; (b) symmetric filling, unsymmetrical discharge (Schulze, 2008).....	41
Figure 39: EDEM calculation cycle.....	44
Figure 40: Illustrative particle overlap (DEM Solutions, 2008).....	45
Figure 41: Contact model using springs, dashpots and friction slider (Chung and Ooi, 2008).....	46
Figure 42: Top view of simulation to show periodic boundaries, yellow arrows show the same clustered particle.....	51
Figure 43: Calibration and simulation chart.....	53
Figure 44: Calibration test; bulk density over particle size.....	54
Figure 45: Particles created from a cluster of 1 to 5 spheres.....	56
Figure 46: Calibration test; angle of repose for the number of spheres per cluster.....	57
Figure 47: Simulation test; angle of repose over the shear modulus with sketched asymptote trend lines (red).....	58
Figure 48: Calibration test; angle of repose over Poisson's ratio with a linear trend line.....	59
Figure 49: Calibration test; angle of repose over coefficient of restitution.....	60
Figure 50: Calibration test; angle of repose over rolling and static friction coefficient, with required 37 degree bar.....	61
Figure 51: Calibration and simulation chart.....	65
Figure 52: Schematic layout of the Tepee (not to scale).....	66
Figure 53: Tepee design in EDEM and system boundaries (red box).....	68
Figure 54: Extended flow; core and mass flow (Jenike & Johanson, 2010).....	68
Figure 55: Typical cumulative size distribution curve of the run-of-mine ore at Tara Mines.....	69
Figure 56: Mix filling conveyor.....	72
Figure 57: Batch filling conveyor.....	72
Figure 58: Heap segregation (Enstad and Mosby, 1998).....	72
Figure 59: Tepee filled with mixed filling method.....	72
Figure 60: Tepee filled with batch filling method.....	72
Figure 61: Schematic top view of observed areas with fines and coarse in the Tepee.....	73
Figure 62: Experimental plan (red) and project objectives and research questions.....	76
Figure 63: Example of a (static) screen capture.....	79
Figure 64: Example of a (dynamic) stream capture.....	79
Figure 65: Example screen capture showing the initial filling of the Tepee.....	80
Figure 66: Example screen capture showing the discharge, where particles are measured in the blue bin.....	80
Figure 67: Particle size histogram by size.....	81
Figure 68: Particle size histogram over time.....	82
Figure 69: Output and cumulative output over time.....	83
Figure 70: Size distribution over output mass with mass intervals of 1 tonne.....	84
Figure 71: Discharge of bulk material showing withdrawal angle (60 deg) and angles of repose (37 deg) after Comminution Technology JV (2011).....	85
Figure 72: DEM simulation showing the angle of withdrawal in red.....	85
Figure 73: 3D model, only one half is displayed.....	89
Figure 74: 3D slice model.....	89
Figure 75: Capture of simulation I.a.....	90
Figure 76: Capture of simulation II.a.....	90
Figure 77: Size distribution graph of simulation I.a.....	90
Figure 78: Size distribution graph of simulation II.a.....	90
Figure 79: Capture of simulation I.a.....	92

Figure 80: Size distribution graph of simulation I.a.....	92
Figure 81: Capture of simulation II.b.....	92
Figure 82: Size distribution graph of simulation II.b; high static friction	92
Figure 83: Capture of simulation II.c.....	92
Figure 84: Size distribution graph of simulation II.c; friction tips	92
Figure 85: Capture of simulation V.....	94
Figure 86: Capture of simulation II.a.....	94
Figure 87: Size distribution graph of simulation V.....	94
Figure 88: Size distribution graph of simulation II.a.....	94
Figure 89: Capture of simulation II.c.....	96
Figure 90: Capture of simulation A2.....	96
Figure 91: Size distribution graph of simulation II.c.....	96
Figure 92: Size distribution graph of simulation A2.....	96
Figure 93: Capture of simulation C; highlighting the ‘necking effect’	98
Figure 94: Size distribution graph of simulation C; input < output rate	98
Figure 95: Simulation D2; showing a growing fill level.....	98
Figure 96: Size distribution graph of simulation D2; input > output rate	98
Figure 97: Simulation H; keeps a 70% fill level.....	98
Figure 98: Size distribution graph of simulation H; input = output rate	98
Figure 99: Capture of simulation II.c.....	102
Figure 100: Capture of simulation III.c.....	102
Figure 101: Size distribution graph of simulation II.c.....	102
Figure 102: Size distribution graph of simulation III.c	102
Figure 103: Capture of simulation IV.a	106
Figure 104: Capture of simulation II.c.....	106
Figure 105: Size distribution graph of simulation IV.a	106
Figure 106: Size distribution graph of simulation II.c.....	106
Figure 107: Capture of simulation VII; total of both outlet.....	108
Figure 108: Size distribution graph of simulation VII; total.....	108
Figure 109: Simulation VII; larger left outlet.....	108
Figure 110: Size distribution graph of simulation VII; left outlet	108
Figure 111: Simulation VII; smaller right outlet.....	108
Figure 112: Size distribution graph of simulation VII; right outlet.....	108
Figure 113: Capture of simulation G.....	110
Figure 114: Size distribution graph of simulation G; where the yellow arrow points the moment that input material reaches the outlet.....	110
Figure 115: Capture of simulation F	111
Figure 116: Size distribution graph of simulation F; two ‘necking effects’ are pointed by the red arrows.....	111
Figure 117: Capture of simulation VI	112
Figure 118: Size distribution graph of simulation VI	112
Figure 119: Sketch to compare stagnant and flow zones for the simulation size and the actual size of the Tepee	113
Figure 120: Flow chart of the ore handling system with the stockpile in the red box.....	128
Figure 121: Flow profile: (a) mass flow, (b) funnel flow with stagnant zones to the top of filling (piping), (c) combination of mass and funnel flow (low stagnant zones) after Schulze (2008)...	129
Figure 122: Contact model using springs, dashpots and friction slider (Chung and Ooi, 2008). 130	130
Figure 123: Angle of repose for the number of spheres in a cluster.....	131
Figure 124: Rolling and static friction calibration for the angle of repose.....	132

Figure 125: Heap segregation (Enstad and Mosby, 1998)	133
Figure 126: The Tepee filled with batch filling method.....	133
Figure 127: The Tepee filled with mixed filling method.....	133
Figure 128: 3D model with mixed filling, only one half is displayed.....	134
Figure 129: 3D slice model with mixed filling.....	134
Figure 130: 3D slice model with batch filling.....	134
Figure 131: Size distribution graph of a full 3D conical stockpile.....	135
Figure 132: Size distribution graph of a wedge-shaped slice model.....	135
Figure 133: Size distribution graph of the model using ‘real’ fines, pebbles and coarse.....	136
Figure 134: Size distribution graph of the model using only coarse sized material to represent fines, pebbles and coarse.....	136
Figure 135: Size distribution graph of a 60 degree wall model	136
Figure 136: Size distribution graph with batch filling under core flow conditions.....	137
Figure 137: Aerial view of the mine location; orebody is given brighter and town of Navan is located on the right (Tara Mines intranet, 2011 <i>unpublished</i>).....	139
Figure 138: Simplified geological map of Ireland, showing the location of Carboniferous Limestone, hosted orebodies and prospects (Tara Mines intranet, 2011 <i>unpublished</i>).....	140
Figure 139: Schematic image of stratigraphic column in the Navan mine area (Peace et al, 2003)	142
Figure 140: Simplified geological plan of Navan Orebody, showing main ore lenses and faulting (Tara Mines intranet, 2011 <i>unpublished</i>).....	143
Figure 141: Representation of the in-house and JORC resource and reserve classification (Ashton, 2011 <i>unpublished</i>)	144
Figure 142: JORC classified mineral resources and ore reserves at 31st December 2010 (Ashton, 2011 <i>unpublished</i>).....	144
Figure 143: Schematic overview of the ore handling system at Tara Mines.....	148
Figure 144: Schematic layout of the Tepee	149
Figure 145: Plan view of the blast design of a typical stope; the red area produces relative fine ore and the green area produces relative coarse ore.....	154
Figure 146: Cross-section of the blast design of a typical stope; the red area produces relative fine ore and the green area produces relative coarse ore	154
Figure 147: Cross-section of the blast design of a typical development drift; the red area produces relative fine ore and the green area produces relative coarse ore	154
Figure 148: Plan view, technical drawing of the Tepee and the regions with a surplus of fine and coarse material.....	157
Figure 149: Point down laser above the outlet measures the same filling height for different Tepee fill volumes	157

List of tables

Table 1: Defined size fractions and the requirements by the AG mill	15
Table 2: Common particle shape descriptors, with their Waddell's sphericity and some examples	21
Table 3: Advantages (in bold) and disadvantages of mass and core flow (Holdich, 2002).	31
Table 4: Overview of calibration tests and the determined particle parameters	53
Table 5: Overview of the calibrated parameters.....	62
Table 6: Results of repeatability test with the calibrated parameters	62
Table 7: Static wall friction angle; literature and modelled	63
Table 8: Tepee dimensions at Tara Mines and in the DEM model.....	67
Table 9: Simplification in fraction and size of particles at Tara Mines and in the DEM model	69
Table 10: DEM particle properties: size, sphericity, roundness, volume and mass.....	70
Table 11: Reasons for filling methods.....	71
Table 12: Results of the filling methods	72
Table 13: The grouped simulation results and the belonging simulation numbers	76
Table 14: EDEM material parameters as used in the simulations.....	77
Table 15: DEM particle properties: size, sphericity, roundness, volume and mass.....	77
Table 16: Tepee dimensions at Tara Mines and in the DEM model.....	78
Table 17: Overview of input and output rate	78
Table 18: Particle colouring	79
Table 19: Overview of the simulation results, the researched parameters and the belonging simulation numbers.....	87
Table 20: Simulation parameters for comparing a slice and cone simulation with low wall friction settings.....	91
Table 21: Simulation parameters for comparing cone with two slice simulation with high wall resistance.....	93
Table 22: Simulation parameters for comparing 'real sized' particles with single sized coarse particles	95
Table 23: Simulation parameters for comparing different methods of filling.....	97
Table 24: Simulation parameters for comparing different ratios between in- and output rate.....	99
Table 25: Simulation parameters for comparing different wall angles.....	103
Table 26: Impact of wall angle on the angle of withdrawal at different discharge steps	104
Table 27: Simulation parameters for comparing the influence of an outlet splitter	107
Table 28: Simulation parameters of simulation G with asymmetric filling.....	110
Table 29: Simulation parameters of simulation F with interrupted discharge.....	111
Table 30: Simulation parameters of simulation G with a 100% fill level	112
Table 31: Impact on size distribution for simulations without input	114
Table 32: Impact on size distribution for simulations with input	115
Table 33: Material properties in EDEM after calibration.....	117
Table 34: Impact on size distribution for simulations with input	118
Table 35: Particle and bulk properties of ore and the AG mill size requirement	130
Table 36: Results of repeatability test with the calibrated parameters	132
Table 37: Overview of the DEM calibrated parameters and the simplified DEM model size fractions.....	133
Table 38: Dimensions of the actual stockpile, the reduced DEM model and in the DEM slice	134
Table 39: Defined size fractions and the requirements by the AG mill	151
Table 40: Blast pattern design using 70 and 76mm drill holes.....	155

Nomenclature

a	[m/s ²]	Acceleration
A	[m]	Area; projected area
b	[m]	Outlet diameter for a wedge-shaped hopper of arching
D	[m]	Diameter of a rathole
D_{10}, D_{50}, D_{80}	[mm]	The particle size at which a percentage (10, 50, 80) of the particles by mass are smaller than that given size; $D_{80} > 130\text{mm}$
D_A	[m]	Projected area diameter
d	[m]	Outlet diameter for a conical hopper of ratholing
D	[m]	Outlet diameter for a conical hopper to arching
d_{max}	[m]	Maximum particle diameter
e	[-]	Coefficient of restitution
E	[Pa]	Young's modulus
ff	[-]	Flow factor
ff_c	[-]	Flowability, calculated for consolidation stress
F	[N]	Force
F_n^d	[N]	Damping force
f_s	[-]	Static friction coefficient, also μ_s is used
$f(\varphi_i)$	[-]	Function for hopper geometry in a rathole
g	[m/s ²]	Gravitational acceleration
G	[Pa]	Shear modulus
h^*	[m]	height above the virtual apex at the critical point in an arch
$H(\theta)$	[-]	Function for hopper geometry
I	[kg·m ²]	Moment of inertia
L	[m]	length
m	[kg]	Mass
m	[-]	Hopper shape; 0 for wedge-shaped, 1 for conical shaped
m_b	[kg]	Mass of loose bulk material
r	[m]	Radius
R	[m]	Radius
R	[-]	Roundness
S	[Nm/rad]	Stiffness
t	[s]	Time
T	[N·m]	Torque
T_R	[s]	Rayleigh time step
V_b	[m ³]	Volume of loose bulk material
v^{rel}	[m/s]	Relative velocity
α or α_M	[degrees]	Angle of repose
δ	[m]	Particle overlap
ϵ	[-]	Porosity
θ_h	[degrees]	Wall friction angle to the horizontal
ρ	[kg/m ³]	Particle density
ρ_b	[kg/m ³]	Bulk density; loose bulk density
ρ_f	[kg/m ³]	Density of fluid
ρ_s	[kg/m ³]	Particle density
σ	[Pa]	Normal stress
σ_1	[Pa]	Major principle stress
σ'_1	[Pa]	Major stress in an arch
σ''_1	[Pa]	Circumferential stress in the wall of a rathole

σ_2	[Pa]	Minor principle stress
σ_c	[Pa]	Compressive strength <i>or</i> unconfined yield strength
τ	[Pa]	Shear stress
θ	[degrees]	Wall angle measured to the vertical
θ_c	[degrees]	Inclination of the wall of a conical hopper to the vertical
θ_p	[degrees]	Inclination of the side walls of a wedge-shaped hopper to the vertical
μ_i	[-]	Internal friction coefficient
μ_r	[-]	Rolling friction coefficient
μ_s	[-]	Static friction coefficient, also f_s is used
ν	[-]	Poisson's ratio
φ_i	[degrees]	Internal friction angle
φ_e	[degrees]	Effective angle of internal friction
φ_x	[degrees]	Angle of static wall friction
ω	[1/s]	Angular velocity

Indices

<i>crit</i>	Critical
<i>i, j</i>	Particle number
<i>n</i>	Normal direction
<i>net</i>	Net/resulting
<i>t</i>	Tangential direction
*	DEM particle equivalent

Abbreviations

3D	Three-dimensional
AG	Autogenous grinding
COB	Coarse ore (underground storage) bin
LHD	Load haul dump machine
SAG	Semi-autogenous grinding
SWEX	Southwest extension

1 Introduction

The aim of the project is to obtain understanding of the behaviour of the material in the Tepepe stockpile. This may be done by computational modelling of the stockpile. This report focuses on the size distribution during discharge. The individual particle characteristics are important to apply in the modelling; hence the discrete element method is very well suited for this type of modelling due to its distinct particle character. In this work the discrete element package used is EDEM, which is a discrete element modelling package developed by the commercial company DEM Solutions. This introduction will first describe the location of the mine and the stockpile and thereafter describes the problem statement and the project aim and objectives.

1.1 General locality

The mine site of New Boliden Tara Mines is located in Ireland some 50km northwest of the capital city Dublin. The mine neighbours the town of Navan in the county of Meath. The Navan orebody has been discovered in the early 1970's and production commenced in 1977. A detailed description of the mine can be found in *Appendix B*. An introductory review is given here.



Figure 1: Geographic location of Tara mines (OpenStreetMaps, 2012)

The Navan orebody lies between 50 and 1,000 metres below surface and stretches over 4km from northeast to southwest with a width of 1,5km. The orebody is hosted by Lower Carboniferous limestones. The majority of the mineralisation is found in sphalerite and galena. The 15 to 80m thick orebody flattens out the southwest and becomes less thick in the Southwest Extension (SWEX).

The total estimated size of the Navan orebody has been initially larger than 105 Mt., making it the largest zinc mine in Europe and the fifth largest worldwide. Annually, the mine produces around 200,000 tonnes of zinc concentrate and 40,000 tonnes of lead concentrate. At the end of 2010, the mine had produced over 75 Mt of ore grading at 8.2% zinc and 1.9% lead.

Zinc is mainly used for galvanising and in alloys, but it is also a major component in the battery industry. The major use of lead is found in the battery industry as well, but is also used because of its high density and low melting point.

After being owned by different companies, Tara Mines is now owned by New Boliden. New Boliden is a Swedish mining and smelting company. The company has mines and smelter in Sweden, Finland, Norway and Ireland. The commodities produced in the four Boliden mines are copper, zinc, lead, silver and gold. The smelters of Boliden refine these raw materials as well as scrap metal to produce pure metals.

Ore at Tara Mines is mined from the underground using conventional drilling and blasting techniques. The mine primarily uses two different mining methods. The first one is the development of drifts and tunnels to gain access to the orebody. The second method is stope and pillar mining, used for the production of ore. These mining methods are described in more detail in *Appendix B*.

The broken ore is loaded and brought to one of the five underground crushers. Via a series of conveyor belts and ore bins, the ore is brought to the hoisting system. Once the ore is skip-hoisted to surface it is stockpiled in the coarse ore storage building called the Tepee. A schematic overview is given in Figure 2 and details on the ore handling system are given in *Appendix B*.

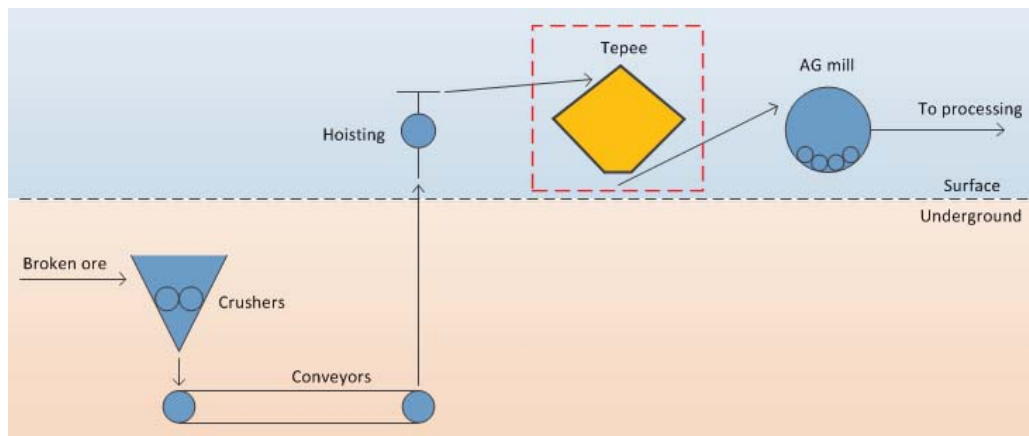


Figure 2: Flow chart of the ore handling system at Tara Mines with the stockpile in the red box

In the processing plant of Tara Mines, the valuable zinc and lead minerals are liberated from the gangue material. The first process of mineral liberation is comminution and the second process is flotation. Flotation is done by a series of cells, in which fine ground ore is added together with water and reagents. Air is dispersed at the bottom of the cells, where air bubbles are formed. The valuable metals attach to the air bubbles and float to surface where froth is formed. The froth is scraped off, cleaned and dewatered to results in a separate zinc and lead concentrate.

The flotation circuit requires ground ore to be smaller than 75 microns, in order to extract the metals effectively. To acquire this feed size, the ore undergoes several stages of comminution. This starts with underground blasting, which liberates the ore from the underground. The broken ore is crushed to minus 150 millimetres by a crusher. Any additional fragmentation caused by the ore handling system is discussed in *Appendix B*. The final step in comminution is the grinding of ore in the recently installed autogenous grinding (AG) mill. The AG mill is fed directly from the surface stockpile Tepee.

The grinding medium in an AG mill is the rock itself. Hence, the AG mill requires a specific size distribution input. The AG mill at Tara Mines needs enough coarse material (P80>150mm) to grind efficiently. Efficiency of the AG mill is of great importance, since it impacts the throughput and the power consumption. The grinding circuit is responsible for up to 50% of the power consumption.

1.2 Problem statement

The AG mill grinds most effectively with a size distribution as coarse as possible, which is depend on the mill dimensions and ore properties. For Tara Mines the mill feed size should be 20 percent above 130 millimetres. The current mill feed does not meet this minimum requirement of coarse material. Therefore, several measures have been taken in the 'Fragmentation Project' at Tara Mines (see *Appendix B*). As part of the fragmentation project the drill/blast patterns have been optimised, which improved the size distribution.

However, the broken ore still does not have the suitable distribution when arriving at the AG mill. This is shown by a 3D optical size measurement camera that records the size distribution at the mill feed. Freshly blasted rock contains enough coarse material, but this is not recorded when it arrives at the 3D mill camera. This implies that there is a loss in coarse material either due to one or more fragmentation steps or due to size segregation of the bulk.

The original proposed topic of this study was to investigate where in the ore handling fragmentation and segregation takes place. During the research, it was concluded that it was too complex to measure the degree of fragmentation at each single stage in the ore handling system. The complexity was caused by the inaccuracy of optical size measurement and furthermore the segregation in ore bins made it impossible to track a single batch of ore. One major finding was that coarse material is produced by the mine, but does not enter the AG mill in the required size distribution.

As a result the research focus was modified to the stockpile Tepee. All material arrives at the Tepee before it enters the AG mill. Therefore, the Tepee is the last stage in the ore handling system that controls the size distribution. At present, it is uncertain what happens with the material after dumping it into the Tepee. This study aims to model the stockpile, to provide understanding of the material behaviour and the resulting size distribution output of the Tepee.

1.3 Aim and objectives

The aim and objectives are discussed in this chapter. The original aim and therefore the original objectives changed during the project. Both the initial and the final aim are discussed, together with their objectives.

1.3.1 Original aim and objectives

The problem statement in the previous section highlighted the initial problem as fragmentation at each stage in the ore handling system. The aim initially set for this project was the following:

Identify the size fragmentation steps in the ore handling system of Tara Mines.

In order to do this the following objectives were defined:

1. Measure the size distribution of ore at conveyor belts by the use of online image analysis.
2. Identify the location of fragmentation steps in the ore handling system.
3. Investigate the degree of size reduction at each fragmentation stage by tracking a single batch of ore throughout the entire ore handling system.

During this research it was concluded that it was too complex to measure the degree of fragmentation at each single stage in the ore handling system. However, one major finding was that coarse material is produced by the mine, but does not enter the AG mill in the required size distribution. Therefore the original aim and objectives were changed to the stockpile Tepee, since this is the last stage in the ore handling system that controls the size distribution.

1.3.2 Final aim and objectives

This resulted in the following final aim of this thesis:

Obtain understanding of the behaviour of the material in the Tepee by using discrete element modelling.

The material behaviour is researched by examining the flow of the material and the size distribution. This is also used in the objectives of this work. The individual particle characteristics are important to apply in the modelling, hence the discrete element method is very well suited due to its distinct particle character. The final objectives are the following:

1. Determine particle properties in discrete element modelling (by calibrating for the material bulk behaviour)
2. Develop an effective simulation model by using discrete element modelling
3. Define an optimal way to operate the Tepee by using discrete element modelling

In discrete element modelling, calibration of the material properties is required in order to simulate the correct bulk behaviour. Subsequently, a simulation model is developed which is effective in calculation time. Finally, an optimal way of operating the Tepee is defined. This optimal operation of the Tepee delivers the ideal size distribution during discharge and the best predictable discharge flow. This was done in two stages. The two stages are explained in Section 1.5 *Report outline*. The objectives are structured as in Figure 3.

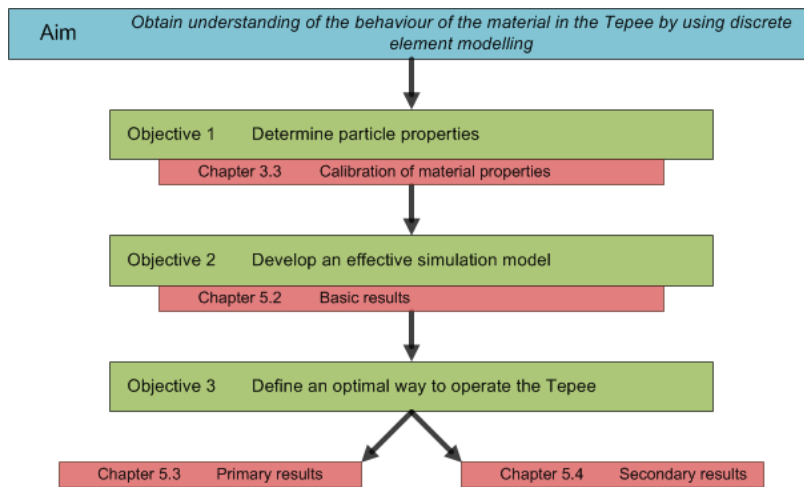


Figure 3: Aim and objectives

1.4 Research question

The objectives as stated in *Section 1.3.2* were investigated according to their research questions. The research questions contribute to achieving the aim of this report; to gain understanding of the material behaviour in the Tepee. The research questions (RQ) are numbered where the first number applies to the objective. The research questions are stated as follows.

Obj. 1. Determine particle properties

RQ1.1: What are the particle properties in the simulation to result in the appropriate bulk behaviour, looking at: the bulk density, the angle of repose and the static wall friction?

Obj. 2. Develop an effective simulation model

RQ 2.1: Is it applicable to model a 3D slice to represent a full 3D simulation?

RQ 2.2: Is it applicable to model single sized coarse particles to represent all size fractions?

Obj. 3. Define an optimal way to operate the Tepee

RQ 3.1: What is the flow mode in the stockpile?

RQ 3.2: What is the size distribution during discharge of the stockpile?

The research questions are placed in a similar diagram as shown for the objectives. The research questions 3.1 and 3.2 are studied in two sections, which will be explained in *Section 1.5 - Report outline*.

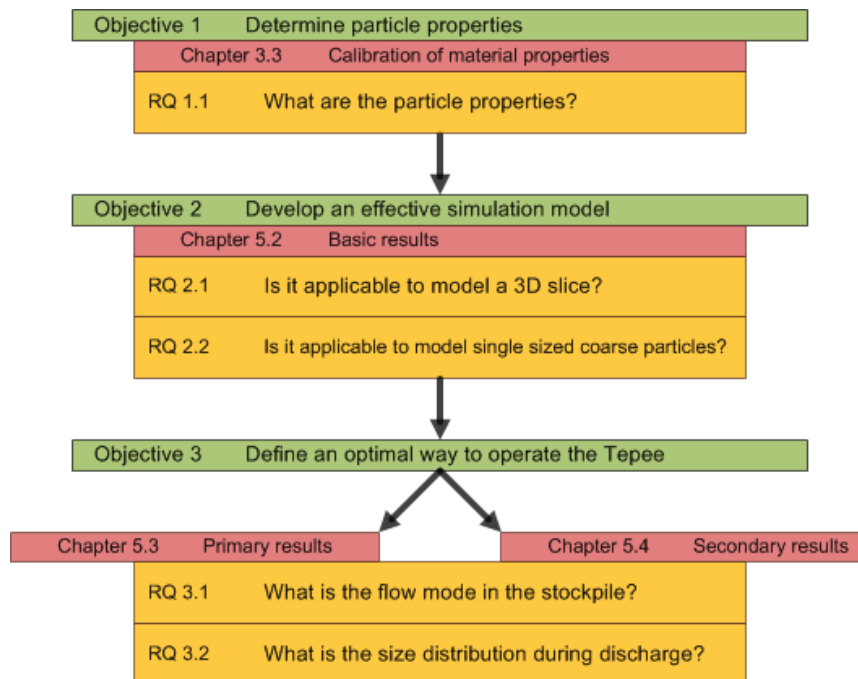


Figure 4: Research questions and objectives

1.5 Report outline

The report contains the following chapters and appendices.

Chapter 1	Introduction
Chapter 2	Review of background information
Chapter 3	Discrete element modelling and material calibration
Chapter 4	Simulation setup and methodology
Chapter 5	Simulation results
Chapter 6	Discussion
Chapter 7	Conclusion
Chapter 8	Recommendations
Appendix A	Paper
Appendix B	Tara Mines
Appendix C	Simulation results

After the Introduction, the necessary background information is given in Chapter 2. This background explains the working of an AG mill, the fundamentals of particles and bulk materials as well as the flow and segregation of bulk materials.

This work uses a commercial discrete element software package called EDEM. The principles of the discrete element method are reviewed in Chapter 3. Subsequently, the parameters in the software package EDEM are discussed. The final part in this chapter is the calibration of the material properties to find the applicable parameters in EDEM.

The setup of the simulation and the methodology are described in Chapter 4. This chapter explains the logic behind the simulations and explains how the results are displayed.

Chapter 5 presents the results of the simulations. These are divided into three sections. These sections are structured in the same way as the objectives and the research questions, shown in Figure 5. Firstly, *Section 5.2 – Basic results* addresses the simulations conducted to develop an effective simulation model. Secondly, *Section 5.3 – Primary results* looks at the simulations that have wider applicability to stockpiles. The final *Section 5.4 – Secondary results* reports on specific Tara Mines' Tepee situations.

The results of the modelling are discussed in Chapter 6. The conclusions and recommendations are given in Chapter 7 and 8.

Appendix A provides a paper of this thesis report. Appendix B presents detailed information about Tara Mines and their fragmentation project. All relevant simulation data are attached in Appendix C.

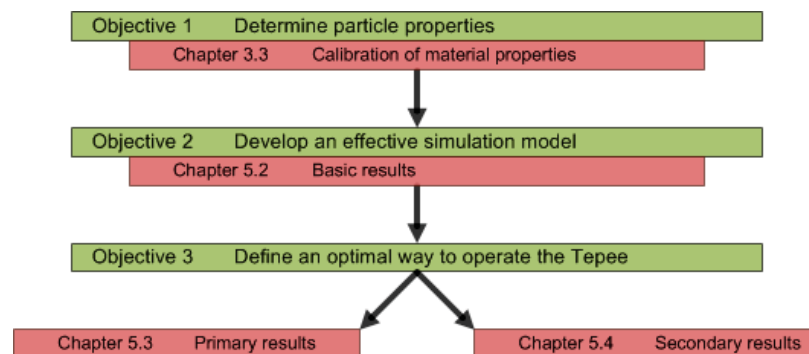


Figure 5: Objectives in the report structure

1.6 Research scope and limitations

The research in this thesis project is defined by the objectives and the research questions. Based on those research questions several decisions were made on the boundaries to include and exclude in this project. The logic of the research scope is explained in *Section 3.3 – Material calibration* and *Chapter 4 – Simulation setup and methodology*. A summary of what is included and excluded in this project is given below.

		Included	Excluded
General		Particle size requirement of the mill	Size requirement per unit mass of the mill
		Zinc/lead ore	Other bulk materials
			Economic impact Feasibility to implement Tepee control measures
Modelling	Particles	Particle size: fines, pebbles & coarse	Full size distribution
		Particle shape	Fines <30mm
		Bulk properties: angle of repose, bulk density & static wall friction	Laboratory experiments to acquire particle properties
			Cohesion
Tepee		Tepee geometry	Feeding & discharge systems
		Tepee wall friction	
Model		Relative particle velocity and direction by stream captures	Validation by particle tracking
		Filling methods	Particle breakage

2 Review of background information

To understand the behaviour of the material in a stockpile at Tara Mines by using discrete element modelling, this chapter provides the background information to bring the basic knowledge that is required to achieve this aim. This chapter introduces the origin of the problem and reviews the parameters that define the behaviour of a bulk material. The background information as given in this chapter is as follows.

1. Autogenous grinding mill
Explains how the AG mill works and what parameters determine the grinding efficiency. This section explains where the size distribution requirements originate and states the importance of an optimal sized mill feed.
2. Particle fundamentals
The fundamentals of particle size and shape are discussed. It reviews the methods of particle size and shape measurements. This section provides background information on two of the individual particle properties that need to be defined in *Objective 1 – Determine the particle properties*; size and shape.
3. Bulk material
The fundamentals of the ore as a bulk material are reviewed, this includes particle size distributions, bulk density and the angle of repose of the bulk material. This section explains the bulk parameters that are researched in *Research question 1.1 – What are the particle properties?*
4. Flow in stockpiles
Background information on the flow in stockpiles is provided to gain understanding of flow mode and material behaviour in the Tepee. This section reviews the required background information to understand *Research question 3.1- What is the flow mode?*
5. Segregation
Segregation methods are review to understand why bulk materials may segregate and how this influences the size distribution as studied in *Research question 3.2 – What is the size distribution during discharge?*

Background information on the discrete element method and the software package EDEM are given in Chapter 3.

2.1 Autogenous grinding mill

Comminution of particles is required to liberate the valuable metal bearing ore from the gangue material around it. By each size reduction step more particle surface area is created, which is needed to improve the metal extraction process. The first step in the comminution process is blasting of the ore, followed by one or more crushing stages. The final comminution step is grinding of lump ore. The principles of autogenous grinding and the requirements on the ore properties are reviewed in this chapter.

2.1.1 Grinding

Grinding is generally performed by tumbling mills that utilise a loose grinding medium. The grinding medium is lifted together with the ore by the rotation of the drum. This induces several breakage mechanisms. These mechanisms are combinations of impact and abrasion and are pictured in Figure 6. In Figure 7 is shown where the regions of different breakage mechanisms occur in the mill.

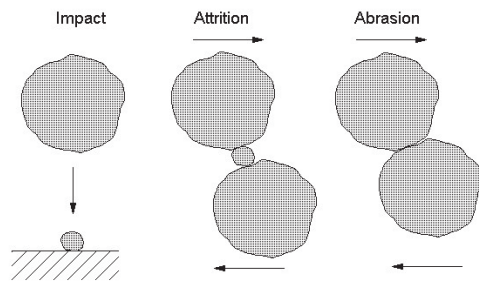


Figure 6: Mechanisms of breakage (Napier-Munn et al., 1996)

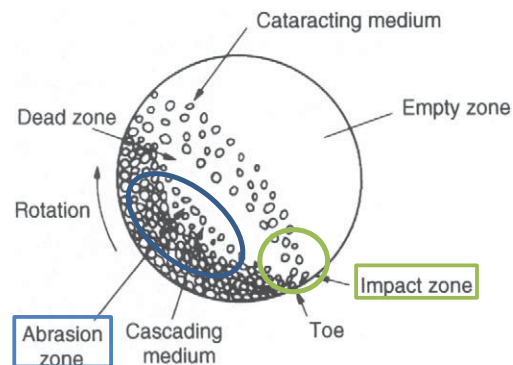


Figure 7: Motions of charge in a tumbling mill (Wills and Napier-Munn, 2006)

Since steel balls or rods are often used as grinding media, these mills are called respectively ball mills and rods mills. An autogenous grinding (AG) mill utilises the ore itself as the grinding medium. A mill using steel balls in addition to the ore as natural grinding medium is called a semi-autogenous (SAG) mill.

A major attraction to use an autogenous mill is the reduction of operating cost derived by the elimination of steel grinding media. Providing that the ore properties are suitable for autogenous grinding, the use of primary autogenous milling may reduce operating cost by 30 to 40 per cent (Lane and Siddall, 2002). Other important reasons that makes AG milling interesting are: the simple grinding circuit compared to ball grinding circuits, the ability to treat a wide range of ore types (including sticky and clayey feeds) and lower capital costs (Wills and Napier-Munn, 2006).

There are two main configurations of the autogenous grinding mill; referred to as high and low aspect ratio mills. The aspect ratio of the mill is the ratio between the inside diameter of the mill over the effective grinding length. High aspect ratio mills have a diameter of 1.5-3 times the length, where low aspect ratio mills range from square to a length of 3 times the diameter (Wills and Napier-Munn, 2006). Low aspect ratio mills are favoured in Scandinavia and South Africa and the high aspect ratio mills are preferred in North America and Australia. Tara Mines' AG mill is a low aspect ratio mill; the length over diameter ratio is 1.1 (Rice, 2012 *personal communication*).

2.1.2 Requirements for AG milling

Optimal AG mill performance is achieved when the mill operates at a high throughput and at a low power consumption. This performance is dependent on several ore feed properties and mill operating settings. The most important properties and settings are reviewed and this section starts with the AG breakage cycle and breakage rate.

The breakage cycle in an AG mill is shown schematically in Figure 8. The feed enters the mill, where it is subjected to breakage by collisions with other particles or with the mill walls. Particles can exit the mill via a grate when its size has become small enough. Otherwise, the material will undergo further collisions.

The breakage rate is the frequency of particle breakage due to collisions. The breakage rate is related to the particle size and typically forms a distribution as given in Figure 9. As will be shown later on the shape of this distribution is largely depended on the particle size distribution of the feed and the mill rotational speed. The particles of the size that are ground by impact and attrition breakage mechanisms, undergo the highest breakage rate and therefore are ground most effectively.

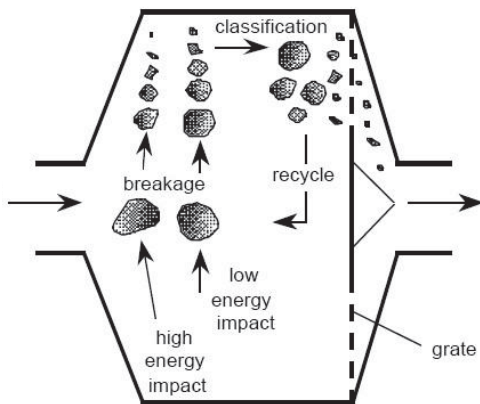


Figure 8: AG mill breakage and classification mechanisms (Napier-Munn et al., 1996)

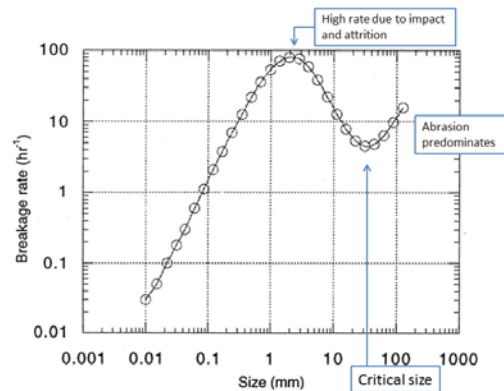


Figure 9: Breakage rate as a function of particle size (Napier-Munn et al., 1996)

The main properties to that influence the mill performance are listed below:

Mill properties	Liner profile
	Mill speed
	Volumetric mill load
	Pulp density
Feed properties	Throughput
	Hardness
	Size distribution

The profile of the mill liner can influence the grinding. Furthermore, the liner may increase the charge lifting height, which provides an increase in kinetic energy. An increase in the rotational speed of the mill generally increases the throughput, since both the frequency of collision and the lifting height are increased. An optimal mill load is generally achieved at 30-40% of the mill volume. A higher mill load may cause a so-called 'soft toe', which decreases the breakage of the critical sized material. Next to that, the mill load has a major influence on the power consumption of the mill, therefore mill load and power consumption should always be balanced. A high pulp density reduces the flow rate through the apertures of the grate.

The throughput of the feed into the mill influences the mill performance, since a low feed rate will reduce the collision frequency. The ore in an AG mill has to be sufficiently competent to establish an impact and not so competent or lacking in lumps that the media charge becomes critical. Hence, the mill product size becomes too fine and thereby decrease the gross circuit efficiency (Lane and Siddall, 2002). Low aspect mills encounter challenges when the ore is competent, due to the difficulty of achieving effective impact breakage since abrasion becomes the dominant grinding mechanism. Therefore, the large diameter together with the short grinding length of a high aspect ratio mill is favourable, since it delivers good impact breakage. The drawback is that a high aspect mill with the same volume draws more power (Gupta and Yan, 2006). The requirement of the mill on the feed size distribution is discussed separately in the next section, since this is a major factor and the reason of this study.

2.1.2.a Size distribution

In AG milling three important size fractions are distinguished, namely: Fines, pebbles and coarse. The influence of these size fractions on the efficiency of grinding are reviewed. Subsequently, the size requirements for the mill at Tara Mines are given and reviewed in this section.

Optimising the mill settings is required for efficient autogenous grinding, since the feed and especially the size of the feed are essential. The mill settings (mill load and speed) may help improving efficiency; although this increases energy consumption in most cases. The feed properties therefore are very important. The hardness of the ore influences the breakage; however, this is an uncontrollable factor. The ore size on the other hand is controllable. Since the grinding medium is defined by the size distribution of the feed itself, this makes the size distribution of the feed the most important and controllable parameter. Each size fraction is reviewed separately.

For the fine material, smaller than the grate apertures, no grinding is required. Since this is essentially “free” throughput for the mill (Valery et al., 2001). The fines size fraction at Tara Mines is defined slightly larger at a size of <50mm, however this material is not causing problems in the grinding process and therefore there are no restrictions to the amount of fines in the distribution.

The pebble sized material is the most difficult size to grind and therefore are also called the critical size fraction. This is observed in Figure 9, by the low breakage rate. These particles are too small to grind other particles and too large to be efficiently ground themselves. Therefore these particles tend to accumulate in the mill, causing a reduction in capacity and thus reduce the throughput of the mill. The size fraction of the pebble material at Tara Mines is 50-100mm and the mill feed should contain no more than 50% of this size, where less is preferred (Rice, 2012 *personal communication*).

Finally, the third fraction is the coarse sized material. In autogenous grinding, the major focus is on the coarse sized material, since this fraction is needed for impact crushing. In this fraction, the size and the number of particles are important. Ideally, the feed should provide lumps large enough to generate high kinetic energies to break smaller rocks. Larger sized coarse particles result in a better mill performance (Napier-Munn, 2006). Also the number of coarse particles should be high enough to provide a high frequency in kinetic breakage collisions.

The difficulties in grinding the critical sized pebbles are largely overcome when there is enough coarse material. Tara Mines uses two mill requirement definitions for the coarse ore fraction; 30% of the feed larger than 100mm and 20% of the feed larger than 130mm. The second

requirement will be used in this study and is referred to as 80% passing a sieve of 130mm (P80>130mm). This one is chosen, since a P80 value is used more often in literature. These size fractions and mill requirements at Tara Mines are listed in the table below (Mc Connel, 2012 and Rice, 2012 *personal communication*).

Table 1: Defined size fractions and the requirements by the AG mill

	Size [mm]	AG mill requirement
Fines	<50	none
Pebbles	50-100	As low as possible, $\leq 50\%$
Coarse	>100	P70 or 30% >100mm P80 or 20% >130mm

Summarising, the ideal AG mill feed consists of a large amount of coarse and fines and furthermore as few as possible of the pebble sized material. A method to reduce the negative effect of the pebble sized material is applying pebble extraction and pebble crushing. Autogenous milling is typically practiced in association with pebble crushing to improve circuit power efficiency. The pebble flow provides an ideal source of media for secondary milling; thereby pebble crushing allows limited ability to improve performance (Lane and Siddall, 2002). The most important factor to achieve efficient autogenous grinding is a constant feed of ore containing enough coarse material, which means that the feed receive from the stockpile should be well mixed.

2.1.2.b The influence on the mill performance

The influence of different parameters is predicted by Morrell (2004) and parts of his results are displayed in Figure 10. The method of grinding in Morrell's predictions is semi-autogenous grinding, whereby steel balls are the grinding medium. In this work an autogenous grinding mill is involved, whereby the ore itself is the grinding medium. To use to predictions by Morrell, the ball size is seen as the coarse particle size and the ball load is seen as the weight of the coarse fraction. The weight of the coarse size fraction is a combination of number of particles and the size of a single particle.

The figure shows that an increase in the mill load and an increase in the size of the coarse fraction have a negative effect on the grinding performance, since these parameters reduce the breakage rate.

An increase in the load of coarse material and an increase in the mill speed both have a positive effect on the grinding performance, since these parameters increase the breakage rate. It is seen that an increase in coarse particle size has the largest influence on the breakage rate.

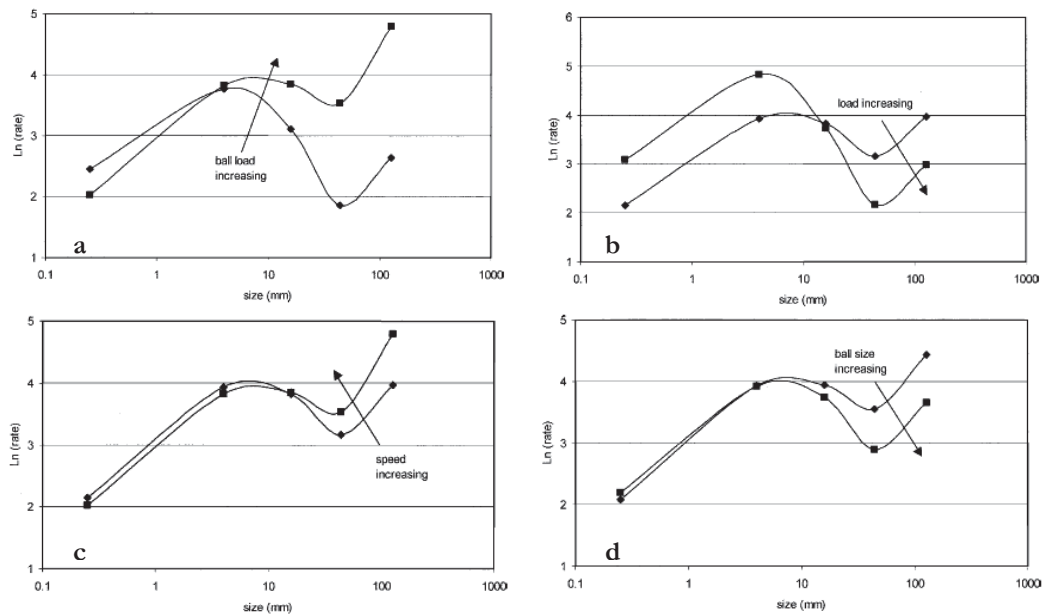


Figure 10: Impact on breakage rate of: a) ball load increase, b) mill load increase, c) mill speed increase and d) ball size increase (Morrell, 2004)

Figure 10.d highlights the impact of an increase in ball size. For an autogenous mill this is an increase in coarse particle size only, where the total weight of the coarse fraction remains the same. It can be concluded that for an equal load of coarse particles with a larger size this reduces grinding efficiency, due to a reduction in the number of coarse particles.

Figure 10a shows an increasing ball load or for an AG mill an increase in the total number of coarse particles. The increase in number of coarse particles significantly increases the breakage rate, which is beneficial for the grinding efficiency. A summary is given here below.

Increase in number of coarse particles	positive
Increasing ratio coarse to total	positive
Increase in coarse particle size	negative, when this reduces the total number of coarse

2.2 Particle fundamentals

Knowledge of the particle fundamentals is essential to understand the size distribution of a bulk material. This chapter reviews the particle size and particle shape, since several methods are applied. Subsequently, the particle size distribution functions are reviewed. Finally the size measurement methods of sieving and image analysis are explained.

2.2.1 Particle characterisation

Particle characteristics influence the behaviour of a particle; for example, a spherical particle rolls more easily than an angular particle. Hence, the particle characteristics also determine the bulk behaviour.

This chapter first describes the size, subsequently the size distribution and finally the shape of the particles. Several other particles characteristics are not discussed, since they are of less relevance to the topic of research in this report. This includes particle features such as particle porosity, chemical properties, strength and abrasiveness.

2.2.1.a Single particle size

Particle size for irregular shaped particles is difficult to represent using a single parameter. This means that more parameters are required. These parameters can be distinguished either in a visual measurement (length and width) or by using an equivalent sphere (Figure 11).

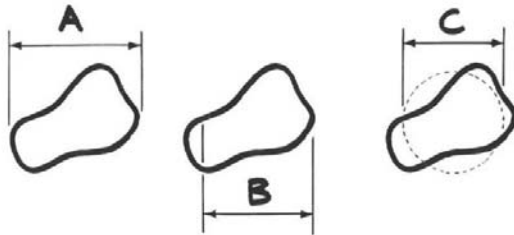


Figure 11: Particle dimensions: (A) Feret's diameter, (B) Martin's diameter, (C) projected area diameter (Filterworld, 2005)

Definitions of the most used dimension parameters are given according to Merkus (2010):

- Length
The longest dimension from edge to edge of a particle
- Width
The longest dimension of the particle measured perpendicular to the length
- Thickness
Height of the particle when it is resting in its position of maximum stability
- Feret's diameter (Figure 11.a)
The distance between two virtual, parallel lines tangent to the a randomly orientated particle
- Martin's diameter (Figure 11.b)
The diameter of a particle at the point where the particle is split into two equal projected areas

In a sieve analysis of the particle sizes, the width and the thickness together define the minimum aperture size through which a particle can pass, since these parameters give the smallest size combination in two perpendicular directions.

The equivalent sphere concept has been introduced to the field of image analysis to make particle size distributions more uniformly interpretable and is especially used in optical size measurement

methods. The diameter of the equivalent sphere defines the size of the particle. By doing this the particles can be given a single size parameter, the equivalent sphere diameter. This is often simply referred to as the diameter or size of the particle, since it is widely used in image analysis.

As long as the particle shape remains the same, the linear dimensions of a particle can change with a constant factor and the equivalent sphere will change with the same factor.

The most used equivalent diameters are given below and defined according to Merkus (2010).

- Equivalent projected area diameter
Diameter of a circle having the same area as the particle's projection
- Equivalent surface area diameter
Diameter of a sphere having the same surface area as the particle
- Equivalent volume diameter
Diameter of a sphere having the same volume as the particle
- Equivalent sieve diameter
Diameter of particles that just pass through the apertures of a sieving medium

The equivalent sieve diameter is usually smaller than the other diameter, since this represents its smallest cross section. Where it should be mentioned that during a sieve test the particle also should find this orientation to fall through the mesh, which can be a source of error for elongated particles.

2.2.1.b Particle size distribution

The size of a single particle may be represented by several parameters, as mentioned in the previous section. This also counts for particle size distributions. The distribution can be based on number, volume or mass of particles. There are also several ways used to display the size variation in a batch of particles.

The size of a collection of particle can be described using: minimum or maximum diameter, a weighted mean size, a D10, D50 or D80 or even with graphs to plot a distribution of particles. A D10, D50 and D80 are the particle size at respectively 10, 50 and 80% undersize in a cumulative size distribution.

There are three major ways to display the particle size distribution; using a histogram, a distribution curve and a cumulative size distribution curve.

The histogram and size distribution curve in Figure 12, show for every size range in the number of particles as well as the fraction of the total number of particles. In this case the distribution curve has been normalised. The normalisation gives a relation between the distribution curve and its cumulative curve: The distribution curve is the derivative of the cumulative curve.

The cumulative size distribution in Figure 13 shows the same data set ('Number'), but is plotted cumulatively. In Figure 13, different functions have been plotted; number and mass of particles is used most often. The particle number curve shows a higher fraction for small particle diameters then the curve on mass. This is naturally caused by the fact that smaller particles have a smaller mass, thus in number more small particles are needed to reach the same mass fraction. The cumulative size distribution is often displayed with the x-axis on a log scale, when there is a wide spread in particle size.

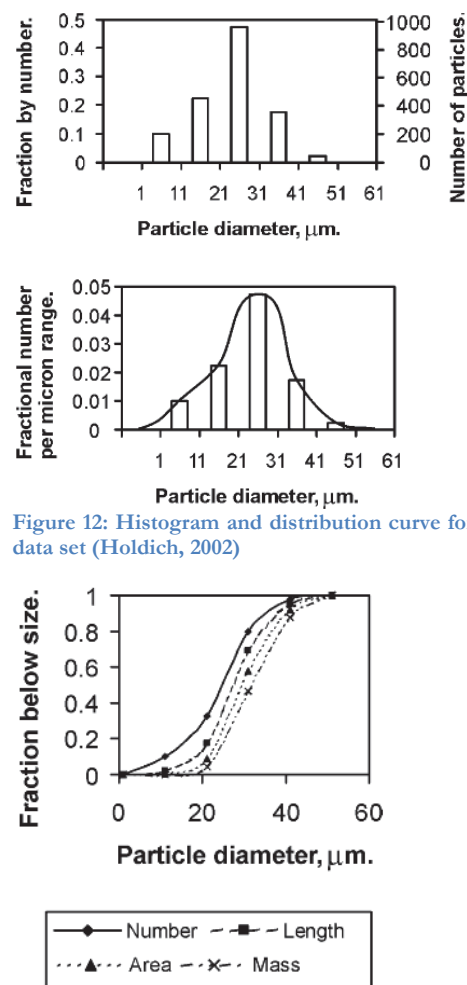


Figure 12: Histogram and distribution curve for same data set (Holdich, 2002)

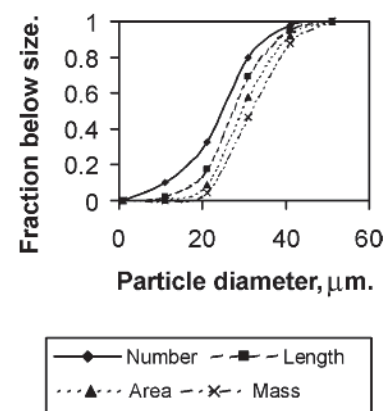


Figure 13: Cumulative size distributions; same data set, different functions (Holdich, 2002)

2.2.1.c Particle shape

When handling bulk materials, the shape of the particle is important as well. The different diameters as discussed before show that there may be large variations in shape. Particle shape can be described in either a qualitative or a quantitative way.

A qualitative description of particles can be given by visual inspection of the evident particle appearance; some examples of shape descriptors are given in Figure 14.

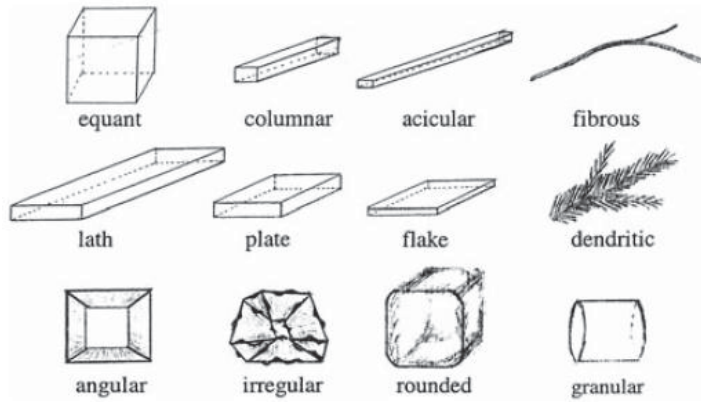


Figure 14: Examples of shape descriptors (Merkus, 2010)

Quantitatively, particles can be described in several ways. Just as for particle size in the previous section, there is not one single approach to describe the shape of a particle. Santamarina and Cho (2004) state that there are three scales to describe particle shape and they all have their opposite scales:

- Sphericity ' S ' versus platiness
- Roundness ' R ' versus angularity
- Smoothness versus roughness

Smoothness or roughness describes the surface unevenness, which are much smaller scale than the particle dimensions. Roundness is on a larger scale and relates the projected area ' A ' and the particle length ' L ' by the following formula (Merkus, 2010):

$$R = 4A/\pi L^2 = (D_A/L)^2 \quad \text{Eq. 1.}$$

The roundness is close to zero for particles that are very angular and roundness will reach one for rounded particles. Furthermore, the roundness is related to the compactness, since it is the square root of the roundness. The compactness is the equivalent projected area diameter D_A over the length of the particle.

Sphericity describes how close a particle approaches a perfect sphere. Different ratios are used to define the sphericity. As an example Wadell's sphericity ' ψ ' is used, which defines sphericity as: The ratio between the surface area of a sphere with equal volume to the particle and the actual surface area of the particle. This can also be described as their equivalent spherical diameters ratio squared, as shown in the formula below (Holdich, 2002).

$$S \approx \psi = (D_V/D_S)^2 \quad \text{Eq. 2.}$$

The use of Wadell's sphericity is well established and therefore common shape descriptors are also described using this sphericity. The table below provides an overview with shape descriptors, Wadell's sphericity and some examples as an indication, as given by Holdich (2002).

Table 2: Common particle shape descriptors, with their Wadell's sphericity and some examples

Descriptor	Wadell's sphericity	Example
Spherical	1.000	Glass beads
Cubic	0.806	Sugar, calcite
Angular	0.66	Crushed minerals
Flaky	0.54	Gypsum, talc

In the previous equations, it is complicated to acquire or measure the correct parameters and the answer is more precise than necessary. Often, the figure below is used to overcome this problem. This is also done in this work for the ore at Tara Mines. A representative sample of ore is taken and compared to the particle examples in the figure.

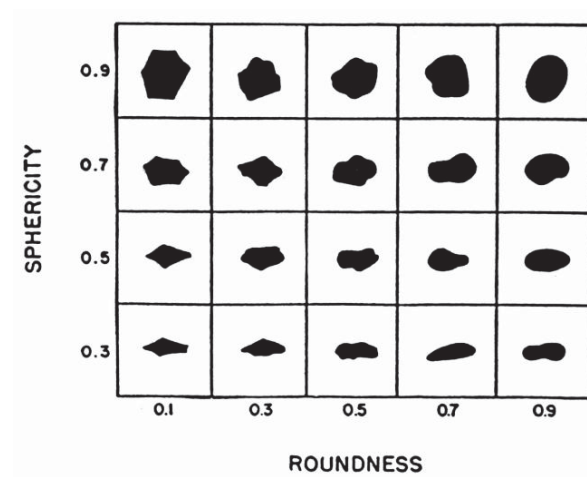


Figure 15: Particle examples with their roundness and sphericity (Santamarina and Cho, 2004).

2.2.2 Size analysis

Reporting on the particle size can be done by using several size descriptions, but also by different measuring methods. In this study, two methods were used to measure particle size distributions; sieve analysis and image analysis. The basic fundamentals of these measuring methods will be described in this chapter.

2.2.2.a Sieve analysis

Sieving subdivides a batch of material in different size fractions. The different size fractions may be weighted and/or counted in number. Generally, this delivers accurate size distributions. Sieving can be done either manually or mechanically. To acquire a size distribution a range of sieves with different mesh sizes need to be used. The material is sieved first using the widest mesh and stepping down in mesh size each time. When the material is poured onto the sieves, the sieves need to be shaken to make sure that all particles will rotate and will pass the sieve when their size is below the mesh opening. The apertures in the sieve can be squared or round, which depends on the way the mesh is constructed. Different apertures have a slight impact on the measuring errors of the particle size.

A major disadvantage of sieving is that relatively large samples are needed to provide a good representation of the whole, which becomes expensive in operating and labour costs. The major benefits of sieving are the very easy principle and low capital costs. Sieve analysis on samples with large rock size is more difficult to carry out, due to the size and weight of the material. An important factor to look at is the so-called 'cut size'. This cut size is the smallest sieve size used and thereby defines the lower limit of the particle size measured.

2.2.2.b Image analysis

An image of a batch of particles may be used to retrieve the particle size distribution by analysing the size of each individual particle in the image. The image used can be a microscopic image, a photograph or a frame from a video camera. The typical cycle to acquire a size distribution from an image is as follows.

1. Image acquisition; produce an optimal image.
Illumination of the material should be optimised to show particle boundaries as clearly as possible, therefore brightness and contrast should be optimised. In a photograph, noise and unfocussed pictures should be avoided. Some digital editing may improve the image to gain slightly better results.
2. Particle delineation; assigning the outlines of the particles.
Depending on the method used for image analysis, particle delineation can be done manually or by using an algorithm. In an algorithm a threshold can be applied based on the grey levels of neighbouring pixels. A very important factor in this stage is the determination of the lower detection limit; what is the smallest particle that detected and delineated? This lowest detection limit is also called a cut-off size. For example, a theoretical cut-off size in digital images is caused by the resolution, since a particle is only detected when its size is at least 4x4 pixels (Split Engineering, 2010).
3. Scaling; relating the number of pixels to the actual size.
A scale is needed to assign an actual value to the particle size. The particle delineation has defined the amount of pixels for each particle. This amount of particle pixels is translated to the actual particle size, using the amount of pixels for the length of the reference object.
4. Particle size measurement; acquiring a size distribution.
Using the delineation and scale the particle can be measured. The required diameter is

extracted from the image for each individual particle. A third dimension is sometimes applied, using a best-fit ellipsoid. In this stage, also estimation of the fines (particle size below the cut-off size) can be applied. Results are often displayed using a cumulative size distribution using particle size on the x-axis and the percentage passing on the y-axis (using an equivalent sieve diameter).

Different algorithms and systems may be used. These steps can be applied on both online and offline systems and based on 2D or 3D imaging. Offline image analysis means that a picture is taken from a sample and processed at a later time. Online image analysis or video analysis can be applied on moving material, whereby captured pictures or video are processed instantly to deliver direct results. Video and pictures are 2D representations of the material; several systems are available, for example: SplitEngineering and Wipfrag. Increasingly online systems are equipped with stereo cameras (Noy, 2006) or an additional laser scanner (Kaartinen and Tolonen, 2008), to provide a 3D image of the material. The benefit of a 3D system is found in detection of the extra dimension and therefore could result in a more accurate measurement of size distribution.

Accurate application of image analysis requires good particle boundary detection, therefore the right illumination is needed, which is explained in detail by Crida (1995).

One of the main errors using image analysis is the estimation of the hidden material (especially on conveyor belts, but also in stockpiles). When material lies underneath other material, this part is out of the cameras' sight. This problem is partly solved when using a 3D system. However, estimation on the 'invisible' material is still required.

Furthermore, an appropriate correction factor is needed for the particle size below the cut-off size. This size fraction is too small to be detected by the system and thus should be corrected for.

Removal of these errors is done by calibrating the measurements. This can be done by sieve testing the same material as used in the images. The image analysis is a very precise method, but needs calibration to be accurate. The difference between precision and accuracy is shown in Figure 16. In the left picture, the four X's are more precise where the four O's are more accurate. The effect of calibration is shown on the right, where it improves the accuracy.

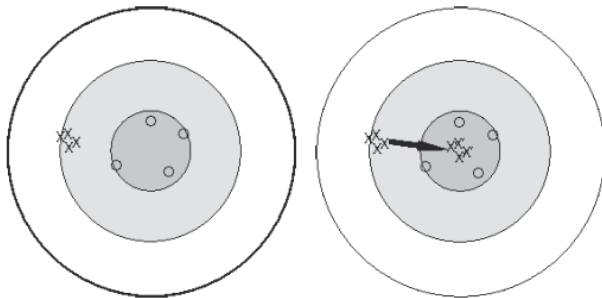


Figure 16: Difference between accuracy and precision in a bull's eye target (Maerz, 2001)

Advantages of image analysis methods are low operating costs and the possibility to automate the recording and analysis. This makes the use of large numbers of images possible. The use of a large number of images is the best method to gain a correct representation of the entire bulk material. The optical measurement is independent from size, so large particles can be measured easily. Another major benefit over a sieve analysis is that the material flow does not have to be interrupted. In addition, an online video analysis system is less influenced by a 'snap shot' effect, since it takes a continuous stream of frames. A calibrated image analysis system can be very effective in detection of the particle size distribution.

2.3 Bulk material

Bulk materials may be defined as materials consisting of a large amount of individual particles. Bulk material is a granular mixture existing in a free-flowing form. The behaviour of a bulk material cannot be described by its material composition only. Next to the individual particle characteristics, the properties of a material as a bulk are important when studying material flow. The characteristics of free-flowing, cohesionless bulk materials are described in this study by particle size, particle size distribution, particle shape, bulk density and angle of repose. For cohesive bulk materials, also the cohesion, adhesion, moisture and even temperature should be taken into account as well. In this study, the material is considered free-flowing and cohesionless, since the focus of this study is on the coarse material. Cohesion plays a more dominant role for fine material.

2.3.1 Particle size and size distribution

As discussed in *Section 2.2*, the particle size, shape and size distribution are parameters that need to be looked at carefully. The particle size and size distribution have a major impact on the flow of bulk materials. The maximum grain size is an important factor in the design of discharge openings and transfer points for conveyor belts (Petermann, 2010). The fine fraction is a dominant factor in the flowability of a bulk material. Fine material can either increase or decrease the flowability of the bulk. In general, a certain amount of small particles functions as a flow medium on which coarse material is transported (Schulze, 2008). Hence, this increases the flowability of the bulk. On the other hand, the fines may reduce flowability as well. This may be caused by the cohesive and adhesive properties of fine-grained materials. Also the water absorption capacity of fines is higher, which may increase the stickiness of the material.

2.3.2 Bulk density

The density of a particle is the ratio of mass of the particle over its volume. The density of a bulk material takes the voids between multiple particles into account; therefore the bulk density is the weight per unit of volume (in: kg/m³ or t/m³) including open voids.

While the density of the material in this study is considered constant (*Section 3.3.1*), the bulk density however may differ considerably. Bulk density depends on the particle size distribution, moisture content and the compactness of the bulk. Bulk materials with a wide range of particle sizes may result in a higher bulk density, when the smaller particles will fill the open voids between the larger particles. This may increase bulk density up to 20% (Petermann, 2010).

Bulk density may also differ due to compaction. However, the bulk density in the Tepee stockpile is loosely formed. This loose bulk density ' ρ_b ' is the mass of a loose bulk material ' m_b ' over the volume of the sampled material ' V_b ', which includes the open voids. The loose bulk density is the most used bulk density, since this incorporates the largest bulk volume to be handled.

$$\rho_b = \frac{m_b}{V_b} \quad \text{Eq. 3.}$$

2.3.3 The angle of repose

The angle of repose is the angle of the slope of a pile formed by free-flowing material. This angle is also referred to as the angle of slope. The angle of repose ' α ' (or ' α_M ' in Figure 17) is the angle between a horizontal line and the sloping line from the top of a freely formed pile of bulk material to the base of the pile.

The angle of repose depends on particle shape, particle surface, particle size and moisture content. The most important parameter is the particle shape. Perfectly rounded particle will roll freely and therefore result in a lower angle of repose. Very angular particles will interlock, which reduces rollability and thereby increase the angle of repose.

A slightly wet material will form a larger angle of repose, because the surface tension between the water and the particles will bound the particles together. High water content will cause liquefaction, which occurs when loose particles become oversaturated with water and the particles loose contact with each other. Liquefaction of bulk material results in a close to zero angle of repose.

The particle size is important in combination with the moisture content, since fines may become sticky. However, also the particle shape may be different for larger and smaller particles. Holdich (2002) states that particle size distributions with a high percentage of fines in general result in a lower angle of repose. The fines act as a flow medium and increase flowability of the material, which reduced the angle of repose.

Roughness is another parameter that needs to be taken into account. For example, rough spherical particles result in steeper angles of repose than smooth spherical particles, even when they both have the same shape.

Since the angle of repose is easily measured from a stockpile photo or by straightforward laboratory tests, the angle of repose is often used in describing bulk materials and their flow characteristics. Different laboratory test are described by Schulze (1998) and shown in Figure 17. A first method is measuring the slope angle of conical pile formed by pouring the unconsolidated bulk material through a funnel. Another method is to measure the slope angle of the material remaining in a flat bottom container after discharge through a centred outlet (Figure 17.b). Furthermore, dynamic repose angle measurements are done, for example by using a slowly rotating drum. The reason for different repose angle measurements is the dependency of the slope angle on the geometry.

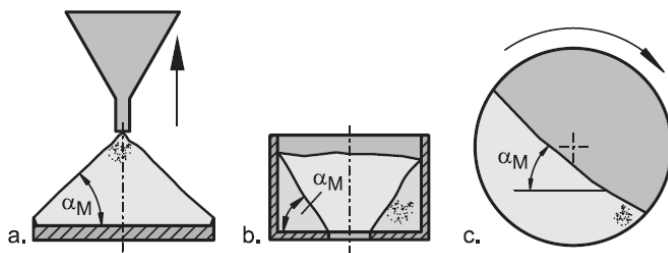


Figure 17: Measurement of repose angle; (a) poured angle of repose, (b) drained angle of repose and (c) dynamic angle of repose (Schulze, 2008)

2.3.4 Moisture content

The moisture content of the bulk material is a dominant parameter for the stickiness of the material when reviewing crushed rock. Especially with finer material, the water content dominates the flowability of the bulk. Small amounts of water may increase particle bonds, where large amount of water cause liquefaction.

Moisture in bulk materials are divided into two groups; bound water (structural water, adsorbed water) and 'free' water between the particles. The 'free' water in the hollow spaces between the particles is most essential. Petermann (2010) states that cohesive materials (the fine particles and powdery material) change their state by varying water content, which is mainly due to the size of the particles. Fine grained material have a relative large surface to their weight, hereby causing a larger impact of the liquid bonds to the particles. A wet, fine material may behave plastic. Coarse material is not affected by small amounts of water and will remain free-flowing.

2.3.5 Bulk stresses and friction angles

The angle of repose is formed due to the internal friction of bulk. In bulk material storage (mainly in silos) the internal friction angle and wall friction angle are important. Since the flowability of bulk materials are related to the stresses and the friction values of the material, the stress states of the bulk material are reviewed first.

The uniaxial compression test measures the shear stress ' τ ' over the normal stress ' σ '. The shear stress is measured by applying a load on a created a freestanding cylinder of bulk material. The normal and shear stress resulting from this test are usually visualised in using Mohr's stress circle, as shown in Figure 18.

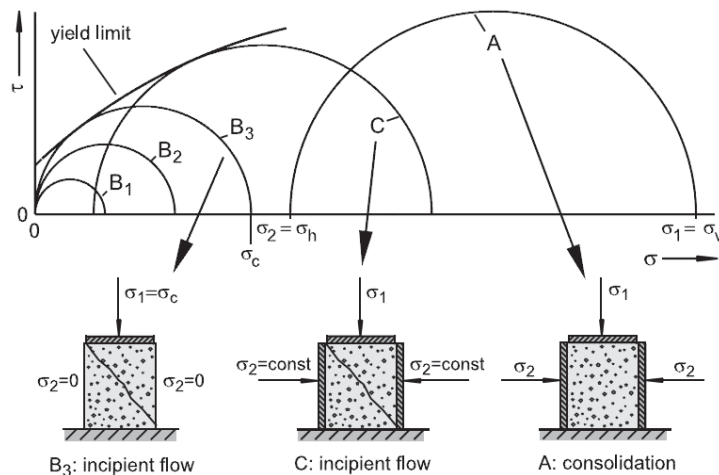


Figure 18: Measurement of unconfined yield strength, shown in Mohr's stress circles (Schulze, 2008)

In the previous figure, different stresses on a bulk specimen are distinguished. Sample B1, B2 and B3 show an increasing vertical load (normal stress ' σ_1 ') where the horizontal stress (minor principal stress, ' σ_2 ') is zero, since there is no horizontal confinement. Sample B1 and B2 show only elastic deformation and stay well below the yield limit. Sample B3 shows a failure of the sample when the load reaches the unconfined yield strength ' σ_c ', also called the compressive stress.

Sample C uses a constant horizontal load on the sample. This shifts Mohr's stress circle to the right and allows larger vertical load on the sample before failure. A Mohr's circle that hit the yield

limit means that the sample is deformed (or commences) plastic deformation. When the Mohr's circle is well below the yield limit (B1, B2 and A) the sample deforms elastically.

Schulze (2008) describes the flowability of bulk materials as a relation between the consolidation stress ' σ_c ' and the compressive stress ' σ_1 ', which is similar to the numerical approach of Jenike (1964) and given by the following equation.

$$ff_c = \frac{\sigma_1}{\sigma_c} \quad \text{Eq. 4.}$$

The flow factor ff_c (for consolidation stress) classifies the material on its flowability, this is displayed in Figure 19. The higher the flow factor, the better the flowability of the bulk material.

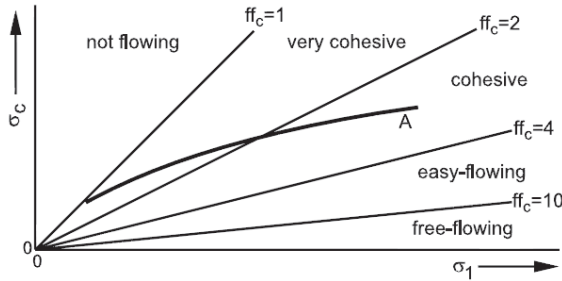


Figure 19: Classification of flow behaviour (Schulze, 2008)

The friction values and the angles of friction are reviewed using Mohr's circles. Mohr's friction law states that there is a linear relationship between the shear stress and the normal stress. This relation is given by the internal friction value ' μ_i '.

$$\tau = \mu_i \cdot \sigma \quad \text{Eq. 5.}$$

The internal friction value can be interpreted as a measure of the strength of the bulk material. The internal friction value is tangential related to the internal friction angle, as shown in the equation below. For bulk materials, the angle of internal friction is almost equal to the angle of repose (Petermann, 2010), (Metcalf, 1965). Therefore, the angle of repose ' α ' is also closely related to the internal friction value.

$$\mu_i = \tan \varphi_i \quad \text{Eq. 6.}$$

$$\mu_i \approx \tan \alpha \quad \text{Eq. 7.}$$

$$\mu_s = \tan \varphi_x \quad \text{Eq. 8.}$$

In a similar way the angle of static wall friction ' φ_x ' (measured to the horizontal) is related to the static friction coefficient ' μ_s ' for solid particles on a solid surface, e.g. the wall of a bin or chute. The inclination of the surface to the horizontal is the wall friction angle. The maximum wall friction angle is the angle at which particles overcome the static friction and start to roll and slide downwards. The static wall friction angle is generally lower than the angle of repose; due to the flat surface of the wall.

2.4 Flow in stockpiles

The flow properties of bulk materials in a stockpile have major influence on the size distribution output since they define the flow mode and invoke segregation and blending effects. To understand why these effects take place the flow within the stockpile need to be understood. The stockpile in this report is conical shaped, therefore many similarities are found with the flow in a conical hopper or silo. The flow patterns discussed are developed mainly for applications in hopper, chute and silo design, however they are very well applicable to the Tepee stockpile at Tara Mines.

2.4.1 Flow regions

Different regions of flow can be distinguished. This can be done either qualitatively or quantitatively. The qualitative approach defines areas with different flow modes visually. A quantitative theory was published by Jenike (1961) and was based on the physical properties of the bulk solids.

Based on visual observations, Brown and Hawksley in 1947 (as quoted in Swedes, 1998) reported five different areas during discharge of free-flowing bulk solids. The different areas A to E are marked in Figure 20. As the discharge flow begins, after each other the areas D, C, A and B are formed. Area A is a fast moving layer compared to layer B. In zone A, single particles roll freely and move as a block over layer B. Zone E is also called a dead/stagnant zone and is not moving at all.

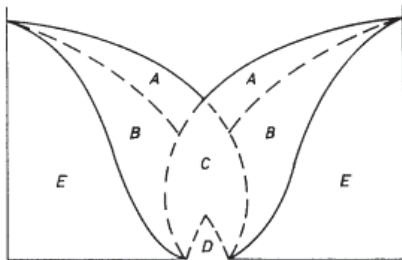


Figure 20: Areas of flow after Brown and Hawksley (as quoted in Swedes, 1998)

The contact plane between B and E is of a greater inclination than the angle of repose, which is maintained by the free surface. Particles moving from zone A and B into zone C will increase velocity. These particles will lose their particle-particle interaction when they move into zone D and will fall freely through the aperture at the bottom.

Another approach based on visual observations is developed by Kvapil (as quoted in Janelid and Kvapil, 1966). Where the Brown and Hawksley approach is limited to small filling heights, the work of Kvapil has no restrictions as such. He distinguished two different movements, namely the ellipse of primary and secondary motion. In primary movement, particles move downwards only, due to gravity. While in secondary motion, the particles can also rotate and move in a horizontal direction. The zones of movement are elliptical shaped. The primary movement can only occur in very tall silos (or in caving zones, where the work of Kvapil started), which is shown left in Figure 21. Secondary movement is very important near the outlet opening in a silo of any shape (Martinez, et al., 2002), which is best shown on the right in Figure 21.

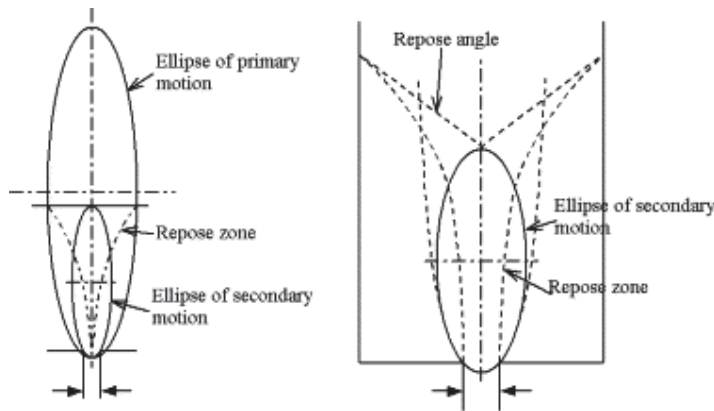


Figure 21: Ellipsoids of motion in bulk materials as proposed by Kvapil (as quoted in Janelid and Kvapil, 1966)

At the start of bulk material discharge, both ellipsoids begin to grow. The primary ellipse continues growing till the upper surface of the filling material is reached. Hereafter a 'repose zone' is formed, which is also called the 'funnel of repose'. The ellipsoid of secondary motion also continues growing until it reaches the deepest surface point of the funnel of repose. At this point, the ellipsoid is decreasing in width and a discharge funnel is formed. This funnel constitutes the interface between regions of slow and fast moving material (Schwedde, 1998). This interface is also referred to as the angle of withdrawal.

2.4.2 Mass and core flow

The first to predict the material flow quantitatively from the properties of the bulk solid was Jenike. Jenike (1961, 1964) predicted the mode of material flow according to the material properties and equipment parameters.

Jenike distinguished two gravitational flows: mass and funnel flow (also known as core flow). The modes of flow are distinguished on their discharge behaviour. In mass flow, all bulk material moves downwards simultaneously. The result is that the first material flowing out is the material that is also poured in first (first-in, first-out). In funnel flow, the material in the centre of the silo/stockpile is discharged first, followed by the side material closer to the walls. As long as the side material is not moving towards the discharge opening, this material is referred to as stagnant. In funnel flow, the material behaviour can be described as 'first in, first out'. Figure 22 highlights the difference between mass and funnel flow.

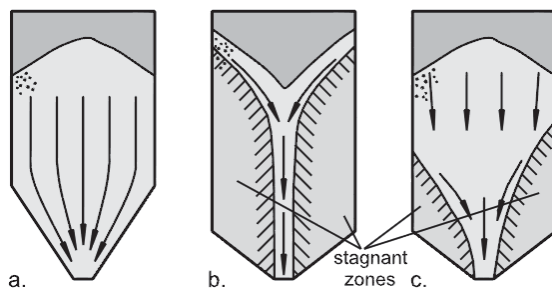


Figure 22: Flow profile: (a) mass flow, (b) funnel flow with stagnant zones to the top of filling (piping), (c) combination of mass and funnel flow (low stagnant zones) after Schulze (2008)

In mass flow, the entire bulk content is in motion when material is discharged; thus the material against the wall moves as well. In core flow, the bulk is moving at different velocities, where some material is not moving at all and remains in a stagnant zone. Due to the discharge of the

moving zone in funnel flow, the stresses on the stagnant zone are relieved, which makes it possible for the top of the stagnant zone to start moving towards the core.

When the walls of a silo are not steep enough for mass flow, the material will flow in core flow. The start of discharge in a filled silo will first form a flow channel above the outlet. The shape of the flow channel differs with the material properties and geometry, however for a centred bottom opening the flow channel will be mostly shaped as a cylindrical funnel. The material in the flow channel starts flowing downwards. As long as the flow channel is filled with material, this material brings horizontal pressure on to the stagnant zone, when this stress is relieved the stagnant zone starts moving under the vertical stress caused by gravity.

Stagnant zones are called unstable if the stagnant zone is slipping over either the walls or another (stable) stagnant zone. Slipping of these stagnant zones causes the stagnant material to enter the flow channel periodically, since it is not a smooth continuous motion. The forces induced by this, cause vibrations that is called quaking. Quaking is a major cause of erratic flow during discharge, which makes output predictions more difficult.

It is widely accepted that three factors are dominant in the flow mode of the bulk material: the internal friction of the material, the material-wall friction and the stockpile design. The design of the stockpile includes the outlet size, the wall angle and basic shape (wedge shaped or conical). These factors are included in the design charts of Jenike (1961, 1964), shown in Figure 23 and Figure 24. Jenike used continuum models, which were valid against experimental data to develop a series of charts, to relate material properties and silo design to the flow mode.

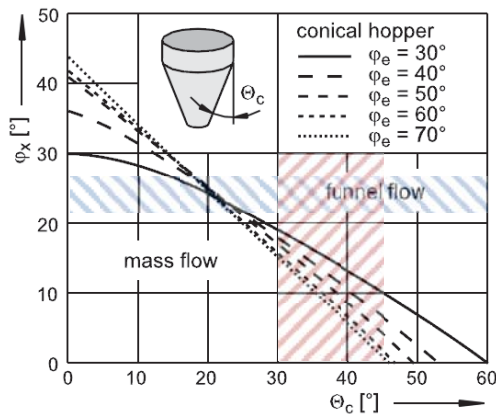


Figure 23: Design chart after Jenike (1961); flow mode in a conical hopper (Schulze, 2008)

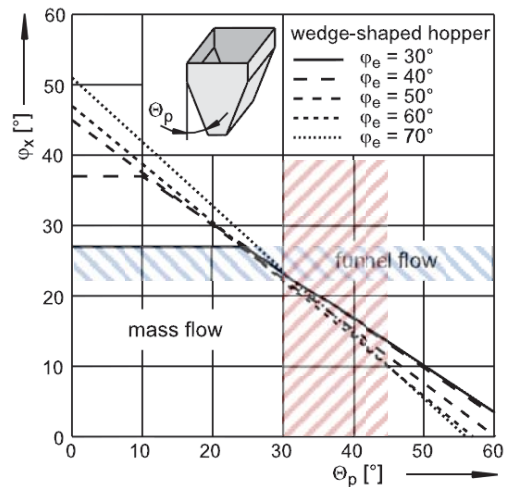


Figure 24: Design chart after Jenike (1961); flow mode in a wedge-shaped hopper (Schulze, 2008)

Jenike's (1961) design charts are specific to the hopper geometry; the conical shape and the wedge-shaped hopper. In addition, the design charts are also specific to the internal friction of the bulk material, represented by the effective angle of internal friction ' φ_e '. Together with the angle of static wall friction ' φ_x ' and the maximum inclination of the hopper wall ' θ_c ' or ' θ_p ', the diagrams determine whether the mass will discharge in mass flow or funnel flow.

The diagrams for a conical and a wedge-shaped hopper show similarities. In both diagrams, mass flow is achieved with a low bulk to wall friction and a low wall inclination ' θ ' (or a steep wall angle ' α ' when measured to the horizontal). A high friction angle and a high wall inclination angle will thus result in funnel flow. The stockpile at Tara Mines is expected to have a wall friction

angle (22-26 degrees Gilbert Gedeon, 1994) and a wall angle between 45-60 degrees ($\theta_c = 30-45$ degrees), therefore funnel flow is expected to be the flow mode.

The impact of the internal friction angle is not considered as a significant factor influencing the flow mode, regarding either a conical or a wedge-shaped design. The flow mode in the Tepee is further discussed in *Chapter 4*. Comparing both diagrams it is seen that for identical material properties (φ_x and φ_e), mass flow is achieved at larger wall inclination (a flatter wall angle) for a wedge-shaped hopper than for a conical hopper. The difference in wall inclination is generally in the range 8-12 degrees (Schulze, 2008).

2.4.3 Advantages and disadvantages of mass and core flow

The advantages and disadvantages of mass and core flow are reviewed. The most important factors are listed in Table 3 (after Holdich, 2002), where the advantages are given in a bold font. In general mass flow results in a more even distributed and better predictable flow. However for large volume of bulk material, the tall design of the storage building required, is not very well applicable. Another reason to go for funnel flow stockpile is better resistance to wear on the wall surface; the bulk slides along the stagnant zones instead of the walls. Especially with hard, large sized and angular rock, wear reduction is an important factor.

Table 3: Advantages (in bold) and disadvantages of mass and core flow (Holdich, 2002).

Mass flow	Core flow
Good output prediction; uniform flow and first in, first out.	Difficult output prediction; erratic flow and last in, first out
No loss of material in stagnant zone	Stagnant zones, which may empty at complete discharge (may reduce capacity)
Absence of bridging and ratholing	Ratholing and bridging may occur
Less segregation; no rolling of particles	Segregation during discharge; particles roll at different velocities
Tall and thin structure required	More efficient, low cost structure required
High wall stresses	Wall stresses may be relieved
More wear on wall surface	Less wear on wall surface

2.4.4 Arching and ratholing

The flow of material is influenced by the outlet size of either a hopper, a silo or a stockpile. A small discharge opening may cause arching and ratholing. These two phenomena are discussed, since they should be and can be prevented by the size of the outlet opening of the stockpile.

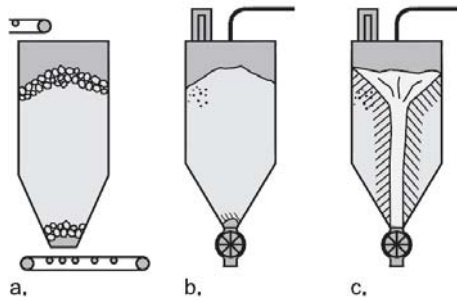


Figure 25: (a) Arching due to interlocking and wedging, (b) Arching due to cohesive strength of bulk material, (c) ratholing (Schulze, 2008)

Arching is a risk to avoid in mass and funnel flow. A narrow outlet has the potential to form a stable arch above the outlet. Two kinds of arching may occur; an interlocking arch (Figure 25.a) or a cohesive arch (Figure 25.b). Especially with coarse-grained bulk material, the particles may form an arch due to interlocking particles and due to wedging of particles. A stable arch directs the forces to the walls and blocks the flow in the stockpile. Mainly in fine-grained bulk material cohesive arching may occur. The cohesive strength of the material is a cause of the adhesive forces of the individual particles (Van der Waals forces for fine-grained bulk or liquid bridges in moist bulk solids).

Arching is avoided by using a sufficiently large outlet size. This increases the span of the arch. Therefore, the required forces to span the outlet become too large to form a stable arch. To prevent arching, it is generally accepted that the outlet opening of a conical hopper needs to be 6-10 times the maximum particle diameter ' d_{max} ' and for a wedge-shaped hopper 3-7 times the maximum particle diameter (Schulze, 2008).

Ratholing (or piping) takes place when the moving material forms a channel above the outlet, as shown in Figure 25.c. The stagnant zones on either side of the channel will not flow into the channel when the material has enough cohesive strength. Hence, the flow channel will remain open when no new material is loaded. Ratholing only occurs in funnel flow since the pipe is formed from the consolidation of stagnant zones, which is the main reason to favour a mass flow system. Ratholing is unwanted when the stockpile is used as a buffer in capacity. In this case, the stockpile is never emptied completely, therefore material remains in the stagnant zone and is never released. This reduces the effective capacity of the stockpile.

2.4.4.a Outlet size for mass flow

Another approach to determine the outlet diameter is the use of flow factor diagrams. Flow only occurs when there is no blockage of the outlet by arching. Arch forming is described by the stresses acting on the bulk material in this section.

Equation 9 was referred to previously in *Section 2.3.5* and gives the flow factor for consolidation stress. This formula can be rewritten to estimate a critical flow factor ' ff_{crit} ', by using the stress required to support a stable arch ' σ'_1 '.

$$ff_c = \frac{\sigma_1}{\sigma_c} \quad \text{Eq. 9.}$$

$$ff_{crit} = \frac{\sigma'_1}{\sigma_c} \quad \text{Eq. 10.}$$

The arch formed in the hopper redirects the weight of the bulk to the walls of the hopper. This force is given by the major stress required to support a stable arch ' σ'_1 '. Figure 26 shows that a stable arch is only possible in the region where the unconfined yield strength is greater than the stress required in a stable arch; ($\sigma_c > \sigma'_1$). The critical flow factor ' ff_{crit} ' therefore becomes smaller than one, which means that the bulk material is considered not flowing (*Section 2.3.5* Figure 19). The figure shows this critical moment in the height point above the virtual apex ' h^* ', from which the critical outlet opening ' d_{crit} ' can be defined. In order to avoid blockage due to arching the outlet opening should be larger than the critical outlet opening.

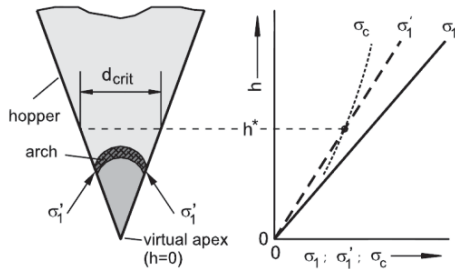


Figure 26: Determination of the minimum outlet size (d_{crit}) to avoid arching (Schulze, 2008)

The major assumptions by Jenike (1964) and Janssen (1895) are: the bulk solid arch is smooth, further the arch has a constant thickness and must only carry its own weight. According to Jenike (1961), this results in the following equation for the major stress:

$$\sigma'_1 = \frac{2r \cdot \sin \theta \cdot g \cdot \rho_b}{1 + m} \quad \text{Eq. 11.}$$

The diameter of respectively a conical hopper and wedge-shaped hopper are represented by the term ' $2r \cdot \sin \theta$ '. Where ' r ' is the distance from the hopper apex to the base of the arch and ' θ ' is the wall angle measured to the vertical. The parameter ' m ' represents the shape of the hopper and is zero for a wedge-shaped hopper and set one for a conical hopper.

The ratio between σ_1 and σ'_1 is called the flow factor ' ff '. The flow factor is constant at the wall of the hopper, since both stresses are proportional to the hopper diameter (which is a function of the arch to apex distance ' r ').

$$ff = \frac{\sigma_1}{\sigma'_1} = \text{constant} \quad \text{Eq. 12.}$$

Jenike shows that the flow factor is dependent on the hopper or stockpile geometry (m and θ) and the bulk flow properties (φ_x and φ_e). The following diagrams are made by Jenike (1964) to determine the flow factor of the bulk in a hopper.

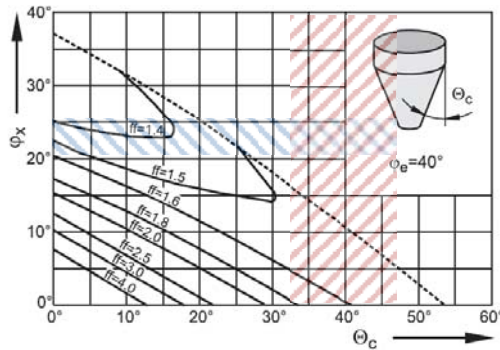


Figure 27: Flow factor diagram for conical hopper (Schulze, 2008)

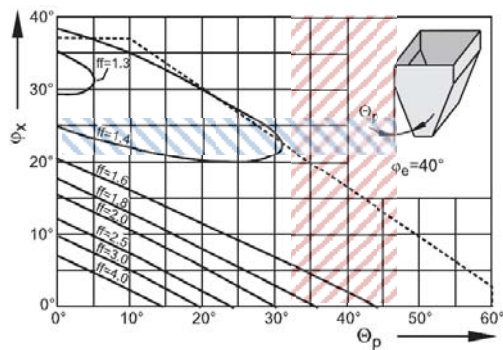


Figure 28: Flow factor diagram for wedge-shaped hopper (Schulze, 2008)

Dotted line is the boundary between mass and funnel flow, defined previously by Jenike's design charts.

The stockpile at Tara Mines is constructed with a wall inclination (θ_c or θ_p) of 30-45 degrees (Plunkett, 2012 *personal communication*). In this study a comparison is required between both flow factor diagrams for the same effective angle of internal friction φ_e and with a uncertain angle of wall friction φ_x . An estimate for the wall friction angle is given in Section 2.4.2 at 22-26 degrees, which confirms core flow in the stockpile Tepee. Even in case a lower wall friction angle applies to this case, this does results in the same flow factor for either hopper shape, namely a flow factor around 1.6.

Using Jenike's flow factor diagram the flow factor can be determined, when applying this flow factor and equation 13 and 14 the critical outlet diameter can be calculated using the follow formulas.

Detailed derivations are found in Schulze (2008).

$$d_{crit} = (1 + m) \cdot \frac{\sigma_{c,crit}}{g \cdot \rho_b} \quad \text{Eq. 13.}$$

$$b_{crit} = (1 + m) \frac{\sigma_{c,crit}}{g \cdot \rho_b} \quad \text{Eq. 14.}$$

The factor m is takes into account the hopper type and geometry. The critical outlet size can be determined more precisely when the factor $(1 + m)$ is replaced by the function $H(\theta)$, which describes the hopper geometry and is shown in Figure 29

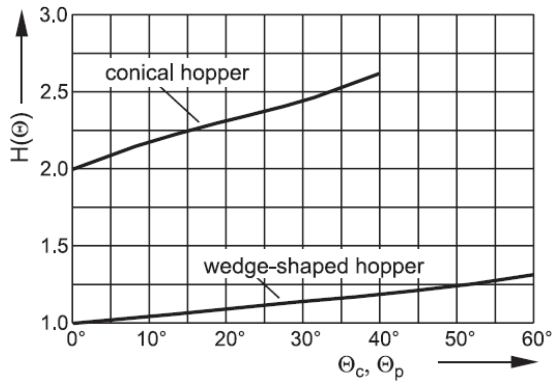


Figure 29: Function $H(\theta)$ for hopper geometry (Schulze, 2008)

The figure shows that for steep hopper walls (low ' θ '), the function ' $H(\theta)$ ' is equal to one for wedge-shaped and two for conical shaped hoppers. For flatter wall angles (high inclination ' θ ') this factor increases faster for conical hoppers. The stockpile at Tara Mines has wall inclination of $30 < \theta < 45$, which means that ratio the critical outlet diameter for a conical to a wedge-shaped hopper is in the order of 2.6 to 1.2; thus the critical outlet of a conical stockpile should be more than two times the diameter of a wedge-shaped hopper.

2.4.4.b Outlet size for funnel flow

Since ratholing only takes place in funnel flow, the method to determine the minimum outlet size in funnel flow is different from mass flow. In mass flow, the critical diameter of the outlet to avoid arching is calculated. However, in funnel flow the critical outlet diameter to avoid ratholing is more important, since this diameter is always larger than the critical diameter to avoid arching; ($D_{crit} > d_{crit}$). This means that for core flow only the critical diameter to avoid ratholing is required, since by this also avoids arching.

Jenike (1964) developed an approach to estimate the rathole dimensions, which is called 'lower bound' approach. This approach assumes that the stresses at the wall of a stable rathole are independent of the filling level. This approach only holds when there is filling and discharge at the same time, so the consolidation of bulk material can be neglected. Jenike states that when a stable rathole diameter is formed, there is a circumferential compressive stress ' σ_1'' ' acting close to the surface of the rathole wall. This is pictured in Figure 30. The rathole remains stable when the unconfined yield stress ' σ_c ' of the bulk solid exceeds the circumferential stress, since this blocks the bulk material from flowing into the interior of the rathole. Using the diameter of the rathole ' D ' and the bulk density of the material ' ρ_b ', the circumferential stress can be calculated as follows (Schulze, 2008):

$$\sigma_1'' = \frac{D \cdot g \cdot \rho_b}{f(\varphi_i)} \quad \text{Eq. 15.}$$

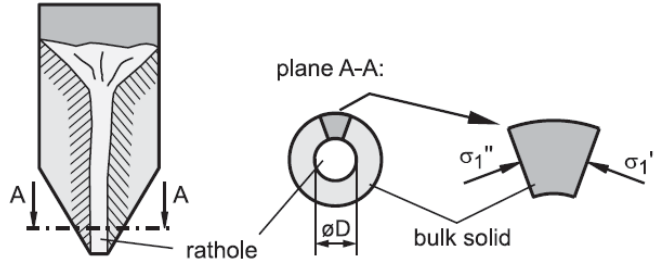


Figure 30: Stable rathole and circumferential stress (Schulze, 2008)

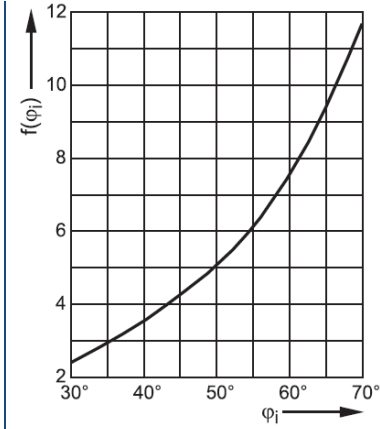


Figure 31: Function $f(\varphi_i)$ (Schulze, 2008)

Similar to the critical outlet diameter for mass flow to avoid arching, the critical diameter for arching in core flow is calculated. This results in the formula given below, where the function ' $H(\theta)$ ' for hopper geometry is replaced by the function ' $f(\varphi_i)$ '. Figure 31 shows the relation between this function and the angle of the local yield locus ' φ_i ', which is the yield locus at starting output flow.

$$ff_p = \frac{\sigma_1}{\sigma_1''} \geq 1.7 \quad \text{Eq. 16.}$$

$$D_{crit} = f(\varphi_i) \cdot \frac{\sigma_{c,crit}}{g \cdot \rho_{b,crit}} \quad \text{Eq. 17.}$$

Since the circumferential stress is not relevant in a wedge shaped hopper with a rectangular output, the design procedure to avoid arching, as seen in *Section 2.4.4.a*, applies here. Therefore the critical width of the outlet ' b_{crit} ' must be calculated, where the values $ff = 1.7$ and $H(\theta) = 1.15$ have to be used according to Schulze (2008).

2.4.5 Gravity reclaim stockpile

Gravity reclaim stockpiles are widely used when handling large volumes of bulk material. Material from the Tepee stockpile at Tara Mines is also reclaimed by means of gravity, therefore similarities are found with gravity reclaim stockpiles. There is however a major difference, since the Tepee is also constructed with a 'bottom cone' and gravity reclaim stockpiles are generally placed on a horizontal surface (see the figure below).

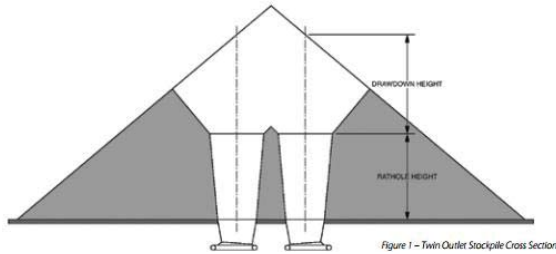


Figure 32: Example of a gravity reclaim stockpile (Roberts, 2009)

The attraction to use gravity reclaim stockpiles are the low costs and the very high storage capacity that can be reached. The major disadvantage is that ratholing may significantly reduce the so-called 'live capacity' of the stockpile. The live capacity is the part of the stockpile where the material is actual moving and discharged, the other parts contain the stagnant material. For more information on the live capacity and the stresses involved there is referred to Roberts 'hoop stress' theory (Roberts, 2009).

This live capacity is also of importance for the Tepee, however this effect is reduced by the design of the Tepee. The bottom of the Tepee is not a horizontal surface where a lot of material is 'lost', but is placed in a downwards pointing cone. This naturally increases the live capacity of the Tepee, compared to a gravity reclaim stockpile.

2.5 Segregation

Segregation in general is the separation of units based on their characteristics. In this study, ore particles tend to segregate mainly based on their size, shape and density. Especially when the ore is free-flowing and non-sticky, particles can easily segregate. Segregation is not wanted in most industries, and in this study also unwanted since it disrupts the mixed size distribution. In order to avoid or deal with segregation an understanding of the segregation processes is required.

Different segregation mechanisms can be distinguished:

- Heap segregation or segregation on an inclined surface
- Percolation
- Trajectory segregation
- Impact segregation

2.5.1 Heap segregation

Heap segregation takes place when material is loosely poured on a surface, where it forms a pile. There are several processes influencing heap segregation described by Enstad and Mosby (1998). They state that rolling and sifting are the most important effects, however in some special cases other effects may be active, such as push-away, angle of repose and fluidisation effects. Since heap segregation is a combination of mechanisms it best referred to as a segregation process instead of a segregation mechanism (Enstad and Mosby, 1998).

Rolling is important at the stage where particles roll down the slope of a heap. Large particles are not stopped by obstacles where small particles are stopped closer to at the top of the pile (Figure 33.a). Similarly, round particle end up at the bottom of the slope, where irregular shapes get hold at the top of the slope (Figure 33.b). The sifting effect (Figure 33.b) occurs when the bulk slides down the slope in layers (Figure 33.c), where small particles are sifting downwards into the open voids between larger particles.

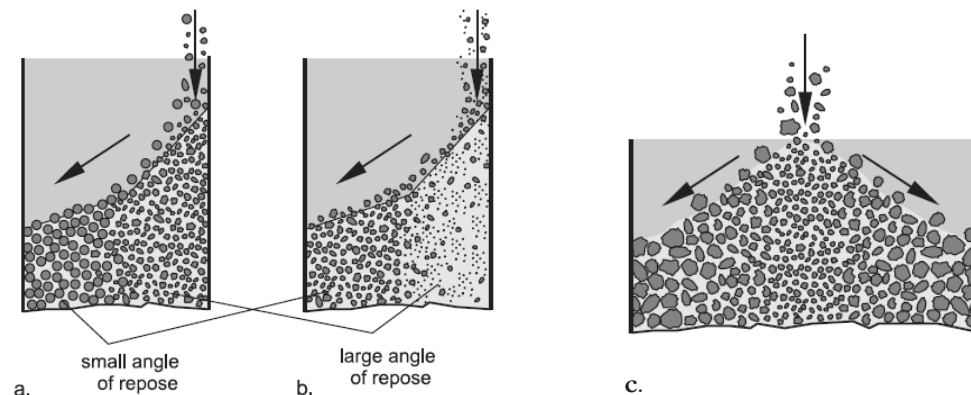


Figure 33: Heap segregation, due to: (a) repose angle and particle shape, (b) repose angle and particle size dominant, (c) particle size and sifting effect (Schulze, 2008)

2.5.2 Percolation

Segregation due to percolation is a separation of different type particles caused by shaking or vibrating of the entire bulk. Jha and Puri (2009) state that percolation segregation is the dominant mechanism during conveying, storage, flow, since heap segregation is not seen as a single segregation mechanism.

Due to movement of the entire bulk, small particles move into the present open voids and thereby move downwards in respect to the coarser particles (Figure 34). This is an effect seen especially during transport on a conveyor belt, in trucks or in silos.

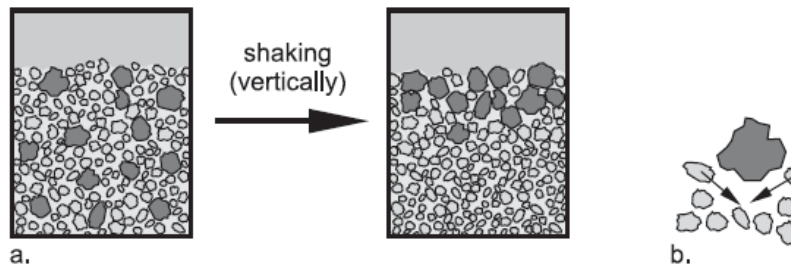


Figure 34: Segregation caused by percolation (a) and the mechanism; fines entering the open voids (Schulze, 2008)

2.5.3 Trajectory segregation

Trajectory segregation also caused by vibrations and thereby a type of percolation. Due to vibration, a large particle is moved upwards and is prevented from returning to its original position, due small particles that fall into the open space.

Especially on conveyor belts, this also causes segregation at the discharge of material as shown in Figure 35. Coarse material lying on top is 'launched' further away from the discharge point than the smaller material at the bottom of the belt. Other factors that increase this effect during discharge are the air resistance (since this has a larger impact on smaller particles) and the stickiness of smaller particles to the belt.

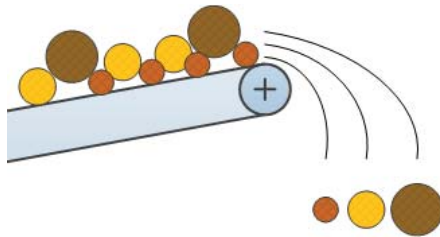


Figure 35: Trajectory segregation on a conveyor belt

2.5.4 Segregation by impact

Material that hits a surface (for example silo walls or the rock plate in a transfer point) are deflected; the deflection may be different for some particles than for others. Size and shape are big factors influencing impact segregation. Segregation of this type is reported in the ore handling system of Tara Mines. However, in this study it is not considered further. Since, other segregation mechanisms are more dominant and impact segregation is not noticed in the stockpile of Tara Mines.

2.5.5 Optimisation of the filling process

Segregation happens more often than not when handling bulk materials. Schulze (2008) states three strategies that can be followed to deal with segregation:

- Modification of the bulk solid
- Remixing the segregated material
- Optimisation of the filling process

In a mining stockpile, the first two strategies are difficult to implement, due to the roughness and the large volumes of material. The third method, optimisation of the filling process, will be further discussed and is applied in the simulations in this report.

Silos that are filled identical, but operate under different flow modes discharge their content differently. This is shown in Figure 36. Segregated silo fill at funnel flow mode discharges the fines in the core of the silo first and coarse material at a later stage. However, when the same load discharged at mass flow mode, it is remixed at the outlet.

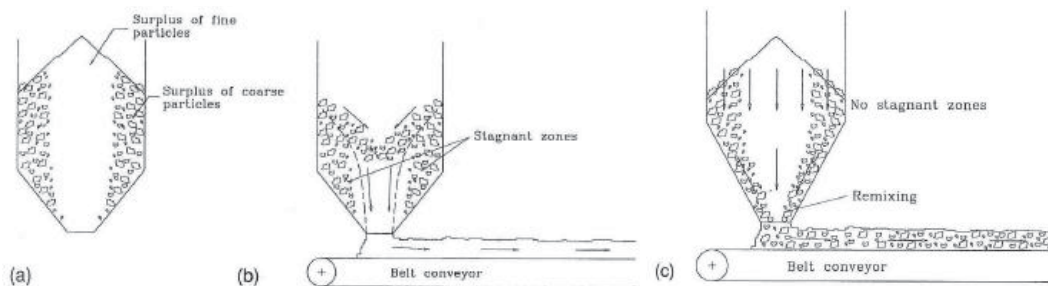


Figure 36: The same silo fill (a) discharged in: (b) funnel flow produces fines followed by coarse and (c) mass flow produces a remixed bulk material (Enstad and Mosby, 1998)

Most gravitational stockpiles for large amounts of rock material are funnel flow systems. Despite this is an unfavourable mode of operating, when looking at the discharge of a mixed size distribution. Optimisation of the filling of the stockpile is an effective measure to deal with these negative effects of segregation in funnel flow mode. An overview of these measures is given in Figure 37 and most of them focus on spreading the material to avoid a core filled with only fine material.

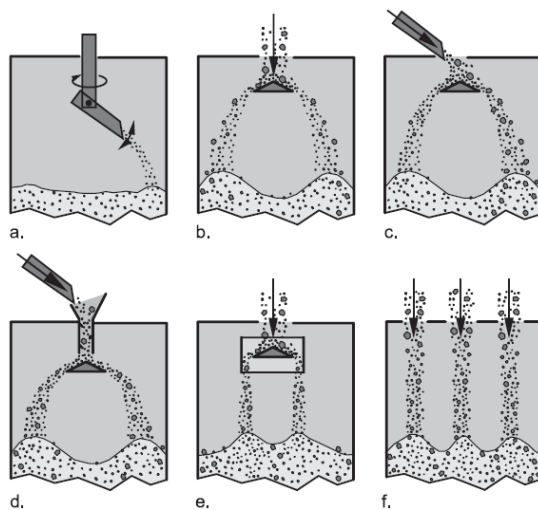


Figure 37: Methods for distributed fill (Schulze, 2008)

Figure 38 shows two scenarios of segregated filling that are also observed at Tara Mines, see *Appendix B*, Figure 148. The chutes at Tara Mines are also used to control the flow. The unsymmetrical discharge in Figure 38.b is modelled with simulation VII in *Section 5.4.1.b*.

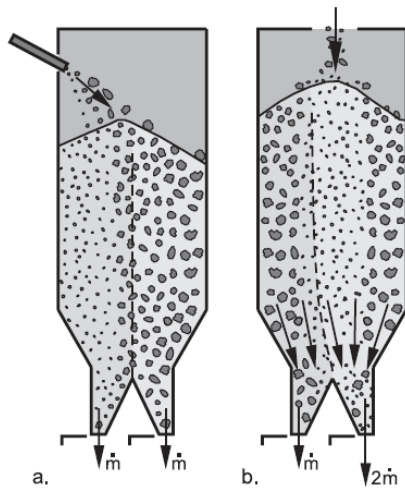


Figure 38: Silo with two outlets: (a) unsymmetrical filling, symmetric discharge; (b) symmetric filling, unsymmetrical discharge (Schulze, 2008).

3 Discrete element modelling and material calibration

The review of background information explained the complexity of flow in bulk materials, due to the influence of individual particles. The aim of the project is to gain understanding of the behaviour of the material in the Tepee stockpile. This may be done by computational modelling of the stockpile. This report focuses on the size distribution during discharge. The individual particle characteristics are important to apply in the modelling; hence the discrete element method is very well suited for this type of modelling due to its distinct particle character.

This chapter first describes the principles of the discrete element method, which is applied to the software package EDEM. Subsequently, the parameter and work cycle in EDEM are reviewed. The final section determines the parameters in EDEM by calibration for the appropriate bulk behaviour.

Section 3.1 Principles of discrete element method

Section 3.2 EDEM parameters

Section 3.3 Material calibration tests

3.1 Discrete element method

Discrete element method (DEM) - also called distinct element method - is a numerical method developed in 1979 by Cundall and Strack, which predicts the motion of individual and independently moving particles. Cundall and Strack developed their computer program BALL in the field of geomechanics. Since then several DEM software packages have been created, that are capable of simulating 3D particle behaviour. The application of DEM and DEM packages moved from geomechanics to mechanical design engineering and more recently into the field of bulk materials. This resulted in the software package used in this thesis EDEM, which is a product of the commercial company DEM Solutions.

3.1.1 Principles

The discrete element method models the dynamic behaviours and mechanical interactions of each individual element in a physical problem through time. This method models bulk material as a group of individual particles that interact at the inter-particle contact points.

The principle idea of DEM is to solve Newton's equations of motion for every possible degree of freedom for all particles.

$$F_{net} = ma \quad \text{Eq. 18.}$$

The forces acting on each individual particle are calculated to predict the future location after a distinct time step. This process - the calculation cycle - is displayed in the figure below and will be explained in more detail.

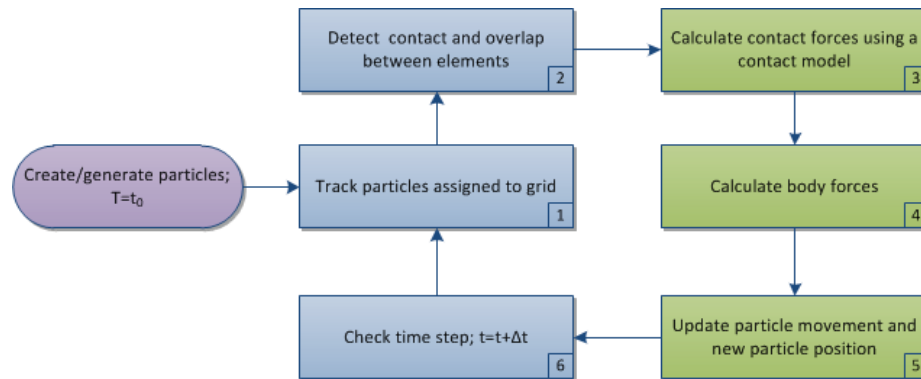


Figure 39: EDEM calculation cycle

The DEM cycle starts with the creation of particles and any geometric element inside a domain. Each time step in the calculation cycle makes it possible to add new particles in the domain or to move any geometric element. Particles outside the domain are removed from the system. All steps in the calculation cycle shown in Figure 39 will be reviewed.

Step 1: Track particles

The domain is divided up in grid cells. The EDEM calculation cycle starts by assigning each particle (and geometric element) to a grid cell. Grid cells with two or more elements are marked as active. Non-active cells are excluded from the calculation, in order to save calculation time.

Step 2: Detect contacts and overlap

All active grid cells are checked for overlap ' δ ', see Figure 40. This may be overlap between either multiple particles or between particles and a geometric element. These overlaps are listed and temporarily stored for calculations in the next step. Particles in EDEM are modelled as rigid spheres using a soft contact model. This way particle overlap is allowed, but individual particle deformation is not allowed. The particle overlap represents the deformation of a particle.

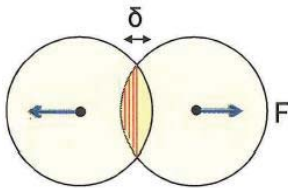


Figure 40: Illustrative particle overlap (DEM Solutions, 2008)

Step 3: Calculate contact forces using a contact model

The amount of overlap measured in the previous step is related to the resulting contact force using a so-called contact model. EDEM is capable of dealing with several build-in contact models as well as custom build models. The simulations in this report use the build-in Hertz-Mindlin contact model, which is described in *Section 3.1.2*.

Step 4: Calculate body forces

This step calculates all other forces on a particle that are not caused by element-element interactions. Gravitational force is the only external force acting on particles in this study. This force is added to the contact forces to provide the resulting force ' F_{net} ' in Newton's second law of motion in *Section 3.1.3*.

Step 5: Update particle movement and new position

Particles movement is divided in translation and rotation, which provides respectively the particle position and orientation. The three parameters to calculate a new particle position/orientation are the old particle positions, the mass of the individual particles and the resulting force acting on each particle. These three parameters are all known from previous steps. They are used to calculate the particle accelerations and velocities by using the laws of motion of Newton and Euler. The manually set time step is used to calculate the new particle positions and orientations.

Step 6: Check time step

Last step in the cycle is a time step check. The cycle is stopped when the end of simulation time is reached, otherwise the cycle continues again with step 1.

3.1.2 Contact model

The default contact model in EDEM is Hertz-Mindlin (no slip). This is also the contact model used in this study. The Hertz-Mindlin (no slip) contact model is based on the work of Mindlin and Deresiewicz (1953). The contacts between two particles or geometric elements are modelled using sets of springs and dashpots and a friction slider, as pictured in Figure 41. Together with particle overlap these springs, dashpots and sliders the particle interaction is modelled in the contact model. The following equations in this chapter are retrieved from the software package documentation DEM Solutions (2011) and DEM Solutions, (2008). These equations will show how all the forces are calculated, which will lead to a resulting force required in Newton's second law of motion.

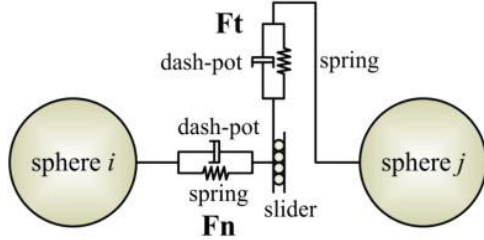


Figure 41: Contact model using springs, dashpots and friction slider (Chung and Ooi, 2008)

The two forces governing the contact model are the normal force ' F_n ' and the damping force ' F_n^d '.

$$F_n = \frac{4}{3} E^* \sqrt{R^*} \cdot \delta_n^{\frac{2}{3}} \quad \text{Eq. 19.}$$

With ' E^* ', the DEM sphere equivalent of the Young's modulus. ' R^* ' is the equivalent radius and ' δ_n ' is the normal overlap.

$$\frac{1}{E^*} = \frac{(1 - \nu_i^2)}{E_i} + \frac{(1 - \nu_j^2)}{E_j} \quad \text{Eq. 20.}$$

$$\frac{1}{R^*} = \frac{1}{R_i} + \frac{1}{R_j} \quad \text{Eq. 21.}$$

The damping force is modelled as the acting of a dashpot. The normal damping force is given by:

$$F_n^d = -2 \sqrt{\frac{5}{6}} \beta \sqrt{S_n m^*} v_n^{rel} \quad \text{Eq. 22.}$$

With ' S_n ', the normal stiffness and ' m^* ' the equivalent mass. The normal component of the relative velocity given by ' v_n^{rel} '. Where coefficient ' β ' is given below as a function of the restitution coefficient ' e '. The coefficient is explained in Section 3.2.

$$\beta = \frac{\ln e}{\sqrt{\ln^2 e + \pi^2}} \quad \text{Eq. 23.}$$

$$S_n = 2E^* \sqrt{R^*} \delta_n \quad \text{Eq. 24.}$$

The tangential force ' F_t ' depends on the tangential overlap ' δ_t ' and the tangential stiffness ' S_t '.

$$F_t = -S_t \delta_t \quad \text{Eq. 25.}$$

$$S_t = 8G^* \sqrt{R^* \delta_n} \quad \text{Eq. 26.}$$

Here is ' G^* ' the equivalent shear modulus.

The tangential damping force ' F_t^d ' is given by:

$$F_t^d = -2 \sqrt{\frac{5}{6}} \beta \sqrt{S_t m^*} v_t^{rel} \quad \text{Eq. 27.}$$

Where ' v_t^{rel} ' is the relative tangential velocity.

The tangential force is limited by Coulomb friction law:

$$F_t \leq \mu_s F_n \quad \text{Eq. 28.}$$

Where ' μ_s ' is the coefficient of static friction. This coefficient is explained in *Section 3.2*.

Rolling friction is accounted for by applying a torque ' τ_i ' to the contacting surfaces.

$$\tau_i = -\mu_r F_n R_i \omega_i \quad \text{Eq. 29.}$$

With ' μ_r ' the coefficient of rolling friction (explained in *Section 3.2*), ' R_i ' the distance of the contact point from the centre of mass and ' ω_i ' the angular velocity.

3.1.3 Calculation of new particle position

An important step in the DEM cycle is the calculation of new particle positions and orientations. These calculations use the net force and the net torque as calculated in the contact model and apply these in respectively Newton's second law of motion and Euler's equations of motion.

The new particle position is calculated using the translational motion of the particle. This means this is only the new position of the particle and does not take into account the rotation of the particle and thereby the orientation of the particle. The formulas used to calculate the new particle position are listed here below.

$$F_{net} = \sum F_i \quad \text{Eq. 30.}$$

$$F_{net} = m_i a_i \quad \text{Eq. 31.}$$

$$m_i \frac{dv_i}{dt} = (F_n + F_n^d) + m_i g \quad \text{Eq. 32.}$$

Where the net force ' F_{net} ' is the sum of all forces in any direction. The forces are the mass times the acceleration ' a '. Integration of the acceleration over a specified time step results in the new particle position.

The new particle orientation is calculated using the formulas below. These formulas take into account the angular velocity of the particles and the torque ' T ' applied to them. A similar integration as for the particle position, will result in the new particle orientation. The symbol ' I_i ' is the moment of inertia, which is the mass over the rotational radius.

$$T_{net} = \sum F_t R_i \quad \text{Eq. 33.}$$

$$I_i \frac{d\omega_i}{dt} = R_i (F_t + F_t^d) + T_i \quad \text{Eq. 34.}$$

3.1.4 Rayleigh time step

The time step is the amount of time between the iterations, in EDEM this time step is fixed throughout the simulation. Hence, a smaller time step will result in a longer calculation time, since this requires more iterations. On the other hand a time step set too large will result in inaccurate simulations, because particles gain too much energy as a result of excessive virtual overlap ' δ '.

In EDEM the time step is given in actual time and as a percentage of the Rayleigh time step. The Rayleigh time step is the time taken for a shear wave to propagate through a solid particle (DEM solutions, 2010). Rayleigh waves account for 67% of the solid collision energy in comparison with the dilational/P-wave (7%) and distortional/S-wave (26%). Hence, in simulations it is a good approximation to assume that all the energy is transferred by Rayleigh waves (Li, Xu and Thornton, 2005) and therefore is a good measure of the estimation of the calculation time.

Rayleigh's time step as given in DEM Solutions (2011) is displayed in the following equation.

$$T_R = \pi R \left(\frac{\rho}{G} \right)^{\frac{1}{2}} / (0.1631\nu + 0.8766) \quad \text{Eq. 35.}$$

The Rayleigh time step ' T_R ' is a function of the smallest available particle radius ' R ', the particle density ' ρ ' as well as the shear modulus ' G ' and Poisson's ratio ' ν ' of the material.

The calculation time is reduced when using: a larger particle radius, higher density, lower shear modulus or a lower Poisson's ratio. It is worth noting that often the shear modulus is most effective to adjust when the behaviour in the simulation allows it. This is tested in *Section 3.3.2.b*.

3.2 EDEM parameters

EDEM is a commercial discrete element modelling package developed by DEM Solutions. EDEM is designed for simulation and analysis of bulk particle handling. The package is operated by a graphical user interface, which follows the following steps:

Creator	Creating geometries, particles and defining the their properties and interaction
↓	
Simulator	Set the simulation settings and run the discrete element simulation
↓	
Analyst	The post-processor play back of the simulation and to extract requested results

EDEM Academic version 2.4 is used for the simulations in this report. The most important settings of the software package will be explained.

3.2.1 Creator

The creator is used to import the particles and the geometries into the simulation, with their specific materials and belonging physical properties.

Physics

The first step in the creator is defining the physics between the different elements in the simulation, in other words how the elements behave when they are in contact with each other. This is the ‘physics interaction’ between the particles themselves and between particles and the geometry. A contact model needs to be applied for each of these interactions. Several build-in contact models can be selected, where in this report the Hertz-Mindlin (no-slip) contact model is used for particle-particle and particle-geometry interactions. Furthermore, gravity is set in this step.

Materials

The second step is to define the materials and their properties. The following material properties need to be set (definitions according to DEM solutions, 2011):

- Poisson’s ratio ν ‘Ratio between transverse contraction strain to longitudinal extension strain in the direction of force’
- Shear modulus G ‘Ratio of shear stress to the shear strain’
- Density ρ Material density; mass per unit volume

Each of the previous mentioned ‘physics interaction contact models’ require several interaction coefficients, which are used in the calculations of the contact model. Interaction coefficients need to be set for each possible contact combination of the different materials; in this work there are rock-rock and rock-wall interactions. The following coefficients are requested in EDEM, with given definitions according to DEM solutions (2011):

- Coefficient of restitution μ_r ‘Ratio of the separation speed to the speed of approach in a collision between elements’
- Coefficient of static friction μ_s ‘When a body rolls on a surface, both the body and the surface can deform to oppose this rolling motion. This is represented as a torque applied to both bodies. This coefficient is a scalar to the amount of torque required to put an object into motion on a flat surface’
- Coefficient of restitution e ‘A scalar value used to determine how much force is required to put it to motion when it is at rest on another material’

Particles

A following step is to define the particle dimensions. Particles are created by clustering one or more spheres. Spheres in one cluster can overlap. The location and diameter of each sphere can be defined. The software package then calculates the volume and mass of the particle.

Model domain and geometric elements

A model domain and some geometrical elements need to be defined. The model domain is the area where the simulation takes place. Particles outside the domain are permanently removed from the simulation. The simulation performs calculations on the entire domain, therefore a larger domain will result in longer calculation time.

Periodic boundaries make it possible to define what happens to a particle when it leaves the domain. Periodic boundaries for a particular direction allow particles leaving the domain in that direction to re-enter instantly on the opposite side (Figure 42). “Thus, the natural three-dimensional packing, as opposed to the altered packing that would occur if a rigid boundary was used, and the particle population is preserved” (McBride and Powell, 2006).

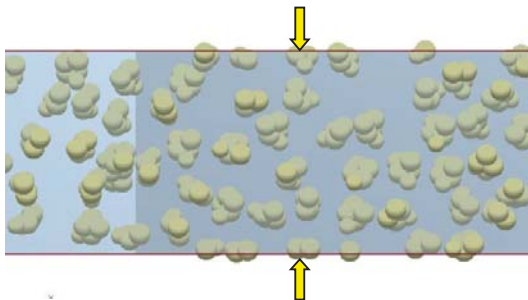


Figure 42: Top view of simulation to show periodic boundaries, yellow arrows show the same clustered particle

Geometric elements can be inserted in the domain and the particles will interact with these elements. Geometric elements of editable size in EDEM are a box, cylinder and a polygon. There is a possibility to apply dynamics to the elements. Further, a material needs to be assigned to these geometric elements when it is a physical element. Geometric shapes can also be assigned as virtual, so it does not interact with anything in the simulation. Virtual geometries are required to define particle factories.

Particle factories

The final step in the EDEM creator is to define where and how particles enter the domain of the simulation. This is done by means of so-called ‘particle factories’. This feature can turn a volume or surface into a particle creator, where predefined particles enter the simulation. Multiple factories can be used in a single simulation, which is done in this report to create distinct locations of particles.

There are two types of factories; static and dynamic. Static factories produce particles at a specified time and thereby enable the user to instantaneously fill a volume or produce a set amount of particles. Dynamic factories produce particles at a specified rate over time, where the production of particles may be limited in time or by total mass to stop production. This rate may be based either on mass or on the number of particles. The initial conditions define the starting conditions of the factories. The initial conditions contain the type and size of particles together with their distribution, position, velocity and orientation.

3.2.2 Simulator

The simulator in EDEM is the discrete element solver in the program, which runs the actual simulation. In the simulator, several parameters need to be set to run the simulation and to define how the data is saved. These parameters are discussed here below and all influence the simulation time. The simulator has a viewer that enables the user to view the simulation during the calculation process. Furthermore a solve report is generated automatically, which displays detailed information on the simulation.

Time step

In the EDEM simulator, one of the important parameters to be set is the time step. The time step is the amount of time between iterations and can be set as the actual time step in seconds or as a percentage of the Rayleigh time step. The Rayleigh time step is discussed in *Section 3.1.4*. The time step is important, since a small step will result in a long calculation time and a large step may result in ‘unnatural’ behaviour of the particles.

Data save

The interval of data saves can be set in this section. This defines how often the data is saved. A save interval set very small may result in a longer simulation time, when the memory write-out can not meet up with the amount of saves. A interval that is set very large may roughen the data since more iteration are included in one data save, this may cause jerky movement when replaying the simulation.

Simulation grid

The simulation domain is divided up in a grid in order to detect particle contacts. Grid cells without particles are excluded in the calculation to save calculation power and thus time. A smaller grid size in general decreases calculation time, since this reduces the number of particles per grid cells and thereby makes the calculations less complex.

3.2.3 Analyst

The result of the simulation is viewed in the EDEM analyst, where also the simulation data can be extracted. The viewing and data extraction aspects are briefly discussed below.

Viewer

The viewer allows the user to replay the simulation as an animation or to view each saved time step separately. The particles can be represented in different ways (e.g. default particles, vectors or stream) and thereby highlighting several particle attributes. Some of the particle attributes possible to display are: size, mass, location, velocity, forces, energies or contacts.

Further, the EDEM viewer gives the possibility to show/hide/colour specified particles or geometries and supports the creation of sections in the simulation. Movies and screen captures can be made at any time in the viewer.

Data extraction

In order to extract the data, a bin or selection needs to be made first. All particle properties inside a bin or selection can be extracted, using the build-in graphing tool or by exporting the data into a database file. All information that is saved at each time step can be extracted from the program.

3.3 Material calibration tests

The success of DEM simulations relies on correct setting of the particle properties and particle interactions. This is done by material calibration and is the first objective of this project. Material calibration is done by finding the particle parameters in EDEM to result in bulk behaviour that corresponds to reality. The parameters in EDEM are set correctly, when the bulk behaviour approaches reality closest. This calibration of the material properties in EDEM are shown in the top half of the following picture. The bottom half shows the Tepee simulations, which are discussed further in *Chapter 4*.

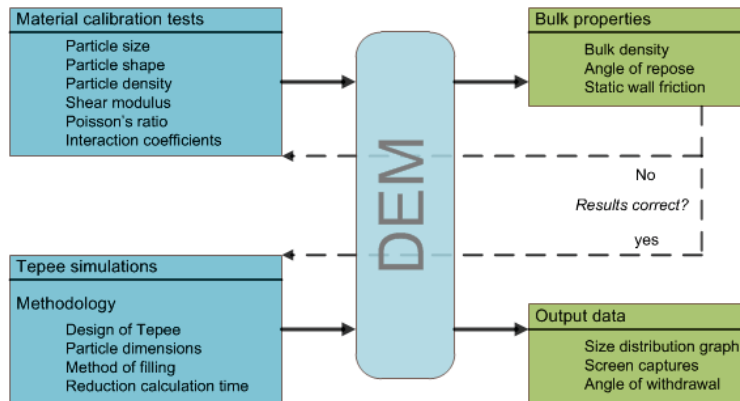


Figure 43: Calibration and simulation chart

Due to simplifications in DEM simulations, the individual particle properties as set in DEM may differ from reality. The EDEM program requires several parameters that are retrieved from the calibration tests, namely the material properties of the particles and interaction properties of the particles. The table below shows the calibration tests that are carried out and which parameters are researched in each test.

Table 4: Overview of calibration tests and the determined particle parameters

Calibration test	DEM parameter
Bulk density	Particle density
Angle of repose	Particle size/shape Particle build up Shear modulus Poisson's ratio Coefficient of restitution Coefficient of static friction Coefficient of rolling friction
Static wall friction	Coefficient of static friction Coefficient of rolling friction
	Particle-particle contact
	Particle-geometry contact

The bulk density test is used to set the particle density. The angle of repose tests is used to set most of the parameters in EDEM, since the angle of repose is used to determine the flowability of the bulk material this is a good simulation to set the parameters correctly. The static friction test is used as a secondary test to avoid abnormalities in the parameters as they are set by the angle of repose tests.

3.3.1 Bulk density

Simulations to test the bulk density are carried out first. Since the second law of Newton is based on the mass of the particles, the density is one of the essential parameters to be set properly.

Bulk density ' ρ_b ' is a relation of particle density ' ρ_s ' and density of the fluid ' ρ_f ' within the voids (Schulze, 2008).

$$\rho_b = (1 - \varepsilon) * \rho_s + \varepsilon * \rho_f \quad \text{Eq. 36.}$$

Since the voids in the bulk solid are expected to be filled with air, the last term can be neglected. Porosity ' ε ' is the ratio of the void volume to the total volume of the bulk solid.

$$\varepsilon = \frac{V_{voids}}{V} \quad \text{Eq. 37.}$$

Schulze (2008) states that a typical values for the porosity of a dry bulk solid ' ε ' is 0.4, when the particle shape does not deviate too much from a sphere. Given equation 36 above, this provides an estimate for the bulk density of 60% of the particle density ' ρ_s '.

Tara Mines has carried out several experiments to measure the particle density (which is the in-situ density of ore). The ore density in this work is taken from the 'Pale Beds' ore, since 97% of the ore mined is 'Pale Beds' ore (details in *Appendix B*). The particle density ' ρ_s ' of these pale beds ores at Tara Mines is measured at 2750 kg/m³ (Pentony, 1991 *unpublished*).

The simulation in EDEM to measure bulk density is a straightforward simulation. A box is loosely filled with particles. To avoid wall effects a smaller virtual bin is created inside this box. The mass of the particles inside the box is extracted from EDEM. This bulk mass and the known dimensions of the bin provided the bulk density of the material; results are shown in Figure 44 and will be discussed.

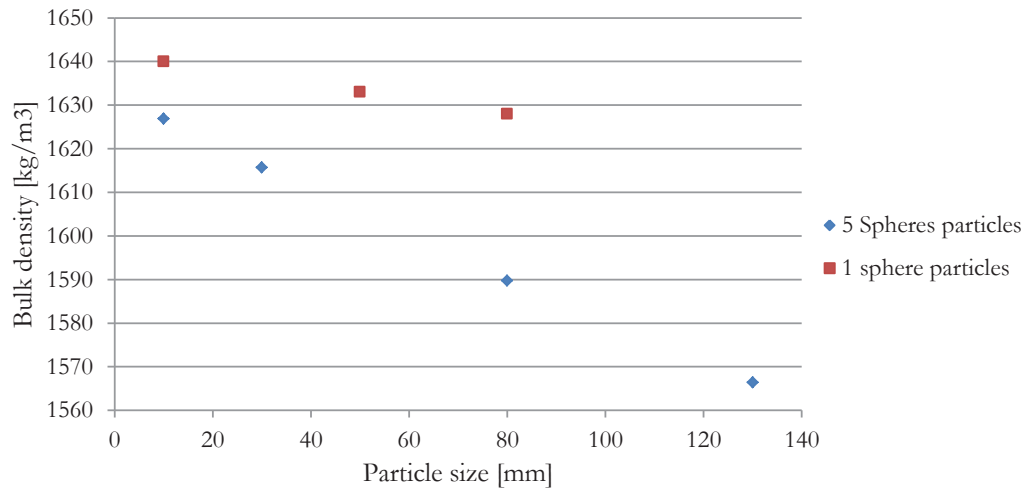


Figure 44: Calibration test; bulk density over particle size

The bulk density of a single sphere particle is around 1640 kg/m³. This is consistent with the theoretical estimate from Schulze on the data from Tara Mines; which results in 1650 kg/m³ (which is 60% of the particle density). The bulk density is reduced slightly (1%) for particles consisting of multiple spheres and particles with a larger diameter.

In the software package EDEM, spheres can be clustered to create irregular shaped particles. The simulations in this report use clusters of five spheres, which is discussed in *Section 3.3.2.a*. The bulk density of the 5 sphere cluster particles show a slight reduction in bulk density for the same size. The irregular shape of the clustered particles creates larger open voids in the volume and thereby reduces the bulk density.

Another phenomenon that can be seen is a lower bulk density for particles with a larger diameter. This effect is not explained by the theoretical estimated bulk density of 60% of the particle density for spherical particles, since for single sphere particles this still equals a spherical shape. The reason may be found in the measuring method of the mass. Particles on the boundary of the measuring bin are only taken into account when their mass centroid is inside this virtual bin.

These simulation show that the difference between the theoretical estimate and the modelled bulk density is very small (1%). Therefore it is concluded that a particle density of 2750 kg/m^3 is a good approximation of reality.

3.3.2 Angle of repose

In the following simulations, the angle of repose was measured for varying material parameters in EDEM. Free-flowing particles were dropped from a height to form an unconfined pile. The angle this pile makes with the horizontal surface was measured. In each simulation, this angle of repose is an average of four repose angles; on both sides of the pile in x and y direction.

Appendix B mentions a measured angle of repose at Tara Mines of 37 degrees. This angle is used to calibrate the EDEM particle properties.

3.3.2.a Particle shape

The first angle of repose simulations are carried out to study the influence of particle shape. EDEM has the ability not only to simulate with spherical particles, but also to incorporate shape. Any number of spherical particles can be used to cluster to form any desired shape. By clustering the spheres, the particles get an irregular shape, which influences the particle behaviour. Purely based on its shape, an angular particle will roll less easy than a perfectly spherical one.

In these simulations, the influence of the number of spheres in a cluster is compared to the angle of repose. An overview of the particles used is given in Figure 45, where each single sphere has a diameter of 50mm.

A single sphere is obviously perfectly spherical and therefore rolls freely in all directions. The shape of a sphere does not give the particle any natural roll friction. All roll friction therefore should be added artificially by the coefficient of rolling friction.

A cluster consisting of two spheres will always be shaped as a roll. The two spheres are always aligned with their centres on a virtual axis. This gives the cluster a more irregular shape, but leaves the possibility to roll round this virtual axis.

Creating a cluster out of three spheres will form either a roll/snake shape or a triangular shape. The triangular shape brings an advantage since the virtual rolling axis is not present. However, a triangular shape has all the spheres placed on a virtual plane. This will limit the potential to roll freely, but a sliding potential remains along this virtual plane.

These effects will be reduced substantially when particles are built up from four or more spheres. The effect of the particle build up by number of spheres is displayed in Figure 46. The impact of the number of spheres is represented by the angle of repose. Parameter settings in EDEM (density, Poisson's ratio and interaction coefficients) are constant in each simulation. The sphere diameters are equal in all simulations, which means that particles consisting of a cluster will have a larger size than of a single sphere particle.

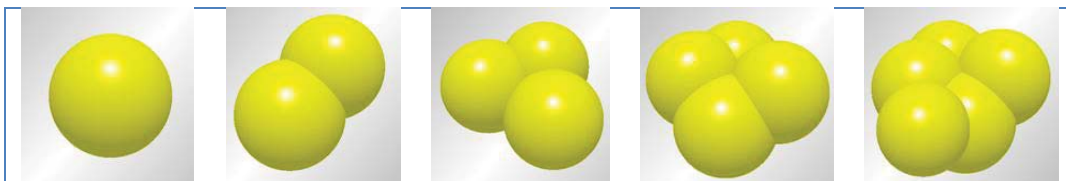


Figure 45: Particles created from a cluster of 1 to 5 spheres

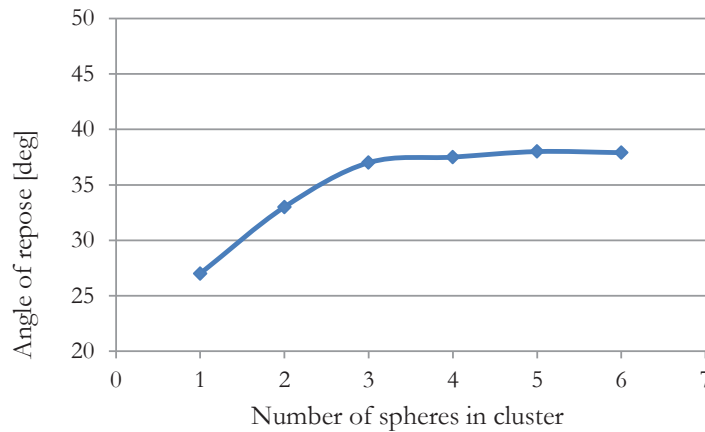


Figure 46: Calibration test; angle of repose for the number of spheres per cluster

As discussed before, the angle of repose is depended on the number of spheres in a particle cluster. Figure 46 shows that a pile of single spherical particles results in a low angle of repose of 27 degrees, which is caused by the missing of ‘natural’ rolling friction by the shape of the particle. The angle of repose increases for each extra sphere in a cluster. This increase levels out after 4 to 5 spheres in one cluster to around 37 degrees.

It should be mentioned that a cluster could be build up in different ways with the same number of particles. This will influence the angle of repose. The particle build-ups in these simulations were chosen such that the irregularity increases when more particles are used in a cluster. Also the size of a particle increases with each additional sphere in a cluster.

A good approximation of a 37 degree angle of repose is achieved when using a particle build up from 5 spheres. Using more spheres will increase calculation time, without improving the accuracy of the repose angle substantially. Clusters with four or less spheres will increase the uncertainty of achieving a 37 degree angle of repose.

3.3.2.b Shear modulus and Poisson's ratio

The material properties calibrated in this section are the shear modulus and Poisson's ratio. Shear modulus ' G ' is ratio of shear stress to the shear strain and is one of the measures of the stiffness of a material. The shear modulus is a relation between the Young's modulus ' E ' and Poisson's ratio ' ν '.

$$G = \frac{E}{2(1 + \nu)} \quad \text{Eq. 38.}$$

In geotechnical reports from Tara Mines (Pentony, 1991 *Unpublished*) and (Helsinki University of Technology, 1997 *Unpublished*), the Young's modulus is measured at 55 MPa and an average Poisson's ratio of 0.20. This gives a shear modulus of 23 GPa.

The shear modulus has a large impact on the calculation time as mentioned in *Section 3.1.4*. Therefore, it is desirable to set the shear modulus on a low value where the bulk characteristics of the material still behave naturally.

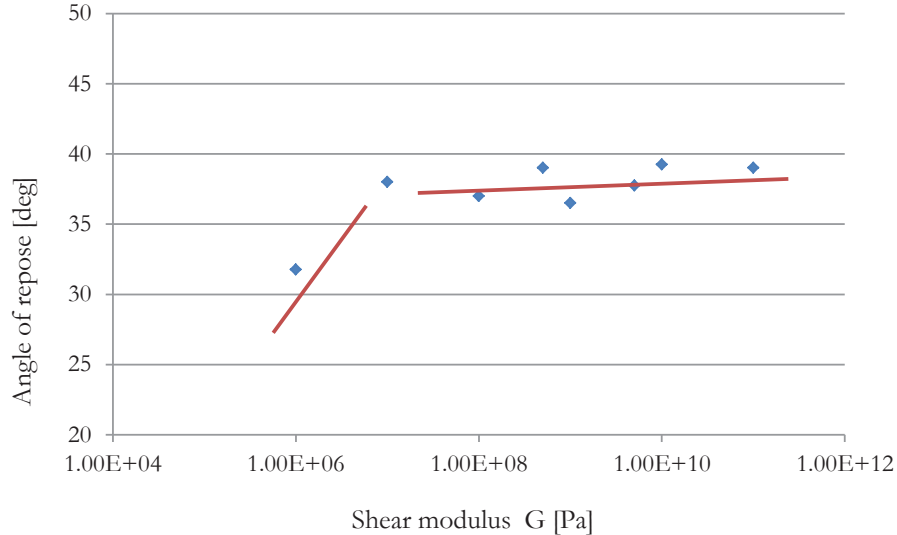


Figure 47: Simulation test; angle of repose over the shear modulus with sketched asymptote trend lines (red)

The results in Figure 47 shows two asymptotes; a 37 degree repose angle asymptote for high shear moduli and a steep dropping asymptote for shear moduli lower than 10^7 Pa.

The shear modulus measured at Tara Mines is $2.3E+10$ Pa. Figure 47 show that this value can be set at a lower value in EDEM to save calculation time, since it is not changing the resulting angle of repose significantly. A low shear modulus that results in a 37 degree angle of repose is found at 10^8 Pa. This value remains on the 37 degree asymptote and is not close to the steeply dropping asymptote for low shear moduli.

Similar tests are carried out to calibrate the Poisson's ratio. The ratio is measured at Tara Mines at an average of $\nu = 0.2$.

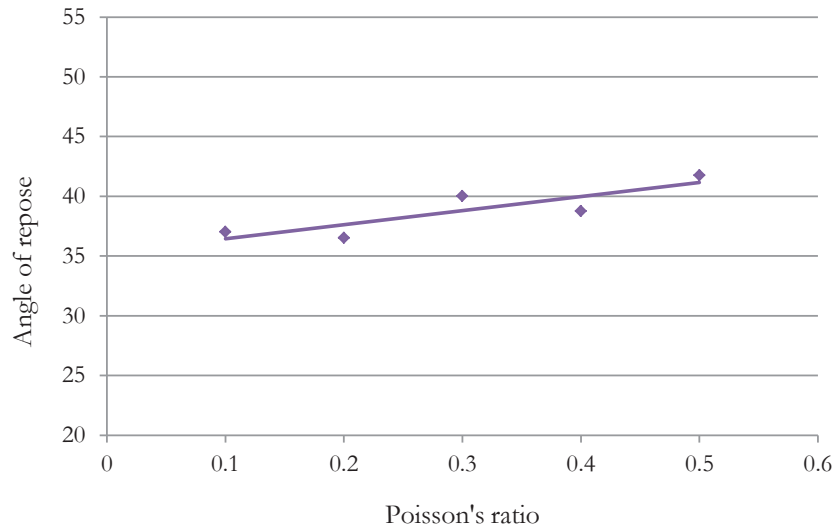


Figure 48: Calibration test; angle of repose over Poisson's ratio with a linear trend line

The angle of repose appears to increase linearly when increasing Poisson's ratio from 0.1 to 0.5. The best suitable value for EDEM is therefore chosen on this linear line; resulting in a Poisson's ratio of 0.25 to acquire a repose angle of 37 degrees. This is a low risk value since this avoids significant variations caused by measuring errors.

3.3.2.c Particle interaction coefficients

The interaction of two surfaces colliding is defined by three parameters; coefficient of restitution, static friction coefficient and the rolling friction coefficient. Calibration of these parameters is carried out by simulation similar to the ones for Poisson's ratio and shear modulus; by the formation of a pile using free flowing material and measurement of the repose angle.

The coefficient of restitution ' e ' is the ratio of speed in separation to the speed of approach in a collision between two elements. This is explained in *Section 3.2.1*.

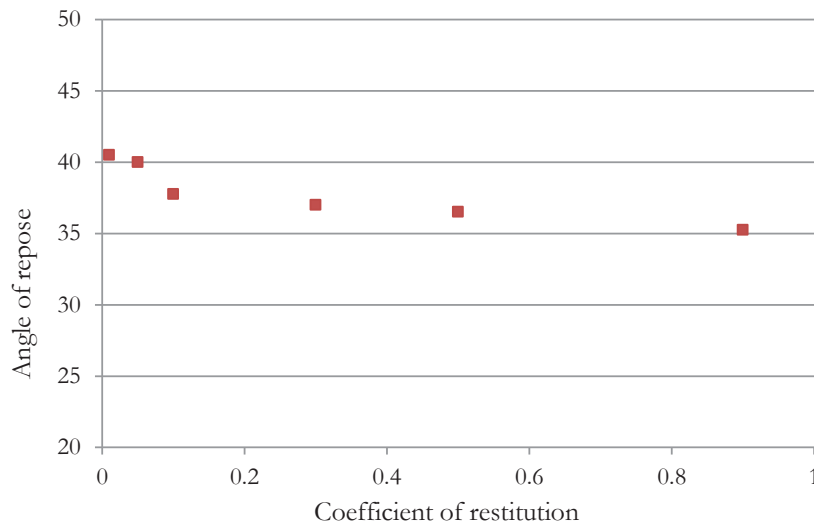


Figure 49: Calibration test; angle of repose over coefficient of restitution

A coefficient of restitution very close to zero results in the highest angle of repose, which is due to the extreme low velocity after collision. Hence, the particle has very low velocity and therefore forms a steeper angle during deposition.

Next to the very low coefficients of restitution, the angle of repose is not significantly influenced by variations in the restitution coefficient. The EDEM restitution coefficient is set at a stable value of $e=0.3$, to minimise the risk of unexpected errors.

Coefficients of static and rolling friction influence each other and have a significant impact on the angle of repose. Hence, these coefficients are varied in relation to each other. In the following simulation, the rolling friction coefficient is set at 0.05, 0.1 and 0.15 for static friction coefficients of 0.2, 0.4 and 0.6.

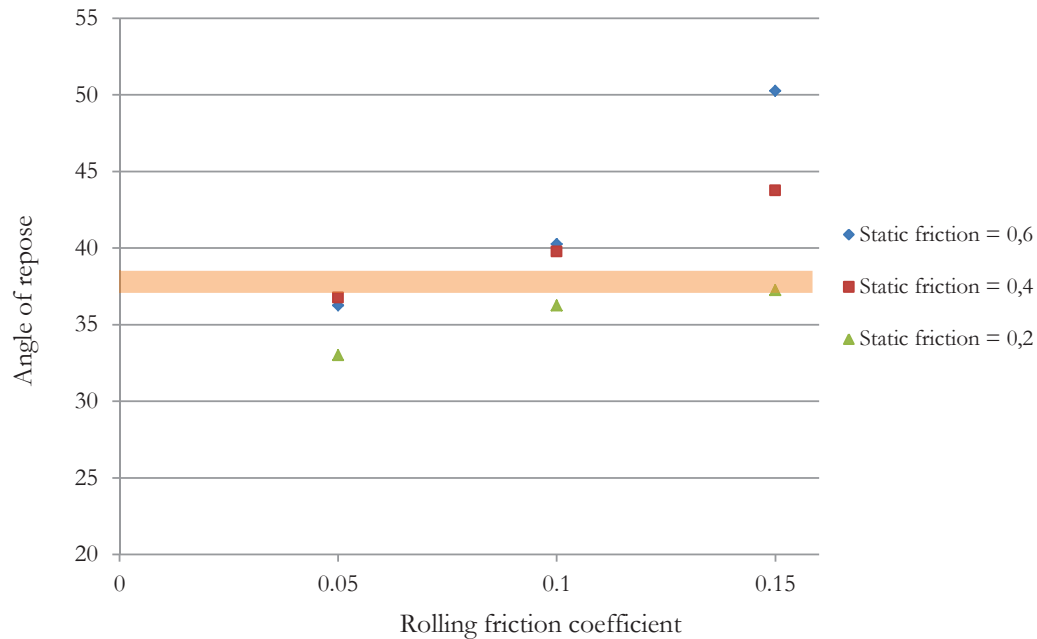


Figure 50: Calibration test; angle of repose over rolling and static friction coefficient, with required 37 degree bar

Figure 50 shows that a higher rolling friction coefficient causes a wider spread for variations in the static friction coefficient, than for lower rolling friction coefficients. This also be caused by a numerical spread and measuring deviations, however due to this the coefficient of rolling friction is set at $\mu_r = 0.1$, which is also a better approach of the 37 degree repose angle. The coefficient of static friction is set such that the resulting angle of repose is 37 degrees for the rolling friction coefficient of 0.1; this is achieved at a static friction coefficient of $\mu_s = 0.25$.

3.3.3 Repeatability test

In the previous simulations, the EDEM parameters were determined. To assess the accuracy of these calibrated values a repeatability test was carried out. The repeatability test was done by running a simulation with the determined parameters several times and measuring the angles of repose in an identical way as before. This results in a spread of the resulting angles of repose and this determines the measuring error.

The repeatability test consists of ten identical simulations where the parameters are set equal. These parameters are retrieved from previous calibration tests and are summarised in Table 5.

Table 5: Overview of the calibrated parameters

Parameter	Value	Unit
Density	2750	kg/m ³
Particle build-up	5	Spheres
Shear modulus	10 ⁸	Pa
Poisson's ratio	0.25	-
Coefficient of restitution	0.3	-
Coefficient of rolling friction	0.1	-
Coefficient of static friction	0.25	-

Simulations in EDEM are carried out ten times with these values. Similar to the calibration tests, the angle of repose was measured four times in each simulation; both sides of the formed pile in x-direction and both sides in y-direction. This results in 40 measurements for the angle of repose in 10 simulations.

Table 6: Results of repeatability test with the calibrated parameters

		10 simulations (average of 4 measurements)	40 measurements
Minimum angle of repose	[deg]	34.75	31
Maximum angle of repose	[deg]	39	43
Mean angle of repose	[deg]	37.2	37.2
Standard deviation	[deg]	1.31	3.10

From these results (Table 6), it can be seen that individual measurements have a standard deviation of 3.10 degrees. This means that a single angle of repose measurement might not be representative for the entire simulation. The standard deviation per simulation (an average of four measurements) is logically lower than for single measurements. The standard deviation per simulation is 1.31, which is significantly lower.

The angle of repose simulations in the calibration tests are also based on an average of four angle measurements per simulations. The deviation in these measurements therefore is in the order of 1-1.5 degrees. This is an acceptable variation, since the selection of parameter settings is based on low risk values.

3.3.4 Static wall friction

The static wall friction is based on particles sliding down an incline. The inclination of the plate where the particles start sliding is a measure for the friction between the particle and the surface of the plate, which is discussed before in *Section 2.3.5*.

$$\mu_s = \tan \varphi_x \quad \text{Eq. 39.}$$

The angle of the inclined plate ' φ_x ' is not exactly equal to the angle of repose since the angle of repose is tested as the angle of a pile formed by bulk material. The angle of the inclined plate will be smaller, since the plate is a smooth and flat plate and thereby lacks the roughness of a particle surface.

This test is mainly carried out to detect any unexpected and unrealistic behaviour of the bulk material. The settings for this simulation are set the same as for the repeatability test, see Table 6. The wall friction simulation uses a smooth and flat plate, which consists of the same properties as the ore particles. Also the interaction properties for particle-wall are set similar as for particle-particle.

The simulation starts with placing 25 particles on a horizontal plate. When the particles are disposed properly, the angle of the plate to the horizontal is slowly increased (with $\frac{1}{2}$ degree extra inclination per second). When the particles start moving the simulation is stopped and the angle of the plate is measured. This static wall friction angle ' φ_x ' is related to the static friction between the wall and the particle, as in Equation 39.

The result of this simulation is that particles start to slide and roll when the inclination of the plate is above 23 degrees. Table 7 shows this result compared to other theoretical wall friction values taken from literature.

Table 7: Static wall friction angle; literature and modelled

Static wall friction angle [deg]		Source
22-26	Limestone on concrete	Gilbert Gedeon, 1994
23	Granite	Elert, 2005
23		EDEM

The measured inclination of 23 degrees in EDEM seems to be an appropriate value compared to the other literature values.

4 Simulation setup and methodology

Figure 51 shows the same simulation chart as shown before in *Chapter 3*. The cycle in the top boxes were established in the calibration tests in *Section 3.3*. The calibrated parameters are used in the Tepee simulation. This chapter will discuss the bottom half of the chart: the Tepee simulations and the output data.

The first part of this chapter describes the methodology (or the logic) behind the decision made in the modelling (the ‘Tepee simulations’ box in Figure 51). Modelling is always an approach of reality, where simplification of the system is required to some extent. It is discussed how reality is approached and which simplification measures were taken. The second part of this chapter provides an experimental plan and summarises the simulation settings. The final part of this chapter explains the way the results are displayed in this report (the ‘output data’ box in Figure 51).

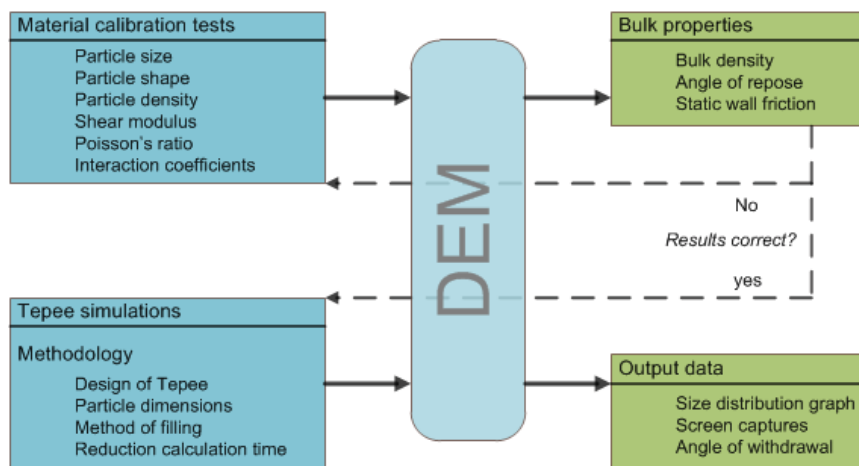


Figure 51: Calibration and simulation chart

4.1 Simulation methodology

This section describes the simplifications and measures taken to simulate the material flow in the Tepee stockpile.

First, simplifications were made by reducing the Tepee dimensions in the computational model. Secondly, the full size distribution was reduced to three particle sizes. Subsequently, two methods of filling were distinguished in order to review their impact on the size distribution. Finally, measures are discussed that were taken to reduce the calculation time.

4.1.1 Design of the Tepee stockpile

The coarse ore surface stockpile Tepee functions as a storage buffer between the mine and the AG mill. A schematic overview of the Tepee design is shown in Figure 52. The design of the Tepee can be seen as two conical shapes. The bottom cone is dug into the overburden with its top down so it forms one large conical funnel. The second cone points upwards and forms a metal roof over the formed conical heap of material. A more detailed description of the Tepee is given in *Appendix B*.

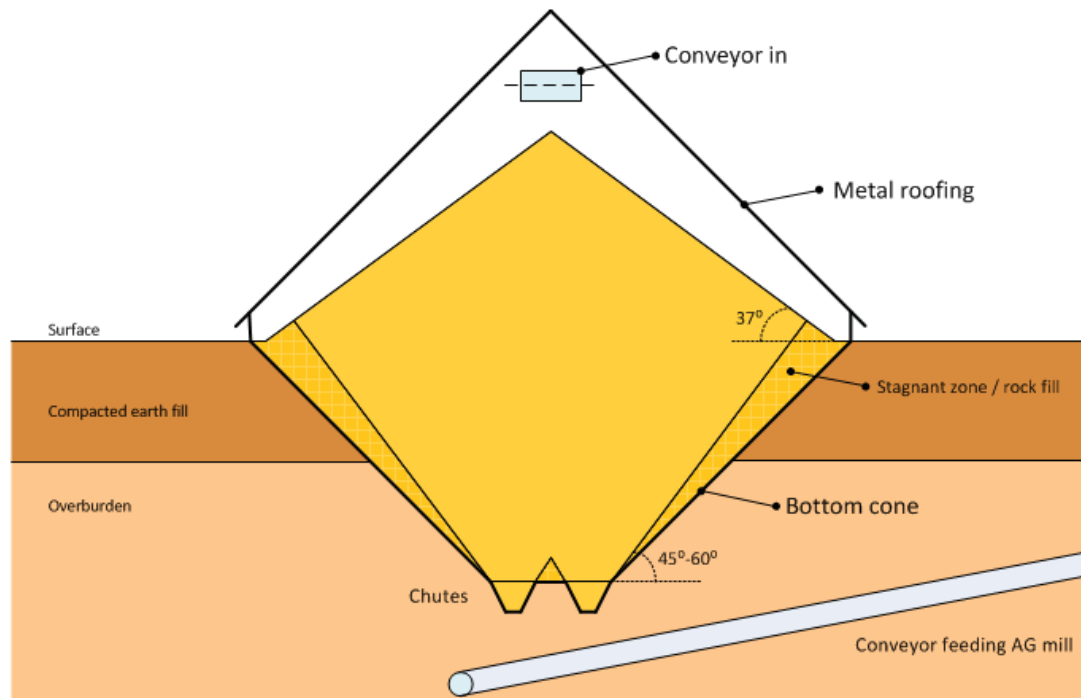


Figure 52: Schematic layout of the Tepee (not to scale)

Feeding of the Tepee is done by a conveyor reaching to the top of the roofing and centred on the axis of the cones. Underneath the Tepee, four chutes, feeders and a conveyor system have been constructed, which are used to extract the ore from the stockpile and feed the mill.

The roofing is not in contact with the ore and is only used as dust prevention. The only walls that are in contact with ore are the walls of the bottom cone. These walls are constructed of compacted earth fill and dug into overburden material. At a 45 degree angle this is covered with the stagnant zone / rock fill. Depending on the fill level of the Tepee, the angle may increase to 60 degrees depending on the amount of stagnant rock fill. The constructed wall material therefore is rock and its properties are comparable to the ore properties.

In order to reduce the calculation time, the size of the Tepee was scaled down in the model. The main Tepee design parameters are listed in the table below.

Table 8: Tepee dimensions at Tara Mines and in the DEM model

	Tepee at Tara Mines	3D DEM model	DEM slice model
Capacity [t]	30,000	170	15-16
Diameter [m]	45	7.5	7.5 (0.8m slice width)
Wall angle [deg]	45-60	45 or 60	45 or 60
Outlet size [m]	4.5	1.3	1.3 or 0.8 or 0.5
<i>Outlet size / maximum particle diameter</i>	<i>35</i>	<i>10</i>	<i>10 or 6.2 or 3.8</i>

In order to maintain similar flow behaviour, the volume of the model was reduced and the wall inclination was kept similar to the Tepee. A major reduction in the capacity of the DEM model is achieved by reducing the diameter and height of the modelled stockpile. The outlet size (diameter) is also substantially reduced to either 1.3, 0.8 or 0.5 meters, depending on the simulation. The outlet size varies in some simulations, since this is a measure to control the output rate.

In *Section 2.4.4* it was noted that in order to prevent ratholing and arching, the outlet size of a conical hopper should be 6-10 times the maximum particle diameter and for a wedge-shaped 3-7 times. The maximum particle diameter is 130mm. The 3D DEM model is conical and thus well within the limits, since the outlet size is 10 times the particle diameter. The DEM slice is wedge-shaped and the outlet size of 1.3 and 0.8m fall well within the limits (10 and 6.2 times the particle diameter). The outlet size of 0.5m is 3.8 times the particle diameter and just within required region.

In Figure 53 the boundary of the system is shown by the red box in a simulation example. The system domain starts with the input of ore, whereby the conveyor itself is not included. The input is simulated by means of a factory plate, which gives control of the amount and the kind of particles entering the system. The walls of the bottom cone are included, since these influence the wall friction and thus the flow of bulk material. The covering roof is not included, since the roof has no influence on the flow of ore in the stockpile. At the bottom, there are restrictions to the geometry, since the chutes, feeders and conveyor are not included. The opening itself is included and in some simulation the impact of multiple outlets is tested, by installing a splitter plate. The system domain ends right after discharging the material. The chutes and feeders are not taken into account since this makes the modelling more complex in this stage of simulating. Another reason not to include the chutes and feeders is that a minor influence is the discharge system is expected. The chutes are expected to result in ‘expanded flow’ (Figure 54). Expanded flow is a ‘hybrid’ flow pattern and develops when a mass flow hopper is placed below a funnel flow system (Jenike & Johanson, 2010). The chutes are not included in the simulation, since the expected funnel flow is maintained in the stockpile itself.

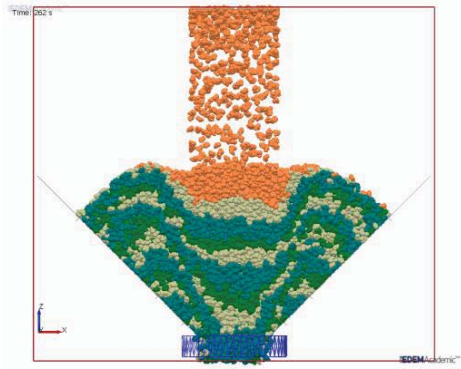


Figure 53: Tepee design in EDEM and system boundaries (red box)

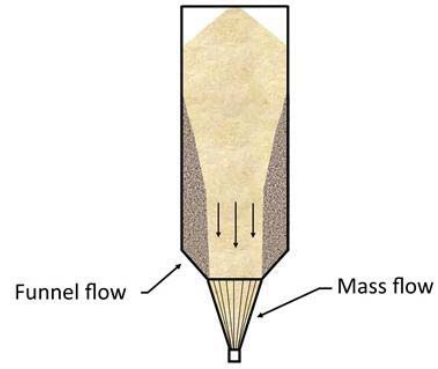


Figure 54: Extended flow; core and mass flow (Jenike & Johanson, 2010)

4.1.2 Particle dimensions

Tara Mines fills the Tepee with the run-of-mine ore, which is a full distribution of ore particles sized from dust to large lumps. A typical cumulative particle size distribution at Tara Mines is displayed in Figure 55. The modelling in this study simplifies this size distribution to three sizes, named: fines, pebbles and coarse.

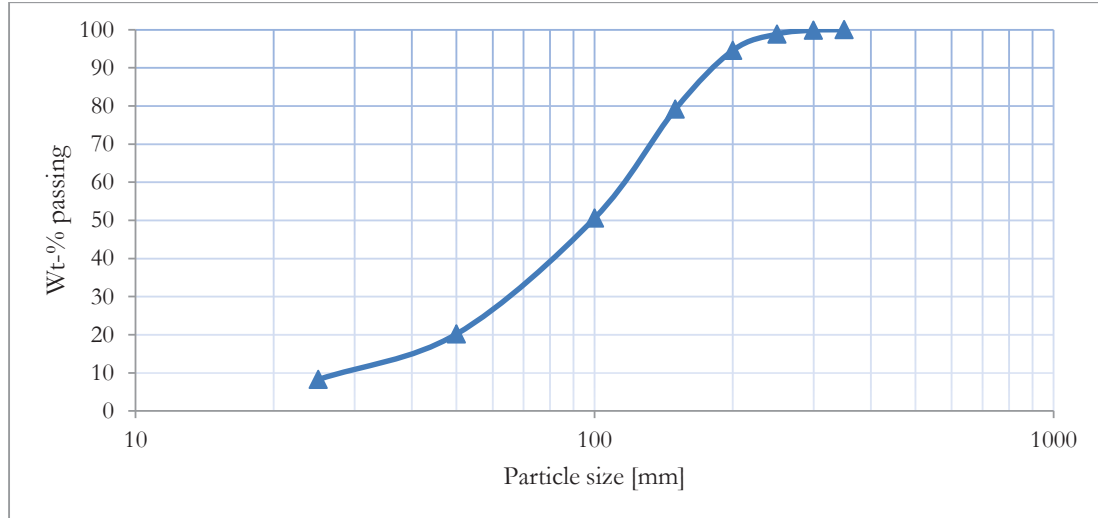


Figure 55: Typical cumulative size distribution curve of the run-of-mine ore at Tara Mines

Based on the requirements of the AG mill (as mentioned in *Section 2.1.2*), simplifications are made to the particle size and the distribution. The AG mill requires a specified fraction of coarse material and this is included in the DEM particle sizes and fractions of sizes in an ideal mix. The DEM particle size and the ideal distribution are given in Table 9. The simplified DEM model particles represent this distribution at Tara Mines.

Table 9: Simplification in fraction and size of particles at Tara Mines and in the DEM model

	Actual Tara Mines		Simplified DEM model	
	Size [mm]	Mill requirement	Size [mm]	Fraction in ideal mix
Fines	<50	none	30	25%
Pebbles	50-100	As low as possible, ≤ 50%	80	50%
Coarse	>100	P70 or 30% >100mm P80 or 20% >130mm	130	25%

This simplification in particle size is an approximation of the actual size distribution at Tara Mines. The mill roughly requires that the fractions of fines, pebbles and coarse particles are proportioned to each other as: 1:2:1. In DEM modelling there are two reasons to simplify the full distribution into three size fractions (fines, pebbles and coarse):

- Reduction of calculation time
- Distinct division in three particle sizes to observe mixing and segregation effects

First, this simplification to these three size fractions, reduces the calculation time significantly by saving a large amount of calculation time for the smallest dust-size particles. The smallest particles take more calculation power, since more particles are needed for the same mass.

Secondly and most important for this work is the division in three distinct particles sizes. The three distinct particle sizes make it easier to observe the influence of blending and segregation

than for full size distributions with a surplus in one size. The effects of particle size are exaggerated by this means, making the effects more clear. Additionally, there is a practical reason; these three sizes are easier to model in the software package. Due to the distinct sizes, the particles have a separate identity, which makes it easy to extract data (e.g. amount, weight, velocity) for one particular category (e.g. pebbles).

Table 10 shows a summary of the particle properties as used in the simulations. The influence of the size and shape of the particle is described in *Section 2.2.1*. The particle properties listed in the table below are particles built in a cluster of 5 spheres. The volume and mass are calculated by the program using a particle density of 2750 kg/m³.

Table 10: DEM particle properties: size, sphericity, roundness, volume and mass

	Size [mm]	Sphericity*	Roundness*	Volume [m ³]	Mass [kg]
Fines	30	0.5	0.4	1,4e-05	0,039312
Pebbles	80	0.5	0.4	0,000223	0,614104
Coarse	130	0.5	0.4	0,000914	2,5141

* Using Figure 15 in *Section 2.2.1.c*

The particle shape is given by the sphericity and the roundness. These parameters are first retrieved from photographs of the rock, where representative particles were chosen. Hereafter, the spheres in EDEM are clustered such that the sphericity and roundness are similar to particles in the photographs.

4.1.3 Filling of the Tepee

The Tepee is a gravity reclaim stockpile, this means that gravity controls the discharge at the bottom. Minor adjustments to control the discharge size can be made using combinations of the four chutes at the bottom. A more important control measure is the way the particles become located in the Tepee, due to the way of filling. Two observations on the filling of the Tepee are seen and discussed below; different filling method and segregation at the incoming belt at the Tepee.

4.1.3.a Different filling methods

At Tara Mines, two different filling methods are distinguished; ‘mixed filling’ and ‘batch filling’. Firstly, mixed filling means that a blend of particles enters the Tepee. In the simulations, this blend suits the requirement of the AG mill by having a large amount of coarse material. Secondly, batch filling means that batches of different sized material follow each other up while feeding into the Tepee. This results in a layering of these batches, where every batch has its own surplus of certain sized particles. These two reasons for these filling methods are discussed here.

Firstly, two different mining cycles are used for development and production mining. These two mining cycles are discussed in more detail in *Appendix B*. The size distribution of ore mined in development mining contains more fines, than the ore mined in production mining. Production mining in general produces the major part of the coarse material.

In a case that bulk material from one mining method is hauled to surface without intermediate blending, this results in one layer of ‘batch filling’. This batch is followed by another batch with differently sized material, which creates a repetition of layers in the stockpile, with large batches in the range of hundreds of tonnes.

When the material from both mining methods is intermediately blended within the ore handling system, this results in a blend and therefore ‘mixed filling’ applies in the Tepee.

Secondly, an observation at Tara Mines shows that there is segregation at the hoisting system. Underground, two skips are filled from the underground ore bin (COB). It is noticed that one of these skips is fed with a smaller sized ore particles than the other one, which is described in *Appendix B*. With their arrival on surface, both skips feed the same conveyor belt one after another.

Due to the size of a skip (14 tonnes), this has a smaller effect on the filling method than the previously mentioned difference in production and development ore. However, this effect can be seen as either a blending mechanism (mix filling) or a reason for batch filling, depending on the material. It is a blending stage, when skips are seen as an alternation between finer and coarse batches. It is a batch filling process, since this creates alternating layers in the Tepee of fine or coarse material. The two filling methods and the reason for occurring are summarized in Table 11.

Table 11: Reasons for filling methods

Filling method	Reason for the filling method
‘Mixed filling’	The product fed into the Tepee is perfectly blended. <ul style="list-style-type: none"> • A perfect size distribution is mined • Blending is achieved at a previous ore handling stage
‘Batch filling’	The product fed into the Tepee is a sequence of batches of fines, pebbles, coarse. <ul style="list-style-type: none"> • Periodically the mine extracts with surplus of a certain size (production or development ore) • Batch feeding into the Tepee due to segregation at hoisting

The method of filling the stockpile will influence the output of the stockpile, since there are not much output and flow controls. Both methods of filling are schematically displayed in Figure 56 and Figure 57.

Mix filling is subjected to heap segregation as mentioned in *Section 2.5.1* and shown in Figure 58. This segregation causes larger particles to roll to the walls of the Tepee, where fines remain in the centre of the stockpile.

By means of batch filling on the other hand, the material enters the Tepee in batches of different size distribution and thereby creating layers of finer and coarser particles.

The resulting fill in the Tepee is schematically displayed in Figure 59 and Figure 60.

Mix filling

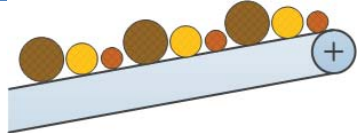


Figure 56: Mix filling conveyor

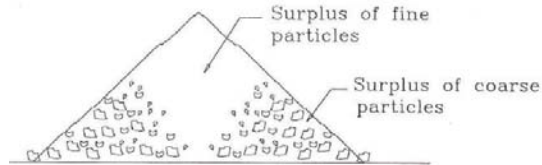


Figure 58: Heap segregation (Enstad and Mosby, 1998)

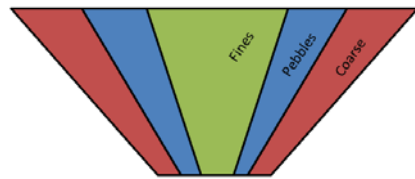


Figure 59: Tepee filled with mixed filling method

Batch filling

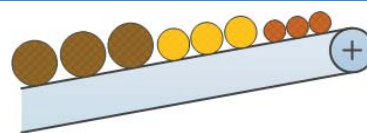


Figure 57: Batch filling conveyor

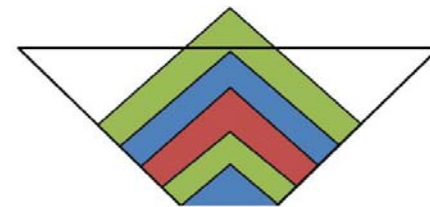


Figure 60: Tepee filled with batch filling method

In order to investigate the behaviour of the different sizes, a very strict boundary is set between the fines, pebbles and coarse particles. For example, areas with a surplus of fines are modelled with only fine particles and areas with a surplus of coarse are modelled using only coarse sized particles. This is not in accordance with reality in a stockpile, but gives the possibility to have a better look on the behaviour of the different filling methods in the stockpile and is easier to model in the EDEM software package.

A summary of the resulting filling in the Tepee is given for both filling methods in Table 12.

Table 12: Results of the filling methods

Filling method	Resulting filling in the Tepee
'Mixed filling'	Due to heap segregation there is a: <ul style="list-style-type: none"> • Surplus of coarse particles near the walls of the Tepee • Surplus of fines located in the centre above the Tepee outlet
'Batch filling'	Is dependent on the incoming batches, layers are formed in the Tepee containing a surplus of fines, pebbles or coarse material

The ratios between the sizes are based on the mill requirements for both filling methods. The ratio of fines/pebbles/coarse is set to 1:2:1. This results in the following tonnages in a slice simulation.

- For the mixed filling mode, the total weight is 16 tonnes, therefore the total weight of the fines area is 4 tonnes, the pebbles area is 8 tonnes and the coarse area is 4 tonnes.
- For the batch filling mode three cycle of fines, pebbles and coarse layering are made. The weight of a single layer of pebbles is 2.5 tonnes, where a single layer of both coarse and fines contains 1,25 tonnes. This gives a total of 15 tonnes filling in the model.

4.1.3.b Segregation due to filling

Investigation of the Tepee stockpile has shown that there are different size regions in the pile. This is also mentioned in *Appendix B*. Trajectory segregation on the belt and the discharge of the belt into the Tepee, result in different allocation of fines and coarse material.

There are two different segregation methods responsible for this segregated discharge. The first is percolation segregation (*Section 2.5.2*, Figure 34); due to the vibration of a conveyor belt, coarse material moves on top of the smaller fraction. The vibrations create open voids, which are filled up with finer material and leaving the coarse material on top. Particles lying on top of the belt tend to be discharge further away from the belt. The second segregation method is trajectory segregation (*Section 2.5.3*, Figure 35). Higher mass and relative less air resistance discharges the larger particles further away from the conveyor belt.

Coarse material is discharged further away from the belt head pulley than the fine material. This effect is independent of the filling method, since even a batch of fines contains some coarse material. It is observed at Tara Mines (*Appendix B*) that this causes areas with more fines and areas with more coarse particles in the Tepee. A schematic top view picture shows these areas in Figure 61. This segregation caused by filling is modelled as an asymmetric filling of the Tepee (*Section 5.4.2*, Simulation G).

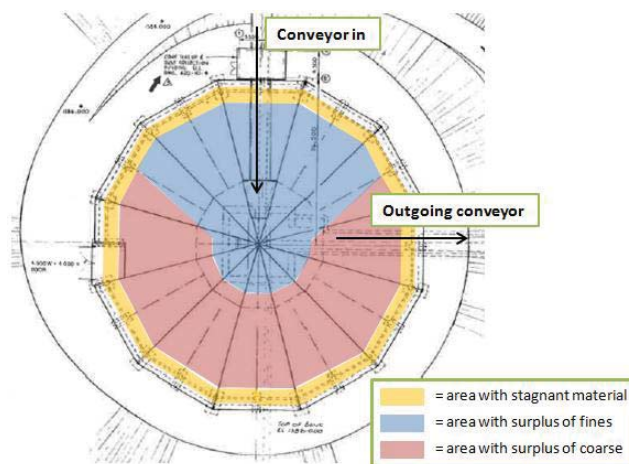


Figure 61: Schematic top view of observed areas with fines and coarse in the Tepee

4.1.4 Reduction of calculation time

Reducing the calculation time is needed to keep the time required for a simulation within workable limits. The idea behind most of the measures to reduce calculation time is to lower the number of spheres in the simulation models. The number of spheres is directly related to the number of particles, therefore a reduction in the number of particles is beneficial for a shorter calculation time. The measures taken to reduce the calculation time are listed below.

- 1. Reduction of the Tepee size**

In DEM modelling a major step to reduce calculation time is to increase the size of the particles in respect to the geometries. This means fewer particles are needed and thereby calculation time is reduced. In order to maintain the right bulk behaviour the decision is made to approach the particle size as close as possible to reality and not to increase particle size. Therefore, the geometry is scaled down.

- 2. Model only a 3D slice of the full 3D stockpile**

A major reduction in calculation time is achieved when a 3D slice of the stockpile is modelled instead of the full 3D conical stockpile. A 3D slice reduces the size of the system to be modelled and thereby reduces the number of particles in the simulation. *Section 5.2.1* studies the applicability of a 3D slice to represent a full 3D simulation. The slice width is set at 0.8 metres, which is more than 6 times the diameter of a coarse particle.

Another approach could have been the use of a 2D model. However, this means that particle movement in three directions is lost and this may influence the bulk flow behaviour. With the use of a 3D slice and the use of periodic boundaries, it is assumed that the bulk flow behaviour is maintained while reducing the calculation time. Periodic boundaries have been described in *Section 3.2.1*.

- 3. Three particle sizes representing a full particle distribution**

Section 4.1.2 mentions more reasons for simplifying a full size distribution to three particle sizes, but this is also a way to reduce calculation time. Calculation time is reduced since there are less fine particles included in the simulation; especially the dust-sized particles are eliminated.

To accumulate the same weight or volume, more fine particles are required than large particles. In DEM modelling not the weight but the number of particles defines the calculation time required. Therefore, it is beneficial to reduce the amount of fines in a simulation.

- 4. Modelling using a single particle size**

One step further to reduce calculation time is the use of a single particle size.

The suitability of modelling only coarse particles in the simulation instead of the three different sized particles is researched in *Section 5.2.2*.

Particles may be given an ID-tag or colour in order to represent their 'size'. Hereby the possibilities remain to extract particle information and size distributions, while modelling is carried out with identically coarse sized particles.

5. Reducing the number of spheres in particle cluster

EDEM particles are constructed by clustering multiple spheres. The benefit of multiple sphere clusters is that a more representative (irregular) particle shape can be created. The disadvantage of multiple spheres is a longer calculation time. Forces are calculated on each sphere in a cluster individually; this implies that more spheres require longer calculation time. The impact of multiple sphere clusters is simulated and discussed before in *Section 3.3.2.a*.

6. Lowering the shear modulus in the model

Mentioned previously, in the *Section 3.3.2.b* is the shear modulus. The shear modulus is the dominant factor in calculation of the Rayleigh time (a measure for the time step). Lowering of the shear modulus in DEM modelling therefore reduces calculation time. The lowest setting for the shear modulus without influencing the bulk behaviour significantly is found in *Section 3.3.2.b* and used in the simulation models.

4.2 Experimental plan and simulation settings

The experimental plan divides the simulation results into three sections: basic, primary and secondary results. The figure below show how these sections are used to reach the project objectives and to find answer to the research questions.

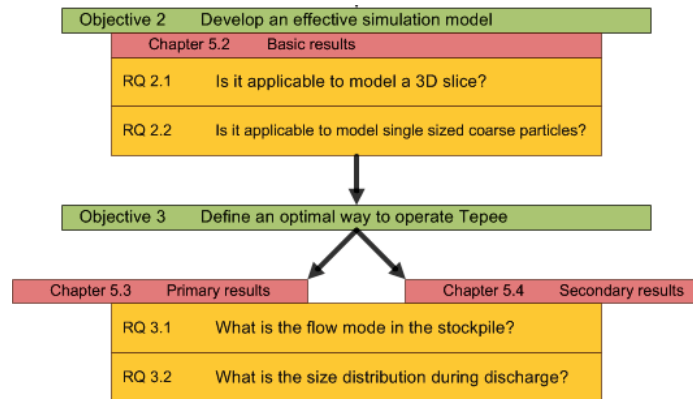


Figure 62: Experimental plan (red) and project objectives and research questions

The simulations to determine an effective simulation model are grouped under *Basic results*. The *Primary results* will report on wider applicable simulations, by researching three parameters that are found in stockpiles. The three parameters are the impact of the filling method, the effect of input during discharge and the influence of the wall angle. Finally, the *Secondary results* will report on simulations that apply specifically to situations at the stockpile of Boliden Tara Mines.

An overview of the simulations is given in the table below. The last column shows the used simulations by their number. Information about the simulations is given before the each of the results in *Chapter 5*. A complete overview of all simulations and their parameters is provided in *Appendix C*.

Table 13: The grouped simulation results and the belonging simulation numbers

Section	Result	Sub-result	Simulations
Basic	3D slice to full 3D	Low wall friction	I, II.a
		High wall friction	I, II.b, II.c
	Using single particle size		V, II.a
Primary	Impact of filling methods		II.c, A2
	Impact of input during the discharge		C, D2, H
	Impact of wall angle		II.c, III.c
Secondary	Outlet splitter	Splitter	IV.a, IV.b
		Asymmetric discharge splitter	VII
	Asymmetric input		G
	Non-constant output flow rate		F
	Fill level of the Tepee at 100%		VI

Mixed filling simulations are numbered using Roman numbering (e.g. I, II.a, II.b, III, IV,..). Batch filling simulations are numbered using capital letters (e.g. A, B1, B2, C,..). Reference to the simulations in *Appendix C* will be as follows: “*Appendix C – XX.X*”, whereby the X’s are the simulation numbers.

As mentioned, the settings that differ per simulation are given before each of the results in *Chapter 5* or can be found in *Appendix C*. There is however a series of parameters that are set similar in each simulation. These parameters will now be discussed.

For each simulation model in *Chapter 5*, the same material properties in EDEM are used. The only exception is the static friction coefficient ' μ_s ' or 'fs' between the wall and ore particles. The static friction coefficient of the interaction between ore and the wall (in this report shortly referred to as 'wall friction') is the only parameter that is set differently across the simulations. The static friction between the ore and wall was initially set identical to ore-ore contact at fs=0.25. Since the walls of the Tepee are constructed from compacted earth and rock fill, this was assumed as a good approach. At later stage in the results, it is shown that it is better to use a higher wall friction (*Section 5.2.1*).

Two different methods are used to increase the wall resistance (*Section 5.2.1*). Either by increasing the static friction coefficient to the value fs=1 or physically by inserting friction plates in the wall (referred to as 'tips'). The notation of both increased wall resistances is respectively: 'high – fs=1' and 'high – tips'. In simulations that are run with friction tips, the static friction coefficient is equal to ore-ore contact at 0.25. Friction tips are small plates, which are placed perpendicular on the Tepee wall and have a height of half a particle diameter. This avoids that the modelled Tepee walls are completely smooth and thus increases the wall resistance.

The material parameters used in the simulations are displayed in Table 14. At the start of each section before discussing the results, an overview of all other simulation parameters are given, in which the wall resistance is given as well.

Table 14: EDEM material parameters as used in the simulations

EDEM parameter		Ore	Wall
Shear modulus	[Pa]	1e8	1e8
Poisson's ratio	[-]	0.25	0.25
Density	[kg/m ³]	2750	2750
		Ore-ore	Ore-wall
Rolling friction coefficient	[-]	0.1	0.1
Restitution coefficient	[-]	0.3	0.3
Static friction coefficient	[-]	0.25	Low = 0.25 High = 1.0

The particles used in all simulations are formed by clustering five spheres. The particle properties as given before in *Section 4.1.2*, are given in the following table.

Table 15: DEM particle properties: size, sphericity, roundness, volume and mass

	Size [mm]	Sphericity	Roundness	Volume [m ³]	Mass [kg]
Fines	30	0.5	0.4	1,4e-05	0,039312
Pebbles	80	0.5	0.4	0,000223	0,614104
Coarse	130	0.5	0.4	0,000914	2,5141

The dimensions of the Tepee as they have been given before in *Section 4.1.1* are summarized in Table 16.

Table 16: Tepee dimensions at Tara Mines and in the DEM model

	Tepee at Tara Mines	DEM model	DEM slice model
Capacity [t]	30,000	170	15-16
Diameter [m]	45	7.5	7.5 (0.8m slice width)
Wall angle [deg]	45-60	45 or 60	45 or 60
Outlet size [m]	4.5	1.3 or 0.8 or 0.5	1.3 or 0.8 or 0.5

The simulation results in *Section 5.3.2* research the importance of the input rate in relation to the output rate. The input rate is controlled by the factory plate in EDEM. For all simulation with input the input rate is set at 6000 kg/s. Except for simulation H, where the input rate equals the discharge at 1200 kg/s. The output rate is controlled by the outlet size. A summary of the flow rates of input and output is given in Table 17.

Table 17: Overview of input and output rate

	Simulation	Rate [kg/s]
Input	Simulation H	1200
	All other simulation with input	2500
Output	With 1300mm outlet	6000
	With 800mm outlet	3000
	With 500mm outlet	1200

4.3 Display of results

After modelling in EDEM, result data is extracted. This section describes the output of the modelling. The method of data extraction and how the data is displayed is discussed. There are three main ways to extract, measure and display the output results of a simulation. First, screen captures of the simulation show the movement of the particles at a specific time or as a velocity factor. Secondly, a virtual bin below the outlet of the Tepee is used to measure and create a size distribution graph. The third output is the withdrawal angle as a measure for the live capacity of the stockpile.

4.3.1 Screen captures

The flow of particles and the flow mode inside the stockpile is best retrieved visually. Therefore, screen captures are made of the simulations. In this report, two different screen captures are used; a static screen capture and a dynamic screen capture of streams.

Both types of capture are shown in Figure 63 and Figure 64, showing the same moment in the same simulation. The static image is simply a still image taken from the simulation playback, where the actual particles are visible. A series of these captures show the way the material flows inside the stockpile. These series of captures are printed for all simulations in *Appendix C*.

In some cases, it is useful to have a more dynamic image of the simulation. This is done using dynamic captures of streams as shown in Figure 64, also referred to as ‘stream captures’. One line in the ‘dynamic capture’ displays the movement of a single particle over 20 iterations. A longer line therefore indicates a higher particle velocity with its direction of movement.

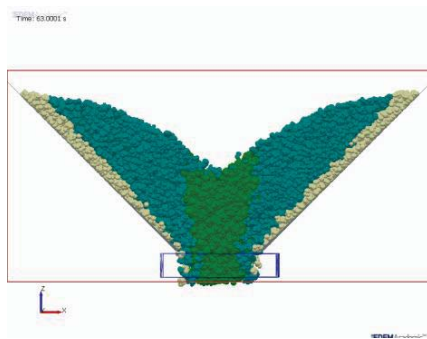


Figure 63: Example of a (static) screen capture

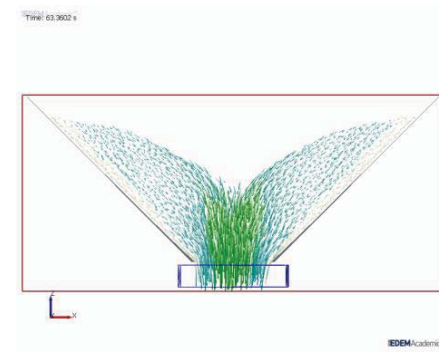


Figure 64: Example of a (dynamic) stream capture

The colours in the captures represent the different particle sizes and these colours are kept identical throughout the entire report. The type of particle with its corresponding colour name are listed in Table 18. Particle colouring is based on the size the particle represents. In the simulations quite often, larger particles are used to reduce calculation time, while they represent a smaller size (reviewed in *Section 5.2.2*).

Table 18: Particle colouring

Particle type	Colour
Fines	Green
Pebbles	Blue
Coarse	Cream
Input particle	Orange

4.3.2 Size distribution graph

Measuring the size distribution at the outlet is required to gain insight on the flow in the stockpile and whether blending takes place in the stockpile. In order to measure the size distribution of the output a virtual bin is created directly below the outlet. Particles entering this bin are recorded. Thereby the properties of the particles, such as size and weight (as well as forces, velocities, etc.), can be extracted at each specified time.

A review is given on how the size distribution at the outlet is displayed and why it is done that way. One simulation is used (Figure 65) as an example. In this example simulation, the modelled Tepee is filled with the ‘mix filling’ method. There is no new material entering the stockpile after this initial stage. The amount of material in the system is fixed and the stockpile is emptied completely. There are several ways to display the size distribution, which will be reviewed in this section.

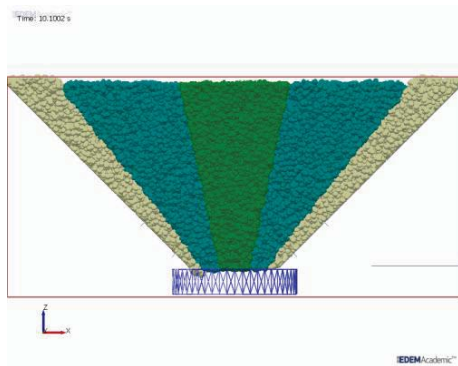


Figure 65: Example screen capture showing the initial filling of the Tepee

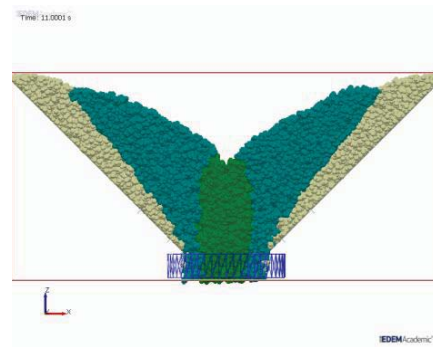


Figure 66: Example screen capture showing the discharge, where particles are measured in the blue bin

Figure 66 shows the material flowing through the virtual bin at the bottom after opening of the outlet. This bin records the particle data that will be discussed on its representation.

Data of all particles passing the bin can be extracted from the program over time. By extracting the size and the weight of particles over time a size histogram was made, which is displayed in Figure 67.

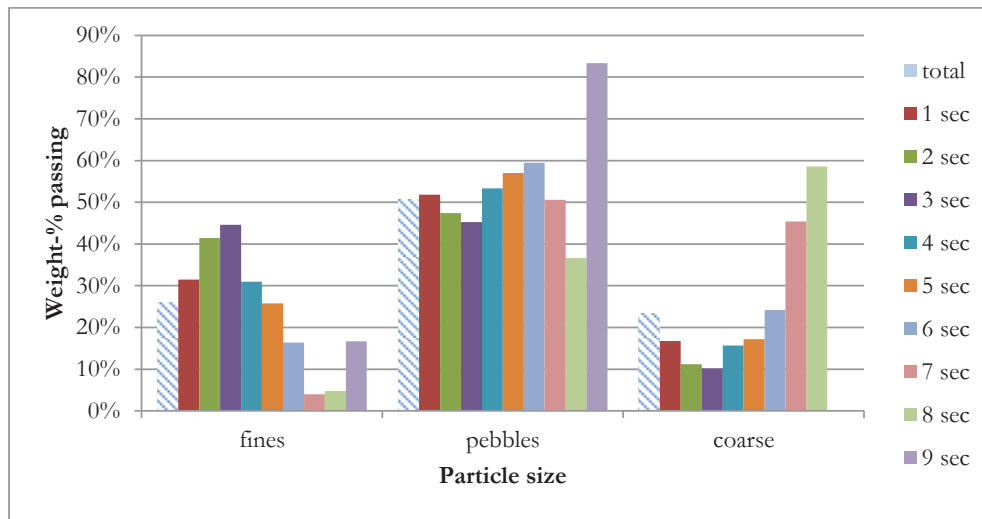


Figure 67: Particle size histogram by size

For each second, the total weight of particles of one size as a fraction of the total weight is plotted on the y-axis. This is called the weight-percent passing. The x-axis shows the different particle sizes, where each colour bar represents a single second. The total of the three size fractions for the same second should always sum up to one hundred. The striped bars are the total of each particle size in the stockpile; this shows the amount of each size that is initially fed into the stockpile. Therefore, this amount has to leave the system as well at a complete stockpile discharge.

This method of displaying the size distribution by size, does show the trend of a single particle size. However, it is difficult to compare what happens at one specific time for all the three sizes. To overcome this problem it is better to plot the size distribution over time instead of over size, this is displayed in Figure 68.

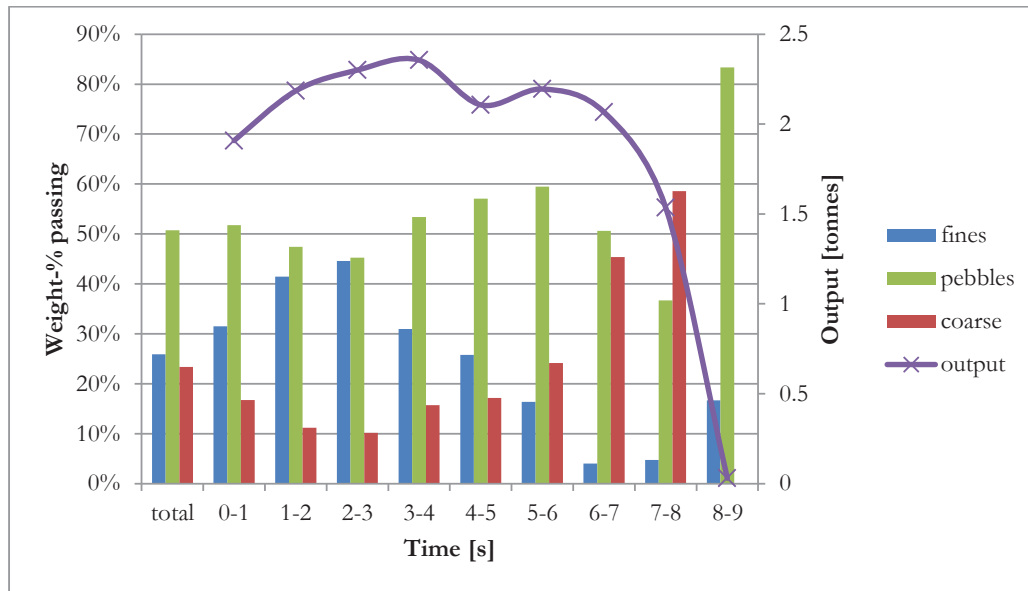


Figure 68: Particle size histogram over time

In Figure 68 the exact same data is plotted, where the weight-percent passing of a size fraction is also plotted on the y-axis. In this figure, the time is shown on the horizontal axis. For each second the bars of fines pebbles and coarse are grouped, where the total of a group of one second should always be 100 percent.

The figure, shows the particle size histograms over time, which provides a good comparison between the different sizes over each time step. However, the output is not constant over time as shown by the line in the graph. The problem this may cause is best noted by the following example: the graph shows a peak in pebble fraction and zero coarse between second 8 and 9. This implies that at that specific time lots of pebbles are discharged, however the amount of material is almost zero tonnes. This effect is caused by only very few particles and therefore this effect can be neglected. To avoid this problem, it is better to plot the weight-percent passing over the total mass (Figure 70) instead of over time (Figure 68).

The variation in output over time (output rate in tonnes per second) can be divided into three sections (Figure 69). The blue output line is the same as in Figure 68 and the red line is the cumulative output using the same data. The three sections are:

1. Start of output
Material only starts moving after the outlet is opened. In the first second material needs to acceleration, which results in a lower output rate.
2. Intermediate flow
There is variation in the intermediate flow, however this variation is relative small (around 10%). A variation of a few hundred kilograms may already be caused by a few coarse-sized particles. Nonetheless, the flow is relative constant; producing even a close to linear line in a cumulative graph as shown in Figure 69.
3. End of output
At the end of the output there is less material in the system. Hence, there is less pressure by other particles on the remaining material, which reduces the output rate. Especially when there is a high wall friction, it may take a while for the last particles to roll down into the outlet and thus there is a low output rate.

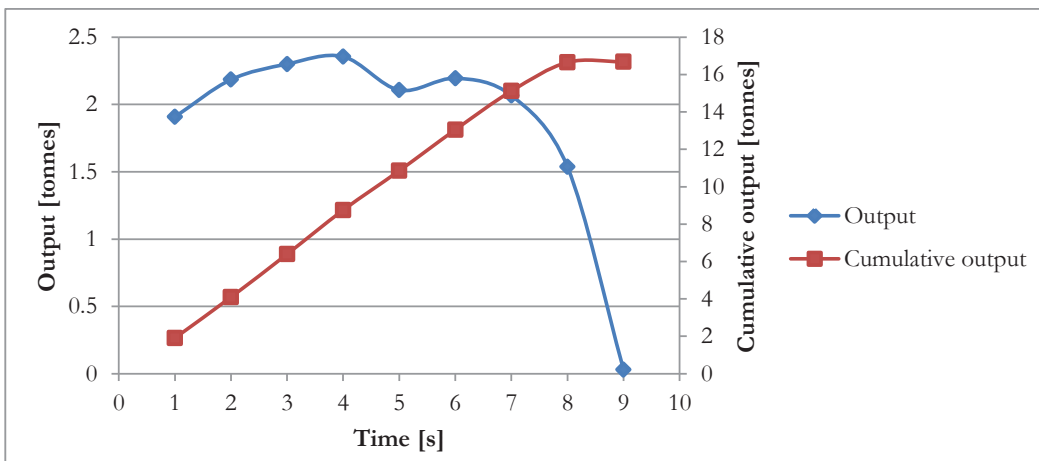


Figure 69: Output and cumulative output over time

Due to the varying output over time, there are two reasons why it is more functional to plot the weight-percent over mass instead of over time:

1. Making it easier to compare multiple simulation results, because the non-constant discharge rate is avoided.
2. The mill requires that a specified size distribution is reached over the mill load and not necessarily over time. The size distribution should be matched of several hundred tonnes (the mill load) and not over a certain period of time.

Figure 70 shows a distribution graph where the weight-percent of the size fractions is plotted over the output in tonnes. The data used in this graph is identical to the graphs before. The method of displaying results as shown here below is the method used in this report, since this gives the best representative overview for comparison.

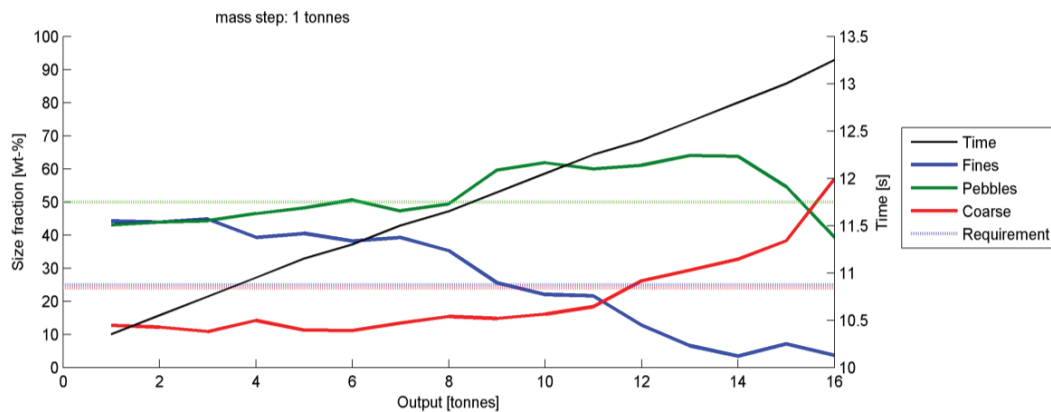


Figure 70: Size distribution over output mass with mass intervals of 1 tonne

The graph in Figure 70 shows the size fraction in weight-percent of the fines, pebbles and coarse in the respectively blue, green and red lines. Furthermore, the mill requirements are given in same coloured dashed lines. The horizontal axis is the output in tonnes. In every graph the mass steps is mentioned (1 tonne in this example), which explains the interval in mass over which a size distribution is measured. This interval varies for some of the simulations, since some simulations require a higher level of detail and the total mass in the stockpile is not similar for all simulations.

The black line shows the time in the simulation related to the output. This makes it possible to relate the moment in the simulation (screen captures) to the size distribution graph. The line is a cumulative of the output and therefore does not make the small variations in the output rate visible, as mentioned before in Figure 69.

The mass step defines the accuracy of the graph. Small mass steps increase the accuracy. However, this is not required in all simulations. The mass step of 0.2 tonnes contains only 80 coarse sized particles, which means that a variation of only eight particles already may cause an inaccuracy of 10%. In mixed filled simulations, this accuracy is not required and this amount of detail only distracts from the important information. Batch filled simulations require this amount accuracy, due of the thin layers formed as a repetition of particle sizes.

4.3.3 Angle of repose and withdrawal angle

The third method to display data is the use of the angle of repose and the withdrawal angle. The angle of repose is the angle of a pile formed by loose pouring of a free-flowing bulk material. The withdrawal angle is the angle that defines the boundary between flowing and non-flowing material in the stockpile during discharge. Steep withdrawal angles imply that more material is stagnant and thus that there is a narrower funnel in core flow. The angle of repose and the withdrawal angle are measured and reported as an angle in degrees in the report. Examples of the angles are shown in the figure below.

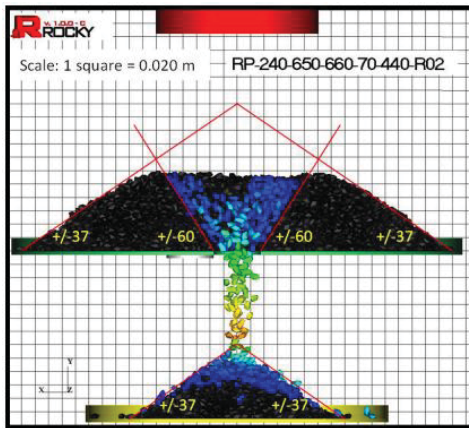


Figure 71: Discharge of bulk material showing withdrawal angle (60 deg) and angles of repose (37 deg) after Comminution Technology JV (2011)

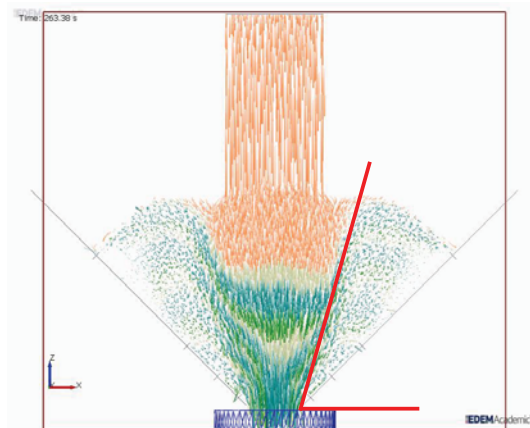


Figure 72: DEM simulation showing the angle of withdrawal in red

The withdrawal angle is measured in the captures of a stream. These captures show several iterations of a particle as a line. Hence, the stream captures shows moving particles as a line and non-moving particles as a dot. This makes it easy to find the boundary (angle of withdrawal) between moving and non-moving material.

5 Simulation results

5.1 Overview of simulations

The experimental plan is discussed in *Section 4.2*. In this section, only a summarising overview will be provided. As mentioned the simulation results are divided into three sections: basic, primary and secondary results. The table below gives an overview of the results and how they are grouped. Most results are a comparison between two or more simulations. The last column mentions which simulations are used in the result. The details of a simulation are given at the start of each results section or can be found in *Appendix C*.

Table 19: Overview of the simulation results, the researched parameters and the belonging simulation numbers

Section	Result	Sub-result	Simulations
Basic	3D slice to full 3D	Low wall friction	I, II.a
		High wall friction	I, II.b, II.c
	Using a single particle size		V, II.a
Primary	Impact of filling methods		II.c, A2
	Impact of input during the discharge		C, D2, H
	Impact of wall angle		II.c, III.c
Secondary	Outlet splitter	Splitter	IV.a, IV.b
		Asymmetric discharge splitter	VII
	Asymmetric input		G
	Non-constant output flow rate		F
	Fill level of the Tepee at 100%		VI

5.2 Basic results

This chapter shows the results on the development of an effective simulation model by two simulation measures. Firstly, the application of a 3D slice and secondly the use of single sized material to represent the fines as well.

Three combinations of model domain size and particle type were used in the modelling. The amount of particles in each model shows the degree of reduction.

3D model with single coarse sized particles	Particles: 33,000+
3D slice model with actual fines, pebbles and coarse	Particles: 127,000+
3D slice model with single coarse sized particles	Particles: 6,000+

5.2.1 3D simulation approach by using a 3D slice

Earlier in *Section 4.1.4*, it is mentioned that a reduction in calculation time is required. An effective way to reduce the calculation power is to simulate a slice that represents the full conical stockpile. The possibility to carry out simulations using a 3D slice is researched in this section. Initially this was done for geometries with a low wall friction and at a later stage the wall resistance has shown to be a dominant factor. Both cases will be discussed.

A vertical slice taken out of a cone will have slightly curved walls from the circularity of the cone. In order to avoid problems in EDEM by using periodic boundaries and these curved walls, it is chosen to use a wedge-shaped slice instead. Periodic boundaries are required in the slice simulation to keep the three dimensional behaviour of the simulation. When no periodic boundaries are used in a simulation a physical wall should be placed instead, which will influence the flow behaviour of the bulk material. Both the geometry of a cone and the geometry of a slice are shown in the following figures. Wall angles, height and outlet opening remain the same in both models.

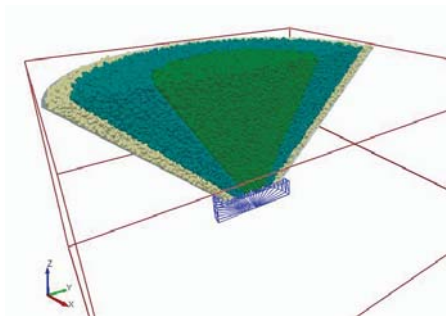


Figure 73: 3D model, only one half is displayed

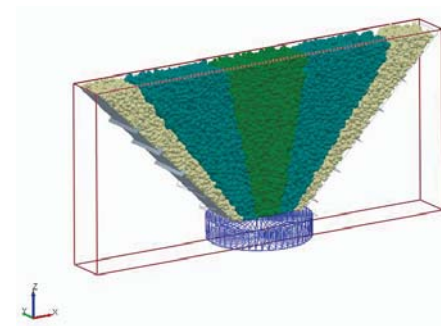


Figure 74: 3D slice model

The simulations grouped in the *basic results* are all filled by the mixed filling method. This filling method is chosen since this will highlight the difference between core and mass flow the best. The mixed filling method has a column of fines in the middle and coarse material close to the walls. For mass flow the discharge will result in a remixing at the outlet, where core flow will discharge first a majority of fines, followed by pebbles and coarse.

Furthermore, in the basic results there is no input during the emptying of the stockpile. For the clarity of the results in these simulations, this input of new material is not taken into account.

5.2.1.a Approach of 3D by using a 3D slice; low wall friction

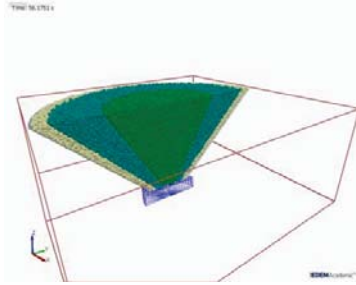


Figure 75: Capture of simulation I.a

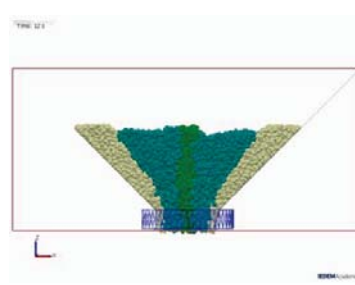


Figure 76: Capture of simulation II.a

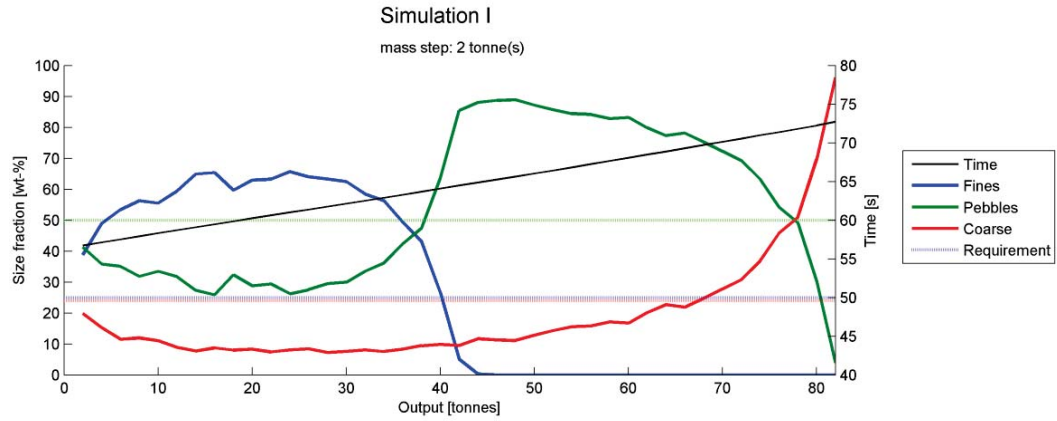


Figure 77: Size distribution graph of simulation I.a

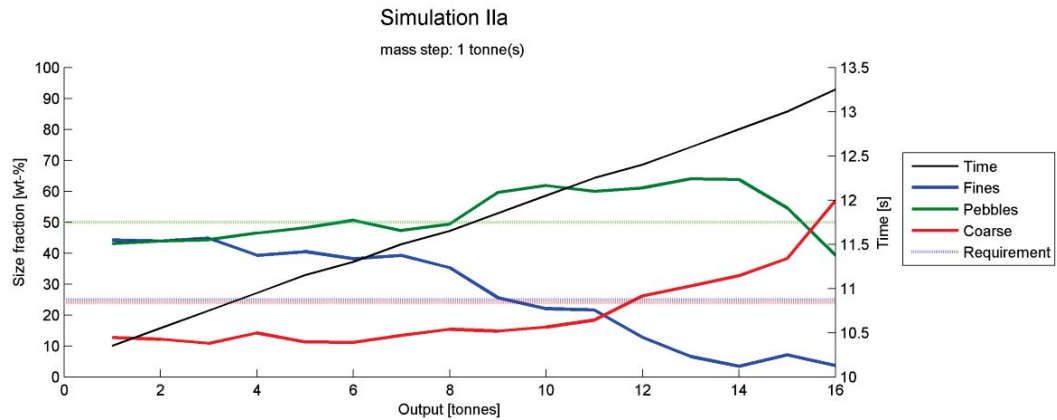


Figure 78: Size distribution graph of simulation II.a

5.2.1.a Low wall friction

A comparison is made between the simulation of a 3D cone and the simulation of a slice, in order to see whether the behaviour of flow in a slice is similar to that in a 3D model. In this comparison, all parameters are set the same for both simulations. The two simulations and their parameters are listed in the following table.

Table 20: Simulation parameters for comparing a slice and cone simulation with low wall friction settings

Parameter	Simulation	
	I	II.a
3D or 3D slice	3D	3D slice
Filling method	Mixed filling	Mixed filling
Particle size [mm]	130	130
Wall angle [deg]	45	45
Wall friction [type]	low - fs=0.2	low - fs=0.2
Outlet size [mm]	1300	1300
Input [-]	no	no
Other	-	-

The resulting size distributions during the discharge are shown in Figure 77 and Figure 78. The 3D simulation shows first a discharge with a majority of fines, followed by a majority of pebbles and in the final stage of emptying the coarse material is discharged.

When comparing the simulation of the slice II.a (Figure 77) with the 3D cone I (Figure 78), it is clearly seen that the size distributions during discharge do not match up. The slice simulation shows a decreasing trend for fines and an increasing trend in coarse, where pebbles vary with 10% margin around the mill requirement. This is significantly different from the 3D simulation, thus the flow must be different in both simulations.

The flow of the simulations is shown in Figure 75 and Figure 76 and in more detail in *Appendix C – I* and *Appendix C - II.a*. The flow mode in the 3D simulation is an example of core flow, where the velocity is the highest in a central column above the outlet and as good as zero at the walls. This agrees with the information in the size distribution graph, where the central column of fines flow out first and the coarse material at the wall the latest. This also agrees with literature in *Section 2.4* and with the observations at Tara Mines in *Appendix B*.

The flow mode in the 3D slice on the other hand does not show core flow. Particles at the wall are moving (which is seen best in the captures of a stream) and this means that the flow mode is mass flow. This movement at the wall induces a remixing effect at the outlet. Although mass flow and thereby the remixing is beneficial for the size distribution, this is not comparable to the 3D simulation and thus not a representative approach of the Tara Mines' stockpile.

The circular shape of the cone results in flow and force in two direction, where the wedge-shaped slice has flow and force in one direction. In a conical funnel effectively more material is pushed through the opening, which results in larger forces pushing the material to the walls of the stockpile. This increases the resistance in respect to a wedge-shaped stockpile. The next section therefore reviews the applicability of a 3D slice with higher wall resistance.

5.2.1.b Approach of 3D by using a 3D slice; high wall friction

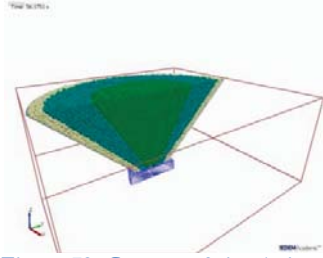


Figure 79: Capture of simulation I.a

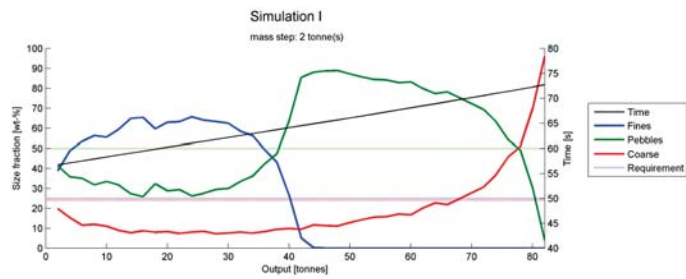


Figure 80: Size distribution graph of simulation I.a

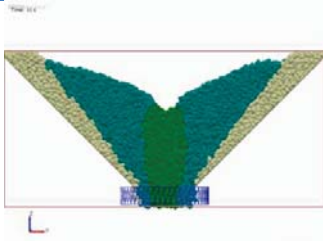


Figure 81: Capture of simulation II.b

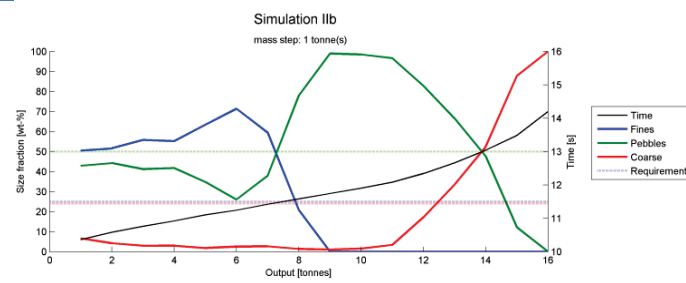


Figure 82: Size distribution graph of simulation II.b; high static friction

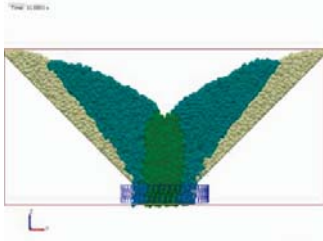


Figure 83: Capture of simulation II.c

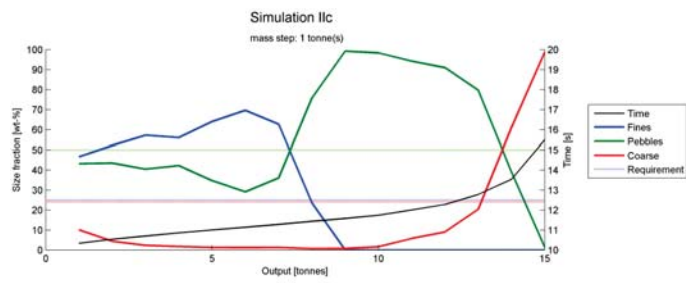


Figure 84: Size distribution graph of simulation II.c; friction tips

5.2.1.b High wall friction

The previous simulation II.c showed that the material flows too easily along the walls and thereby does not approach the 3D simulation I. By increasing the resistance along the wall, the material is expected to flow less easily along the wall. This may result in a core flow mode and thereby a better representation of the 3D simulation and thus of the Tepee.

Two different ways to increase the material resistance with the wall are tested; an increase in the static friction coefficient and the addition of tips in the wall. The tips will physically stop some particles at the wall and thereby create a surface of particles at the wall, which will increase resistance. The properties of the two simulations and the 3D simulation for comparison are shown in the table below.

Table 21: Simulation parameters for comparing cone with two slice simulation with high wall resistance

Parameter	Simulation		
	I	II.b	II.c
3D or 3D slice	3D	3D slice	3D slice
Filling method	Mixed filling	Mixed filling	Mixed filling
Particle size [mm]	130	130	130
Wall angle [deg]	45	45	45
Wall friction [type]	low - fs=0.25	high - fs=1	high - tips
Outlet size [mm]	1300	1300	1300
Input [-]	no	no	no
Other	-	-	-

The distribution graphs of both slice simulations in Figure 82 and Figure 84 show a similar profile. These simulations show a better approach of the 3D simulation I (Figure 80) than the low wall friction simulation in the previous section. The intersection of the fines and pebbles occurs at the same output tonnage and so does the intersection between pebbles and coarse material at the end of the discharge.

Comparing both slices simulations with the 3D cone simulation this shows a very good relation. The intersections between fines and pebbles as well as pebbles and coarse are found at the same relative output tonnage and at the same size fraction. Therefore, a slice with high wall resistance represents full 3D simulation very well, making it an effective measure to reduce calculation time.

The flow in both slice simulations (*Appendix C – II.b and II.c*) show both a very similar core flow, with one clear difference at the end of discharge. The final part of discharge shows particles sliding along the wall for the high static friction simulation, where the friction tips simulation show rolling and tumbling motion along the wall at the end of discharge. The friction tips simulation compares better to reality, since a completely flat surface off the wall is not expected at Tara Mines. Therefore, this is the advised method of applying high wall resistance. Subsequently, the use of tips also avoids the need to find a threshold value for a static friction.

The full 3D simulation is run with high wall friction as well in *Appendix C – I.b*. The higher wall friction for the full 3D simulation does not influence the flow much compared to the low friction in simulation I.a. Therefore, it is concluded that a threshold in wall friction should be reached in order to simulate core flow in the stockpile. The amount of wall resistance does not influence the flow behaviour much after the threshold value is exceeded. The threshold value is not further investigated, since the scenario has been chosen that approximates reality closest; by installing friction tips to create a natural friction plane of particles.

5.2.2 Real sized versus only coarse sized

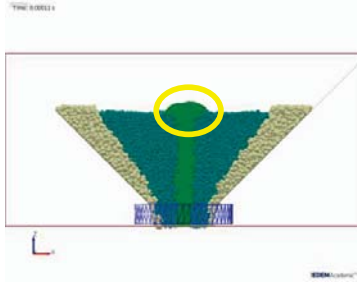


Figure 85: Capture of simulation V

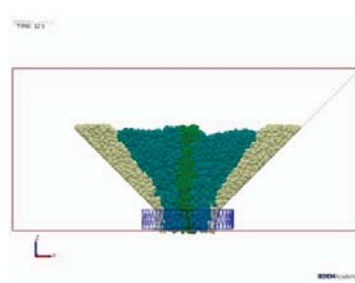


Figure 86: Capture of simulation II.a

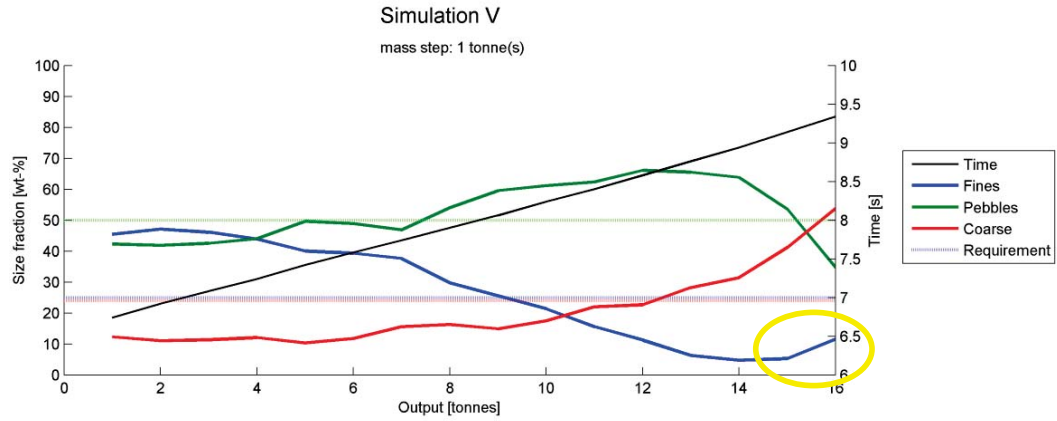


Figure 87: Size distribution graph of simulation V

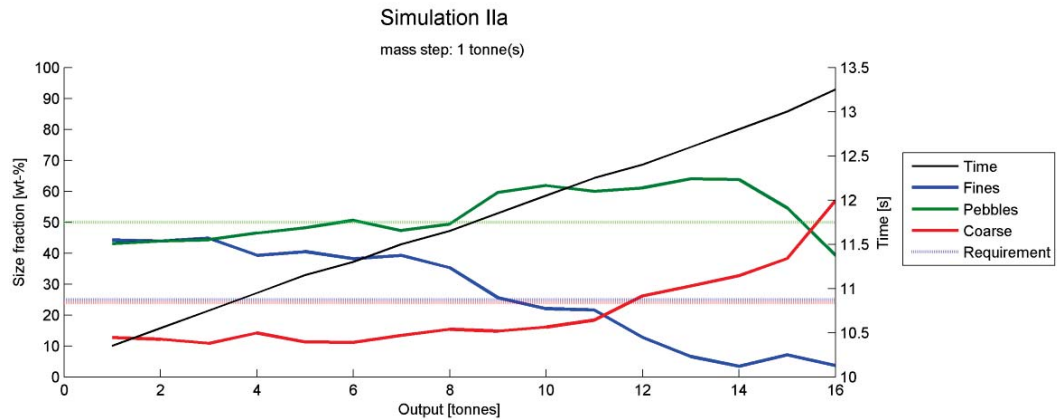


Figure 88: Size distribution graph of simulation II.a

5.2.2 Using a single particle size

Another major step in calculation time reduction can be achieved when large particle can be used to simulate the small particles. Furthermore, this simulations show the effect of particle size. Two simulations are compared. Simulation V was run with actual fines, pebbles and coarse material (respectively 30, 80 and 130mm) and simulation II.a was run with coarse material (130mm) representing the fines, pebbles and coarse.

It is important to mention that both simulations were carried out using a low wall friction, where we have seen that a high wall friction results in a better approach of reality.

Table 22: Simulation parameters for comparing 'real sized' particles with single sized coarse particles

Parameter	Simulation	
	V	II.a
3D or 3D slice	3D slice	3D slice
Filling method	Mixed filling	Mixed filling
Particle size [mm]	30, 80 & 130	130
Wall angle [deg]	45	45
Wall friction [type]	low - fs=0.25	low - fs=0.25
Outlet size [mm]	1300	1300
Input [-]	no	no
Other	-	-

The simulation II.a is also shown in *Section 5.2.1.a*. The size distribution graphs of both simulations (Figure 87 and Figure 88) result in a similar discharge profile. Since, both simulations discharge in mass flow mode. The pebble fraction of both simulations fluctuates around the mill requirement (+/- 15%). The fines fraction shows a decreasing trend starting at 45% and the coarse fraction shows an increasing trend. In both simulations the fines and coarse intersect at a similar location around 20% size fraction.

A difference is noticeable is the fines area. Simulation V - where actual fines are used - shows a plume of fines originating during discharge (highlighted in yellow in Figure 85). A more complete view on the way this plume forms is shown in the screen captures in *Appendix C – V*. This plume is not seen this clearly when using only large sized particles. The cause of this plume is that the coarser material from the sides starts moving to the centre, which will be referred to as 'necking behaviour'. The fines are too light to give enough pressure to prevent the coarse material from falling in. This plume is not expected to occur in the Tepee, since the availability of a minor fraction of coarse particles in a fines area is expected to reduce this effect.

Except for this minor difference caused by the plume, the similarity is very good. Therefore, it is a good measure to reduce the calculation time by using large sized particles that represent the finer material. On the effect of particle size, it is concluded that the particle location is dominant over modelling particle size, because both simulation produce a very similar size distribution graph. There is how ever a small influence caused by the particle size, which causes the formation of the plume.

5.3.1 Impact of filling method

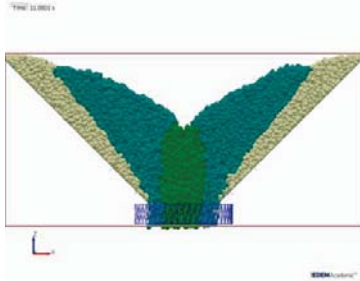


Figure 89: Capture of simulation II.c

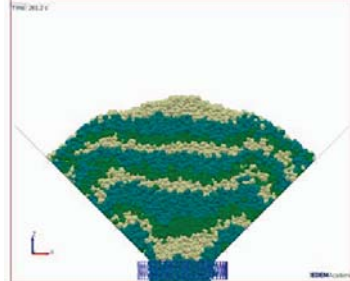


Figure 90: Capture of simulation A2

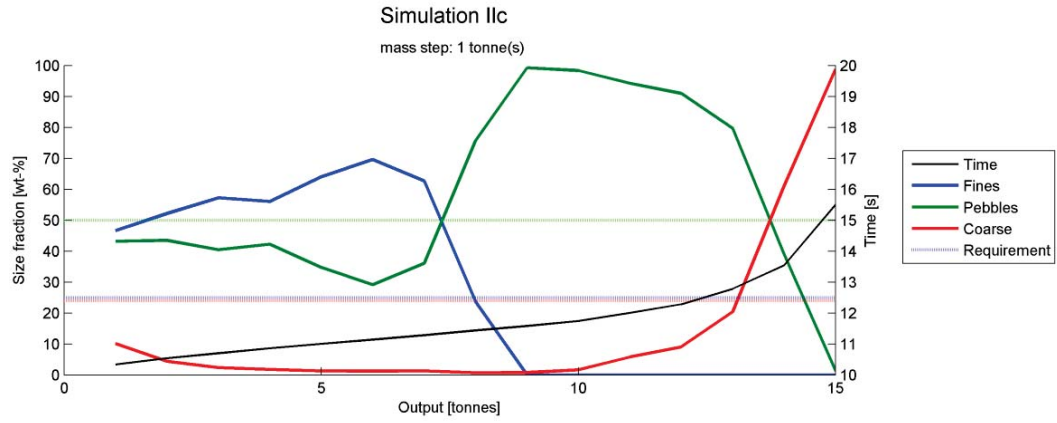


Figure 91: Size distribution graph of simulation II.c

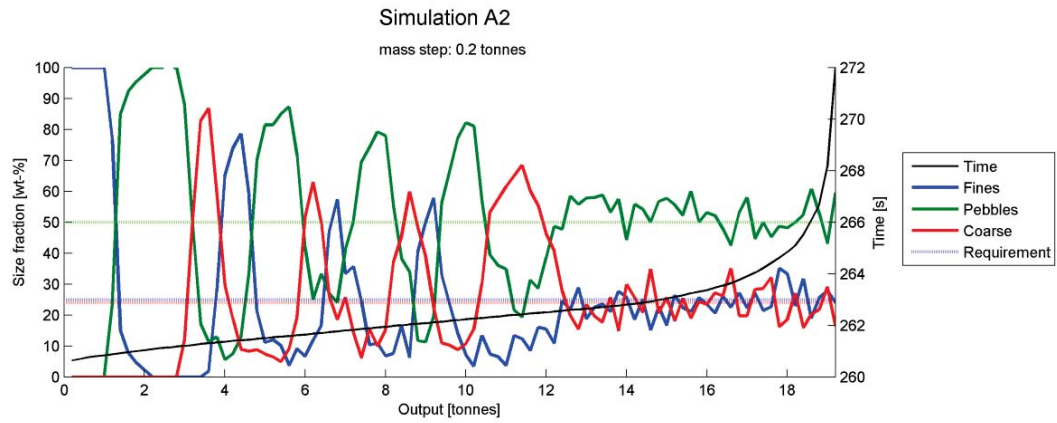


Figure 92: Size distribution graph of simulation A2

5.3 Primary results

In this section *Primary results*, the influence of generally applicable scenarios for stockpiles are reviewed. First, different methods of filling are compared. Thereafter the influence of the ratio between input and output rate is shown. Finally, the result is shown on the impact of the wall angle on the flow mode.

5.3.1 Impact of different filling methods

Section 4.1.3.a mentions the two methods of filling the Tepee. These two methods are compared, on their resulting size distribution output. The simulations were carried out under the same conditions, where only the method of filling is different, as shown in the table below.

Table 23: Simulation parameters for comparing different methods of filling

Parameter	Simulation	
	II.c	A2
3D or 3D slice	3D slice	3D slice
Filling method	Mixed filling	Batch filling
Particle size [mm]	130	130
Wall angle [deg]	45	45
Wall friction [type]	high - tips	high - tips
Outlet size [mm]	1300	1300
Input [-]	no	no
Other	-	-

The size distribution graph of simulation II.c was reviewed before in *Section 5.2.1.b*. Hence, only the simulation A2 will be described before comparing both simulations.

The size distribution graph of simulation A2 (Figure 92) appears to consist of two parts. The first part is a batch wise discharge and the second after ~ 11 tonnes there is a blending during the discharge. The first part shows a peak at the discharge for each of the batches in the same sequence as how they are initially filled. The discharge peaks of the pebble material have a higher weight-fraction and a wider tonnage, which is due to the 1:2:1 ratio of fines, pebbles and coarse. The second part of the discharge shows good mixing of the three sizes and thereby producing the ideal blend that meets the mill requirement.

In comparing both filling methods, it is observed that the batch filling of simulation A2 produces a more ideal discharge for the AG mill, since the quickly varying first part may results in an optimal mill load and the second part is ideally mixed.

The AG mill requires to receive the ideal mix over a certain amount of tonnage. The mill load should contain this ideal mix. This is achieved when batch filling is performed with batches small enough, so that a 'peak' of each of the three size fractions is included in one mill load.

For the second part of the A2 size distribution, the re-mixing delivers an ideal distribution. Thus both parts of the A2 simulation provide a good size distribution for the mill. The output of simulation II.c however is not ideal at one single moment. There has been too much segregation to be re-mixed while discharging in core flow. Although simulation II.c is not ideal, this scenario is the mostly likely to occur at the Tepee stockpile, therefore this simulation is used in other results as well.

5.3.2 Impact of input/discharge ratio

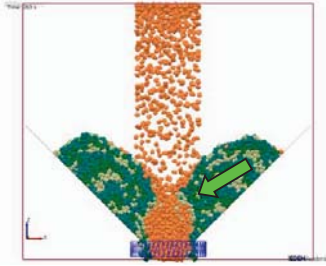


Figure 93: Capture of simulation C; highlighting the 'necking effect'

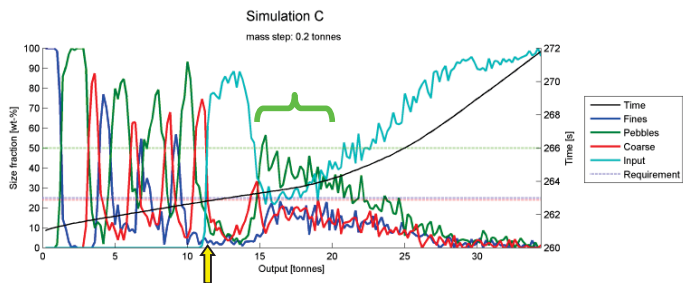


Figure 94: Size distribution graph of simulation C; input < output rate

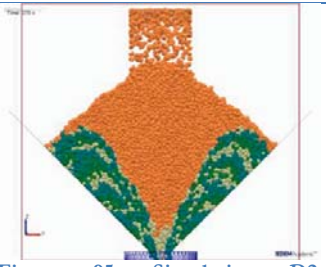


Figure 95: Simulation D2; showing a growing fill level

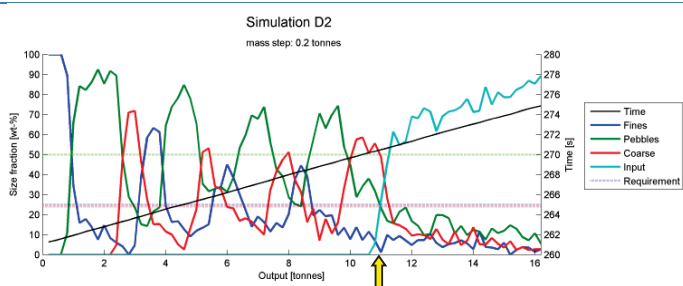


Figure 96: Size distribution graph of simulation D2; input > output rate

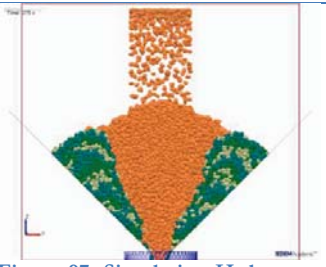


Figure 97: Simulation H; keeps a 70% fill level

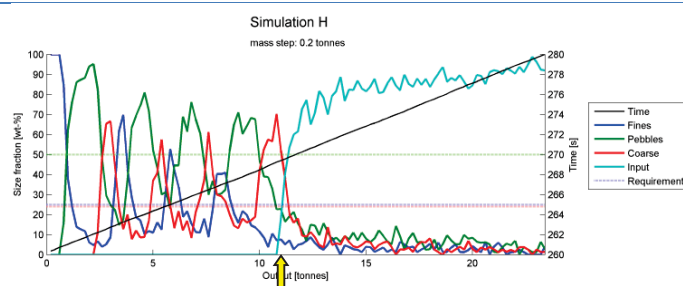


Figure 98: Size distribution graph of simulation H; input = output rate

5.3.2 Impact of the ratio between input rate and output rate on the discharge

The second part reviewed in the *primary results* is the comparison between different ratios between input and output rate. In an operating stockpile, input rate and output rate are not constant. Which results in three possible scenarios; input rate lower than output rate (simulation C), input rate higher than output rate (simulation D2) and equal input rate and output rate (simulation H). The effect of these scenarios is researched in this section.

Table 24: Simulation parameters for comparing different ratios between in- and output rate.

Parameter	Simulation		
	C	D2	H
3D or 3D slice	3D slice	3D slice	3D slice
Filling method	Batch filling	Batch filling	Batch filling
Particle size [mm]	130	130	130
Wall angle [deg]	45	45	45
Wall friction [type]	high - tips	high - tips	high - tips
Outlet size [mm]	1300	500	500
Input [-]	yes	yes	yes; at a lower rate
Other	-	-	input rate = output rate

The table above shows the settings for each simulation. The input rate at simulation C and D2 is set equal at 2.5t/s and the ratio between input and output is controlled by the size of the outlet. Simulation C is set with a wide outlet size, resulting in a higher output rate. Simulation H uses the same smaller outlet diameter as simulation D2, whereby the input rate is lowered to equal the output rate. The output rate of simulation D2 is measured and as input rate in simulation H (1.2t/s).

Comparing the size distribution results shown in Figure 94, Figure 96 and Figure 98 it becomes clear that the size distribution graph can be divided into two parts (similar to what was seen in *Section 5.3.1*). The first part is the interval 0-11 tonnes, where a repetition of size peaks is seen caused by the batch filling method. This first part is similar in each of the three simulations. This repetition of peaks is practically identical to the previous simulation A2 (Figure 92) which did not have input in the simulation, therefore it can be concluded that the discharge of the first part is independent of the input rate.

The second part of the simulations (after 11 tonnes) is different for each of the three simulations and depends on the ratio between in- and output rate:

- Simulation C: The input rate is lower than the output and this is causing a ‘*necking effect*’, due to missing of material in the core that supports the wall material.
- Simulation D2: The input rate is higher than the output and thus the stockpile is slowly filling up more. This creates a heap and causes heap segregation. The effect of heap segregation is dependent on the input material, which is reviewed in *Chapter 6 – Discussion*. The second part of the distribution graph shows that the input material is dominant in the discharge and that there is little mixing with the initial material close to the stockpile wall.
- Simulation H: The input rate is equal to the output rate, so the filling level remains the same. The moment the input material reaches the outlet (at 11 tonnes discharge), the input material is dominant and similarly as in D2 there is little mixing with the material located at the walls.

The ‘*necking effect*’ is seen in all simulation where the input rate is lower than the discharge (e.g. *Appendix C – D1*) and the stockpile thus empties in the simulation. The core in the middle empties, which creates open space in the centre. When the angle of the material at the wall exceeds the angle of repose this side material will slide to the centre and fill the open space (shown with a green arrow in Figure 93). In this work, this movement to the middle is referred to as a ‘*necking effect*’ that narrows the input stream. This effect is also noted by the flow regions of Brown and Hawksley (*Section 2.4.1*), where zone A is comparable to this fast moving layer.

This ‘*necking effect*’ can also be recognised in the size distribution graphs. For example in Figure 94 between 15 and 19 tonnes, where the input fraction is reduced and a mixture of fines, pebbles and coarse fills its empty space. At 19 tonnes, all the material from the sides is discharged. Hereafter the input fraction increases again, although at a slower output rate (black line).

The input/output rate shows impact on the flow mode, especially when looking at the dynamic stream captures in *Appendix C – C, D2* and *H*. The angle of withdrawal is measured for each of the simulations, after 11 tonnes of bulk has been discharged.

Sim C Input rate < output rate → withdrawal angle is 73 degrees

Sim H Input rate = output rate → withdrawal angle is 70 degrees

Sim D2 Input rate > output rate → withdrawal angle is 64 degrees

The input/output ratio influences the angle of withdrawal. A higher input rate puts more material on top of the heap, which puts more pressure on the filling of the Tepee. This results in the smallest angle of withdrawal. The contrary is seen for a lower input rate, where the stress on the material is less, which results in a steeper angle of withdrawal.

The ‘live capacity’ is the moving material in the stockpile. This live capacity is bounded in the core by the angles of withdrawal. The smaller the withdrawal angle the larger the live capacity. Hence, the live capacity is largest when the input rate is higher than the output rate.

5.3.3 Impact of wall angle

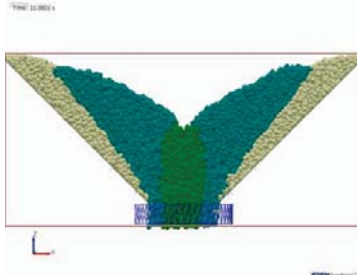


Figure 99: Capture of simulation II.c

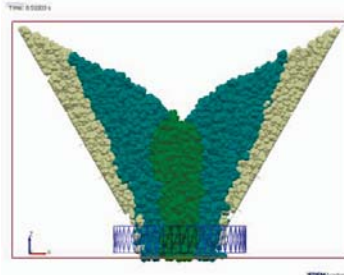


Figure 100: Capture of simulation III.c

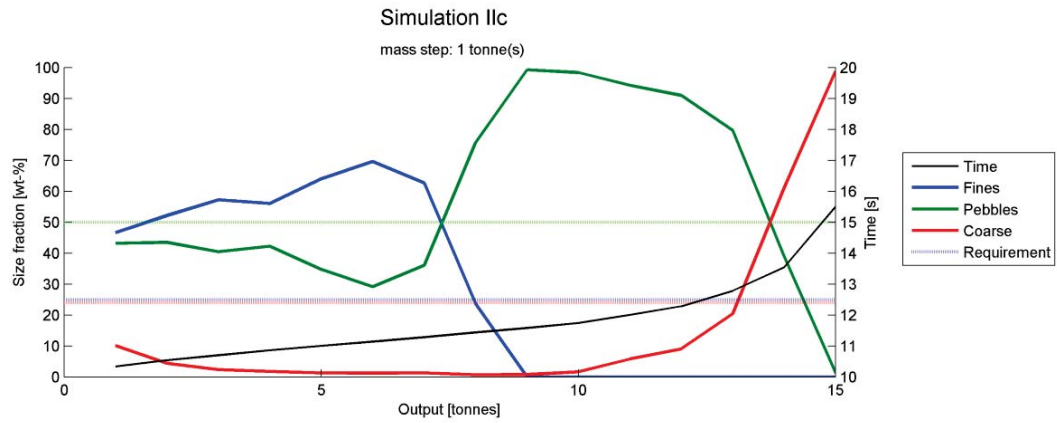


Figure 101: Size distribution graph of simulation II.c

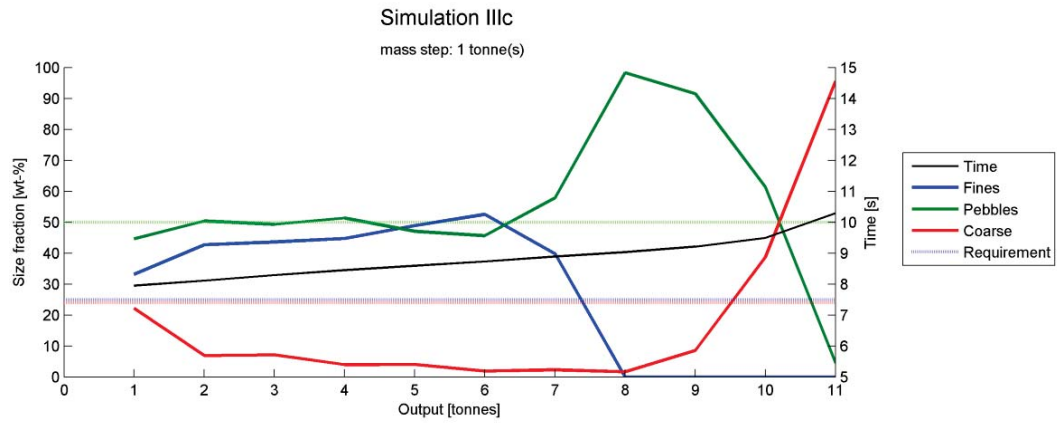


Figure 102: Size distribution graph of simulation III.c

5.3.3 Impact of the wall angle

The wall angle is the last parameter researched in *primary results*. The wall angle is expected to influence the flow and discharge size of the stockpile. The wall angles that are compared are 45 and 60 degrees as summarised with all other parameters in the table below.

Table 25: Simulation parameters for comparing different wall angles.

Parameter	Simulation	
	II.c	III.c
3D or 3D slice	3D slice	3D slice
Filling method	Mixed filling	Mixed filling
Particle size [mm]	130	130
Wall angle [deg]	45	60
Wall friction [type]	high - tips	high - tips
Outlet size [mm]	1300	1300
Input [-]	no	no
Other	-	-

Both simulation have friction tips and are operating in funnel flow as the Figure 99 and Figure 100 show. The total amount of material is different in both simulations, since the geometry of the stockpiles is different. Due to the funnel flow, the size distribution graphs show a similar behaviour after the moment all the fines are discharged. For both wall angle after discharging the fines, the pebble fraction increased first and is followed by an increase of coarse material from the side of the walls.

The start of the discharge however is different, which is caused by the different wall angles. The steeper wall angle shows a relatively longer period that discharges the fines. The fractions of fines and pebbles are quite constant for a significant period of discharge, where the pebble fraction meets the mill requirement. Therefore the 60 degree wall angle is preferred over a 45 degree wall angle, however the discharge is still not ideal.

The screen captures in *Appendix C –II.c* and *III.c* show core flow in both simulations, where the velocity is much higher for steeper walls. This results almost in a mass flow mode for the simulation with a 60 degree wall. This is also stated in the design charts of Jenike (*Section 2.4.2* Figure 24). The location in the graph moves to the left in the intermediate zone between core and mass flow.

However, the higher velocity in the core for the steeper wall does not result in a higher discharge rate. The discharge rate over the first 10 tonnes is very constant and equal for both flow modes, namely 6t/s. After the discharge of 10 tonnes, the flow rate in for the 45 degree wall is reduce substantially (the black line becomes steeper). This is caused by the missing out of particles in the core of the stockpile.

Furthermore, the captures of a stream show that there is less stagnant material in a 60 degree wall model. This is the reason why there is a more constant discharge of fines and pebbles at the first stage of discharge.

The screen captures of a stream in the *Appendix C – II.c* and *III.c* were used to measure the angles of withdrawal after a specific discharge weight, see the table below.

Table 26: Impact of wall angle on the angle of withdrawal at different discharge steps

	Discharged ore	4t	6t	8t
45 degree wall angle II.c	<i>time</i>	<i>10.8s</i>	<i>11.2s</i>	<i>11.5s</i>
Measured withdrawal angle [deg]		73	67	55
60 degree wall angle III.c	<i>time</i>	<i>8s</i>	<i>8.5s</i>	<i>8.9s</i>
Measured withdrawal angle [deg]		75	69	62

The tonnages in the distribution graph are converted to time, using the output line. The time is used to find the corresponding stream captures, on which the withdrawal angles are measured.

The withdrawal angle is not constant over time (or better, not constant over the discharged mass) for these simulations without input. The shortage of material in the core reduces the pressure on the stagnant bulk. Therefore, the material at the walls starts to flow to the centre. This lowers the angle of withdrawal. The angles of withdrawal for a 45 degree wall are lower than for steeper walls. Especially when a large amount of material is discharged, this may be caused by a lower pressure since the material is stacked over a wider area and to a lower height.

The discharge of material from a steeper stockpile is beneficial for the size distribution during discharge, due to a more constant first part of discharge. Hence, this is better predictable than for a stockpile with a 45 degree wall.

An even better size distribution discharge is achieved in a more unrealistic case with low wall resistance. The results in *section 5.2.1.1* show that low wall resistance result in an evenly distributed and ideally blended output. Low wall resistance and a wall angle of 60 degrees results in an ideal discharge, although this may not be a realistic scenario. This unrealistic scenario is printed in *Appendix C – III.a*.

5.4.1.a Comparing outlet with splitter and without splitter

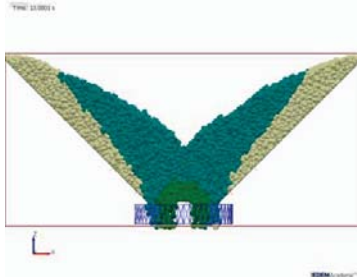


Figure 103: Capture of simulation IV.a

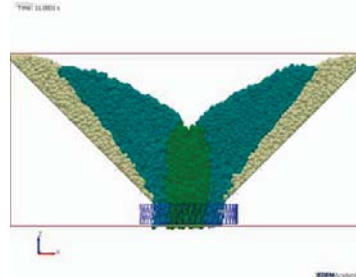


Figure 104: Capture of simulation II.c

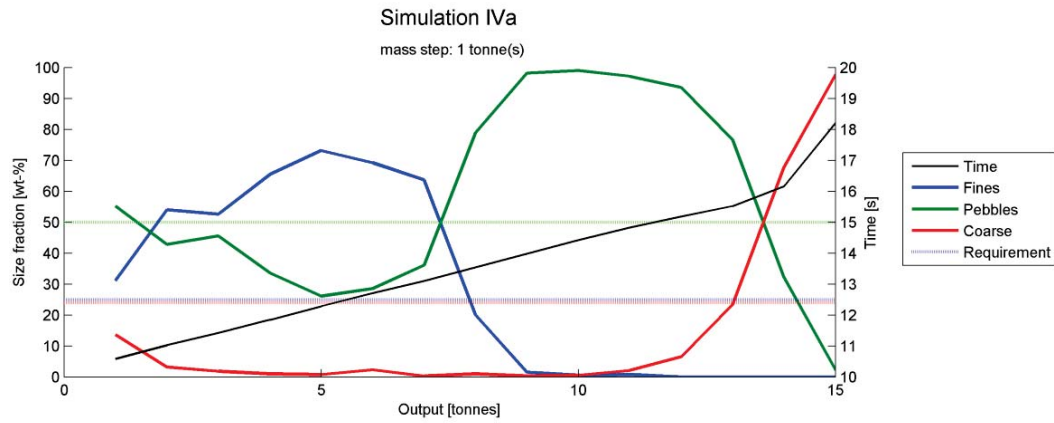


Figure 105: Size distribution graph of simulation IV.a

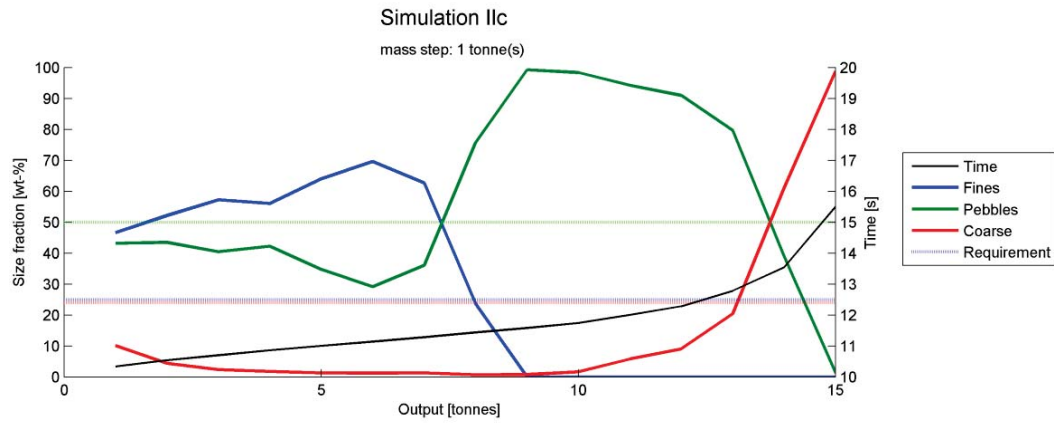


Figure 106: Size distribution graph of simulation II.c

5.4 Secondary results

In the *Secondary results* the results are reviewed of several simulations that specifically apply to situations at Tara Mines. The first situation includes the discharge system of Tara Mines by means of a splitter. Secondly, an asymmetric placement of the input in the stockpile is researched. Subsequently the impact of an interrupted discharge is simulated. A last simulation shows the discharge of a 100% filled Tepee and filled under mix filling conditions.

5.4.1 Outlet splitter

There are two parts studied to retrieve the impact of the output splitter. The outlet splitter in the simulation is used to represent the chutes in the discharge system at the Tepee of Tara Mines. The first part reviews the influence of a symmetric splitter and the second part reviews the influence of an asymmetric placed splitter.

5.4.1.a Influence of a splitter

Simulation IV.a has an output splitter at the outlet and is compared to an identical simulation without a splitter (II.c). The parameters of the simulations are summarized in the table below.

Table 27: Simulation parameters for comparing the influence of an outlet splitter

Parameter	Simulation	
	IV.a	II.c
3D or 3D slice	3D slice	3D slice
Filling method	Mixed filling	Mixed filling
Particle size [mm]	130	130
Wall angle [deg]	45	45
Wall friction [type]	high - tips	high - tips
Outlet size [mm]	1300	1300
Input [-]	no	no
Other	output splitter	-

The size distribution graphs in Figure 105 and Figure 106 as well as the screen captures in *Appendix C- IV.a* and *II.c* show core flow for both scenarios. The splitter as it is used in simulation IV.a does not influence the flow mode as such, the flow mode remains core flow.

The flow profile is clearly influenced by the splitter, since the geometry of the outlet is different. The core flow, splits in two directions. However, the main flow mode is not influenced; there is core flow and the stagnant material at the wall remains similar.

The influence of the splitter on the size distribution during discharge is only seen at the start of discharge. At the first tonne of discharge, the amount of fines is lower for the simulation with a splitter. This is caused by the blockage of fines in the centre due to the splitter plate. This effect recovers after 2 tonnes of discharge, when the discharge flow of material is steady. Even though there is a slight difference in the flow profile, the implementation of a splitter plate as used in this simulation is not influencing the size distribution discharge.

5.1.4.b Asymmetric discharge splitter

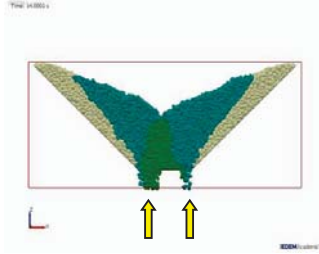


Figure 107: Capture of simulation VII; total of both outlet

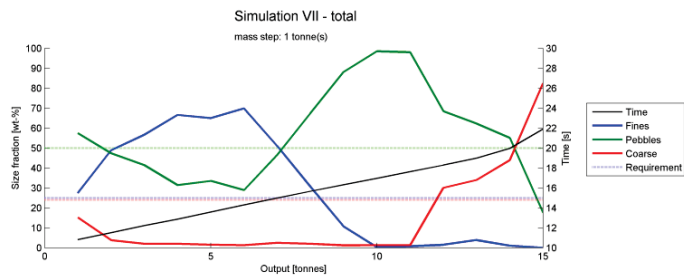


Figure 108: Size distribution graph of simulation VII; total

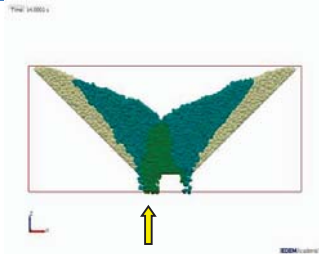


Figure 109: Simulation VII; larger left outlet

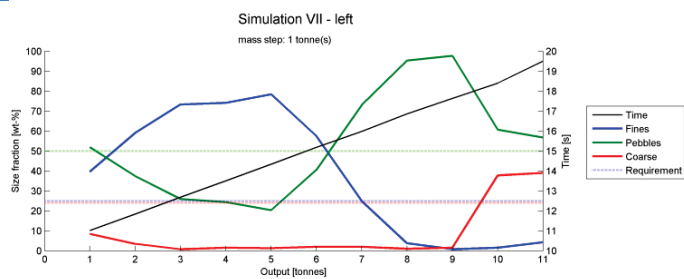


Figure 110: Size distribution graph of simulation VII; left outlet

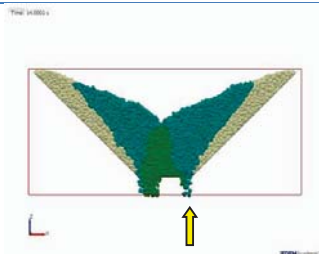


Figure 111: Simulation VII; smaller right outlet

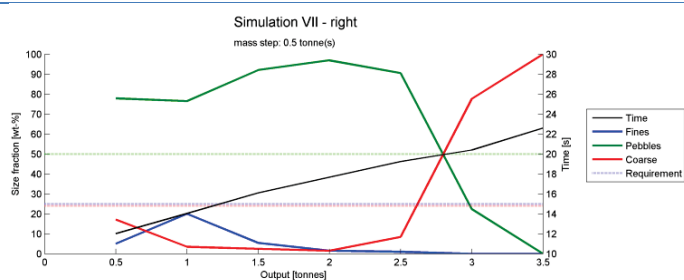


Figure 112: Size distribution graph of simulation VII; right outlet

5.4.1.b Asymmetric discharge splitter

One of the controllable parameters in the Tepee is the opening of the discharge chutes. Simulation VII has a discharge splitter installed, which is placed asymmetrically. This creates a larger outlet size on the left and a smaller one on the right. This simulation displays the impact of asymmetric discharge on the size distribution.

Parameter	Simulation
	VII
3D or 3D slice	3D slice
Filling method	Batch filling
Particle size [mm]	130
Wall angle [deg]	45
Wall friction [type]	high - tips
Outlet size [mm]	left: 600mm, right:300mm
Input [-]	no
Other	-

The screen captures belonging to this simulation in *Appendix C – VII* show core flow. However, the different discharge rates for the left and right outlet show two separate core flow regions. Both outlets have their own core flow region. This is different from simulation IV.a in the previous section, which was modelled with equal sized outlet openings. The two core flow regions in simulation IV.a form one larger region of core flow. The captures of streams from this simulation VII show a large difference in velocity above the left and right outlet. A significant fraction of particles that are located on the right side are discharged via the left outlet, this is due to this difference in velocity and the different core flow regions.

The result of this simulation is shown in three size distribution graphs; the total of both outlets, the left outlet and the right outlet. The distribution graph of the total discharge is in rough lines similar to simulation II.c, where no splitter is installed. Furthermore, this distribution graph is even better related to the one of simulation IV.a, where an equal spaced splitter is installed. Hence, the total distribution is not influenced much by the asymmetric splitter.

However, there is a major difference seen when comparing the left and right distribution graphs. The larger left outlet produces a size distribution similar to the total. Though, in a mixed filling situation the right outlet with a low flow rate show a very different distribution. The right outlet produces mainly pebbles and only at the end of discharge a coarse size distribution. Very notable is the extreme low fraction of small material in the right outlet. This is caused by the different core flow profiles. The left profile has a higher velocity and therefore ‘pulls’ all fine material in the centre in its own directions. The flow rate in the right outlet is too small to ‘pull’ the fine material in its own direction.

5.4.2 Asymmetric input

The feeding of material into the Tepee is expected to be centred above the outlet. However, it is worth full investigating an asymmetric filling of the Tepee, since there is segregation during the discharge of material from the incoming conveyor belt (*Section 4.1.3.b*, Figure 61). This section reviews the impact of an asymmetric filling. This means that the input is not centred directly above the outlet, but is placed closer to the walls of the Tepee. A summary of the parameters used, is given in the table below.

Table 28: Simulation parameters of simulation G with asymmetric filling

Parameter	Simulation
	G
3D or 3D slice	3D slice
Filling method	Batch filling
Particle size [mm]	130
Wall angle [deg]	45
Wall friction [type]	high - tips
Outlet size [mm]	800
Input [-]	yes
Other	asymmetric filling

5.4.2 Asymmetric input

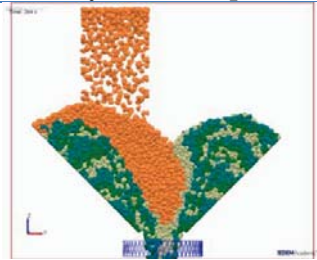


Figure 113: Capture of simulation G

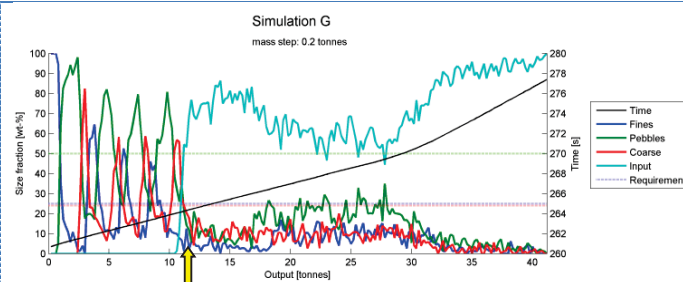


Figure 114: Size distribution graph of simulation G; where the yellow arrow points the moment that input material reaches the outlet

The size distribution graph of the asymmetric input (Figure 114) is best compared with its symmetric counterpart in *Appendix C – D1*. The size distribution graphs are very comparable. The only slight difference seen just after the input material reaches the outlet (pointed out by the yellow arrow). This period with a high input fraction, between 11 and 17 tonnes, is lower for this simulation with asymmetric input. This is caused by more stagnant material falling into the core. This is stagnant material coming from opposite the input location. At both simulations, the ‘necking effect’ is registered at the same discharge tonnage between 20 and 30 tonnes.

This is a surprising result when looking at the flow profiles in the screen captures in *Appendix C – G* and *D1*. The asymmetric input simulation shows core flow, but there is a smaller stagnant zone at the side of the input and a large stagnant zone on the opposite side. The flow is asymmetric but this is not influencing the size distribution much, since it still behaves as core flow.

5.4.3 Interrupted discharge

Production at the mine and in the mill is not constant; this is caused by either the nature of work, maintenance or accidental breakdowns. Therefore, the ratio between input and output is not constant. A scenario where this ratio varies, was modelled in simulation F.

The following schedule was used in the simulation F:

1. Initial batch filled
2. Output and input start at the same time; with a slightly lower input rate than output rate
3. Discharge is stopped for 7 seconds, while input continues at the same rate
4. Discharge is started again; input rate still slightly lower than output.
5. Simulation stopped at the moment that most of the originally placed layers are discharged

Table 29: Simulation parameters of simulation F with interrupted discharge

Parameter	Simulation
	F
3D or 3D slice	3D slice
Filling method	Batch filling
Particle size [mm]	130
Wall angle [deg]	45
Wall friction [type]	high - tips
Outlet size [mm]	800
Input [-]	yes
Other	Interrupted discharge

5.4.3 Interrupted discharge

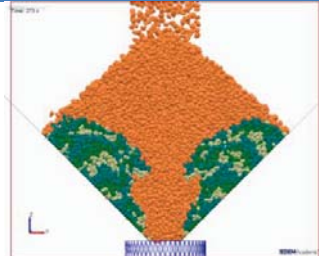


Figure 115: Capture of simulation F

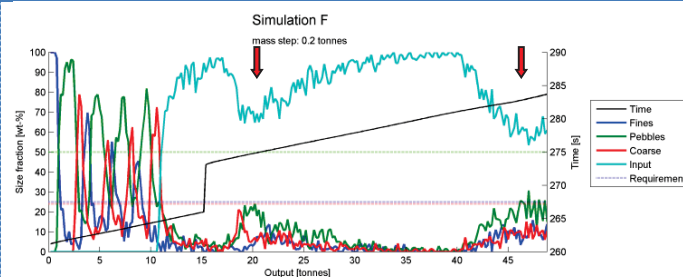


Figure 116: Size distribution graph of simulation F; two 'necking effects' are pointed by the red arrows

Simulation F with interrupted discharge is best compared to simulation D1, which is an identical simulation only without the interruption in step 3 and 4 (see *Appendix C – D1*). The size distribution graph in Figure 116 shows two times a 'necking effect' located at the red arrows. The first one is comparable to the one in simulation D1. Due to the refilling in step 3, the discharge of input material increases again. This continues until the discharging creates open space in the centre again. This is again filled by stagnant side material and creates the second 'necking effect'.

It can be concluded that the heap segregation and the necking effect as concluded in section 5.3.2 simulation D2, may also be caused by periodical stops in input or output. Ideally, the ratio between the input rate and output rate should be maintained the same without interrupting one of the flows. This would optimise the possibility to predict the size distribution output, since this creates a 'last-in, first-out' system.

5.4.4 Fill level of the Tepee at 100%

In the previous simulations with mixed filling, only the bottom half of the Tepee is modelled. Therefore a simulation was run to investigate the influence of a 100% fill level of the Tepee, when the input is a mixed fill. The parameters of the simulation are listed in the table below. Friction tips have proven to be the most realistic measure to increase the wall resistance and are therefore applied.

Table 30: Simulation parameters of simulation G with a 100% fill level

Parameter	Simulation
	VI
3D or 3D slice	3D slice
Filling method	Mixed filling
Particle size [mm]	130
Wall angle [deg]	45
Wall friction [type]	high - tips
Outlet size [mm]	1300
Input [-]	no
Other	100% fill level

5.4.4 Fill level of the Tepee at 100%



Figure 117: Capture of simulation VI

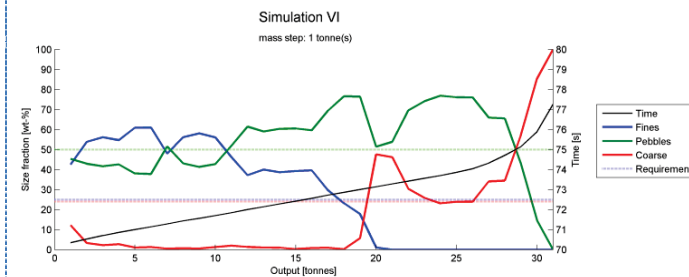


Figure 118: Size distribution graph of simulation VI

The size distribution graph in Figure 118, points out that the size output is in rough lines similar to an identical simulation where only the bottom half is filled (*Appendix C - II.e*). There are roughly parts; part one between 0 and 18 tonnes and part two after 18 tonnes until a full discharge at 31 tonnes. In part one, the fines and pebbles vary around the 50% fraction, where no coarse material is present. In part two the fines are gone and there is only coarse and pebbles sized material in the output. This is roughly similar to the discharging of only a bottom half cone. This is also shown in *Appendix C - VI*, where the screen captures show core flow.

However a difference is seen in the second part, where the coarse fraction shows two peaks. The first peak is caused by coarse material in the top that is discharged earlier. This is followed by a dip in coarse material, due to an increase in pebbles coming from the sides. The second peak is similar to the peak in a model of only the bottom half cone, since this is the discharge of coarse material at the walls on the bottom half of the Tepee.

6 Discussion

Two main topics will be discussed so that the simulation results are placed in a correct perspective.

1. Reflection on the validity of the simulations
2. The optimal way of operating the Tepee
 - 2.1 Simulations without input
 - 2.2 Simulations with input

The first topic is a reflection on the validity of the simulation compared to the real stockpile at Tara Mines. The second topic will discuss the third objective - define an optimal way to operate the Tepee - by using the simulation results.

6.1 Reflection on the validity of the simulations

The simulations as used in this report are scaled to a fraction of the real size of the Tepee. Therefore, it is good to validate these models to reality. However, there is no complete picture of the flow in the Tepee to validate for, due to the large scale. Hence, the use of these scaled simulations is justified by several observations and literature findings that are found back in the simulation results.

Two observations at Tara Mines indicate that material is discharged in core flow. The first observation is the 'last in, first out' system in the Tepee. This occurs in funnel flow the when the 'fresh' material is directly discharged through the centre of the stockpile. The second observation is that a crater is formed when there is no input during discharge. The crater is formed in the centre, right above the outlet. Both observations would not occur in mass flow mode. Based on the wall angle and friction factors, the flow diagrams by Jenike (*Section 2.4.2*, Figure 23) also confirm core flow. This establishes the flow mode in the simulations.

Those observation validate the flow mode, but not the entire simulation model, since the downscaling should be taken into account as well. The withdrawal angles in the simulation appear to be very reasonable, although they have not been verified in this study. Based on these angles, the material is distinguished as flowing or stagnant. Comparing the modelled size and the actual size of the Tepee (Figure 119) this shows that the stagnant zone are relative larger in the actual Tepee for the same withdrawal and wall angles.

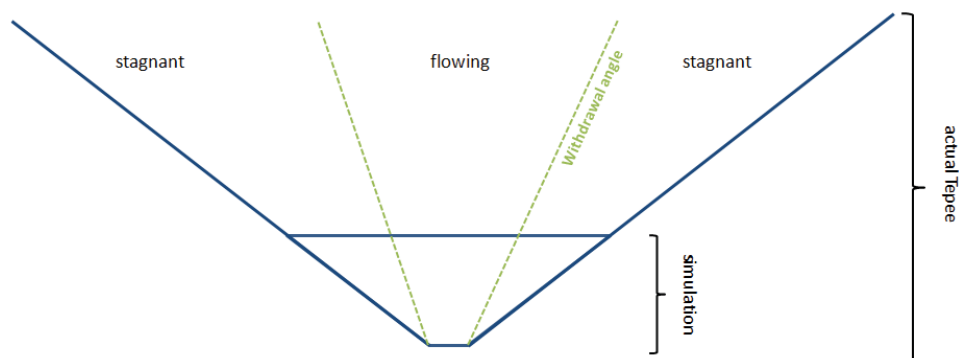


Figure 119: Sketch to compare stagnant and flow zones for the simulation size and the actual size of the Tepee

Therefore, effects seen in the results of the simulation are expected to be larger in the actual Tepee. This may mean that negative effects on the size distribution in the Tepee may become

even more negative and positive effects more positive. Hence, this scaling effect would be of interest for future research.

It should be stated clearly that the distinct separation between the particle sizes in the different filling methods is not the actual case at Tara mines. This is done to gain good insight in the segregation mechanisms and the blending of the sizes at the outlet. This should be taken into account when reviewing the results. Fines represent an area with a surplus of fines, pebbles an area with a surplus of pebbles and coarse a surplus of coarse.

6.2 The optimal way of operating the Tepee

The simulation results show that there is not a single way of operating the Tepee that delivers the optimal size distribution output. It is entirely dependent on the combinations of the filling method and the flow mode.

An overview of the combinations will be provided in the next two sections. The size distribution output will be reviewed and labelled positive, negative or neutral.

6.2.1 Simulations without input

The simulations without the input of new material are discussed in this section. This provides a good overview how the combination of filling method and flow mode influence the size distribution during discharge.

The flow mode is mainly defined by the wall angle and the wall resistance. A steep (60 degree) wall angle and a low wall resistance result in mass flow (*Appendix C – III.c*), where a 45 degree wall angle and high wall resistance result in funnel flow (*Appendix C – II.b and II.d*).

Table 31: Impact on size distribution for simulations without input

Filling method	Flow mode	Impact on discharged size distribution
Mixed filling	Core flow	Negative
	Mass flow	Positive
Batch filling	Core flow	Positive
	Mass flow	Positive (expected from simulation III.c)

Batch filling in general provides a better size distribution, where it should be mentioned that the thickness of the layers and the size ratio is of great importance. Hence, good control on the repetition of filling layers is required. Less control is required for mixed filling, since this is a natural occurring segregation. However, mixed filling and core flow results in the most negative size output, because discharge produces completely separated sizes. Mass flow is not expected to occur in the Tepee, but brings remixing at the outlet and results in a good mixed size distribution, also for mixed filling.

6.2.2 Simulations with input

For simulations with input, the ratio between input rate and output rate defines the segregation and blending effects. Hereby the size of the input material is important to control, which is discussed below. The simulations that highlight these different ratios between input and output rate are Simulation C, D2 and H in *Section 5.3.2*.

Table 32: Impact on size distribution for simulations with input

Ratio of input and discharge	Input size	Impact on discharged size distribution
Input > output	Fines	Positive
	Coarse	Negative
	Ideal mix	Negative
Input = output	Fines	Negative
	Coarse	Neutral
	Ideal mix	Positive
Input < output	Fines	Positive in batch fill mode only
	Coarse	Neutral
	Ideal mix	Positive

Moments that the input rate is higher than the output rate, will fill the Tepee with more material and will thereby create a heap. Segregation mechanisms taking place in this heap, will cause the input material to segregate. This has a negative effect when the input is coarse or ideal mixed material, since the large material will end up near the walls of the Tepee and results in a segregated size distribution at discharge. An input of fines however, will create a layer of fines over the heap, which is beneficial for blending at the output.

A constant level in the Tepee is achieved when the input rate equals the output rate. In combination with the expected core flow, this results in a 'last-in, first-out' system. Hence, in this scenario it is positive to feed the ideal mix into the Tepee, since this flows directly through the stockpile into the AG mill. Secondly, this may be a beneficial scenario the feed coarse material into the Tepee, however this may lead to a lack in coarse material at a later stage and therefore labelled neutral. Finally, the feed of fine material is not recommended, since this will fill the AG mill with only fines, giving trouble reaching a high throughput of the mill.

Scenarios where the input rate is lower than the output rate result in the formation of a crater and eventually in a complete discharge of the Tepee. Feeding fines is not recommended, unless the stockpile is filled using the mixed filling method and the coarser, stagnant material is discharged at that specific time. For only at that specific moment remixing will result in a good size distribution for the mill. Feeding coarse material in this scenario is in general positive; however, this may lead to a lack in coarse material at a later stage. Therefore, this is labelled neutral. The best feed to use is an ideal mix, since there is no segregation in this scenario and thus an ideal mix will be discharged.

7 Conclusion

The aim of the project was to obtain understanding of the material behaviour in the Tepee of Tara Mines. This goal was achieved by the use of the discrete element modelling package EDEM. This chapter presents the conclusions on this study and the simulations.

RQ 1.1 What are the simulation particle properties that result in appropriate bulk behaviour?

Calibration of the material properties in the discrete element modelling software is essential to acquire correct behaviour of the bulk material. The material properties in Table 33 result in appropriate behaviour of the bulk material. The bulk density is 1650 kg/m³, the resulting angle of repose is 37 degrees and the static wall friction angle is 23 degrees.

Table 33: Material properties in EDEM after calibration.

EDEM parameter		Ore	Wall
Shear modulus	[Pa]	1e8	1e8
Poisson's ratio	[-]	0.25	0.25
Density	[kg/m ³]	2750	2750
		Ore-ore	Ore-wall
Rolling friction coefficient	[-]	0.1	0.1
Restitution coefficient	[-]	0.3	0.3
Static friction coefficient	[-]	0.25	Low = 0.25 High = 1.0

RQ 2.1 Is it applicable to model a 3D slice to represent a full 3D simulation?

The 3D slice in simulation II.c proves to be a good representation of a full 3D model. Therefore, a 3D slice is very well applicable to represent a full 3D simulation in order to save calculation time.

RQ 2.2 Is it applicable to model single sized coarse particle to represent all size fractions?

Modelling single sized coarse particles is applicable to represent all size fractions. It is shown by simulation V that the location of particles is dominant over modelling of particle sizes. Hence, the use of single sized coarse material is an applicable measure to save calculation time.

The following paragraphs highlight the optimal way to operate the Tepee in order to achieve an ideal size distribution during discharge. This is done first by answering the research questions RQ 3.1 and RQ 3.2 in short. Secondly, conclusions are given on the optimal size distribution in scenarios with input in the stockpile.

RQ 3.1 What is the flow mode in the stockpile?

The expected flow mode in the stockpile is core flow. Under specific conditions (described in the next paragraph), also core flow results in a good size distribution during discharge. However, it is shown by simulation II.a en III.c that a mass flow in the stockpile results in a more optimal size distribution than core flow. Measures that may not be feasible but result in mass flow mode are steep wall angles and low wall resistance.

RQ 3.2 What is the size distribution during discharge of the stockpile?

The size distribution during discharge depends on the method of filling and on the flow mode. To achieve the optimal size distribution during discharge, batch filling of the stockpile is recommended. Batch filling in general provides a good blended size distribution. It should be mentioned that this is slightly dependent on the size of the batches (or the thickness of layers formed in the Tepee). The other method of filling, mixed filling, only results in the ideal size distribution when the stockpile operates in mass flow mode. This is not likely to take place at Tara Mines, since mass flow is not the expected flow mode.

In the following paragraphs, conclusions are given on the scenarios with input in the stockpile during the discharge.

The angles of withdrawal define the live capacity of the stockpile. Steeper angles of withdrawal reduce the live capacity of the stockpile. This increases the predictability, since fresh material reaches the outlet even faster in the 'last-in, first-out' system. However, the smaller live capacity reduces the effective storage capacity of the stockpile.

High fill levels increase the load on the material, which increases the angle of withdrawal. Hence, the withdrawal angles are steeper at the moments that the input rate is higher than the output rate. In addition, steep wall angles of the stockpile contribute to steeper withdrawal angles and thus a smaller live capacity.

The measures to control the material flow inside the Tepee are: the input and output rate and the size of the input material. Combinations of these parameters therefore are very important. The impact on the discharged size distribution is shown in Table 34.

Table 34: Impact on size distribution for simulations with input

Ratio of input and discharge	Input size	Impact on discharged size distribution
Input > output	Fines	Positive
	Coarse	Negative
	Ideal mix	Negative
Input = output	Fines	Negative
	Coarse	Neutral
	Ideal mix	Positive
Input < output	Fines	Positive in batch fill mode only
	Coarse	Neutral
	Ideal mix	Positive

The input of fine material is positive when the input rate is higher than the discharge and in batch fill mode at a high output rate. Inputting only coarse material is either negative or neutral, since this may lead to a lack in coarse material at a later stage. The input of an ideal blend is mostly beneficial and therefore recommended, except when the input rate exceeds the discharge rate and causes heap segregation.

The optimal way to operate the Tepee is not influenced by an outlet splitter. The resulting size distribution is not influenced. However, different flow rates in the discharge chutes show to have a minor influence on the size distribution, since different core flow regions are formed. This asymmetric discharge splitter, provides a minor control parameter in the stockpile. The size discharge is not significantly influenced by asymmetric filling, although the material flow inside the modelled stockpile is strongly influenced. A disruption in the discharge mainly causes negative effects on the resulting size distribution, especially when fines are fed during the disruption.

All these conclusions together improve the understanding of the material flow in the Tepee and its resulting size distribution. This may help to optimise the use of the Tepee by predicting the discharged size distribution.

8 Recommendations

Recommendations derived from the work in this thesis are presented in two steps.

1. Recommendations on the modelling
2. Practical recommendations for Tara Mines

The following recommendations that are related to the discrete element modelling may be considered to enhance the work in this study.

- **Simulation validation by particle tracking**
The current simulations are validated by literature research and major visual observations that confirm core flow. However, details of the flow inside the stockpile is still relatively unknown. Particle tracking at Tara Mines and comparing the path and the residence time with the simulations may improve the confidence of these simulations
- **Simulations with a complete size distribution**
A boundary in the simulations is the use of three sizes to represent the full size distribution. This neglects the effect that may be caused by fines smaller than <30mm. Simulations are recommended to confirm that the cohesion and stickiness of the ore by particles smaller than <30mm may be neglected.
Measures are taken to use a representative particle shape, however it is recommended to carry out simulation to measure the influence of particle shape.
- **Particle calibration with laboratory tests**
Calibration of the particle properties in this study is done by a limited number of parameters. Therefore, it is recommended to carry out laboratory tests on the ore to find particle and bulk properties. Subsequently these properties may be calibrated in the simulations again. Laboratory tests to considerate are: particle friction (by e.g. Jenike's shear cell test) and angles of repose and withdrawal tests. Where possible, also wall friction tests may be carried out.
- **Included a discharge system in the simulations**
In the current simulations, the discharge system is not included in the scope of this work. The bulk material is discharged purely on gravity. Simulations using a complete discharge system (chutes, feeders and conveyors) may show a reduction of the flow velocity in the core of the simulated stockpile.

Practical recommendations are given on the way of operating the Tepee and to enhance the controllability of the Tepee. The following practical recommendations may be considered.

- **The recommended filling mode is batch filling**
The results and the discussion highlight that the best method of filling is batch filling. In order to control the feed and achieve batch filling some size separation measures and storage capacity is required. This provides a new possibility for Tara Mines; controlling the size of material that feeds the Tepee.
- **Measure the size of the input**

Installing an online measurement system on the Tepee feed creates the possibility to relate the incoming feed with the discharged material (measured with the current system at the AG mill feed). This may provide accurate data whether enough coarse material is mined and how this influences the flow in the Tepee.

The relation in size distributions of incoming and outgoing material would increase the predictability of the mill feed.

- Timing the moment to discharge material with a surplus of fines
There are moments for Tara Mines that are suitable to feed the Tepee with fine particles (slimes). The best moment to feed the Tepee with fines is at a high fill level, when a heap is formed. Feeding fines at this moment creates a layer of fines over the heap, which will be blended due to the core flow.

References

- Anderson, I.K., Ashton, J.H., Boyce, A.J., Fallick, A.E., and Russell, M.J., 1998. Ore depositional processes in the Navan Zn-Pb deposit, Ireland. *Economic Geology*, Vol. 93(5), p.535-563.
- Andrew C.J. and Ashton J.H., 1985. The regional setting, geology and metal distribution patterns of the Navan orebody, Ireland. *Transactions of the Institution of Mining and Metallurgy*. Vol. 94(B) p.66-93
- Ashton, J.H., 1995, Guide to the geology of the Navan orebody. In: Anderson, et al. (eds). *Irish carbonate-hosted zn-pb deposits: society of economic geologists guidebook series*, Vol.21, p.151-168
- Ashton, J.H., Holdstock, M.P., Geraghty, J.F., O'Keeffe, W.G., Martinez, N., Peace, W., and Philcox, M.E., 2003. The Navan Orebody—discovery and geology of the South West Extension., In: Kelly, J.G., Andrew, C.J., Ashton, J.H., Boland, M.B., Earls, G., Fusciardi, L., and Stanley, G., (eds), *Europe's Major Base Metal Deposits: Irish Association for Economic Geology*, p. 405-436.
- Ashton, J.H., Blakeman, R.J., Geraghty, J., Beach, A., Collier, D.W., Philcox, M., Boyce, A.J., Wilkinson, J.J., 2010. The giant Navan carbonate-hosted Zn-Pb deposit – A review. In: Archibald, S.M., (eds), *Zinc 2010: Extended Abstracts Volume*. Cork: Irish Association for Economic Geology. 139pp.
- Chung, Y.C. and Ooi, J.Y., 2008. A study of influence of gravity on bulk behaviour of particulate solid. *Particology*, Vol.6(6), p.467-474.
- Comminution Technology JV, 2010. *Lab: Determining particle flow calibrations*. [online] Available at: <<http://www.conveyor-dynamics.com/rocky%20files/Rocky%20Particle%20Calibration%20Supplement.pdf>> [Accessed 24 June 2012]
- Crida, R.C., 1995. *A machine vision approach to rock fragmentation analysis*. Ph.D. University of Cape Town. 234pp
- Cundall, P.A. and Strack, O.D.L., (1979). A discrete numerical model for granular assemblies. *Géotechnique*, Vol. 29(1), p.47-65
- DEM Solutions, 2010. *EDEM 2.3 user guide*. [Commercial technical operators manual]. Edinburgh. 139pp
- DEM Solutions, 2011. *EDEM 2.4 user guide*. [Commercial technical operators manual]. Edinburgh. 142pp
- DEM Solutions, 2008. *DEM Solutions training: EDEM technical overview*. [Commercial technical training]. Rev. 2.1/2 Edinburgh
- Elert, G., 2005. *The physics textbook: Coefficient of friction for steel*. [online] Hyper textbook. Available at: <<http://hypertextbook.com/facts/2005/steel.shtml>>
- Enstad, G.G. and Mosby, J., 1998. Segregation of particulate solids in silos. In: C.J. Brown and J. Nielsen ed. 1998. *Silos: Fundamentals of theory, behaviour and design*. London: E & FN Spon. Ch.3.5. 836pp

- Filterworld, 2005. *Filtration Technical Page*. [online] Available at: <<http://www.filterworld.co.uk/tech.html>> [Accessed 10 May 2012]
- Gupta, A. and Yan, D.S., 2006, *Mineral processing design and operations: An introduction*, Amsterdam: Elsevier BV. 718pp
- Gilbert Gedeon, P.E., 1994. *Design of sheet pile walls*. Continuing Education and Development, Inc. [online] Available at: <<http://www.cedengineering.com/upload/Design%20of%20Sheet%20Pile%20Walls.pdf>> [Accessed at: 16 May 2012]
- Holdich, R.G., 2002. *Fundamentals of particle technology*. Loughborough: Midland Information Technology and Publishing. 173pp
- Janelid, I. and Kvapil, R., 1966. Sublevel caving. *International Journal of Rock Mechanics and Mining Sciences and Geomechanics*. Vol 3(2). p.129-132
- Janssen, H.A., 1895. Versuche über Getreidedruck in Silozellen, *Zeitschr. d. Vereines deutscher Ingenieure* 39, p.1045-1049
- Jenike, A.W., 1961. *Gravity flow of bulk solids*, bulletin 108, Utah Engineering Experiment Station, University of Utah. p.307-309
- Jenike, A.W., 1964. *Storage and flow of solids*, bulletin 123, Utah Engineering Experiment Station, University of Utah, 20th printing revised 1980. p.194-198
- Jenike & Johanson, 2010. *Functional Design of Silos, Bins, Hoppers*. [online] Available at: <<http://www.jenike.com/Services/Engineering/FunctionalDesign/Silo-Hopper-Design.html>> [Accessed 07 June 2012]
- Jha, A.K. and Puri, V.M., 2009. Percolation segregation of multi-size and multi-component particulate materials. *Powder Technology*, Vol. 197(3), p.274-282
- Kaartinen, J. and Tolonen, A., 2008. Utilizing 3d height measurement in particle size analysis. In: *Proceedings of the 17th IFAC World Congress*, Seoul, Korea: International Federation of Automatic Control, Vol. 17(1)
- Lane, G.S. and Siddall, G.B., 2002. SAG Milling in Australia: Focus on the Future Metallurgical Plant Design and Operating Strategies. *Metallurgical Plant Design and Operating Strategies*. Sydney, Australia, April 15-16, 2002. Sydney, Australasian Institute of Mining and Metallurgy
- Maerz, N.H., 2001. Automated Online Optical Sizing Analysis. In: Mular, A.R. and Barrett, D.J. (eds) *Proceedings International autogenous and semiautogenous grinding technology 2001, Vol 2*. Vancouver, 30 Sep-3 Oct p.250-269
- Martínez, M.A., Alfaro, I. and Doblaré, M., 2002. Simulation of axisymmetric discharging in metallic silos. Analysis of the induced pressure distribution and comparison with different standards. *Engineering Structures*. Vol. 24(12), p.1561–1574
- McBride, A. and Powell, M., 2006. A structured approach to modelling sag mill liner wear – numerical modelling of liner evolution. In: Mular, A.R. et al (eds), *Proceedings International autogenous and semiautogenous grinding technology 2006*, Vancouver, Sep. 24-27, Published CIM, p.120-132

- Mc Cabe, A., 2010. *Boliden Tara Mines Annual Environmental Report 2009*. Submitted by: Boliden Tara Mines Limited, Environmental department. 71pp. [Online] available at: <http://www.epa.ie/licences/lic_eDMS/090151b280367357.pdf> [Accessed 16 March 2012]
- Merkus, H.G. 2010. *Particle Size Measurements: Fundamentals, Practice, Quality*. New York: Springer. 536pp
- Metcalf, J.R., 1965. Angle of repose and internal friction. *International Journal of Rock Mechanics and Mining Sciences*. Vol. 3, p.155-161
- Mindlin, R.D. and Deresiewicz, H., 1953. Elastic spheres under varying oblique forces. *Journal of Applied Mechanics*. Vol. 20, p.327-344
- Mitchell, C.J., Mitchell, P. and Pascoe, R.D., 2008. Quarry fines minimisation: can we really have 10mm aggregate with no fines? In: Walton, G., (ed.) *Proceedings of the 14th Extractive industry geology conference*. Cardiff: EIG Conferences, 25-27 June 2008, p.37-44, 109pp
- Morrell, S., 2004. A new autogenous and semi-autogenous mill model for scale-up, design and optimisation. *Minerals Engineering*, Vol. 17(3), p.437-445
- Moys, M.H., 1993. A model of mill power as affected by mill speed, load volume, and liner design. *Journal of the South African Institute of Mining and Metallurgy*, Vol. 93(6), p.135-141
- Napier-Munn, T.J., Morrell, S., Morrison, R.D. and Kojovic, T., 1996. *Mineral Comminution Circuits: Their Operation and Optimisation*. Brisbane: Julius Kruttschnitt Mineral Research Centre. 413pp
- Noy, M.J., 2006. The latest in on-line fragmentation measurement - stereo imaging over a conveyor. In: *Proceedings of the Eighth International Symposium on Rock Fragmentation by Blasting*, Santiago: Fragblast 8, p.61-66.
- OpenStreetMap, 2012. Tara Mines, 53°39'13.94"N, -6°43'11.19"W, transport map layer. [Online] available at: <<http://www.openstreetmap.org>> [Accessed 2 August 2012]
- Peace, W.M. and Wallace, M.W., 2000. Timing of mineralization at the Navan Zn-Pb deposit: A post-Arundian age for Irish mineralization, *Geology*, Vol. 28(8) , p.711-714
- Peace, W.M., Wallace, M.W., Holdstock, M.P. and Ashton, J.H., 2003. Ore textures within the U lens of the Navan Zn-Pb deposit, Ireland, *Mineralium Deposita*, Vol. 38(5), p.568-584
- Petermann, L., 2010. *Bulk materials handling*. By: FAM Team of authors. English ed. FAM Förderanlagen Magdeburg. 144pp
- Philcox, M.E., 1984. *Lower Carboniferous lithostratigraphy of the Irish Midlands*. Dublin: Irish Association for Economic Geology, 89pp
- Rizzi, G., 1992. *The sedimentology and petrography of Lower Carboniferous limestones and dolomites; host rocks to the Navan zinc-lead deposit, Ireland*. Ph.D. University of Glasgow, 369pp
- Roberts, A.W., Wiche, S.J. & Krull, T., 2009. Optimising the live capacity of gravity reclaim stockpiles. *Australian Bulk Handling Review*. February 2009. p.72-76

Santamarina, J.C. and Cho, G.C., 2004. Soil Behavior: The Role of Particle Shape. *Advances in Geotechnical Engineering: The Skempton Conference*, Jardine, R.J., Potts, D.M. and Higgins, K.G. (eds), 29-31 March 2004, London, p.604-617

Schulze, D., 1998. Measurement of the flowability of bulk solids. In: C.J. Brown and J. Nielsen ed. 1998. *Silos: Fundamentals of theory, behaviour and design*. London: E & FN Spon. Ch.2.2. 836pp

Schulze, D., 2008. *Powder and bulk solids: Behavior, characterization, storage and flow*. English ed. Berlin: Springer-Verlag. 516pp

Split Engineering, 2010. *Split-Desktop: Version 3.0 Help Manual*. [software manual] Split Engineering, LLC. 116pp

Schwedes, J., 1998. Flow patterns. In: C.J. Brown and J. Nielsen ed. 1998. *Silos: Fundamentals of theory, behaviour and design*. London: E & FN Spon. Ch.3.1. 836pp

Valery, W., Morrell, S., Kojovic, T., Kanchibotla, S.S. and Thornton, D.M., 2001. Modelling and simulation techniques applied for optimisation of Mine to Mill operations and case studies, *VII Southern Hemisphere Meeting on Mineral Technology*, Rio de Janeiro, Brasil. p.107-116 [online] available at: <[http://www.metso.com/miningandconstruction/mct_service.nsf/WebWID/WTB-120117-22576-74168/\\$File/115.pdf](http://www.metso.com/miningandconstruction/mct_service.nsf/WebWID/WTB-120117-22576-74168/$File/115.pdf)> [Accessed 12 July 2012]

Wills, B.A. and Napier-Munn, T.J., 2006. *Wills' Mineral Processing Technology: An Introduction to the Practical Aspects of Ore Treatment and Mineral Recovery*. 7th ed. Oxford: Elsevier Ltd. 444pp

Unpublished data accessed through Tara Mines repository

Ashton, J.H., 2011. *Mine Geology Department Handout*. Guide on the geology, mine geology and the resource estimations at Tara Mines

Boliden Tara Mines and Boliden TG, 2011. Internal documentation of Boliden Technical Group and Tara Mines on the fragmentation project. May 2011

Helsinki University of Technology, 1997. *The physical properties of rock at Tara Mines*. Internal documentation Tara Mines providing geotechnical data

Mc Connell, P., 2011. *Tara Mines Mine Engineering Department Handout*. Guide on the mining method, production and the backfill process at Tara Mines

Pentony, J., 1991. *Report of Rock Mechanics Tests to Tara Mines Ltd*. Internal documentation Tara Mines providing rock properties of Pale Bed ore

Tara Mines intranet, 2011. Unpublished Tara Mines archive with images and photos

Personal communication

Mc Connell, P., 2012. *Area Planning Engineer*. Mine production and operation. Blast fragmentation, optical size measurement and the mill feed size requirements. [conversation January-February 2012]

Plunkett, B., 2012. *Chief Mine Engineer*. Operation of the mine. Discussion on the underground ore handling system and the operation of the stockpile Tepee. [conversation January-February 2012]

Rice, C., 2012. *Process Engineer*. Introduction and discussion on mill geometry and mill feed size requirements. [conversation January-February 2012]

Appendix A: Paper

Modelling of material flow and size distribution of ore in a stockpile at Tara Mines, Ireland

E.J. Dolman¹, M.W.N. Buxton² and D.L. Schott³

Abstract

This study aims to understand the material behaviour of ore inside a coarse ore stockpile by discrete element modelling. This is of importance since the stockpile is the last stage to control the size distribution of ore in the ore handling system before feeding the grinding circuit. An optimal size distribution is required for efficient grinding in an autogenous grinding (AG) mill.

To investigate the material behaviour in the stockpile this work focussed on the flow mode inside the stockpile and the size distribution during discharge. The individual particle characteristics are important to apply in the modelling; hence the discrete element method is very well suited for this type of modelling due to its distinct particle character. In this work the discrete element package used is EDEM, which is a discrete element modelling package developed by the commercial company DEM Solutions.

In order to study this aim, several measures in the modelling were taken. The size distribution was divided into the three important sizes, as they are determined by the AG mill. Fines are sized 30mm, pebbles are 80mm and coarse particles are 130mm. A calibration of the parameters of these particles was carried out in order to acquire the correct bulk density, angle of repose and static wall friction of the material in the simulations. Furthermore, an effective simulation model was found by the application of two measures. Firstly, the use of a 3D slice instead of a full 3D simulation showed good results. The second measure was to simulate only coarse sized material to represent each of the particles sizes, which also proved to be very well applicable.

Based on segregation mechanisms two different methods to fill the stockpile were determined; batch and mixed filling. The influence of these filling methods was simulated for different flow modes in order to review the impact on the discharged size distribution.

It was found that the best suitable mill feed was obtained by batch filled stockpiles, especially since core flow was the expected flow mode. Furthermore, it was found that the ratio between input and output rate has a significant impact on the size distribution at the discharge, since this ratio determines whether there is a 'last-in, first-out' system. High input rates result in heap formation, which leads to segregation of coarse sized material. Therefore, at a high input rate it is advised to feed finer material. Feeding of coarser material at moments with a low input rate result in a more optimal size discharge, then when this is done at moments with high input rate.

-
1. Delft University of Technology – Resource Engineering
 2. Delft University of Technology – Resource Engineering
Stevinweg 1, 2628 CN Delft, The Netherlands Email: m.w.n.buxton@tudelft.nl
 3. Delft University of Technology – Transport Engineering and Logistics
Mekelweg 2, 2628 CD Delft, The Netherlands Email: d.l.schott@tudelft.nl

Introduction

This work studies the material flow and particle size distribution in a coarse ore stockpile. The stockpile functions as a buffer between the underground mine and the grinding circuit, where it stores coarse zinc/lead ore. The coarse ore is crushed underground to below 150mm and is stored into the stockpile at surface level (Figure 120). The stockpile directly feeds the grinding circuit, therefore the stockpile is the last stage that controls the size distribution before the material enters the autogenous grinding (AG) mill.

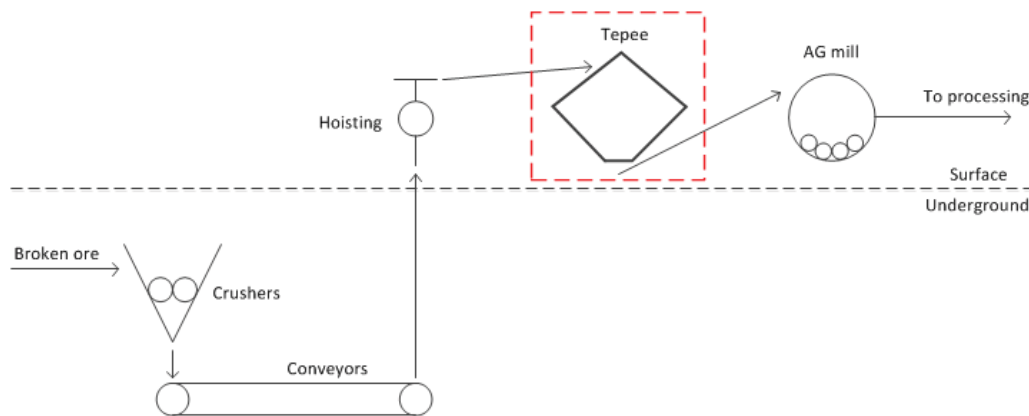


Figure 120: Flow chart of the ore handling system with the stockpile in the red box

The size distribution of the AG mill feed is important, since the grinding medium in autogenous grinding is the ore itself. Hence, the size distribution determines the efficiency of grinding. Generally, three size fractions in the feed of an AG mill are distinguished; fines, pebbles and coarse. The size of ore and the required amounts are taken from unpublished data from a typical Irish style carbonate hosted zinc deposit. In this work, fines are particles smaller than 50mm. Pebble sized material is also called the critical size, since this is the most difficult fraction to grind. The pebbles are too small to grind others and too large to be efficiently ground themselves. The pebbles tend to accumulate in the mill and block the throughput. In this work the pebbles size is 50-100mm and the feed should not contain more than 50% of this fraction, where less is preferred. The third fraction is the coarse sized material. This coarse fraction is needed for impact crushing. Ideally, the feed should provide large enough lumps to generate kinetic energies that are high enough to break smaller rocks and thus to overcome trouble with the critical size fraction. The coarse size fraction is material above 100mm, where the mill requirement is set at $P_{80} > 130\text{mm}$.

Flow in stockpiles

The stockpile that feeds the AG mill is the last step in the ore handling system that controls the size distribution that enters the mill. Due to segregation, a uniformly sized filling of a stockpile is not probable. Therefore, the flow mode is one of the main factors influencing the size distribution during discharge. Several method regions of flow have been distinguished; Brown and Hawksley in 1947 (as quoted in Swedes, 1998) and Kvapil in 1966 (as quoted in Janelid and Kvapil, 1966) defined different region visually. The first to define the material flow quantitatively by the properties of the bulk solid and the storage bin was Jenike (1961). Jenike defined two flow modes; core flow and mass flow (Figure 121). In mass flow (a), all material is moving at relative same velocities, also the material close to the wall. This causes a first-in, last-out system. Core flow (b and c) causes a 'last-in, first-out' system, since the material in the core has a higher velocity and is discharged before the material close to the walls (called the stagnant zone).

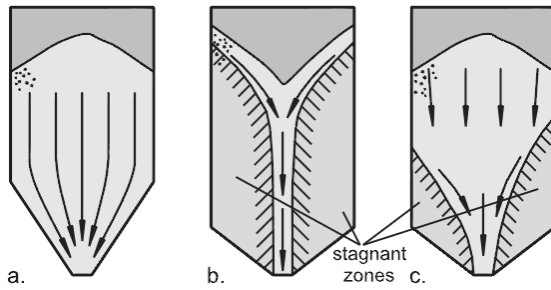


Figure 121: Flow profile: (a) mass flow, (b) funnel flow with stagnant zones to the top of filling (piping), (c) combination of mass and funnel flow (low stagnant zones) after Schulze (2008)

Two goals are set to gain understanding of the material flow in the stockpile by modelling. The first goal is to determine the flow mode in the stockpile. The second goal is to determine the size distribution during the discharge of material. The influence of stockpile geometry, filling methods and the ratio between in- and output rate on these two goals was researched.

To simulate the stockpile accurately, the particle properties were calibrated first by small bulk simulations. Subsequently an effective model was created, by using a slice and single sized particles. The applicability of these measures is reported later in this work.

Discrete element calibration and parameters

Discrete element modelling can be used to model the material flow in the stockpile. The discrete element solves Newton's second law of motion $F = m \cdot a$ for every contact between elements. Detailed description of the discrete element method can be found in Cundall (1979).

This work has been carried out using the software package EDEM version 2.4.1 by DEM Solutions. The default contact model in EDEM was used; the Hertz-Mindlin no-slip contact model. This contact model is based on the work of Mindlin and Deresiewicz (1953), where the contact between particles is modelled using sets of springs and dashpots and a friction slider (as pictured in Figure 122).

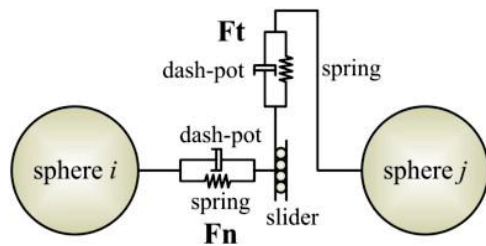


Figure 122: Contact model using springs, dashpots and friction slider (Chung and Ooi, 2008)

Each calculation step assigns the particles to a grid and thereby measures the overlap between the geometric elements. This overlap is used to calculate the friction and damping in between the particles, using the spring and dashpot modelling in both normal and tangential direction. Contact damping is modelled as dashpots and is related to the coefficient of restitution. The tangential force is limited by the Coulomb friction law, and therefore related to the static friction coefficient. The rolling friction of a particle is accounted for by applying a torque to the contacting surfaces. The applied torque is a relation between the normal force, particle radius and angular velocity and the coefficient of rolling friction.

Material

Actual material properties

The required parameters in this contact model are the shear modulus, Poisson's ratio and the contact coefficients and finally the size and mass of the particles. The shear modulus, Poisson's ratio have been determined by Tara Mines in laboratory tests. The contact coefficients (restitution, static friction and rolling friction) are calibrated for by DEM modelling of the bulk characteristics. An overview of the real particle properties in this work is given in Table 35.

Table 35: Particle and bulk properties of ore and the AG mill size requirement

Particle			Size [mm]	AG mill requirement
Sphericity [-]	0.5	Fines	<50	none
Roundness [-]	0.4	Pebbles	50-100	As low as possible, ≤ 50%
Shear modulus [GPa]	23	Coarse	>100	P80 >130mm
Poisson [-]	0.2			
Density [kg/m ³]	2750			
Bulk				
Angle of repose [deg]	37			
Density [kg/m ³]	1650			

DEM calibration of material properties

Although DEM is widely used, the success of the simulations relies on the correct setting of particle properties and particle interactions to reflect realistic bulk behaviour. DEM simulations are always an approach of reality. This work calibrates the material properties by two bulk characteristics; the bulk density and the angle of repose.

The bulk density of the material is the weight of the particles in a volume including the open voids. It is stated by Schulze (2008) that a bulk material the open space between particles takes around 40% of the volume for spherical particles. The particle density was measured extensively of which an average gives the particle density of 2750 kg/m³. Thus, the bulk density is assumed to be 60% of this: 1640 kg/m³. In DEM calibration test for the bulk density a box of known size is filled with particles to measure the bulk density. Calibration with a single sphere particle of small size (15mm) results in the assumed bulk density of 1640 kg/m³. The simulation shows that for large single sphere particles the bulk density drops slightly, which is most likely caused due to looser packing of particles near the wall. The simulation for 5-sphere particles shows a steeper decrease in bulk density, than for single spherical particles. This is caused by the irregularity of the particles, which creates large open voids. The difference between the theoretical estimate and the modelled bulk density is very small (1%). Therefore, a modelled particle density of 2750kg/m³ is a good approximation of reality.

The angle of repose is a measure for the flowability of the bulk material. A major parameter influencing the flowability of the bulk is the shape of the particles, e.g. a perfect sphere will roll and flow more easily. Irregular shaped particles are constructed using overlapping spheres in a cluster. The relation between the number of spheres and the angle of repose is tested, where it should be mentioned that a high number of sphere requires more calculation time. The result shows that the angle of repose increase for the number of sphere. After four or more spheres in a cluster, the angle of repose settles between 37-38 degrees. A good approximation of the actual 37 degree angle of repose is achieved when using a particle build up from 5 spheres.

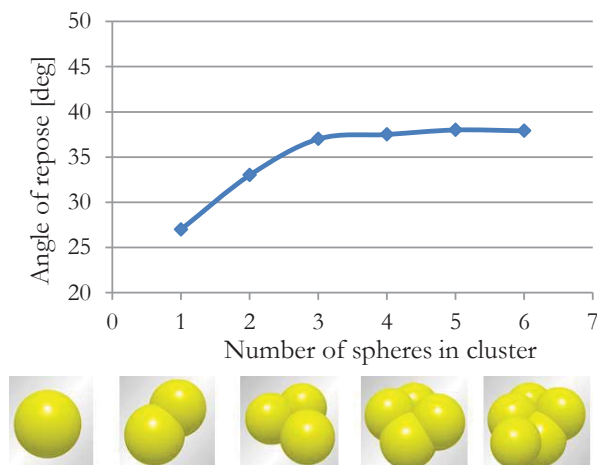


Figure 123: Angle of repose for the number of spheres in a cluster

The angle of repose is also used to calibrate the DEM parameters; shear modulus, Poisson's ratio and the interaction coefficients.

The calibration of shear modulus shows that lower moduli than the real sampled $2.3E+10$ Pa can be applied without influencing the angle of repose significantly. A suitable low risk value for the shear modulus is found at 10^8 Pa.

The Poisson ratio shows a slow increase in repose angle for higher Poisson's ratio. The value for the Poisson's ratio is calibrated at 0.25 very close to the sampled value of 0.2 to gain a repose angle of 37 degrees.

The three interaction coefficients are likewise calibrated using the angle of repose. The coefficient of restitution defines the velocity after a collision as part of the initial velocity. The calibration test shows that very low restitution coefficients (<0.1) results in an increasing angle of repose, due to the very low velocity after a collision. For higher coefficients the impact on the angle of repose is less, therefore the value of 0.3 is a good approximate.

The coefficient of rolling and static friction are influencing each other and have a significant impact on the angle of repose. The calibration test therefore varies the coefficients in relation to each other. Figure 124 shows that a 37 degree angle is found for a rolling friction coefficient of 0.1 in combination with a static friction coefficient of 0.25.

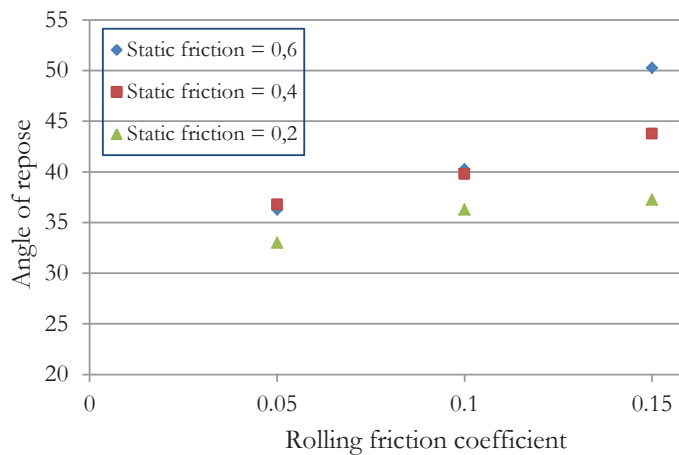


Figure 124: Rolling and static friction calibration for the angle of repose

The simulation to measure the angle of repose is repeated, to acquire the level of error in the measurements. The repeatability shows a standard deviation of 1.3 in the angle of repose for these calibrated parameters, as seen in Table 36.

Table 36: Results of repeatability test with the calibrated parameters

		10 simulations
Minimum angle of repose	[deg]	35
Maximum angle of repose	[deg]	39
Mean angle of repose	[deg]	37.2
Standard deviation	[deg]	1.3

Model

Particle size and shape

The particle size and shape are estimated in simulations. The particle shape is defined from representative particles. Based on the AG mill requirements, simplifications are made on the particle size (Table 37). The particle shape is identical for each particle size and constructed using 5 overlapping spheres; sphericity of 0.5 and roundness of 0.4. The separation in three distinct sizes may exaggerate changes in the particles size distribution, which makes identification of a change in the distribution more clear.

An overview of the parameters as they are retrieved from the calibration test is given in Table 37 together with the simplified particle size fractions as they are used in the DEM modelling.

Table 37: Overview of the DEM calibrated parameters and the simplified DEM model size fractions

Calibrated DEM parameter	Value	Unit
Density	2750	kg/m ³
Particle build-up	5	Spheres
Shear modulus	10 ⁸	Pa
Poisson's ratio	0.25	-
Coefficient of restitution	0.3	-
Coefficient of rolling friction	0.1	-
Coefficient of static friction	0.25	-

	Actual data		Simplified DEM model	
	Size [mm]	Mill requirement	Size [mm]	Fraction in ideal mix
Fines	<50	none	30	25%
Pebbles	50-100	As low as possible, ≤ 50%	80	50%
Coarse	>100	P80 >130mm	130	25%

Filling method

The location of the particles after feeding in the stockpile in combination with the flow mode defines when the material is discharged and thus the size distribution during discharge. There are two different methods of filling distinguished in this work. These filling methods define the location of particles after feeding. The first method is mixed filling, where a (ideal) mixed product is fed into the stockpile. Due to natural occurring heap segregation, different regions are formed with a surplus of fines, pebbles and coarse (Figure 127). The second method is batch filling, whereby size segregation has occurred before filling. This may be caused by different types of ore as well as segregation in the underground ore handling. The filling is simulated as a sequence of batches of fines, pebbles and coarse material (Figure 126).

Mix filling

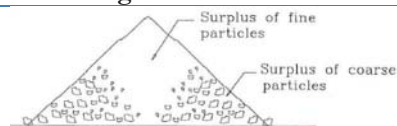


Figure 125: Heap segregation (Enstad and Mosby, 1998)

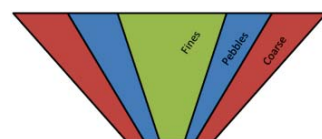


Figure 127: The Tepee filled with mixed filling method

Batch filling



Figure 126: The Tepee filled with batch filling method

Methods to reduce calculation time

The discrete element method solves Newton's second law of motion for every contact between elements. This may result in very long calculation times when many particles are used. Several measures were taken in the modelling to reduce the calculation time as listed below. Most measures reduce the number of spheres in the model.

- Reduction of stockpile size
- Simulation of a 3D slice
- Modelling three sizes representing a full size distribution
- Application of only large material, representing all sizes
- Reducing EDEM parameters: spheres per cluster and the shear modulus

Three combinations of model domain size and particle type were used in the modelling. The amount of particles in each model shows the degree of reduction.

3D model with single coarse sized particles	Particles: 33,000+
3D slice model with actual fines, pebbles and coarse	Particles: 127,000+
3D slice model with single coarse sized particles	Particles: 6,000+

Simulation setup

The simulations in this work use the DEM parameters as shown in Table 37. Furthermore, substantial reductions are made to the size of the stockpile in order to reduce computational power (Table 38). The wall angle of the stockpile is normally 45 degrees, unless stated differently.

Table 38: Dimensions of the actual stockpile, the reduced DEM model and in the DEM slice

	Tepee at Tara Mines	DEM model	DEM slice model
Capacity [t]	30,000	170	15-16
Diameter [m]	45	7.5	7.5 (0.8m slice width)
Wall angle [deg]	45-60	45 or 60	45 or 60
Outlet size [m]	4.5	1.3 or 0.8 or 0.5	1.3 or 0.8 or 0.5

Figure 128 shows an example of the DEM model and Figure 129 shows an example of the DEM slice model, both with mixed filling. An example of the DEM slice model is also shown with batch filling in Figure 130.

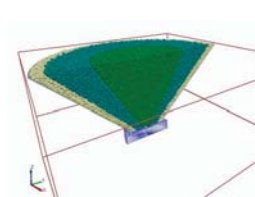


Figure 128: 3D model with mixed filling, only one half is displayed

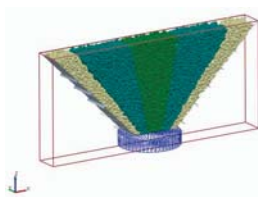


Figure 129: 3D slice model with mixed filling

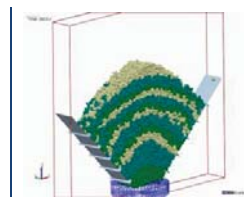


Figure 130: 3D slice model with batch filling

Simulation results and discussion

The results in this work are given using size distribution graphs. These graphs show the size distribution over the discharged tonnes of material. Furthermore as a reference the mill requirement is given for each particle size.

Results of the development of an effective DEM model

This chapter shows the results on the development of an effective simulation model by two simulation measures. Firstly, the application of a 3D slice and secondly the use of single sized material to represent the fines as well.

3D slice

A representation of a full 3D conical stockpile is found in simulating a wedge-shaped slice. The slice has periodic boundaries in y-direction on the virtual walls and the thickness of the slice is 6 times the diameter of the largest particles to maintain the three dimensional flow behaviour. It is found that the wall resistance in a wedge-shaped slice needs to be higher to achieve a similar core flow as in full 3D conical stockpile (Figure 131 and Figure 132). This wall resistance is found best representative when friction plates are used. These small plates perpendicular to the stockpile wall holds particles attached to the wall and creates a natural friction plane of particles. The conical stockpiles model and the wedge-shaped with friction plates result in a very similar size distribution output, caused by the first-in, first-out system due to core flow. This proves good representative use of a wedge-shaped slice.

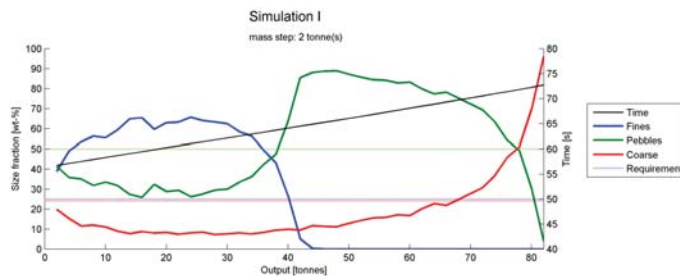


Figure 131: Size distribution graph of a full 3D conical stockpile

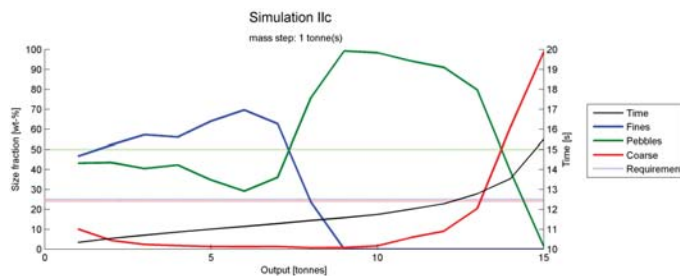


Figure 132: Size distribution graph of a wedge-shaped slice model

Single sized coarse particles

Another measure in the model to reduce computational power is to use large sized particles that represent the fines, pebbles and coarse. These simulations have a low wall resistance and therefore result in mass flow mode (Figure 133 and Figure 134). The results show very similar size distribution graphs, which legitimates the use of large particles to represent all sizes. It shows that the location of particles is dominant over modelling particle sizes in these simulations.

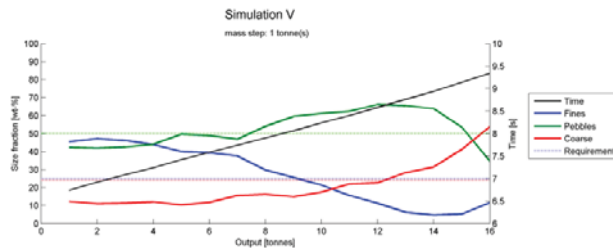


Figure 133: Size distribution graph of the model using 'real' fines, pebbles and coarse

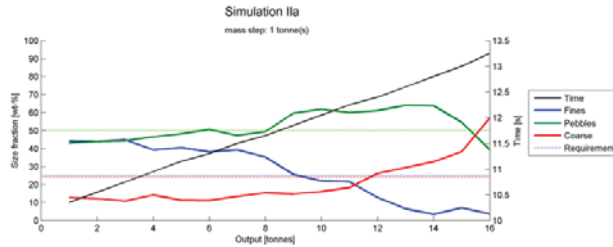


Figure 134: Size distribution graph of the model using only coarse sized material to represent fines, pebbles and coarse

Results of stockpile simulations

The understanding of the flow mode and the size distribution during discharge is acquired by three simulations. First the impact of the wall angle, secondly the different filling methods and finally influence of input during the discharge of the stockpile.

Impact of wall angle

Figure 135 shows the size distribution graph of a 60 degree wall model and is best compared with Figure 132 II.c. Both graphs models have identical properties except for their wall angles. It is noticeable that the steeper wall angle shows a combination between core flow and mass flow. The first part of output shows a mix of fines and pebbles, similar to the blending of mass flow discharge. The second part of the output results in separated sized, due to the stagnant material in core flow. This creates an intermediate stage between mass and core flow, which is the transition in the design graphs of Jenike (1961). In order to reach the AG mill requirement the model with 60 degree walls is slightly better, however the coarse fraction is still discharged separate.

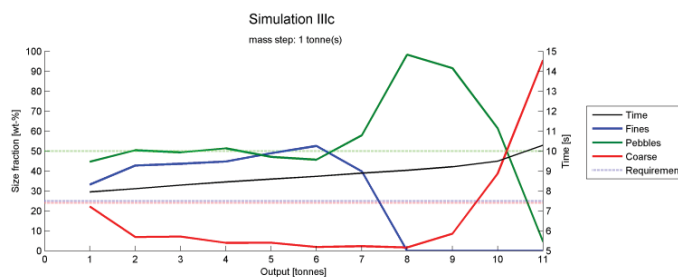


Figure 135: Size distribution graph of a 60 degree wall model

A more optimal discharge of material is achieved when the material is batch filled instead of mix filled. The batch filled model is shown in Figure 136 and the identical simulation with mixed filling is shown in Figure 132 II.c. In combination with core flow mode, the layering in batch filling the size results in a repetition of the size fractions. Over a period of discharge, this may

deliver the required size distribution in case the layers are thin enough. After 12 tonnes of discharge, the size distribution is in very good agreement with the required size distribution. It is concluded that batch filling is the best method of filling in a core flow environment.

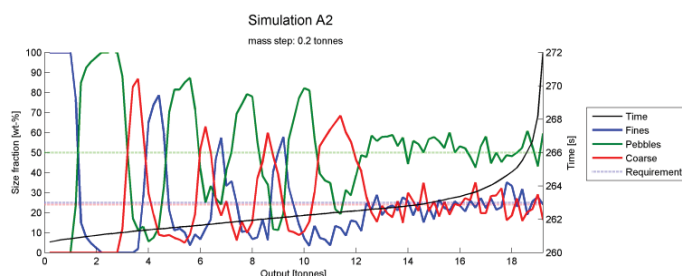


Figure 136: Size distribution graph with batch filling under core flow conditions

Impact of input/output ratio

In an operating stockpile the input and discharge rate are not constant, which influence the flow. Three scenarios are distinguished and modelled; input rate higher than the output rate, equal in- and output rate and a scenario with higher output rate than input rate. In the model, the input rate is controlled by the rate of particle creation and the discharge rate is controlled by the size of the outlet.

Moments that the input rate is higher than the output rate, fill the stockpile with more material and thereby create a heap. Segregation mechanisms taking place in this heap, will cause the input material to segregate. Feeding with coarse and mixed size material has a negative effect on the discharged size distribution, since the coarse material ends up close to the wall due to heap segregation. A finer input however, creates a layer of fines over the heap, which is beneficial for blending at the output.

A constant level in the stockpile is achieved when the input rate equals the output rate. In combination with the expected core flow, this results in a typical 'last-in, first-out' system. Hence, in this scenario it is positive to feed the ideal mix into the stockpile, since this flows directly through the stockpile into the AG mill. Feeding of coarse material may be beneficial in this case, however this may lead to a lack in coarse material at a later stage. Feed fine material is not recommended, since this fills the AG mill with only fines, giving trouble reaching a high throughput of the mill.

Scenarios where the input rate is lower than the output rate result in the formation of a crater and eventually in a complete discharge of the stockpile. Feeding fines is not recommended, since this is immediately discharged as a result of core flow. In the very specific case that a mixed filled stockpile is almost empty and in core flow mode the coarse stagnant material is discharged, mixing at the outlet may result in the required mill size distribution. Feeding coarse material in this scenario is in general positive; however, this may lead to a lack in coarse material at a later stage. The best feed to use is an ideal mix that meets the mill requirements, since there is not much segregation in this scenario and thus an ideal mix will be discharged as well.

Conclusion

The flow mode that provides an optimal size distribution during discharge is mass flow mode. However, the flow mode in the Tepee is expected to be core flow. Measures that may result in mass flow mode are steep wall angles and low wall resistance.

Batch filling in general provides a good blended size distribution, but is dependent on the size of the batches. Only in a mass flow system, mixed filling method is well suited.

The angles of withdrawal define the live capacity of the stockpile. Steeper angle of withdrawal reduce the live capacity of the stockpile. This increases the predictability, since fresh material reaches the outlet even faster in the 'last-in, first-out' system. However, the smaller live capacity reduces the effective storage capacity of the stockpile.

High fill levels increase the load on the material, which increase the withdrawal angle. Hence, the withdrawal angles are steeper at this that the input rate is higher than the output rate. In addition, steep wall angles of the stockpile contribute to steeper withdrawal angles and thus a smaller live capacity.

The input of fine size material is positive when the input rate is higher than the discharge and in batch fill mode at a high discharge rate. Inputting only coarse material is either negative or neutral, since this may lead to a lack in coarse material at a later stage. The input of an ideal blend is mostly beneficial and therefore recommended, except when the input rate exceeds the discharge rate and causes heap segregation.

References

- Chung, Y.C. and Ooi, J.Y., 2008. A study of influence of gravity on bulk behaviour of particulate solid. *Particology*, Vol.6(6), p.467-474.
- Cundall, P.A. and Strack, O.D.L., (1979). A discrete numerical model for granular assemblies. *Géotechnique*, Vol. 29(1), p.47-65
- DEM Solutions, 2011. *EDEM 2.4 user guide*. [Commercial technical operators manual]. Edinburgh. 142pp
- Enstad, G.G. and Mosby, J., 1998. Segregation of particulate solids in silos. In: C.J. Brown and J. Nielsen ed. 1998. *Silos: Fundamentals of theory, behaviour and design*. London: E & FN Spon. Ch.3.5. 836pp
- Janelid, I. and Kvapil. R., 1966. Sublevel caving. *International Journal of Rock Mechanics and Mining Sciences and Geomechanics*. Vol 3(2). p.129-132
- Jenike, A.W., 1961. *Gravity flow of bulk solids*, bulletin 108, Utah Engineering Experiment Station, University of Utah. p.307-309
- Mindlin, R.D. and Deresiewicz, H., 1953. Elastic spheres under varying oblique forces. *Journal of Applied Mechanics*. Vol. 20, p.327-344
- Schulze, D., 2008. *Powder and bulk solids: Behavior, characterization, storage and flow*. English ed. Berlin: Springer-Verlag. 516pp
- Schwedes, J., 1998. Flow patterns. In: C.J. Brown and J. Nielsen ed. 1998. *Silos: Fundamentals of theory, behaviour and design*. London: E & FN Spon. Ch.3.1. 836pp

Appendix B: Tara Mines

Introduction

Boliden Tara Mines is located in Ireland and the mine site is located 50km away from the capital city Dublin (see Figure 138). The Navan zinc-lead orebody neighbours the town of Navan, Co. Meath, where the underground workings pass directly under river Blackwater, public roads, residential areas and agricultural land, as displayed in Figure 137.



Figure 137: Aerial view of the mine location; orebody is given brighter and town of Navan is located on the right (Tara Mines intranet, 2011 *unpublished*)

A survey by the Irish Agricultural Institute published in 1968, highlighted zinc and lead trace element anomalies in stream sediments just west of Navan. In 1969, the Tara Exploration & Development Co Ltd, a Canadian company, began exploring for mineral deposits in the region. A year later, a shallow soil geochemical survey discovered very high levels of lead and zinc in the area around the river Blackwater. Where after an extensive diamond drilling programme commenced, which indicated an orebody of almost 70 million tonnes at a grade of 10.1% zinc and 2.6% lead; the largest zinc-lead deposit of Europe.

Diamond drillings carried out in the 90s discovered two new ore lenses to the southwest of the mine, which added 18 million tonnes to the resource. This area is known as the South West Extension or SWEX. In addition, an extra 1 million tonnes was found to the northwest of the original orebody and is called the Nevinstown area. The total initial size of the deposit is now over 105 million tonnes.

The mine started development in 1973, by driving tunnels into the orebody and constructing production shafts. Production of the underground ore commenced in 1977. Since then the mine has changed ownership a number of times. In the early 1980s Noranda, a Canadian mining company, was the major stakeholder of the mine. The Finnish company Outokumpu bought into Tara Mines in 1986 and became the full owner in 1989. Since 2004, Tara Mines is part of the Boliden Group, which is a Swedish mining and smelting company.

Since the start of production, Tara Mines has been an important employer in the region. Currently around 690 permanent employees are working together with contractors. Indirect employment is estimated up to three times the direct employment.

Geology

Tara Mines is located within the Navan deposits that are found a kilometre northwest of the town of Navan in the country of Meath. The Navan deposit is the largest of several zinc-lead orebodies of the Irish Midlands and is found in Lower Carboniferous limestones and dolostones. It forms part of the Dublin basin and have been classified 'Irish Type'. The Irish deposits are a variety of carbonate-hosted zinc/lead deposits and are very similar to the Mississippi Valley-type deposits (Peace and Wallace, 2000). They differ however in having more copper, silver and iron than most MVTs and are therefore named 'Irish Type'.

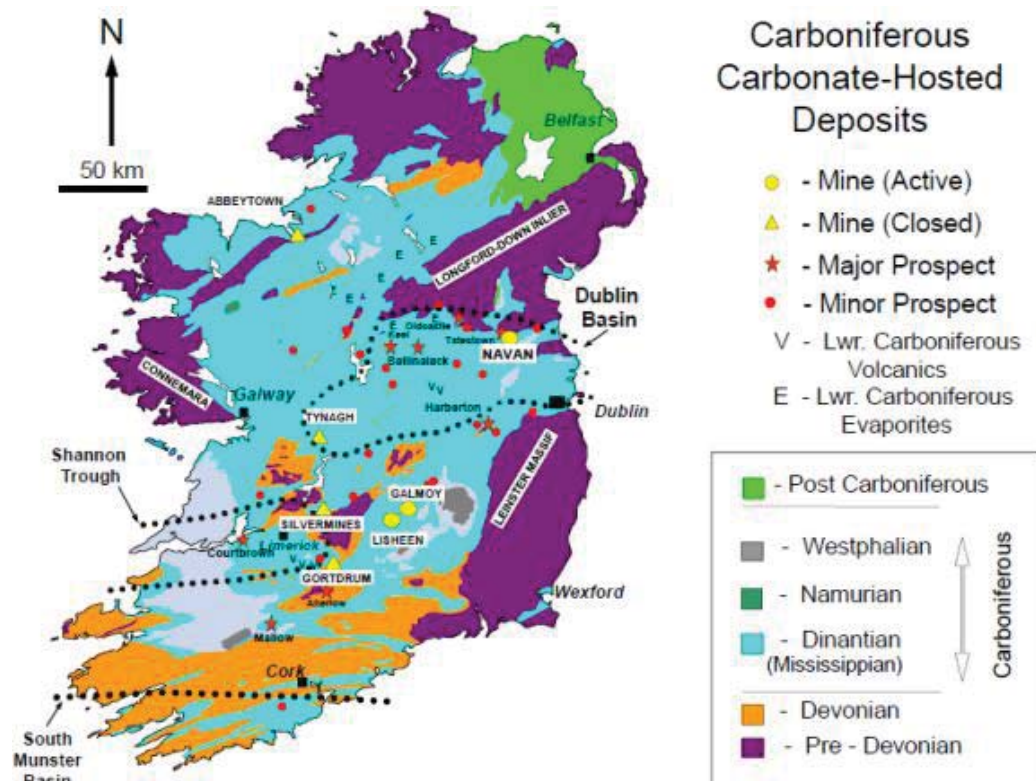


Figure 138: Simplified geological map of Ireland, showing the location of Carboniferous Limestone, hosted orebodies and prospects (Tara Mines intranet, 2011 unpublished)

Regional geology

The Lower Palaeozoics are structurally complex and unconformably underlie the Lower Carboniferous, by the group called Navan Group. The orebody occurs within Lower Carboniferous limestones ranging in age from Courceyan to Chadian (360 – 345 Ma) and are generated in a tropical climate, see Figure 139 (Ashton et al., 2003).

The transition from the alluvial Lower Palaeozoics to the first shallow-marine sediments is indicated by the oldest Carboniferous layer, called the Red Beds. The Red Beds are overlaid by two shallow-marine sediments; Laminated Beds and Muddy Limestone. The Muddy Limestone is the first carbonate horizon of significance. These rocks are thought to be of shallow marine lagoonal origin but, to the west of the mine, limestone conglomerates occur as channel deposits and cut into the underlying Laminated Beds sequence (Rizzi, 1993)

The Navan orebody is hosted by the Pale Beds, which are lying upon the Laminated Beds. These Pale Bed sediments are formed in a shallow-marine environment producing a varied sequence of carbonates, dolomites and subordinate sandstones and shales (Anderson et al., 1998). The majority of ore (97%) is hosted by the Pale Beds (Anderson et al., 1998). This mineralisation occurs in several stratigraphic intervals, reaching up to vertical thickness of 120 metres. The bulk of the main orebody is composed in a series of mineralised lenses, which dip between 15 and 20 degrees to the southwest. The Pale Beds have been interpreted as being deposited in gradually deepening water in a high-energy carbonate ramp or broad tidal belt environment (Andrew and Ashton, 1985).

In the main orebody, the ore lenses are numbered in ascending order; 5 being the lowest and 1 being the highest. To the southwest, economic mineralisation has also been delineated in a higher stratigraphic level in the Pale Beds, referred to as the 'U lens' (Peace et al., 2003).

The ongoing transgression of the environment is proven by the presence of the overlying Shaley Pales limestones; an indication of deeper water conditions (Ashton, 1995). The Shaley Pales are overlain by another limestone; the Argillaceous Bioclastic Limestone Group (Philcox, 1984), with the Waulsortian Limestone Formation scattered through this formation. In more southern parts of the Irish Midlands this limestone is the host rock of mineral deposits like Lisheen and Galmoy.

Substantial parts of the Courceyan succession have been removed in Chadian. The unconformity forms the 'Erosion Surface' and is overlain by a debris-flow breccia-conglomerate. The remainder of the ore (<3%) at Navan is hosted by this Boulder Conglomerate, that overlies the southward-sloping submarine erosion surface (Ashton et al., 2003). The Boulder Conglomerate varies in thickness between 1m and >50m.

The Boulder Conglomerate is regionally overlain by a thinly bedded mudstone of up to 20m in thickness. This is called the Thin Bedded Unit and is mainly found in the southeast of the Navan deposit. Together with the Thin Bedded Unit the Boulder Conglomerate is overlain by a thick sequence of well-bedded limestone, known as the Upper Dark Limestones. The Upper Dark Limestones ranges in age from late Chadian to Asbian (Ashton et al., 2003)

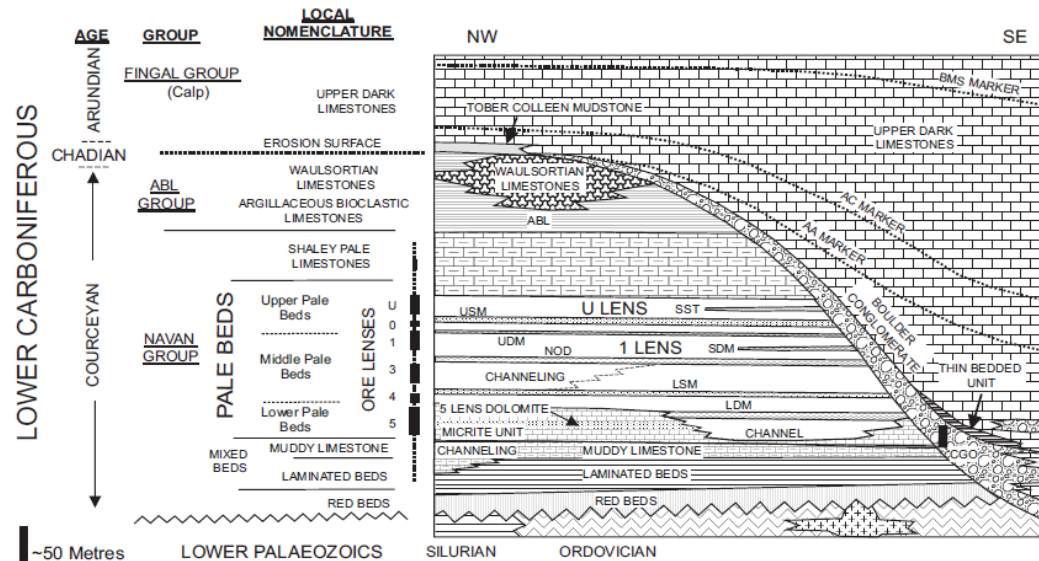


Figure 139: Schematic image of stratigraphic column in the Navan mine area (Peace et al, 2003)

The Orebody

The orebody mined at Tara Mines consists of the following areas: the Main Orebody, the extension in the southwest (SWEX), Liscartan and Nevinstown (Peace et al., 2003). The mineralisation of the rocks was caused by the flow of hydrothermal fluids through the normal faults and along the bedding planes, intersecting the basement structures at the north west of the Dublin Basin (Anderson et al., 1998). The main constituents from the ore are sphalerite and galena, with generally subsidiary amounts of pyrite, marcasite, barite, dolomite, calcite and rare sulphosalts. Ore within the Pale Beds can be characterised by low iron content and a fine grain size (Anderson et al., 1998).

Mineralisation in the Main Orebody is most developed near the base of the Pale Beds (ore lenses 1 to 5), while in the SWEX mineralisation is found in the Upper Pale Beds in ore lens U (Ashton et al., 2010). The ore lenses 1 to 5 generally have a dip of 15 to 20 degrees to the southwest. In the north-eastern part of the mine this dip can increase up to 45 degrees. The vertical thickness of the orebody can be as thick as 200 metres in the Main Orebody and flattens out in the Southwest Extension.

There are major faults dividing the orebody into three zones (see Figure 140). Zone 1 is found north of the B-fault. Zone 2 is in between A, B and T. Zone 3 includes a small zone in the southeast between the A- and C-fault, furthermore zone 3 includes all areas south of the T-fault that are also known as SWEX.

The Nevinstown orebody is an extension northwards of the Main Orebody, from which a crown pillar of 30 metres will remain as major support. It outcrops at surface and steeply dips below the river Blackwater into the Main Orebody. The Liscartan orebody is smaller in size and is found northwest of the main orebody.

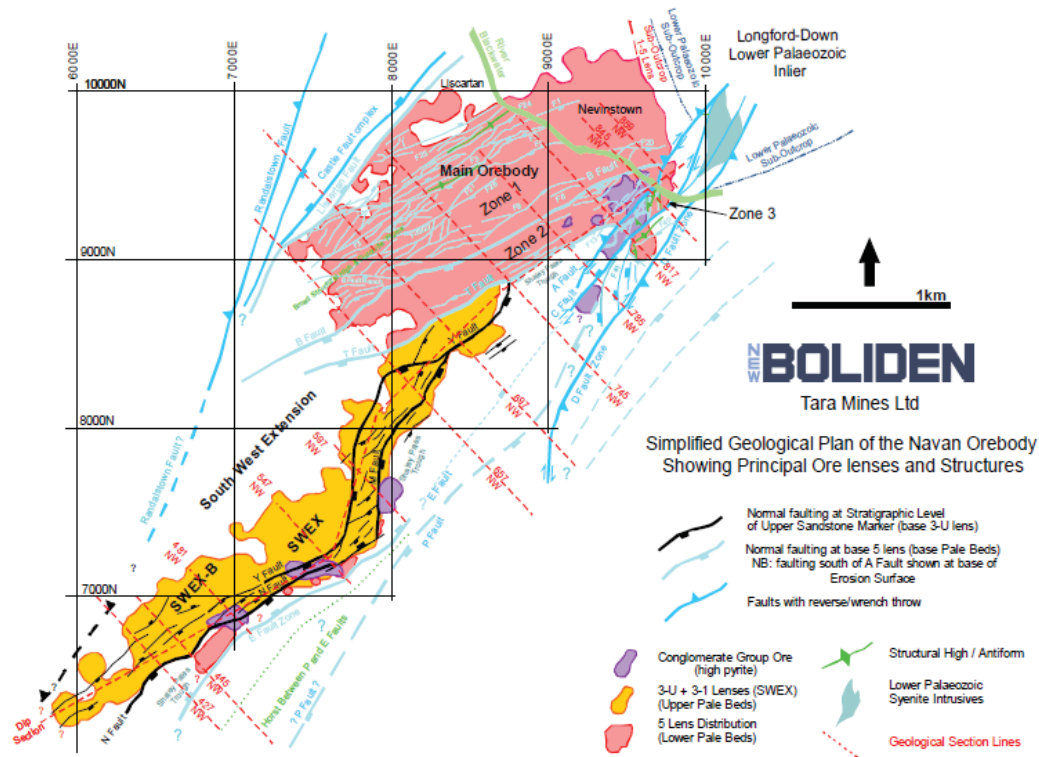


Figure 140: Simplified geological plan of Navan Orebody, showing main ore lenses and faulting (Tara Mines intranet, 2011 unpublished)

Mine geology: reserves and resources

Surface drilling, underground diamond drilling, stope outlines and technical-economic studies define the mineral reserves and mineral resources in the orebody. For their reserves and resources, Tara Mines uses an in-house classification system and the JORC classification system for external reporting. These classification systems are both shown in Figure 142.

Initial exploration is followed up in areas with ore-grade mineralisation by surface drilling in a 60-180m spaced grid. This surface drilling is used to delineate Inferred and locally Indicated Resources. Parts of these resources may be transferred to Probable Ore Reserves after technical-economic studies.

The next step in resource estimation is the underground diamond drilling from hanging walls in fans with a spacing of 20-25m. This drilling information defines the amount of Indicated Resource. After the design of long-term mining blocks, access drifts, provisional stope outlines and permitting, these Indicated Resources may become Probable Reserves.

By completion of the in-stope development, diamond drilling spacing is reduced to 10-15m. This data together with final stope outlines and blasts lines, defines the Measured Resources and the Proven Reserves.

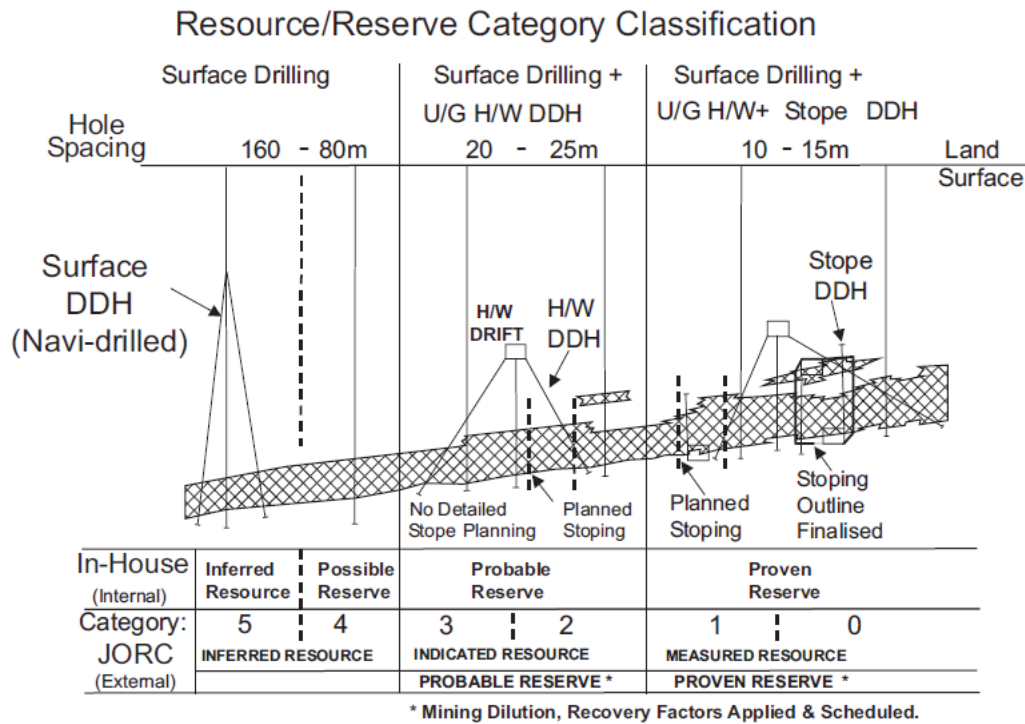


Figure 141: Representation of the in-house and JORC resource and reserve classification (Ashton, 2011 unpublished)

Figure 142 shows the JORC classification of mineral resources and reserves at December 31st, 2010. At the end of 2010 the mine had produced 75.7 Mt grading 8.2% zinc and 1.9% lead. The annual production rate reaches 2.7Mt, or 9,500 tonnes per day. The Mineral Resource cut-off is more than 4Mt at a grade of >5% zinc and lead combined. The Ore Reserve cut-off is more than 5Mt.

JORC Mineral Resources (undiluted)				JORC Ore Reserves (diluted, recoverable, scheduled)			
	Mt	Zn %	Pb %		Mt	Zn %	Pb %
Measured	0.3	7.8	1.9	Proven	3.5	8.3	2.0
Indicated	4.6	6.8	2.1	Probable	12.5	6.8	1.7
Measured + Indicated	4.9	6.9	2.1	Total Ore Reserves	16.0	7.1	1.8
Inferred	7.0	7.3	1.8	The Ore Reserves are additional to the Mineral Resources			
Total Mineral Resources	11.9	7.1	1.9				

Figure 142: JORC classified mineral resources and ore reserves at 31st December 2010 (Ashton, 2011 unpublished)

Mining cycle

The underground rock is excavated using conventional mining in a cycle of drilling, charging, blasting and excavating. Blasted ore is mucked and hauled by LHDs (Load Haul Dump machines or scoops) to drawpoints. Broken waste is mostly dumped into empty stopes. When distances between mucking at the face and dumping at drawpoints became long, a dumptruck is used. The LHD mucks out the rock and loads the dump truck, which hauls the rock and dumps it at the drawpoints.

Several mining methods are used, though they all use drilling and blasting. The reason for using various mining methods is mainly due to geological constraints, but also due to the function of the openings. The function of the openings could be development or production. The development mining only uses the driving of tunnels using drilling and blasting. The production mining uses a few methods. The main production method used is stope and pillar mining and applies to roughly 90% of the production. Stopes are sequenced with pillars. Backfilling is applied to make pillar extraction possible. When the valuable ore covers only 6 metres in height a similar method, drift and slash, is used. Drift and slash produces less tonnage and therefore only is feasible when the grade of ore is relative high. Another method used is room and pillar mining. This is used for selective mining in small areas and with a medium height. Higher costs of operating limits the use of the room and pillar method, but due to the flattening of the orebody in SWEX this method is used more often nowadays. Since stope and pillar mining is the main method applied in production, only this production method is discussed together with the development mining cycle.

Exploration and main development is generally done in waste rock or low-grade ore. Exploration and main development is scheduled at 4000 metres per year and stope development is planned at 9500 metres per year. The yearly extraction rate of ore from development is 25% of the total at 800 ktonnes (Mc Connell, 2011 *unpublished*). The major 75% is mined in production (stope mining) at 1800 ktonnes per year (Plunkett, 2012 *personal communication*).

Development

Development is the driving of drifts at gradients close to horizontal (maximum inclination of 15%). Mine development extends the mine, constructs an access to the orebody and creates access to mine infrastructure. Exploration and main development drifts are constructed in either waste rock or ore, to create initial access to mining blocks. Stope development is done in the mineable ore and creates access for drilling, blasting and mucking from stopes and pillars.

Depending on the intended use and the location, the dimension of the tunnel may vary. A typical stope production drift is 4.7m wide and 5.0m high (Mc Connell, 2012 *personal communication*). This is slightly smaller than a typical haulage drift of 5.6m wide and 5.5m high, due to the trucks that need to travel through the haulage roads.

The development of drifts is done by drilling the drift face with two-boom electric hydraulic drilling jumbo. This jumbo typically drills 55-60 blast holes per drift face with a diameter of 45mm (Mc Connell, 2011). The same jumbo drills four relief holes to create open space for the blast. The advance made with each drill and blast cycle is approximately 4.5 metres. Significant improvements are made with the use of modern Atlas Copco Boomer drill rigs in accuracy and efficiency. These drill rigs are able to position by use of laser guidance and drift coordinates can be uploaded by memory-card. More complex drifts (e.g. spiral ramps) are developed more accurate and low-grade ore from the over-break is reduced.

The blast holes are charged with a pumpable bulk emulsion explosive. The nonelectric delay detonators are inserted in a primer. The detonators are sequenced to break progressively outwards from the 'cut', which is formed by the first blastholes around the relief holes.

After each cycle of drilling, charging, blasting and mucking the drift is scaled and reinforced where necessary. Reinforcements used in the main drifts are a combination of rock bolts, mesh and shotcrete. In some areas with stable walls, only the use of fiber-reinforced shotcrete is sufficient.

Production

Production mining is the extraction of large quantities of the orebody in the most economical way. At Tara Mines, the production of stopes is mining in a vertical direction. Stopes and pillars are generally designed with the long axes close to parallel to the strike and/or principal stress of the orebody. This reduces the amount of footwall development in waste rock and allows a series of stopes to be accessed through drifts that are aligned along the dip of the orebody.

Production mining uses a similar cycle of drilling, charging, blasting and mucking as with development mining, but the equipment and the used method are essentially different. The blastholes are drilled upwards using a longhole drill (more than 80% of the stopes are only uphole). The modern longhole drills use navigational control to position the drill string via previous set orientation marks, which ensures accurate drilling. The explosives used to fill the long holes are a bulk emulsion, which are primed and initiated with non-electric detonators. The yearly amount of emulsion needed is 1.9 million kilos and one blast of 3-6 rings produces around 5,000 tonnes of broken ore (Mc Connell, 2011 *unpublished*).

After a blast, which takes place after the end of shift, the stope is ventilated out to remove blast fumes and dust. The broken ore is mucked using remote controlled scoops. The operator controls the LHD from outside the stope area. The mucked ore is dumped either directly at a drawpoint or loaded onto a 45 tonne dump truck.

Once a stope is completely blasted and mucked out the open void is surveyed with a laser scanner. The scan is analysed to know the amount of overbreak and underbreak to know the dilution and the loss of ore. After the scan is completed and analysed, it is also used to design the best parameter for backfill, such as backfill holes and the bulkhead.

A typical stope has a width between 13 and 20 metres (Mc Connell, 2012 *personal communication*). Stopes are designed on an individual basis to match the local geological features, including faults, joints and bedding planes. The height of a stope depends on the thickness of the ore. When the stope height exceeds 25 metres a hanging wall drifts is developed first, followed by downwards longhole drilling in the stope. The tonnage of a stope ranges from 5,000 to 50,000 tonnes (Mc Connell, 2011 *unpublished*).

A second cycle is used in production mining; the cycle of mining and backfilling of stopes and pillars. The stope and pillar method start with the excavation of a stope (primary stope), with two solid ore pillars on either side. The primary stope is backfilled with a cemented backfill and left to harden for a few months. The remaining ore pillars are extracted using the same mining method. The open void after mining the pillars is filled with weakly cemented waste rock. By extracting these pillars, almost 100% of the ore can be extracted.

A total of 120 separate stopes and pillars are scheduled for 2012 production. Due to the flattening ore body in the SWEX, the average stope size is only 18,000 tonnes (Mc Connell, 2011 *unpublished*).

Crushing and underground transportation

Broken ore from development and production areas reaches underground crushers via direct dumping or dumping at drawpoints. There are five underground crushers to reduce the size to a maximum of 150mm. All the crushers are jaw crushers and they differ in age and capacity (ranging from 350 to 1000 tonnes). The crushers are fed by storage hoppers, which are designed underneath the tips where trucks dump the ore. After crushing, the crushed ore is loaded on a conveyor.

The crushed ore is transported via several conveyors and storage bins to the skip hoist to bring the ore to surface. The layout of this ore handling systems is shown schematically in figure XX. In this figure, the technical detail around the #5 crusher is higher than for the other crusher installations. It should be mentioned that the figure is not to scale.

The newest crusher, number 5, is located in the SWEX area and therefore responsible for crushing of the majority of ore. Crusher #5 loads the crushed ore via two shorter, high capacity conveyors (5-1 and 5-2) to the post-crusher coarse ore storage bin. This bin is used as a buffer for the crusher in case of a breakdown. After this bin, the ore is loaded onto the 5-3 conveyor, which loads onto the 5-4 conveyor. This conveyor in its turn, loads onto the 4-1 conveyor.

The 4-1 conveyor is also loaded by the crusher ore from the #4 crusher. Via the 4-2 and 4-3 conveyor, the material is transported to the underground coarse ore storage bin (COB) at the base of the production shaft. The combined 4- and 5-system is only one of the conveyors loading to this 3,600 tonnes capacity coarse ore bin.

The other two conveyors feeding into the COB are the 1-1 conveyor and the 2-2 conveyor. The 1-1 conveyor is fed solely fed by the #1 crusher. The 2-2 conveyor is fed by both the #2 and #3 crusher systems. At the production shaft, the COB loads two short conveyors that feed the skips. The skip loading by the C1-C2 pocket loaders is done automatically at a rate of 570 tonnes per hour. The two skips are in balance and a single skip can hold 14 tonnes. Hoisting speed reaches up to 7.6 m/s. Through the production shaft, the ore is hoisted 365 metres up to surface, where a conveyor feeds to the surface coarse ore storage building called the Tepee.

All transfer points and crushing stations are monitored by PLC control and real time video cameras that are linked to the control rooms. After the crusher stations, magnets are placed above the conveyor to protect from scrap metal.

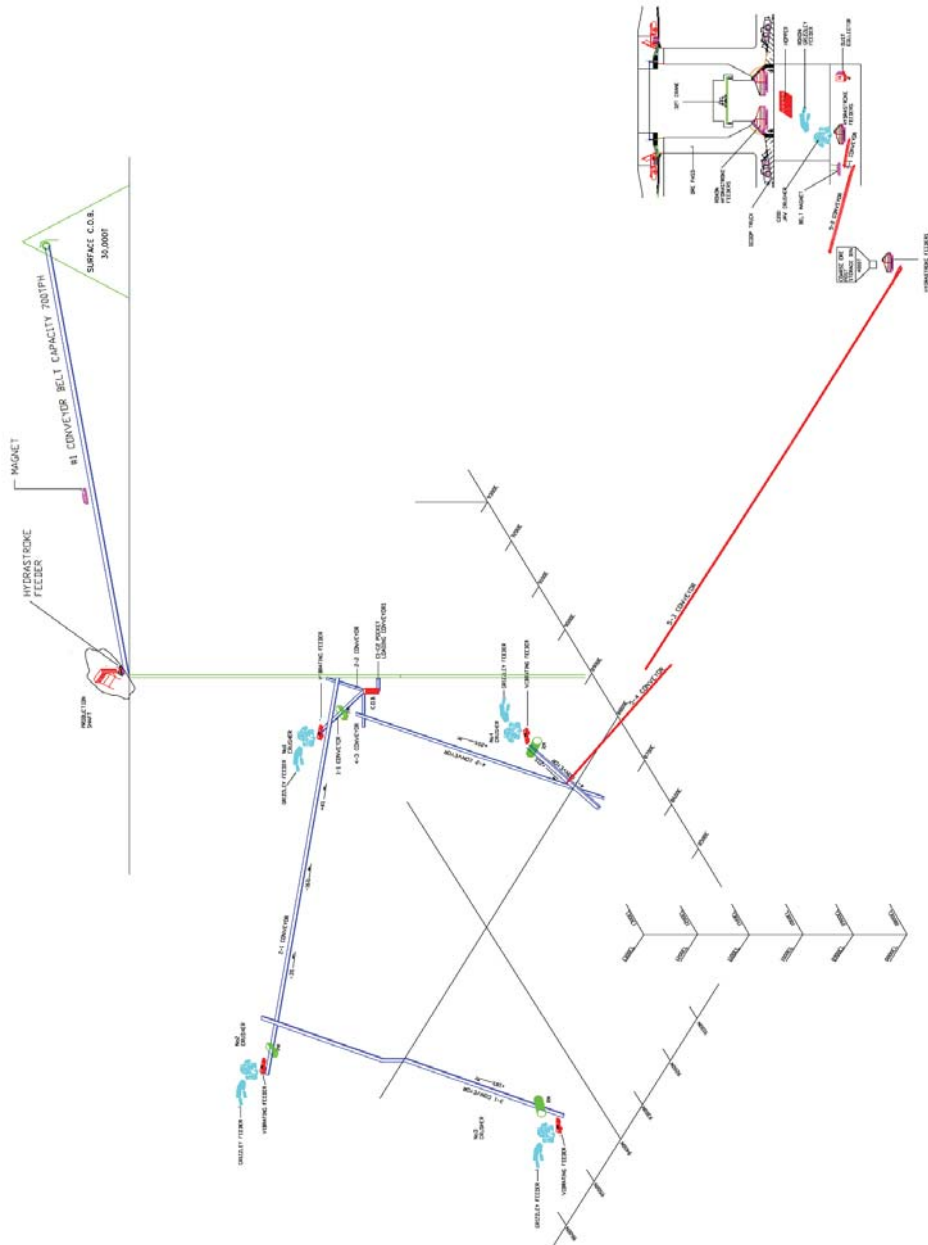


Figure 143: Schematic overview of the ore handling system at Tara Mines

Stockpile

The surface coarse ore storage building, called the Tepee, has a maximum capacity of 30,000 tonnes. The Tepee stores all run-off-mine ore before it enters the AG mill and thereby the Tepee functions as a buffer in case of downtime. The conical storage building is shown schematically in Figure 144.

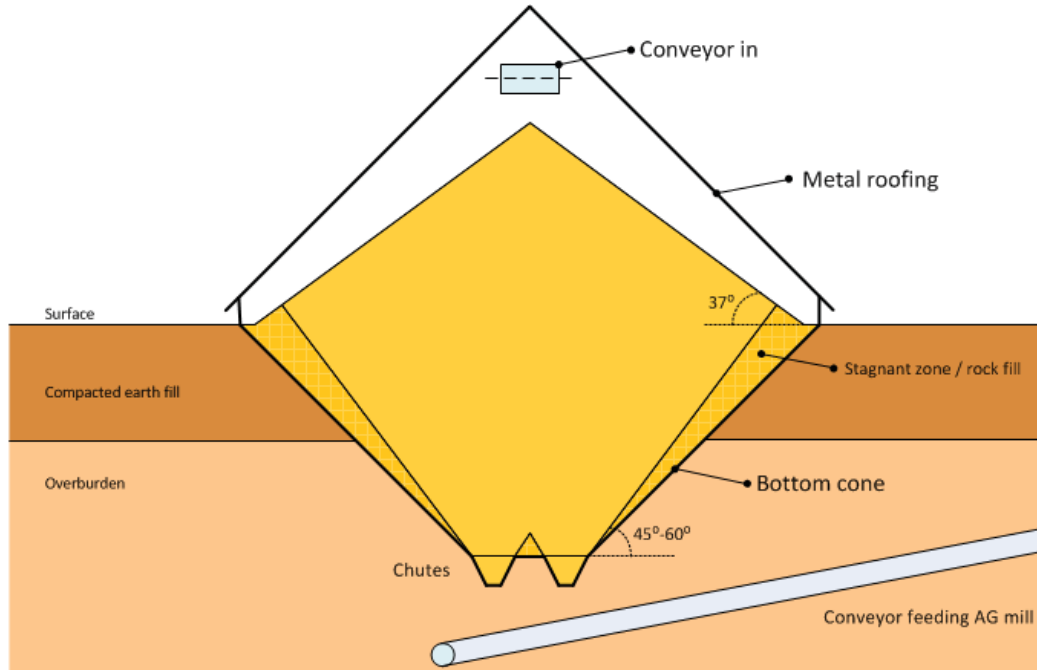


Figure 144: Schematic layout of the Tepee

The bottom half of the Tepee is a downward pointing cone, which is dug into the overburden to reduce the visual impact. The diameter of the cone is 45 metres and the walls are constructed at an angle of 45 degrees. Due to stagnant ore in the stockpile, this angle could reach up to 60 degrees. The conical bottom half has a height (or depth in this case) of 19 metres.

By filling of the stockpile a second cone is formed, inversely on top of the bottom cone (pointing upwards). This material is free flowing and not bounded by any of the walls or the roof. The conical roof gives the Tepee its characteristic shape. The metal roof with a height of 15 metres above surface is needed to reduce dust emissions.

After hoisting, the ore is dumped on the same conveyor belt. The ore enters the surface stockpile by this conveyor and is discharged centred in the top of the Tepee. At the bottom of the Tepee, four chutes are constructed, designed in a square. From these four chutes, two chutes are opened at the same time. This provides some control of the material flow in the Tepee. The chutes feed onto two short conveyor belts, where always one chute loads on one of these conveyors. These dual conveyors at the discharge are angled horizontally at 45 degrees to the incoming conveyor. The dual conveyors are loading on the same single conveyor that feeds directly into the autogenous grinding mill.

Processing

The processing plant at Tara Mines recovers the saleable concentrates of zinc and lead from the ore. The ore of Tara Mines not only contains zinc and lead, but also smaller amounts of less valuable metals. The separation and liberation of zinc and lead from the host rock is done by the grinding of ore, which is followed by a flotation circuit.

Processing of the run-of-mine ore starts with the grinding of ore to 80 weight percent below 75 microns. Grinding is done using an autogenous grinding (AG) mill, which uses the ore itself as a grinding medium. A small ball mill is used for the secondary grinding of pebbles sized material and is applied when necessary.

The AG mill was installed in 2009 as a replacement of the fine crushing and ball/rod mill grinding circuit. The diameter of the autogenous mill is 8.5 metres with an effective mill length of 9.5 metres. The AG mill has a throughput of more than 350 tonnes per hour and the mill is driven by two 4MW motors (Rice, 2012 *personal communication*). Since the mill is responsible for almost 50% of the total power consumption at Tara Mines (Mc Cabe, 2010), efficiency is of great importance. The efficiency of the mill is also important to achieve the annual throughput.

Water and chemical reagents are added to the mill feed. A 15 by 30mm grate is placed in the mill to let the fines pass and to reuse the oversize in the mill for grinding, since it is the grinding medium. The AG mill slurry discharge is typically 62% solids by weight. A spiral classifier is used to remove the coarse fraction, which is send back to the AG mill for regrinding. The fine fraction is send to the flotation circuit and now typically contains 45 wt.-% solids (Rice, 2012 *personal communication*).

In the flotation circuit, chemical activators and flocculants are added, to activate the flotation of lead first. In the froth flotation, the valuable minerals are carried to the top of the flotation cell by the air bubbles. The lead bearing froth is removed from the slurry, after which it is concentrated using a series of roughers and cleaners.

The remaining slurry is treated similarly, while using different additives to activate the zinc metal. Zinc metal froth comes to the top of the flotation tank after which it is removed. Both metal concentrates (respectively 67% lead and 56% zinc) are dewatered and brought to the rail transportation area. The zinc and lead concentrate are stored separately. A train brings the concentrates to the harbour, where it is shipped to preferably Boliden smelters in Norway and Finland.

When the valuable minerals have been recovered in the flotation circuit, the material remaining is known as tailings. From these tailings, the slimes and fine particles are removed using hydrocyclones and are pumped to the tailings pond. At the tailings pond the slimes settle out and clean water is recycled to the mine for varies purposes. The more coarse material remaining from the flotation process, called sand, is stored in tanks. Together with water and cement, this sand is added for a cemented backfill. The water, cement and sand mixture is pumped into the open stopes through boreholes. Over 1 million tonnes of tailings sand is used every year as backfill.

Fragmentation project

The replacement of the grinding circuit by the AG mill brings new requirements to the mined ore, due to the different method of grinding. Tara Mines experiences a need for coarse material to achieve efficient grinding. This section describes the requirement from the mill as well as the measurements that are taken to achieve an optimal size distribution. The current status of the fragmentation project is stated as well as which factors influence the fragmentation and not least important at what locations segregation occurs.

The AG mill is designed to reach a throughput of 360-390 tonnes per hour. The AG mill at Tara Mines has proven to grind most cost effective when: the feed rate (tonnes/hour) is constant and the particle size distribution is P80>130mm or P70>100mm.

A constant feed rate into the AG mill is required to maintain an even distributed mill load. The AG mill demands more energy when the mill load varies over time, because an increase in mill load demands extra energy to keep the mill rotating at a similar velocity.

An essential factor in autogenous grinding is the size distribution of ore. Since the grinding medium is the ore itself, there is a need for coarse particles in order to gain impact grinding. The size distribution is divided into the following three size fractions:

Table 39: Defined size fractions and the requirements by the AG mill

	Size [mm]	AG mill requirement
Fines	<50	none
Pebbles	50-100	As low as possible
Coarse	>100	P70 or 30% >100mm P80 or 20% >130mm

It should be stated that the names used for these size fraction are not conform literature, since fines are in general the size of a powder and given in micrometers. The fines (<50mm) do not form any problem in the AG mill. The problematic size fraction is the pebble size, which is why this size fraction is also called the ‘critical size fraction’. The particles are too small to deliver sufficient kinetic energy to be used as a grinding medium and they are too large to be broken (see *Section 2.1*). The coarse sized particles are all particles above 100mm. Although the crusher opening is set to <150mm, coarse particles up to 300mm may enter the mill from time to time. The coarse fraction is the essential fraction in an autogenous grinding mill, since this sizes make the particles an ideal grinding medium. At Tara Mines, the mill feed should contain 20% by weight of particles above 130mm. This is generally denoted as 80% passing a sieve size of 130mm; P80>130mm. Another coarse indication is P70>100mm, however a P80 is more commonly used.

Requirements of the AG mill are currently not met at Tara Mines. Although the mill feed can be delivered at a constant feed rate, the size distribution does not meet the requirements. Several indications (point down laser at the mill feed and some scarce image analysis) show that the main reason is that the feed does not contain an even distribution of the coarse material. An image analysis study as well as a newly installed 3D vision system at the AG mill show that coarse material is mined in substantial amounts. Therefore, it is assumed that the coarse material is not delivered as an evenly distributed size to the mill feed.

Current status of the fragmentation project

Tara Mines is working on a long-term fragmentation project to optimise the fragmentation. This fragmentation project is mainly initiated to optimise the particle size distribution for grinding. However, several other parameters are also taken into account; such as efficiency of operation and operational costs.

Previous work done on the fragmentation project has started by optimising the blast patterns. The blasting of fresh rock is the first stage of comminution. Thus, ideally the size distribution after blasting should be as ideally as possible, since this save crushing and grinding energy. Furthermore, optimal crusher settings have been studied.

Another stage in fragmentation project is predicting the size distribution feeding into the AG mill. Predicting at this moment is done by placement of a 3D camera system (by MBV Systems) on the mill feed, which measures the size of ore going into the mill. Tracking the ore from blasting all the way up to the mill has been tried to find locations in the mine where ore fragmentation takes place. It has shown to be very complicated to track the ore throughout the entire ore handling systems; even with the use of Metso SmartTags this shows to be problematic. The tracking of ore (and thereby prediction of the size) is made difficult by large coarse ore storage bins, where ore may remain for a few hours or even for weeks. Next to that size distribution measurements in an underground environment appeared to be inaccurate when using photo analysis or became expensive when using a more accurate online 3D video system.

Parameters influencing the fragmentation

The size of ore is dependent on many variables, ranging from the rock properties to the ore handling system bringing the ore up to surface. The size distribution of ore is influenced by:

- 1 Geology
- 2 Mining method
- 3 Blast patterns and explosives
- 4 Crushers and settings
- 5 Ore handling system
 - Drawpoints
 - Ore bins
 - Conveyors and transfer points
 - Hoisting

1 Geology

There are a few different ore lenses at Tara Mines, which have their own specific rock properties. A low impact of different ore types on the fragmentation is expected, since the ore hardness and fracturing of the ore does not differ significantly. There are however some regions where the ore has got a higher iron contents or is more sticky.

A major impact on the size of ore is due to the geological constraints. The geology limits the boundaries of the economically minable reserves. Due to the narrowing of the orebody in direction of the SWEX, the size of the stopes is smaller in the SWEX than in the Main Orebody. A smaller stope makes it more difficult or even impossible to produce large lumps of ore.

2 Mining method

There are two main different mining methods used at Tara Mines; development and production mining. Development mining creates tunnels to gain access to the ore and infrastructure. These tunnels have blast patterns (shown in Figure 147), whereby the drill holes are relatively closely spaced. Production mining is the large scale blasting of stopes in the mineralised areas. The larger the stope, the wider the drill holes can be spaced and thus a coarser fragmentation can be achieved. Production mining still produces significant amounts of fine muck, however production ore is coarser sized than development ore. Around 15% of the ore is produced in development mining.

3 Blast patterns

The spacing of drill holes, the amount of explosives and delay time define the fragmentation of the ore to a great extent. In Figure 145, Figure 146 and Figure 147 some typical blast patterns of a stope and development drift are show. In red areas is displayed where fine muck is produced and in green the areas with relative coarse muck.

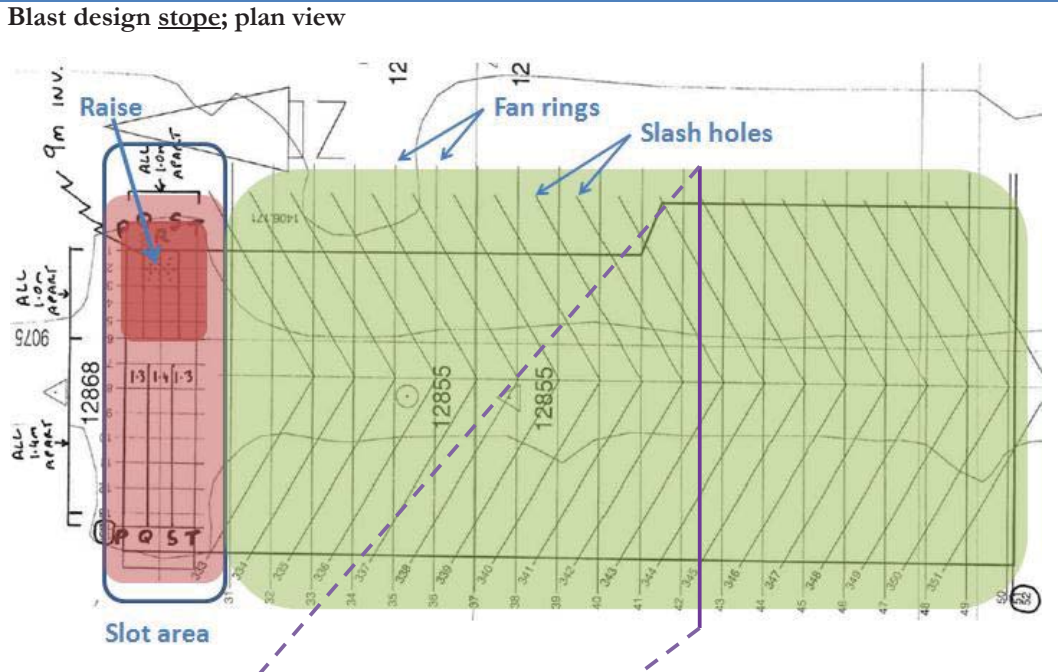


Figure 145: Plan view of the blast design of a typical stope; the red area produces relative fine ore and the green area produces relative coarse ore

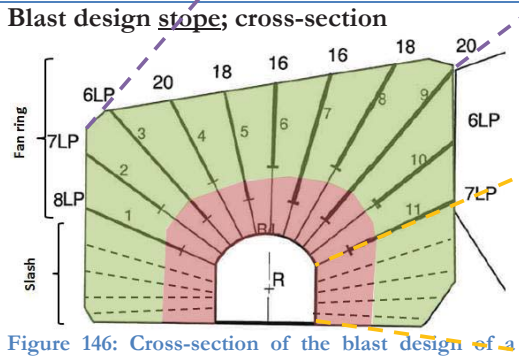


Figure 146: Cross-section of the blast design of a typical stope; the red area produces relative fine ore and the green area produces relative coarse ore

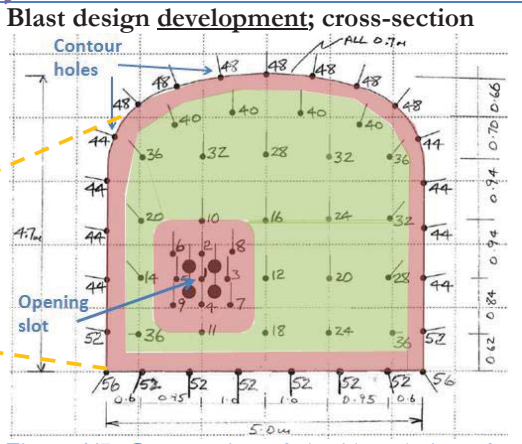


Figure 147: Cross-section of the blast design of a typical development drift; the red area produces relative fine ore and the green area produces relative coarse ore

The areas with an opening slot or a raise (in red) produce finer material, since per volume more explosives are needed to create the first opening. After blasting of the slot area, the fan rings are blasted with increasing burden, which produces coarser ore. The contour blast holes in a development drift that outline the shape of the drift are a source of finer muck. Figure 146,

shows that the fan ring drill holes are not filled completely with explosives, this is also a measure to reduce the amount of explosives and thus achieve a coarser fragmentation.

Part of the fragmentation project is to increase the burden spacing and reduce the total amount of explosives. Larger drill holes may be filled with more explosives; this allows an increase in spacing to achieve a coarser fragmentation. Tara mines reported (Boliden Tara Mines and Boliden TG, 2011 *unpublished*) that the use of a 76mm production drill may increase the ring burdens from 2.3 to 2.6 m (Table 40). This results in a size distribution where >87% of the muck is assigned as coarse material and only up to 4% as fine muck.

Table 40: Blast pattern design using 70 and 76mm drill holes

Drill bit [mm]	70	76
Front tilt angle	15° (rings), 30° (slash)	10° (rings), 15° (slash)
Burden spacing [m]	2.3 (rings), 2.0 (slash)	2.5-2.6 (rings), 2.4 (slash)
Spacing [m]	2.5-2.8 (rings), 1.4 (slash)	2.8-3.0 (rings), 2.6 (slash)
Subdrilling [m]	0.8	1.0
Pivot point [m]	1.5	1.5

4 Crusher settings

The crusher reduces the size of very large boulders to a size that the conveyor systems are capable of handling. There are five underground jaw crushers, with a jaw opening of 150mm. It is studied (Mitchell, Mitchell and Pascoe, 2008) that ‘choke feeding’ of a jaw crusher maximises the capacity and improves stone-on-stone crushing of slabby particles resulting in a more cubical particle size. Choke feeding increases the area on the jaw of the crusher, which is in contact with the rock, thereby making crushing more efficient.

For a non-choke fed crusher at Tara Mines, large slabs are not crushed. This may cause blockage in transfer points or chutes further away in the ore handling system. Inconsistent feeding the jaw crushers produces large slabs when they are not choke fed. This is causing blockage in chutes later on in the ore handling system. Since the crushers are not constantly choke fed, the crusher opening cannot be opened wider to increase the particle size.

5 Ore handling system

The ore handling systems brings the ore from the crushers to the hoisting system by a series of conveyor belts. Several stages in the ore handling system may cause extra (and unwanted) fragmentation.

Drawpoints and ore bins are meant to transport the ore in vertical direction by making use of gravity. The drawpoints and ore bins are short term buffers used to bring the ore to a centralised location, furthermore they feed crushers and conveyors. The vertical drop that the ore makes, can reach up to 30 metres; this may cause (unwanted) breakage of the ore. Inside a bin the ore particles slide among each other, this causes friction. The friction may also reduce the particle size.

The rehandling of ore may cause an impact on the ore particles and thus breakage. This is noticed at transfer points where ore is dropped from one belt onto the other. A second location where rehandling may cause high impact on the particles is at the loading and unloading of the skips for hoisting. The ore is loaded at high velocity using the pocket loaders and during unloading the muck makes another drop of over 10 metres.

Segregation locations

The fragmentation of ore is one of the important function in order to achieve a good size distribution for the mill. Another important function is segregation. Segregation splits the particles in the bulk by their size, which may cause separated periods of finer and coarser particles arriving at the mill, in contrast to the mix that suits the mill best.

Segregation is found at the following locations at Tara Mines:

- 1 Conveyor belts
- 2 Coarse ore bin
- 3 Skips
- 4 Tepee

1 Conveyor belts

On the conveyor belts most of the coarse material is carried on top of the fine material. This can be seen at several conveyors and is seen most clearly at the end of the longer conveyors. The vibration of the belt moves the smaller particles downwards and the coarser material upwards. During discharge of the conveyor into an ore bin this is also of influence, as described in *Section 2.5.3*.

2 Coarse ore bin

The underground coarse ore bin is located near the hoisting installation. All ore is buffered in this bin before hoisting. As mentioned, the discharge of the conveyor belts segregates the particles due to their size. This means that there are regions with a surplus of fines and of coarse material inside the coarse ore bin. At the bottom of the coarse ore bin are two outlets. These two outlets confirm that there is segregation of the material inside the coarse ore bin, since one of the outlets predominantly produces fines and the other one predominantly coarse material.

3 Skips

The two outlets of the coarse ore bin feed their segregated product onto two pocket loaders. The pocket loaders carry the exact amount for one skip load and load the skips in sequence. The skips are coupled; so when one goes up loaded with ore, the other one comes down empty. Due to the segregated ore on the pocket loaders one of the skips also hoist coarse ore than the other. This can also be seen at the discharge of the skips at surface and can even be seen at the conveyor feeding into the stockpile Tepee.

4 Tepee

All ore arrives at surface is first stockpiled in the Tepee. The two skips unload the ore one after another onto the same conveyor belt, which directly feeds the Tepee. The material undergoes mixing and blending effects in the Tepee, which is studied in this report. *Section 4.1.3.b*, mentions that there are regions in the Tepee with a surplus of fines and coarse material. Furthermore, it is observed that two of the Tepee discharge chutes produce smaller muck. The two chutes producing small muck are located at the same side of the Tepee where the regions of finer muck are reported, this is shown in Figure 148.

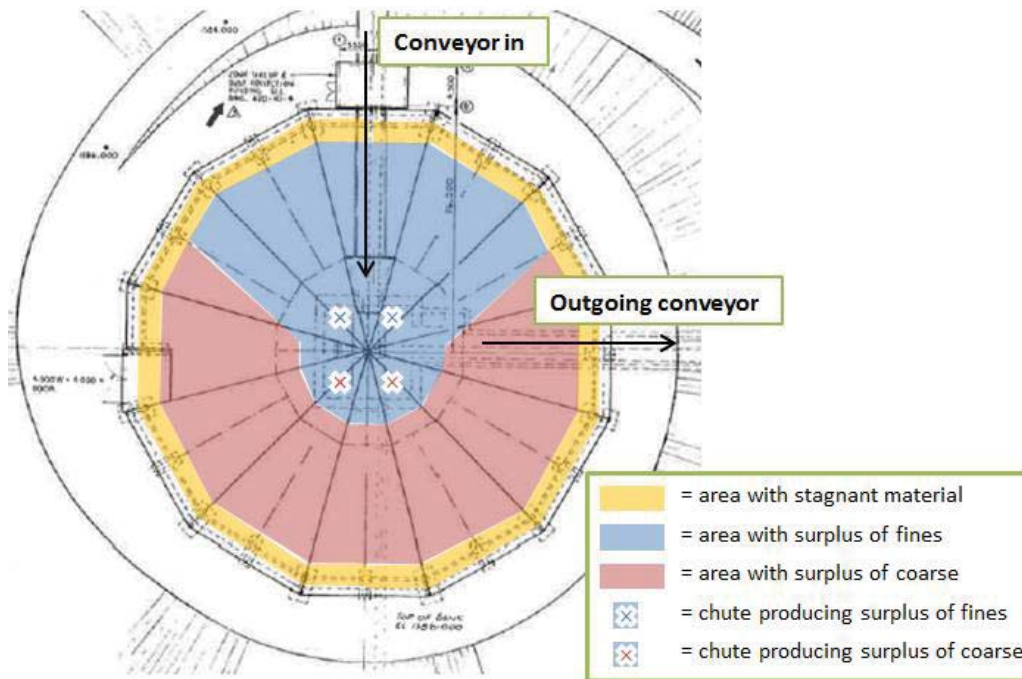


Figure 148: Plan view, technical drawing of the Tepee and the regions with a surplus of fine and coarse material

Observations on the Tepee stockpile

Segregation is not the only observation on the Tepee. There are several more observations that will be reviewed in this section.

The fill level of the Tepee is constantly measured by a point-down laser located directly next to the feeding conveyor belt. This laser measures the height of filling. The fill level as it is used by Tara Mines is based on the fill volume and not the filling height.

The laser measurement is influenced by the operation of the Tepee, which is shown in Figure 149. A computer script tracks the weight of the incoming and outgoing material and together with the point down laser calculates the filling level. The fill levels that are mentioned in this report are based on the volume, and thus not directly on the height of filling.

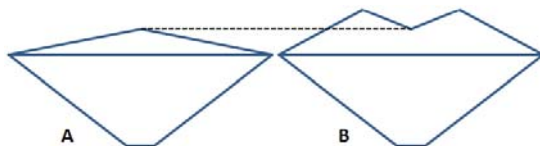


Figure 149: Point down laser above the outlet measures the same filling height for different Tepee fill volumes

Laser surveying of the rock pile inside the Tepee housing has given a good 3D image of the pile formed in the Tepee. This image is used to measure the angle of repose of the ore pile. The laser survey was carried out at a fill level of 70%. The measured repose angle is 37 degrees.

Another observation is the formation of a crater during discharge. Figure 149.B already shows that at a high Tepee discharge rate a crater is formed. The reason of crater formation is that the

material in the core of the Tepee flows faster than the material close to the wall. This report refers to this flow mode as funnel or core flow, after Jenike (1961).

One more observation that agrees with core flow is that the mine reports a 'last-in, first-out' system. Tracking of material in the stockpile, using Metso SmartTags, has shown that the 'fresher' material in the core flows through the stockpile faster than material to the side of the Tepee. The material tracking also indicates that when there is no discharge in the Tepee, the material may end up near the walls of the Tepee, which increases the residence time of those particles in the Tepee.

Appendix C: Simulation results

This appendix provides the simulation results in detail. This chapter first provides an overview with the parameters of all simulations with mixed filling. Subsequently, an overview of simulations with batch filling is given. Hereafter the results of each simulation are given.

Overview of all simulations

Parameter overview of all simulations with mixed fill as filling method

Parameter	Simulation			
	I.a	I.b	II.a	II.c
3D or 3D slice	3D	3D	3D slice	3D slice
Filling method	Mixed filling	Mixed filling	Mixed filling	Mixed filling
Particle size [mm]	130	130	130	130
Wall angle [deg]	45	45	45	45
Wall friction [type]	low - fs=0.25	high - fs=1	low - fs=0.25	high - tips
Outlet size [mm]	1300	1300	1300	1300
Input [-]	no	no	no	no
Other	-	-	-	-

III.a	III.b	III.c
3D slice	3D slice	3D slice
Mixed filling	Mixed filling	Mixed filling
130	130	130
60	60	60
low - fs=0.25	high - fs=1	high - tips
1300	1300	1300
no	no	no
-	-	-

V	VI	VII
3D slice	3D slice	3D slice
Mixed filling	Mixed filling	Batch filling
30, 80 & 130	130	130
45	45	45
low - fs=0.25	high - tips	high - tips
1300	1300	left: 600mm, right:300mm
no	no	no
-	bottom + top filled	-

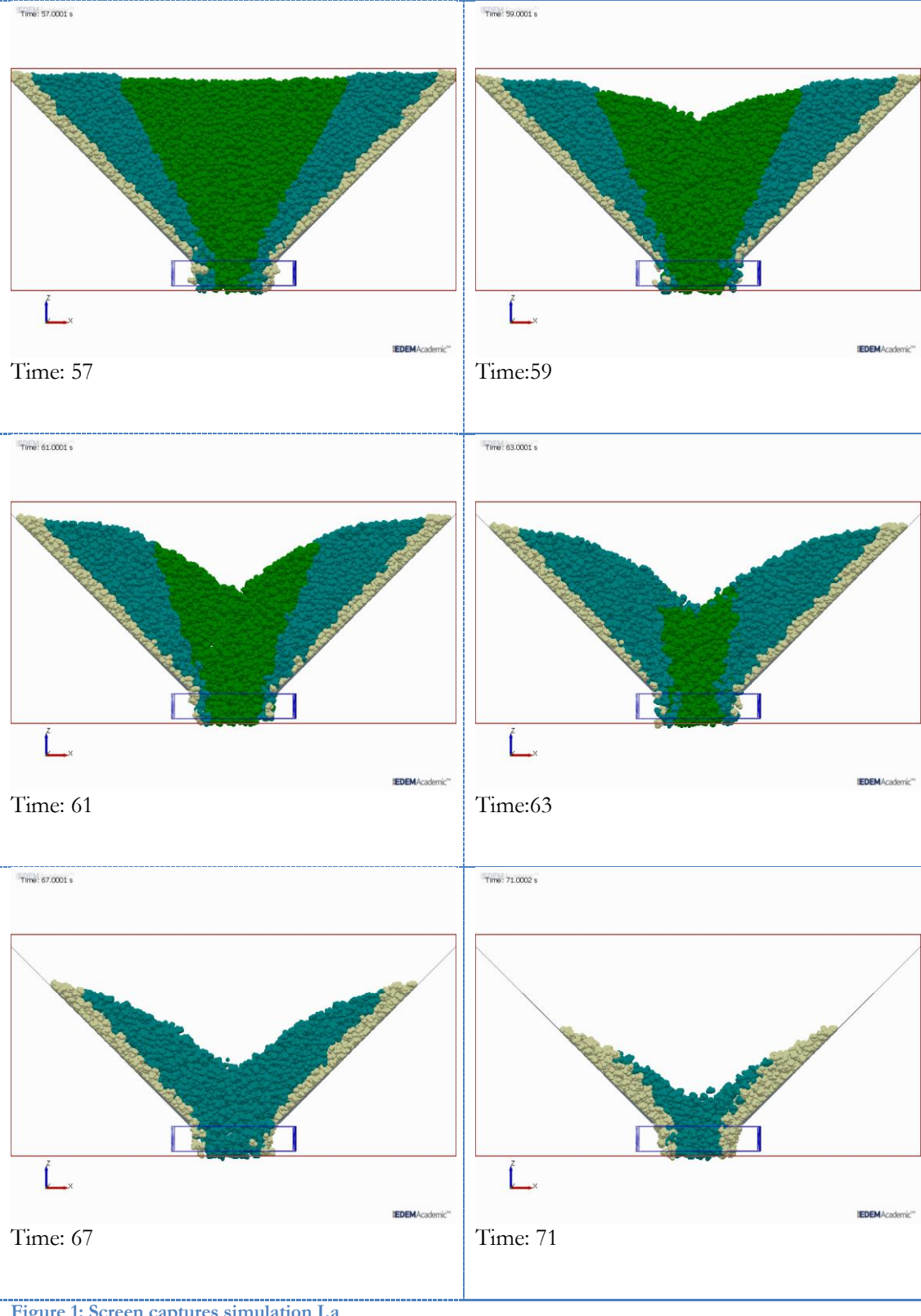
Parameter overview of all simulations with batch fill as filling method

Parameter	Simulation			
	A1	A2	B	C
3D or 3D slice	3D slice	3D slice	3D slice	3D slice
Filling method	Batch filling	Batch filling	Batch filling	Batch filling
Particle size [mm]	130	130	130	130
Wall angle [deg]	45	45	45	45
Wall friction [type]	low - fs=0.25	high - tips	low - fs=0.25	high - tips
Outlet size [mm]	1300	1300	1300	1300
Input [-]	no	no	yes	yes
Other	-	-	-	-

D1	D2	F	G	H
3D slice	3D slice	3D slice	3D slice	3D slice
Batch filling	Batch filling	Batch filling	Batch filling	Batch filling
130	130	130	130	130
45	45	45	45	45
high - tips	high - tips	high - tips	high - tips	high - tips
800	500	800	800	500
yes	yes	yes	yes	yes
-	-	Output intermittent	asymmetric filling	input rate = output rate

Simulation I.a

Screen captures



Screen captures of stream

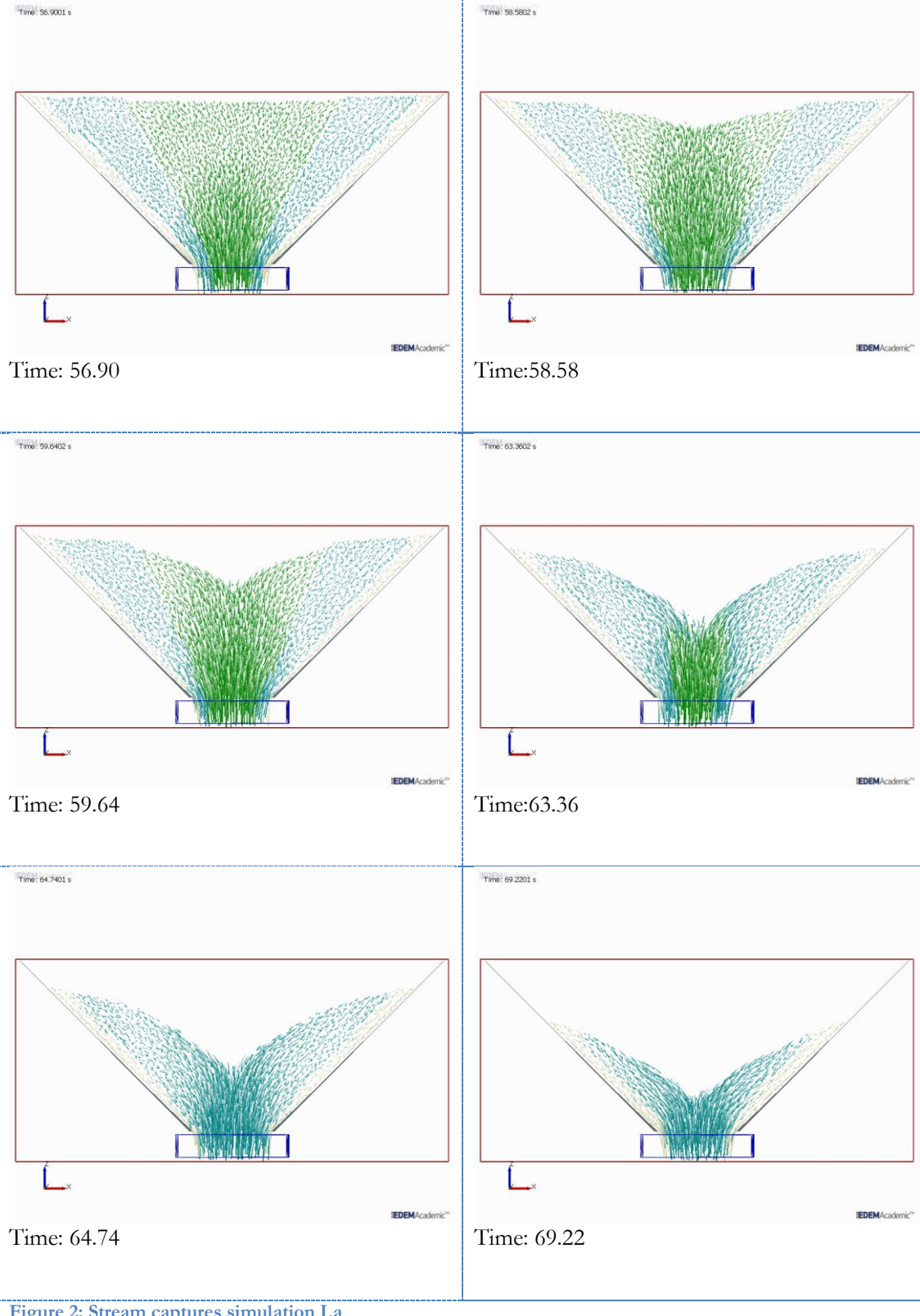


Figure 2: Stream captures simulation I.a

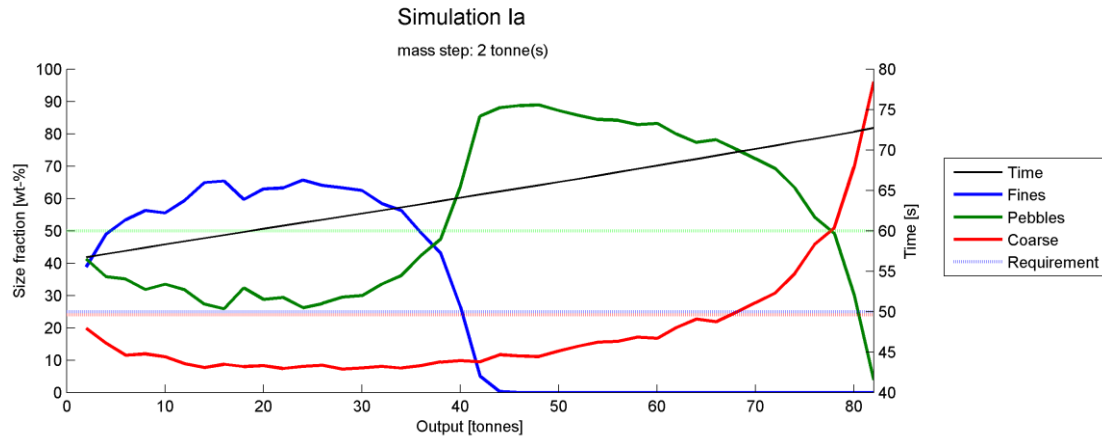


Figure 3: Size distribution graph of simulation I.a

The screen captures show core flow in this simulation; the material in the core is discharged first, followed by the material from the sides. The streams highlight that the velocity is highest close to the outlet. The stream captures also show the growing of the ellipse of secondary motion by Kvapil at 58.90 and 58.58 seconds. Furthermore, these captures also shown that the material at the wall starts moving around 60 seconds, this is earlier than *Simulation I.b* where more wall friction is applied.

The size distribution graph shows a clear example of core flow in combination with mixed filling; the fines are discharged first, followed by the majority of pebbles and at last the coarse material.

Simulation I.b

Screen captures

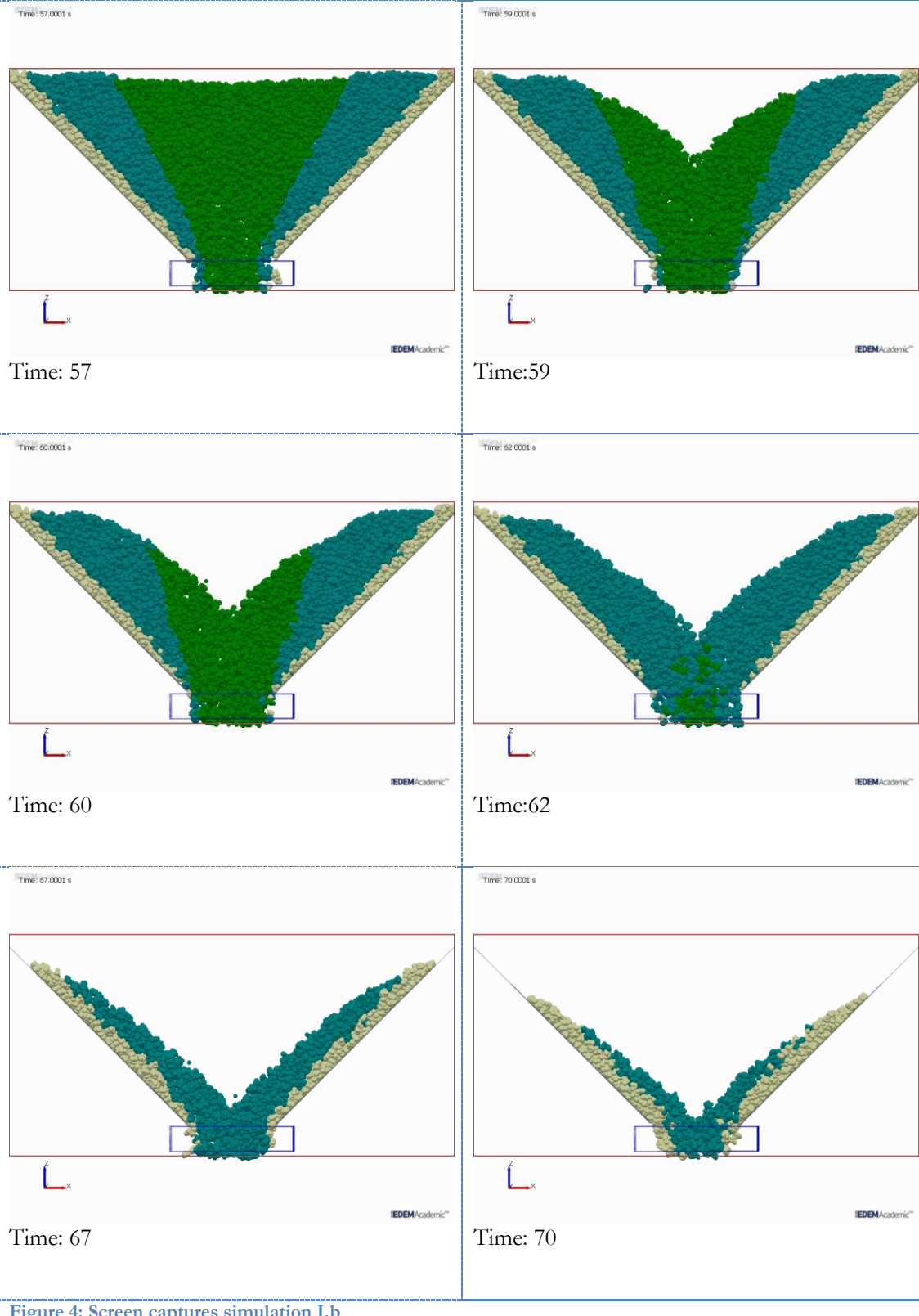
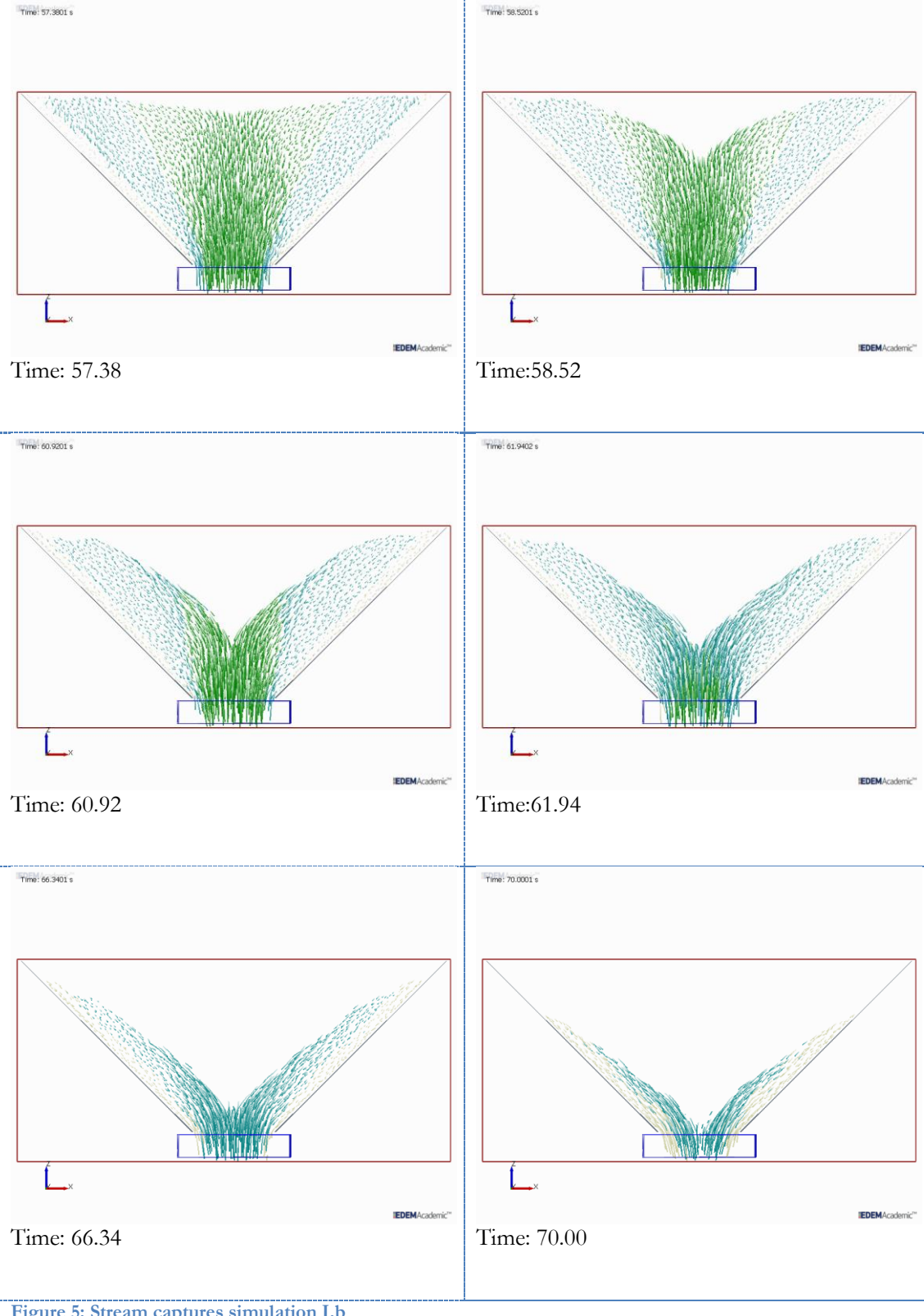


Figure 4: Screen captures simulation I.b

Screen captures of stream



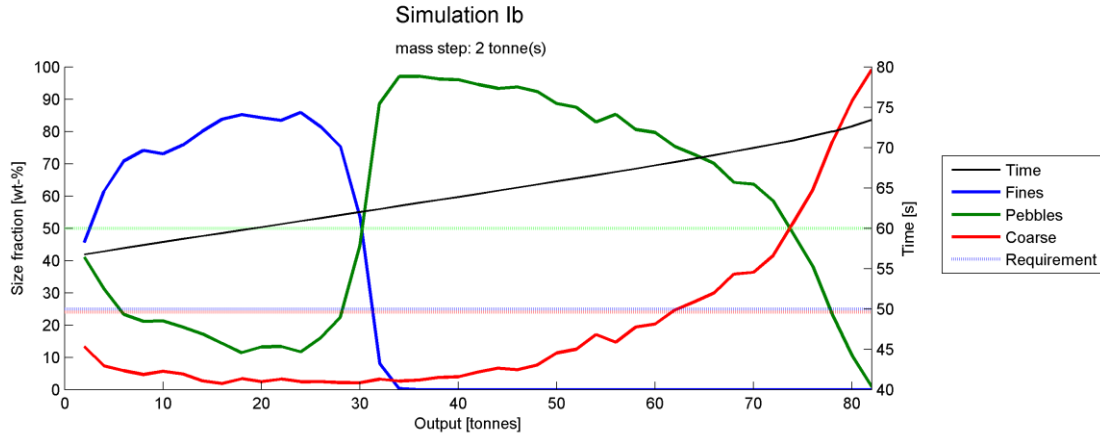


Figure 6: Size distribution graph of simulation I.b

The screen captures show core flow in this simulation; the material in the core is discharged first, followed by the material from the sides. The streams highlight that the velocity is highest close to the outlet. The stream captures also show the ellipse of secondary motion by Kvapil at 57.38 seconds. The angle of withdrawal is very steep in this simulation, even close to 90 degrees; this is due to the very high wall friction in combination with the conical shape of the stockpile. Furthermore, these captures also shown that the material at the wall starts moving around 66 seconds, this is later than *Simulation I.a* where less wall friction is applied.

The size distribution graph shows a clear example of core flow in combination with mixed filling; the fines are discharged first, followed by the majority of pebbles and at last the coarse material. Due to the high wall friction, this separation in sizes during discharge is even more distinct than for *Simulation I.a*. Between 10 and 40 tonnes discharge the coarse fraction is almost zero. Also the pebbles fraction is very low between 10 and 25 tonnes, where it is very high around 35 tonnes.

Simulation II.a

Screen captures of stream

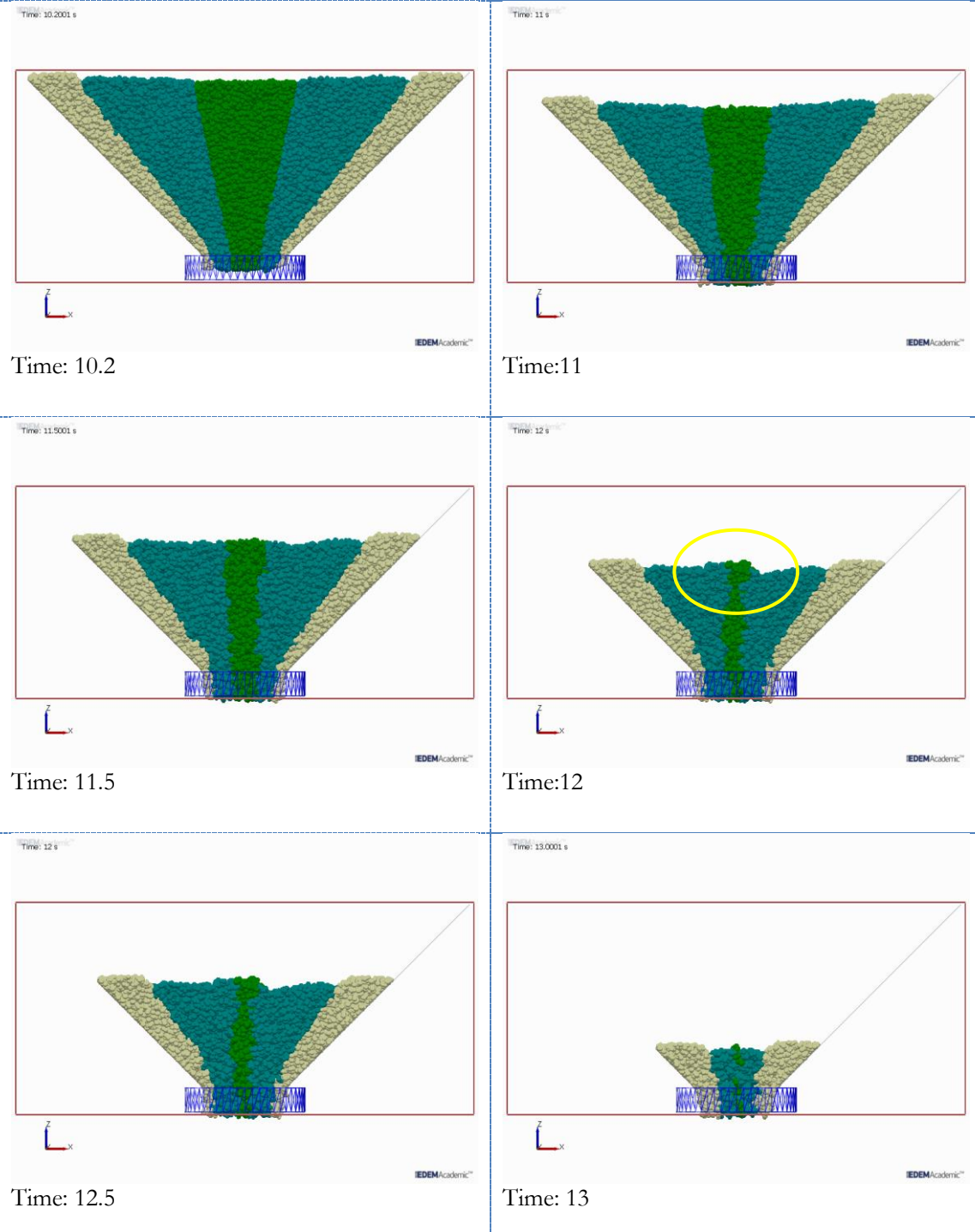
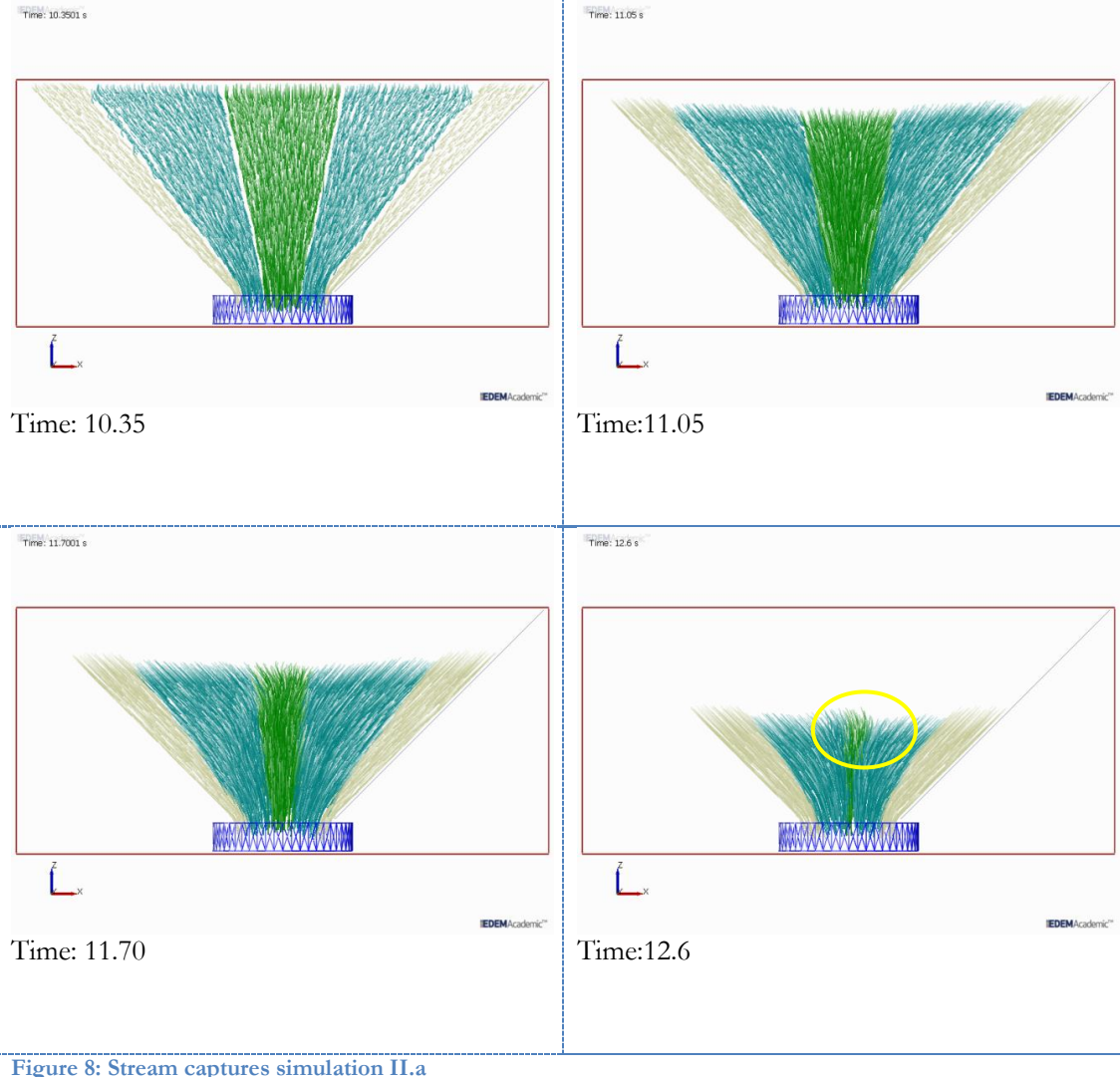


Figure 7: Screen captures simulation II.a

Screen captures



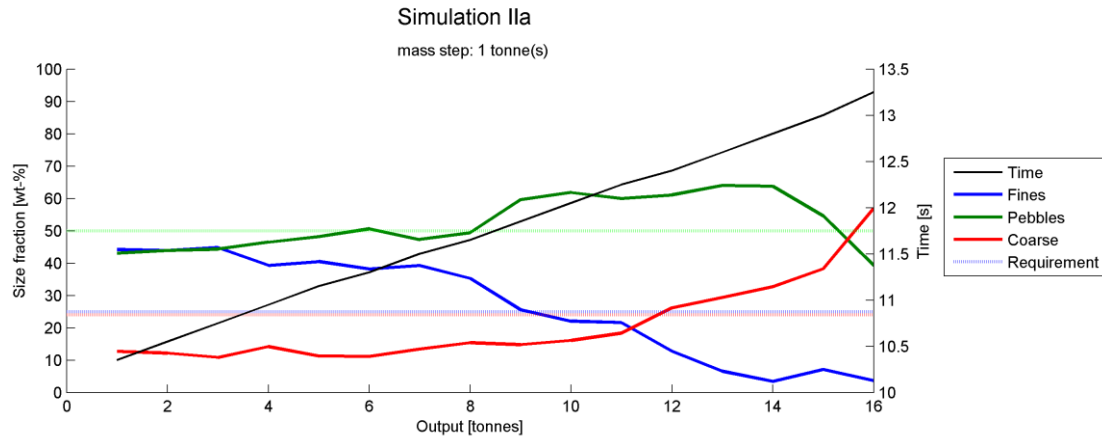


Figure 9: Size distribution graph of simulation II.a

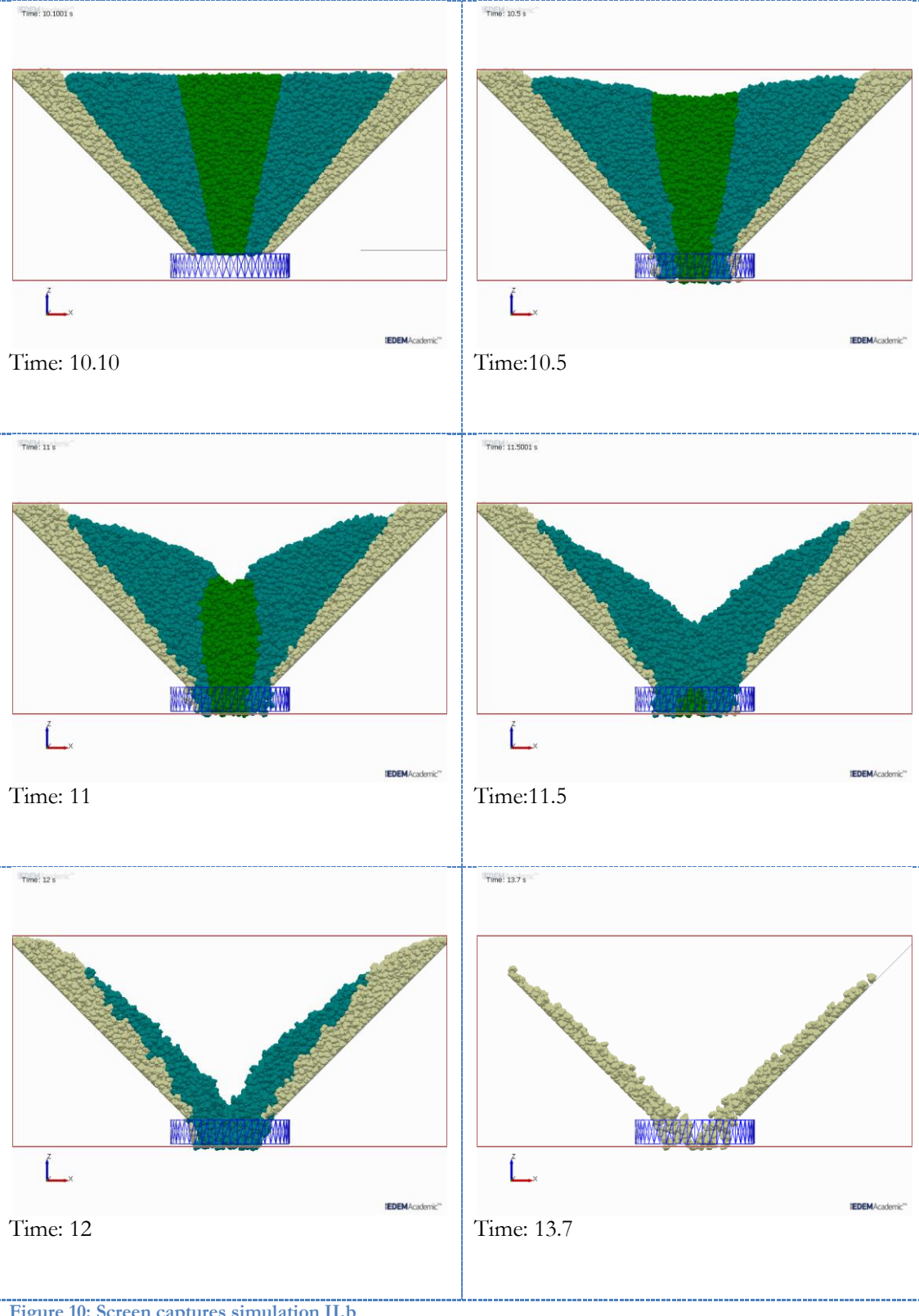
The screen captures in this simulation show very clearly mass flow in the stockpile. In the stream captures, it is seen that all material is moving and has a similar velocity. A notable fact is shown in the stream capture of 12.6 seconds, where a small plum is formed above the outlet (marked by yellow ovals). This is also registered in *Simulation V* and *Section 5.2.2*. This probably caused by the squeezing of the material, since in mass flow all material moves down the funnel simultaneously.

Also the size distribution graph shows clearly mass flow. The material is better mixed than in core flow. The pebble fraction averages around the mill requirement. However, the fines and coarse interchange as well and do not deliver a good blend.

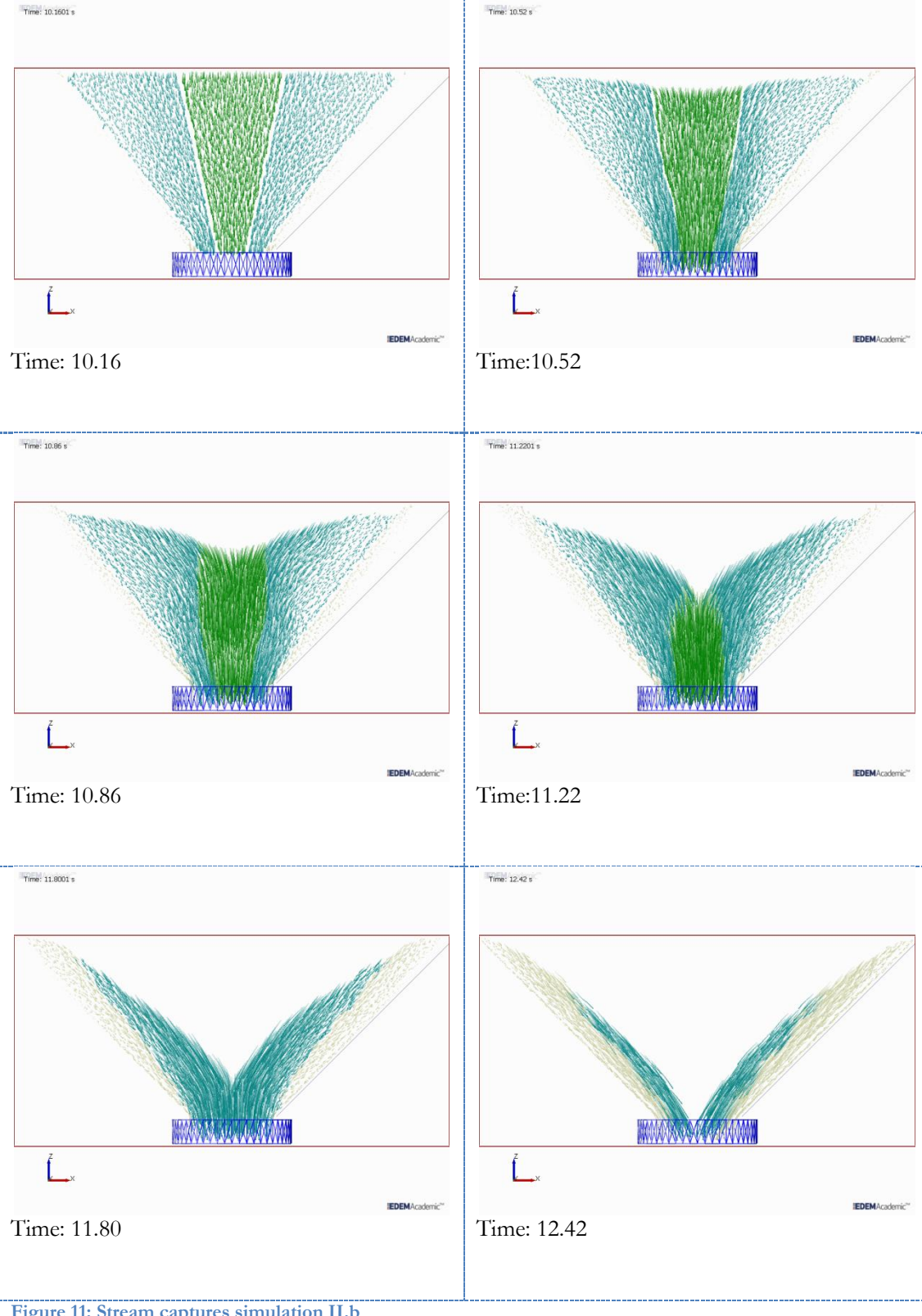
Low wall friction at a 45 degree wall results in mass flow.

Simulation II.b

Screen captures



Screen captures of stream



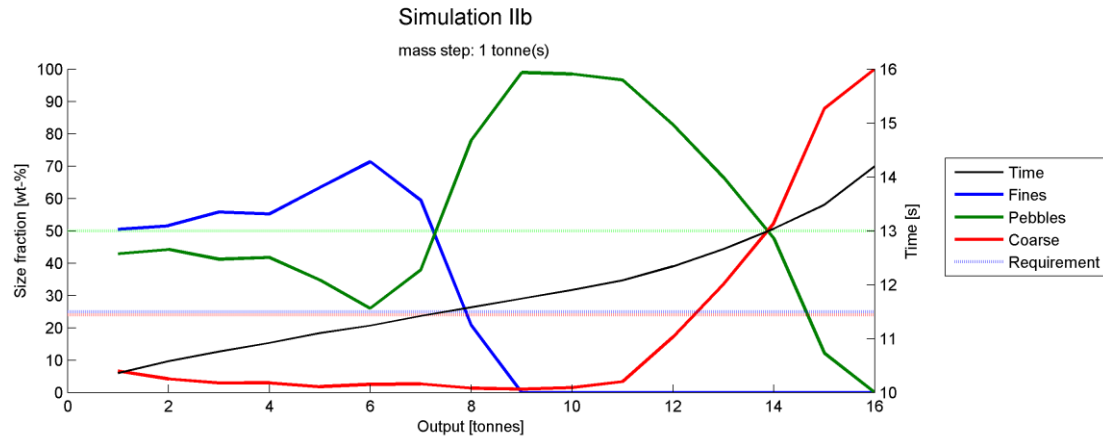


Figure 12: Size distribution graph of simulation II.b

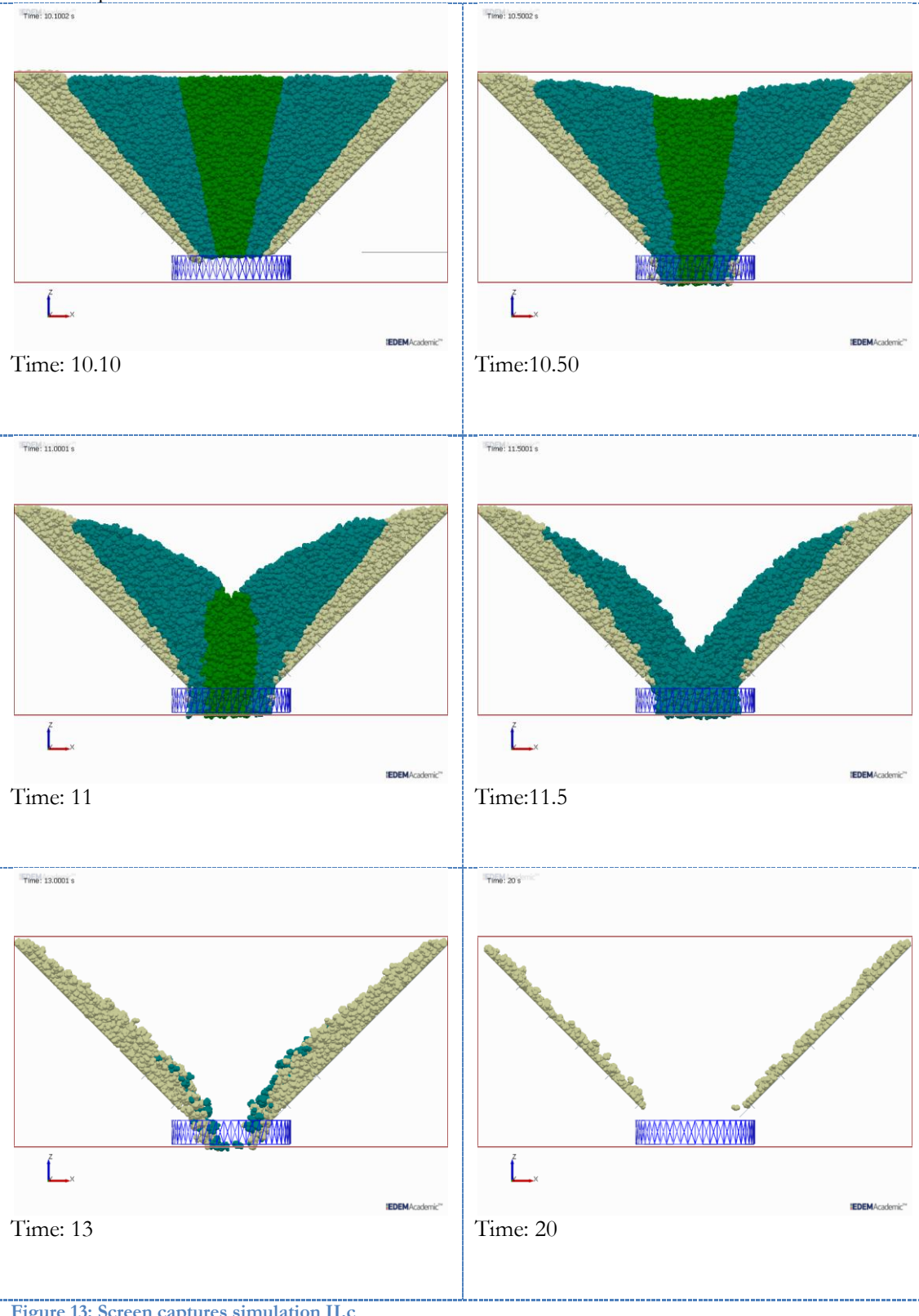
Compared with the previous *Simulation II.a*, only the wall friction is increased. The screen captures show core flow, since the core material is discharge first and is followed by material closer to the walls. The stream captures show an increasing angle of withdrawal, when the core becomes more empty and relieves the pressure on the side material.

The distribution graph shows core flow, with a period of very low coarse material in the beginning.

High wall friction at a 45 degree wall results in core flow.

Simulation II.c

Screen captures



Screen captures of stream

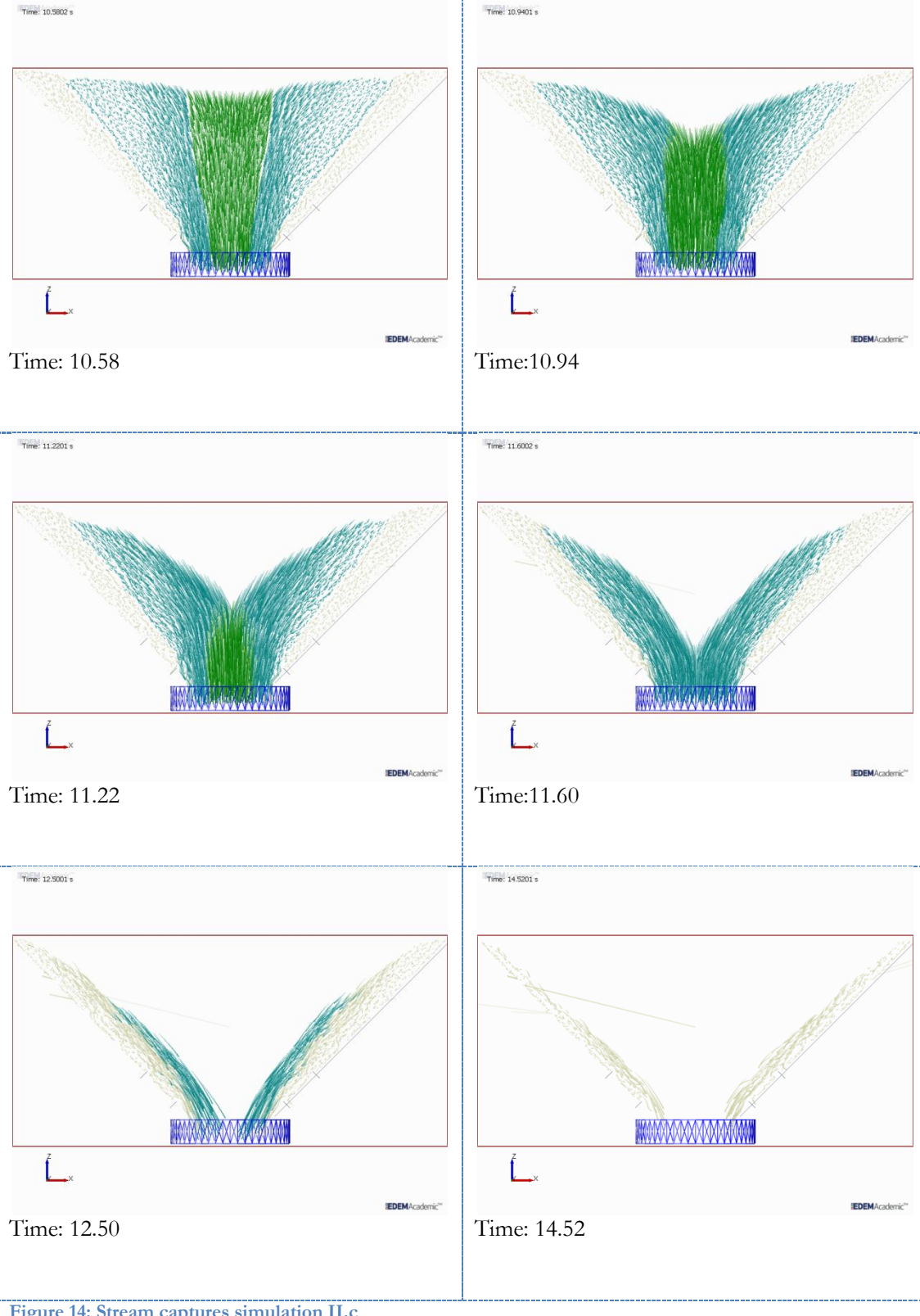


Figure 14: Stream captures simulation II.c

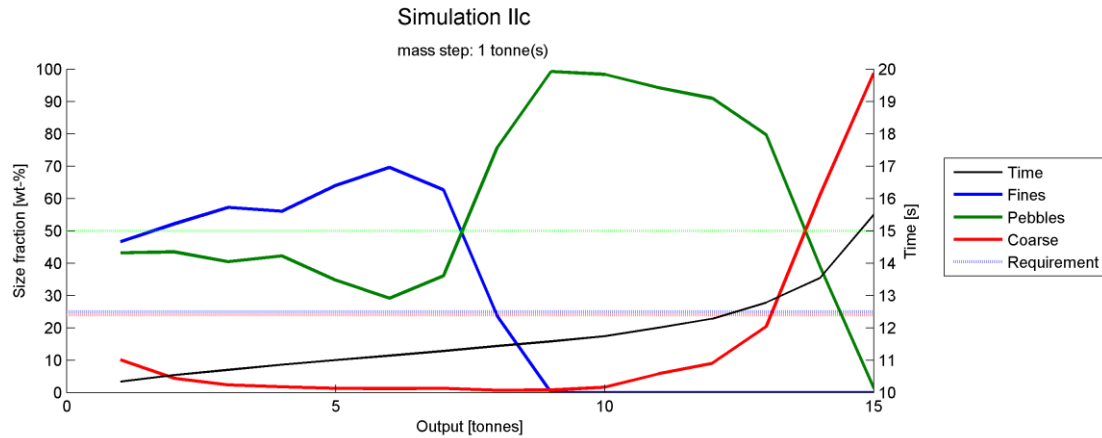


Figure 15: Size distribution graph of simulation II.c

This simulation uses friction tips to increase the wall resistance. The distribution graph and the screen captures show core flow very similar to *Simulation II.b* with high static wall friction. A minor difference is found in the first part of the coarse fraction, which is closer to zero with the use of friction tips. The use of friction tips makes the model behaviour closer related to the 3D conical model with high static wall friction in *Simulation I.b*.

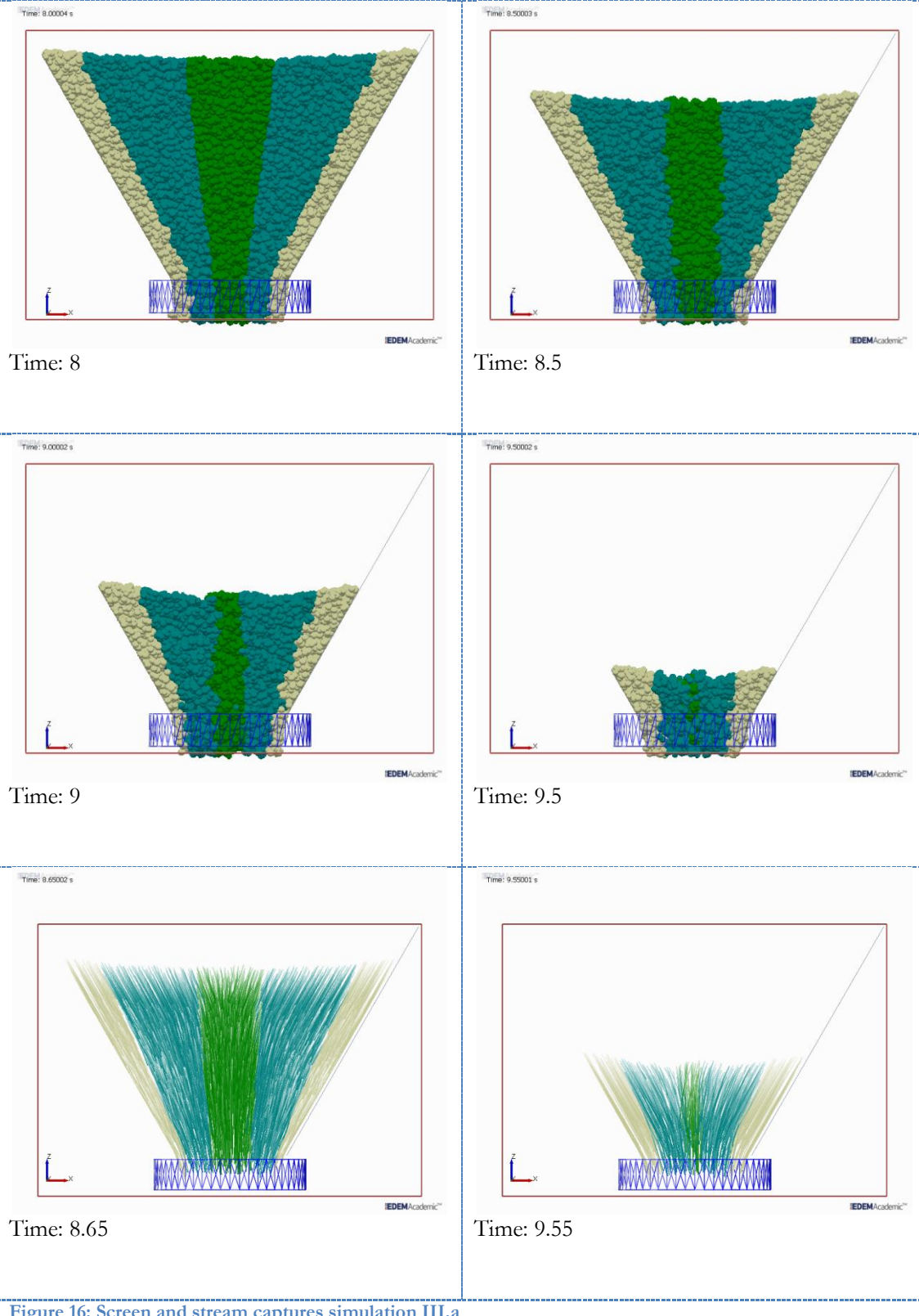
This minor difference is caused by the different methods of applying a high wall resistance. This is seen when comparing Figure 11 and Figure 14 both at 11.22 seconds; in *Simulation II.c* the friction tips hold more coarse material in the stagnant zone, resulting in a very low fraction of coarse material. Therefore, the height of the material directly above the outlet is lower in the simulation with friction tips.

Modelling with friction tips is in better agreement with the 3D conical simulation than the model with high static friction applied.

The friction tips in combination with a 45 degree result in core flow.

Simulation III.a

Screen and stream captures



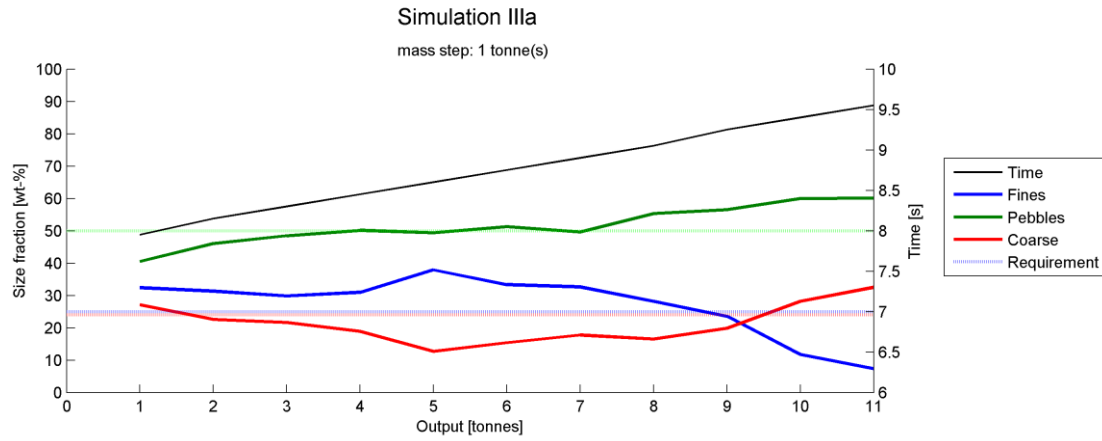


Figure 17: Size distribution graph of simulation III.a

The increased wall angle (60 degrees) and low wall friction results in mass flow. The screen captures show that all material is moving during the discharge. There is a horizontal front moving downwards.

The size distribution during discharge is well mixed and thus matches the mill requirement well. This model is not expected to occur in the stockpile at Tara Mines, due to the low wall friction.

Simulation III.b

Screen and stream captures

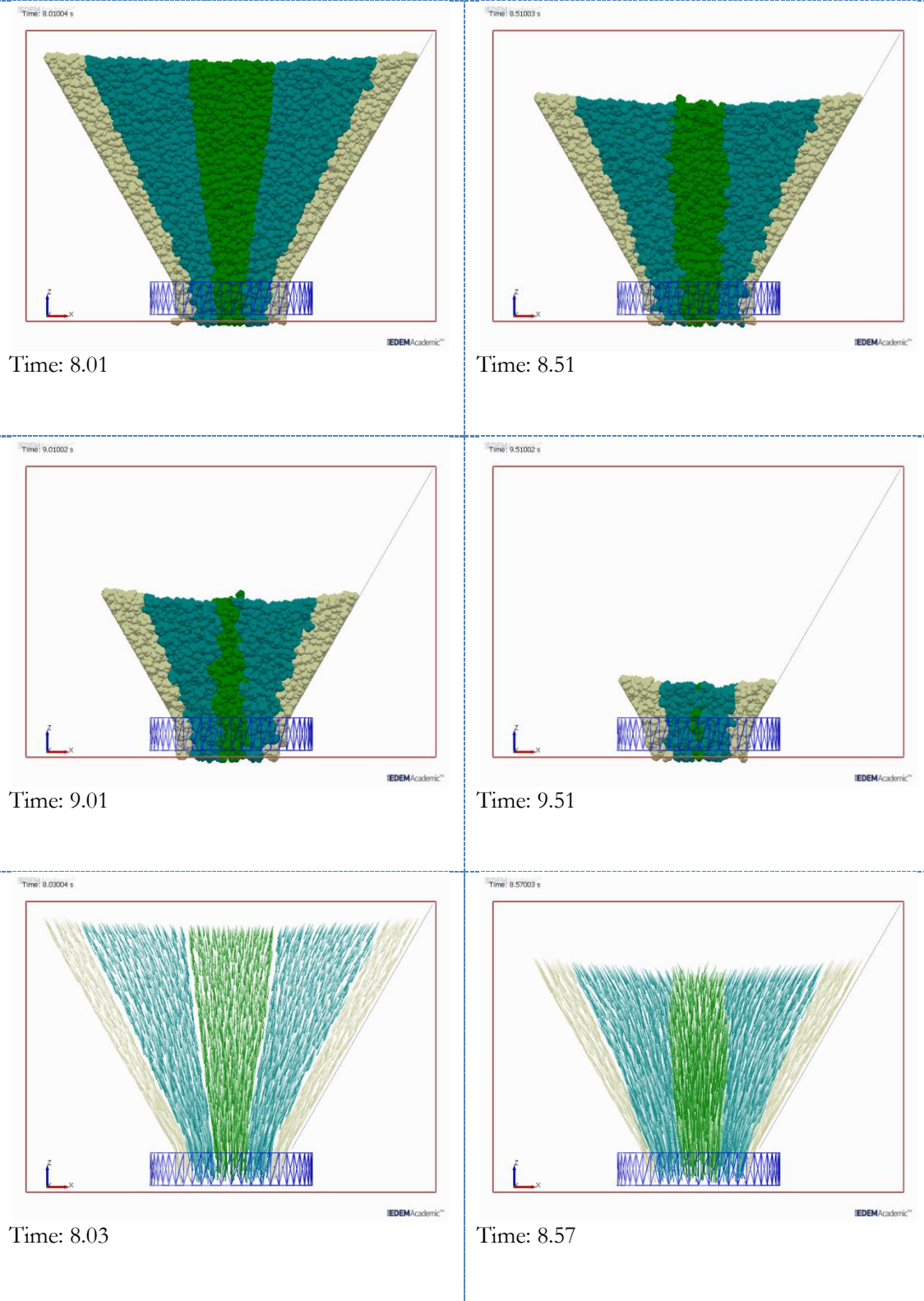


Figure 18: Screen and stream captures simulation III.b

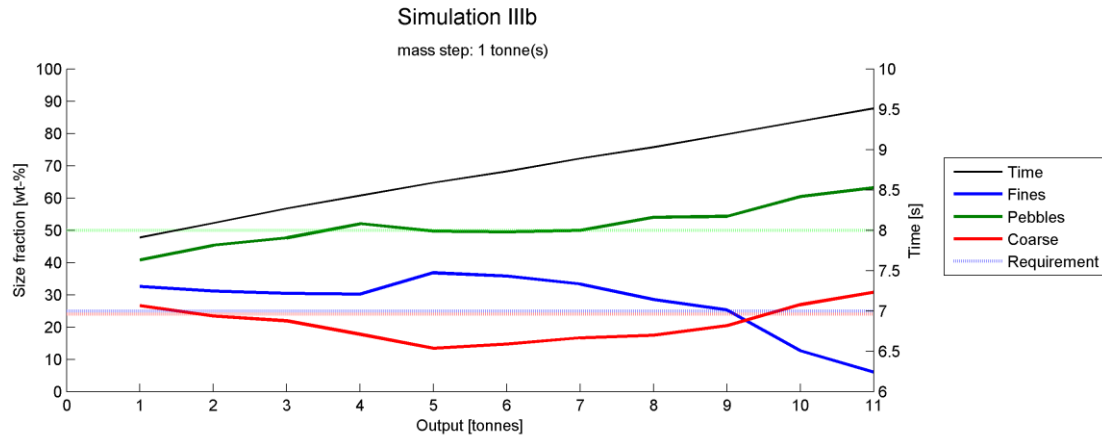


Figure 19: Size distribution graph of simulation III.b

This model uses a high static wall friction. The results are best compared to *Simulation III.a*, which is an identical simulation with low wall friction.

The screen captures and especially the stream captures show that there is mass flow, since all material is moving at a similar velocity. There is not much difference spotted compared to *Simulation III.a*, neither in the size distribution graphs. Therefore, it is concluded that the wall angles are dominant over the static wall friction in establishing the flow mode.

Simulation III.c

Screen captures

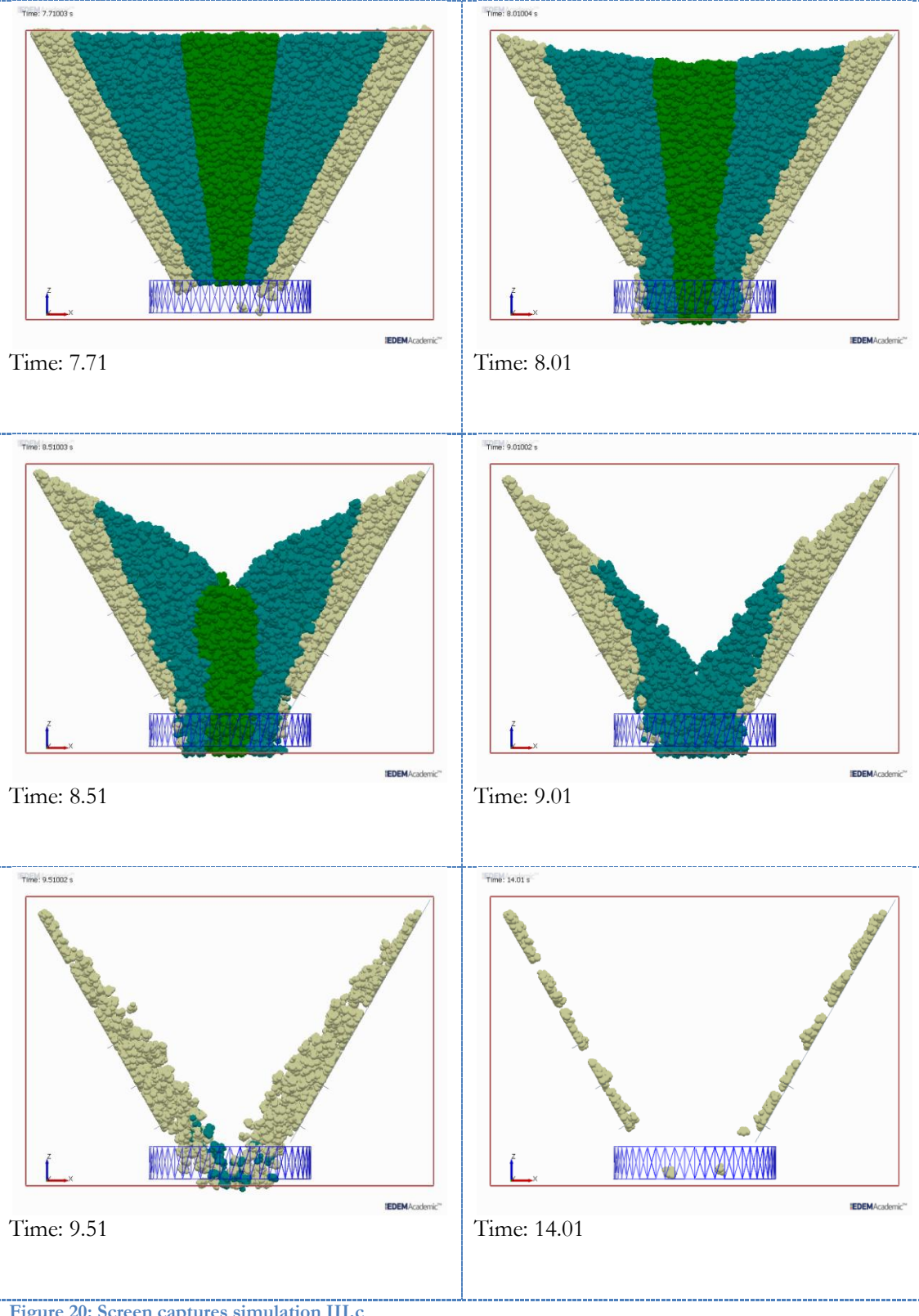
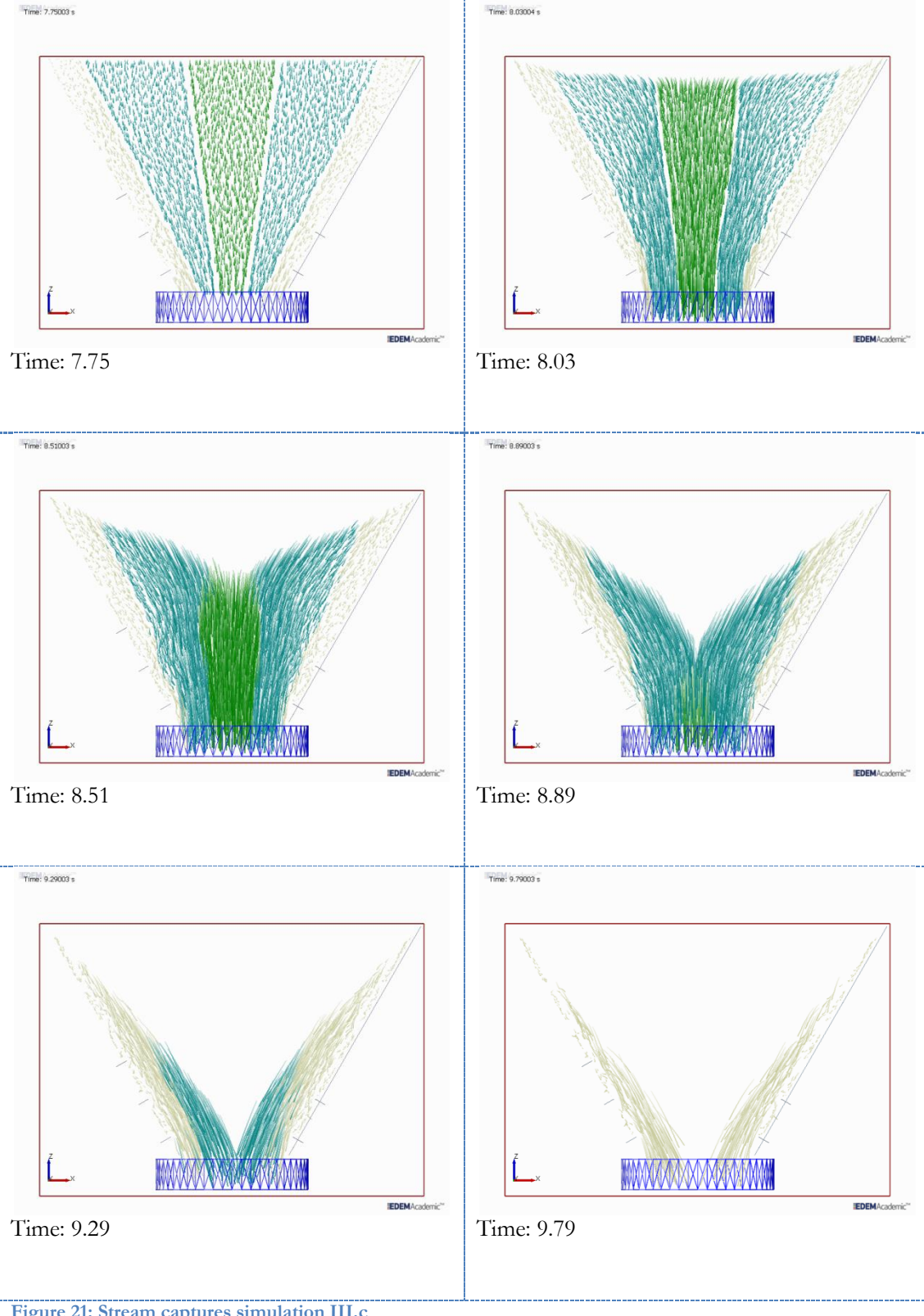


Figure 20: Screen captures simulation III.c

Screen captures of stream



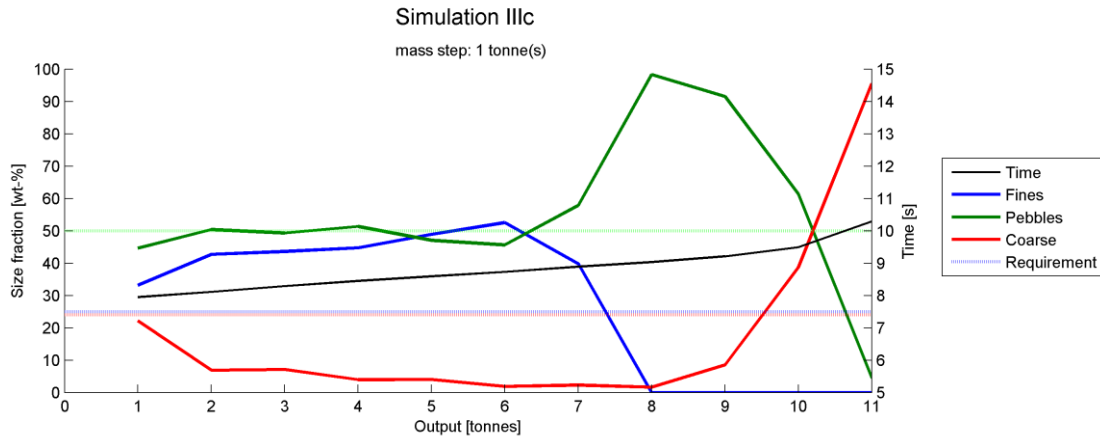


Figure 22: Size distribution graph of simulation III.c

This simulation uses identical parameters as for *Simulation III.a* and *III.b*, except that the wall resistance was increased by installing friction tips.

The screen captures show the formation of a funnel and the stream captures show different particle velocities. Therefore, the flow mode is core flow. However, the distribution graph shows a combination of core and mass flow. The first part is comparable to *Simulation III.b* and shows mass flow, where the second part shows an identical profile as *Simulation II.c* in core flow.

It is concluded that the friction tips invoke more wall resistance and thereby results in core flow. This model is the intermediate zone, between mass and core flow. When the Tepee at Tara Mines has a 60 degree wall angle, this is the most representative simulation. The higher wall angle compared to *Simulation II.c* results in a more favourable discharge size distribution, due to the partly mass flow discharge.

Simulation IV.a

Screen captures

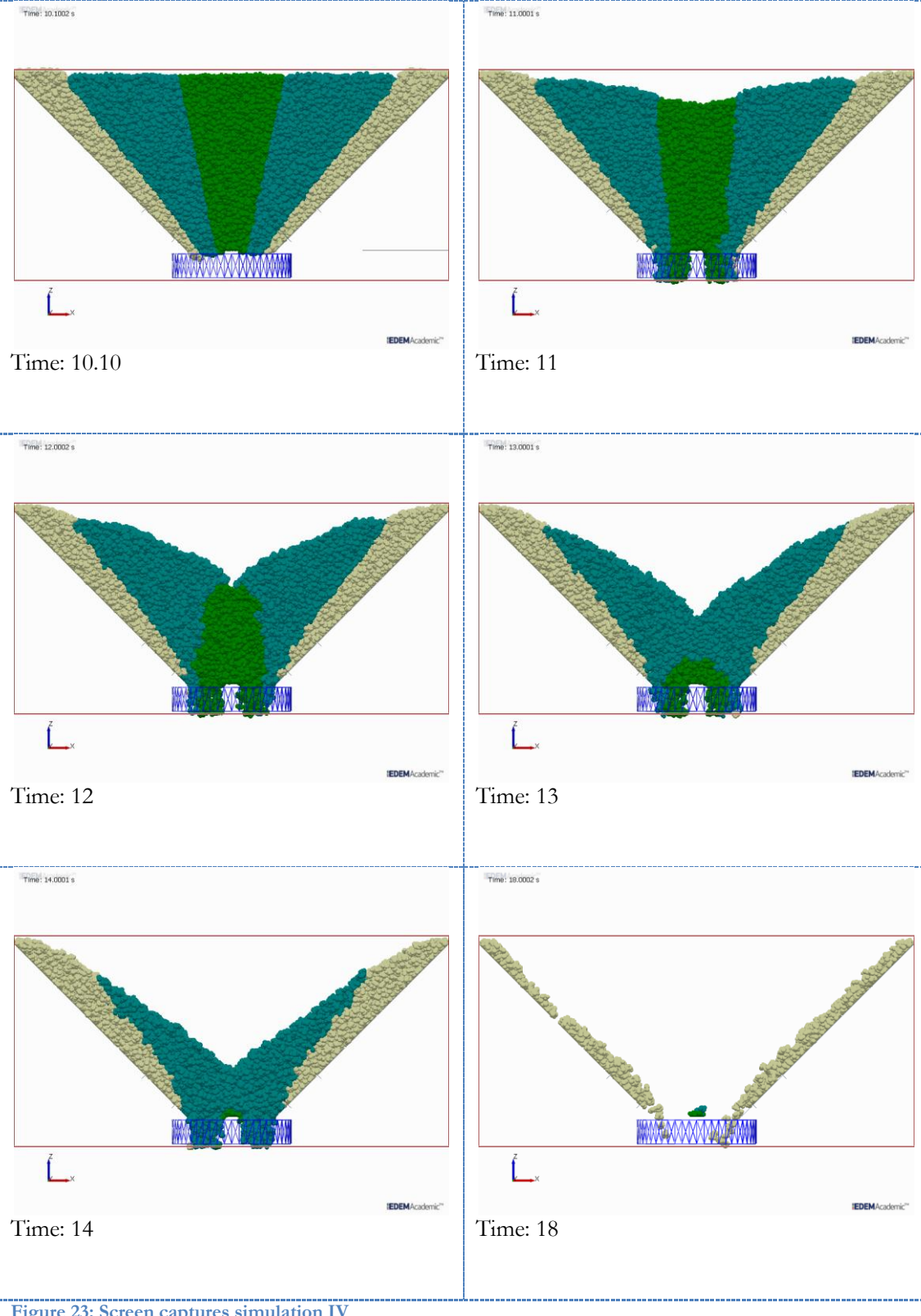


Figure 23: Screen captures simulation IV

Screen captures of stream

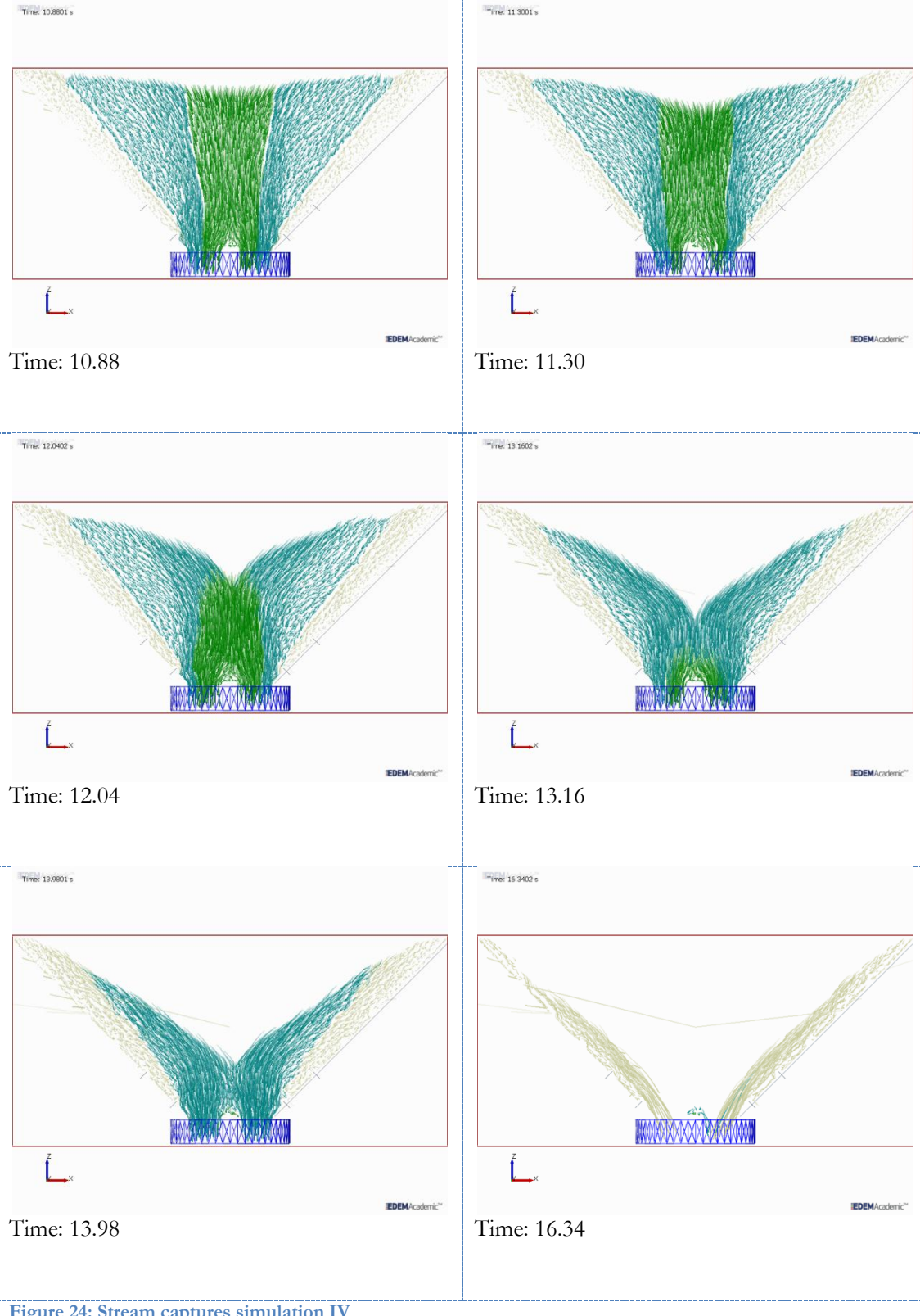


Figure 24: Stream captures simulation IV

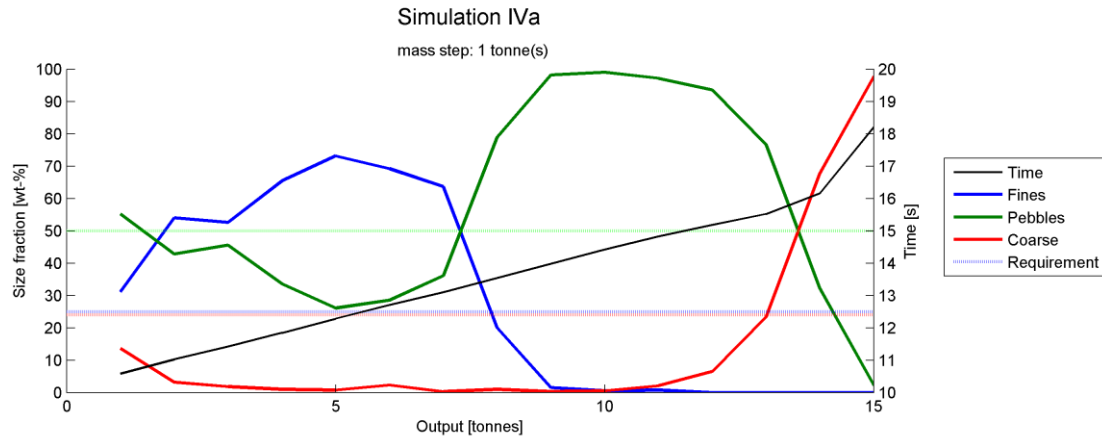


Figure 25: Size distribution graph of simulation IV.a

The results of a model with an installed outlet splitter are shown here. The outlet splitter represents partly the influence of the discharge system at the Tepee.

The friction tips and the 45 degree wall angle result in core flow. The outlet splitter shows no impact on the flow mode. The main influence of the splitter is a reduction of the discharge flow rate, caused by the reduction of outlet size. This is seen when comparing this simulation with the identical simulation without a splitter in *Simulation II.c*. Furthermore, a minor difference is registered at the start of discharge, where the fines region is temporarily blocked. This recovers after 3 tonnes of discharge, which is also seen in the screen captures.

Simulation V

Screen captures

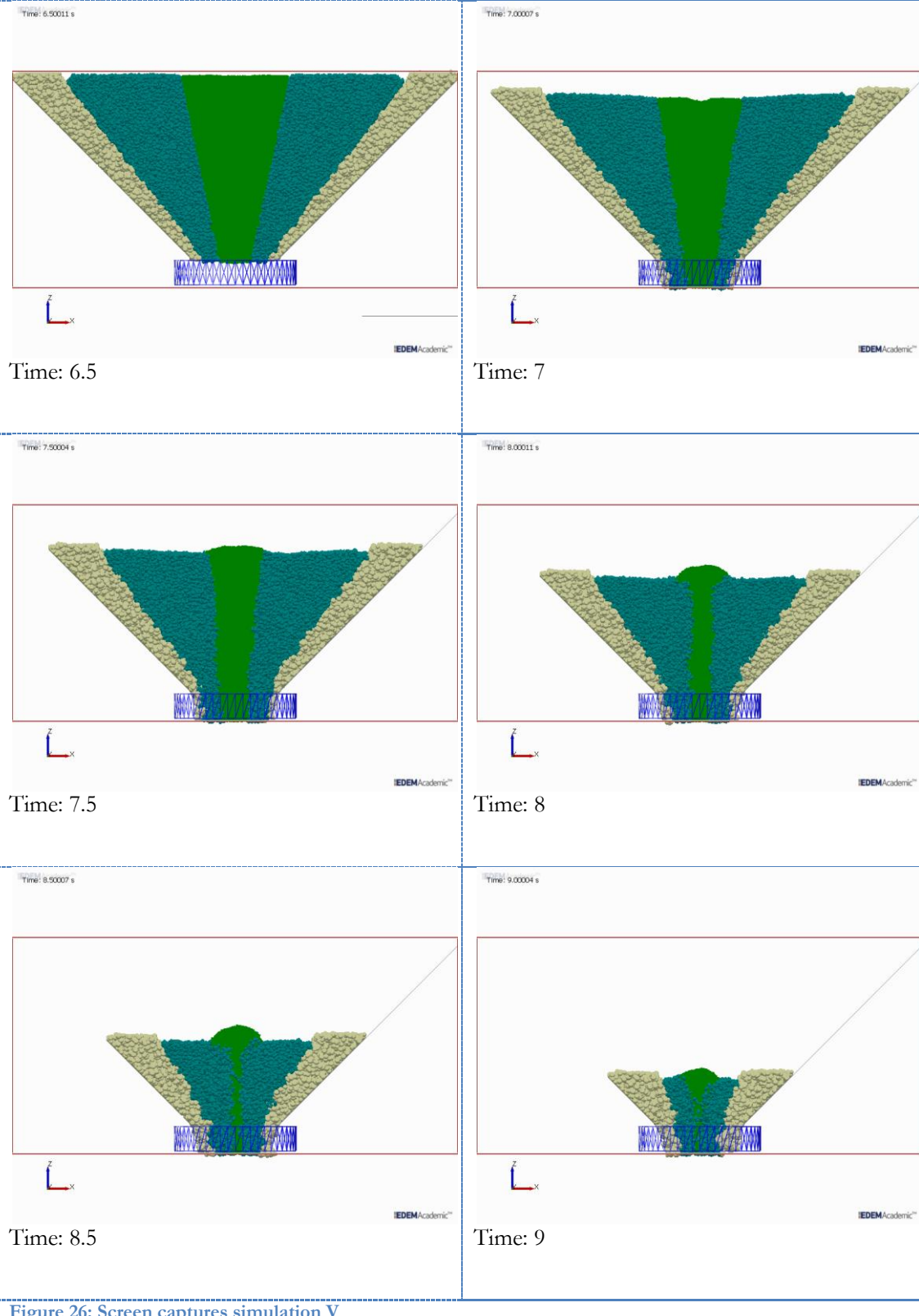
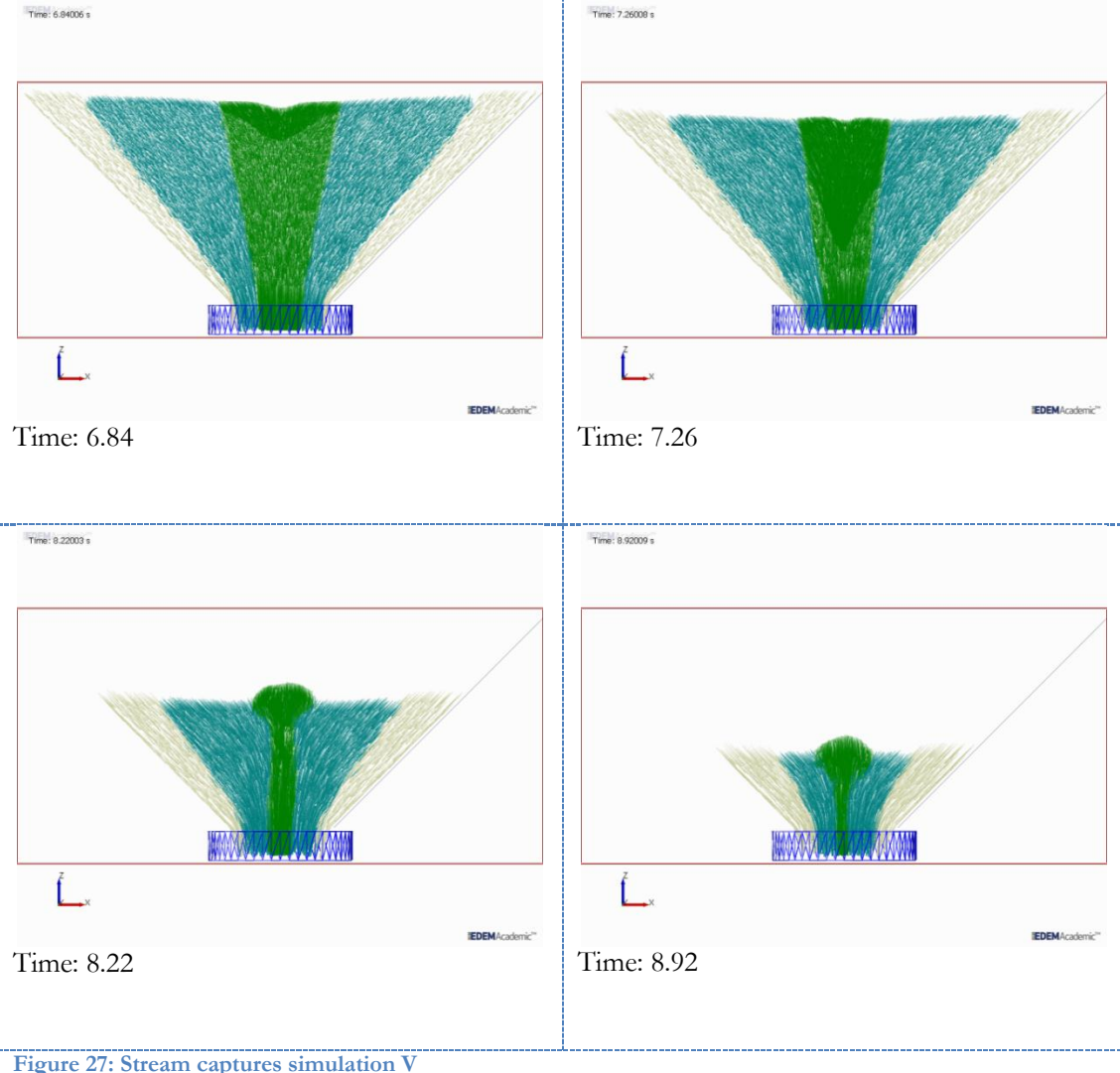


Figure 26: Screen captures simulation V

Screen captures of stream



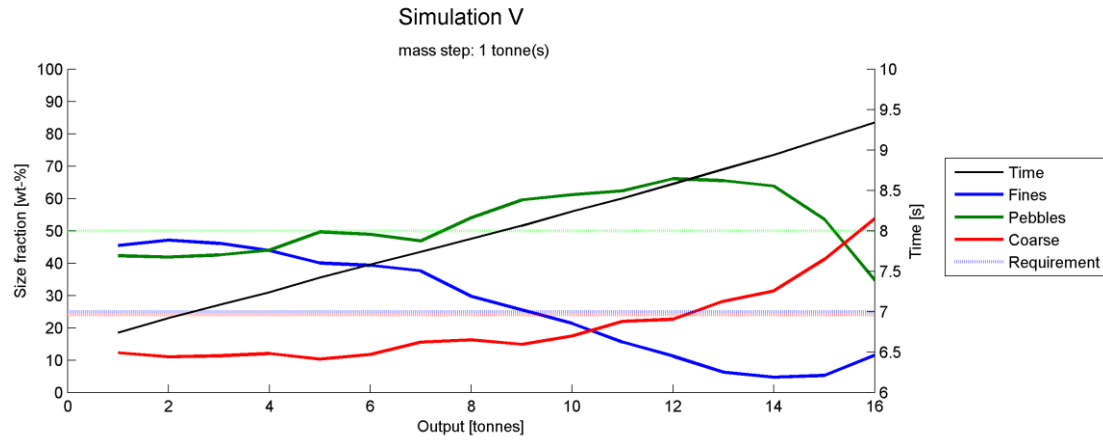


Figure 28: Size distribution graph of simulation V

This model uses ‘real’ sized fines, pebbles and coarse. Except for one observation given below, the results are discussed in *Section 5.2.2*. Due to the low static wall friction this model shows mass flow.

The first two captures of the stream show an increase of velocity at the top of the filling, directly above the outlet. It only occurs with fine particles. This shows that different sized particles behave differently. However, the overall flow of material in the Tepee is not influenced.

Simulation VI

Screen captures

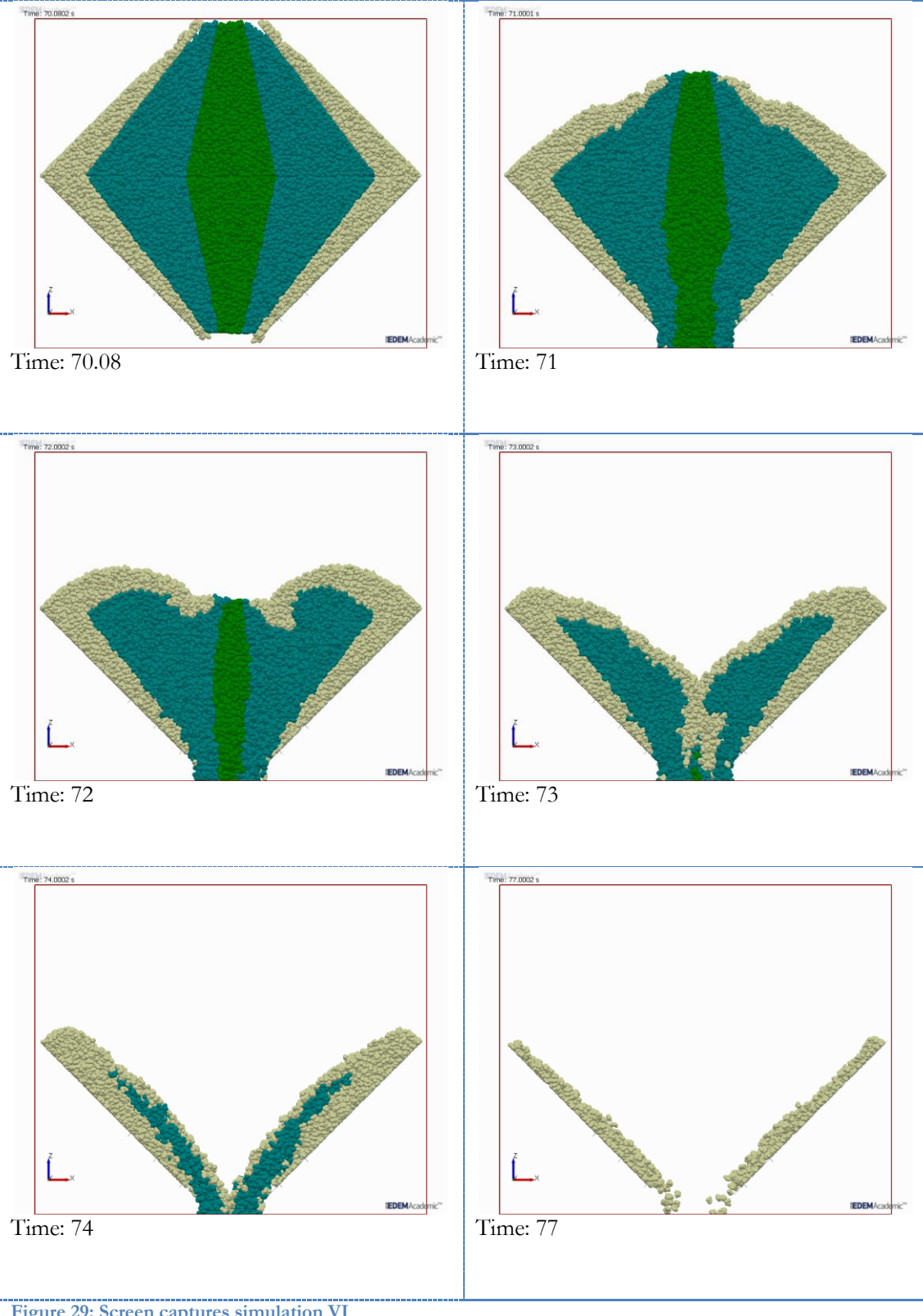


Figure 29: Screen captures simulation VI

Screen captures of stream

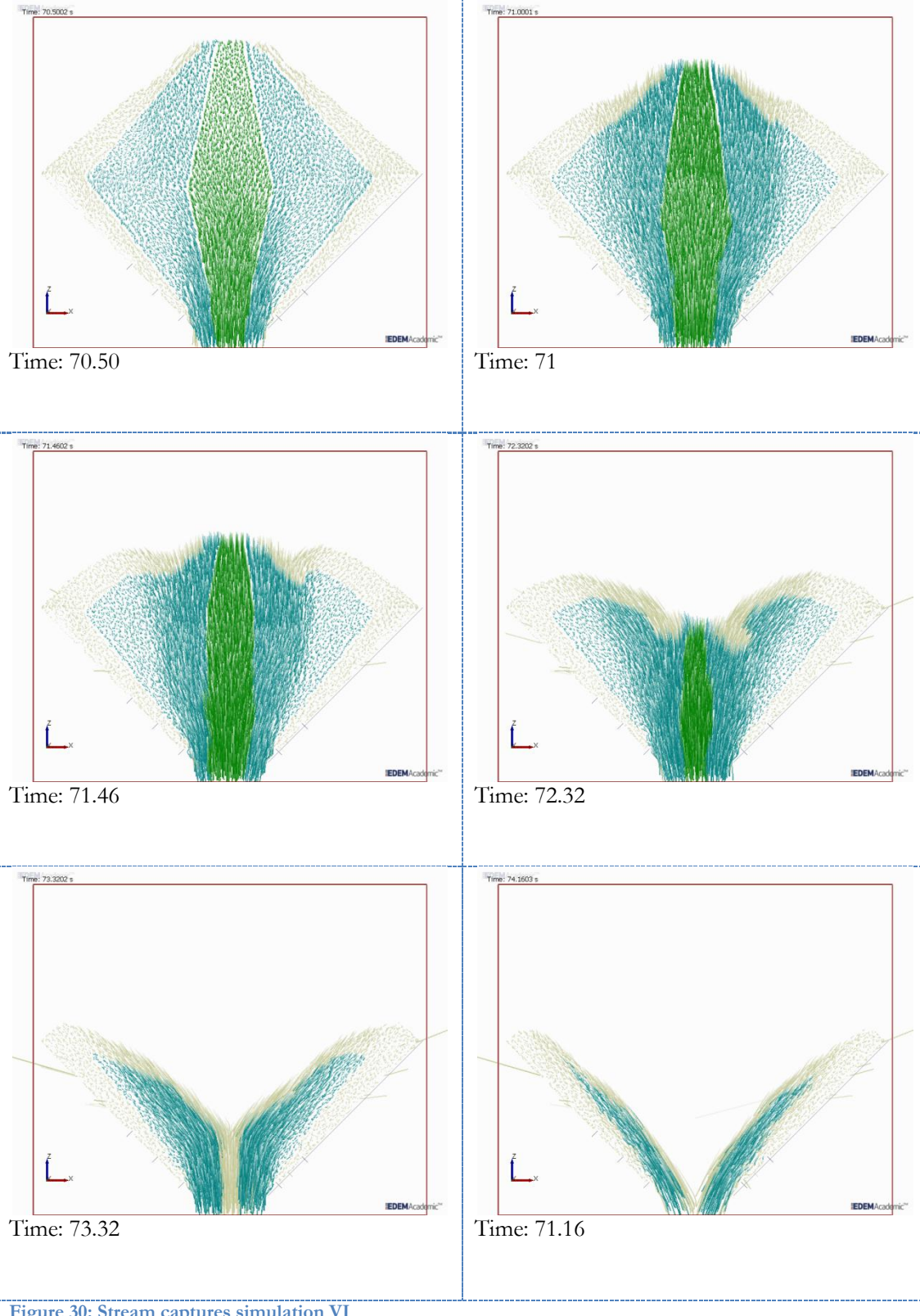


Figure 30: Stream captures simulation VI

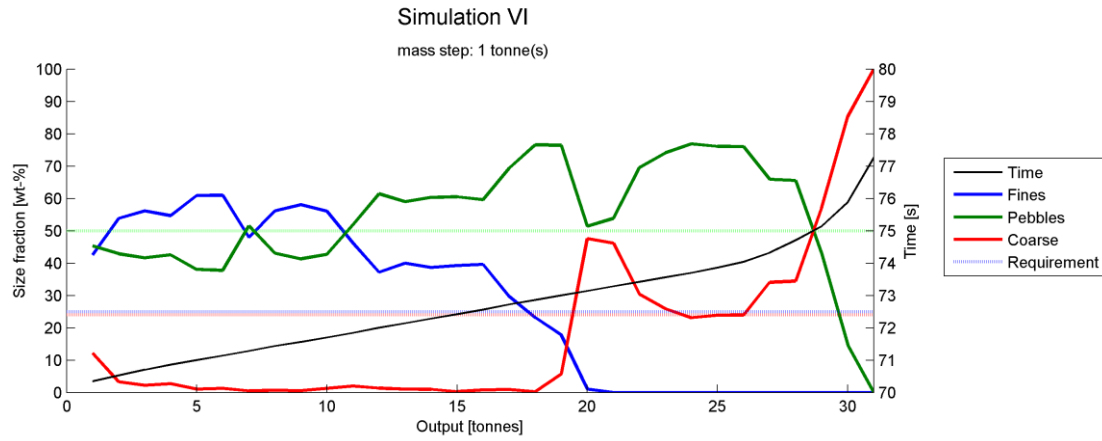


Figure 31: Size distribution graph of simulation VI

The results of this simulation are discussed in *Section 5.4.4*. This section shows the screen captures belonging to that section.

The screen captures show very clearly the falling in of the top stagnant layer, which is called the ‘*necking effect*’ in this report and is comparable to zone A in the flow regions of Brown and Hawksley in *Section 2.4.1*.

Simulation VII

Screen captures

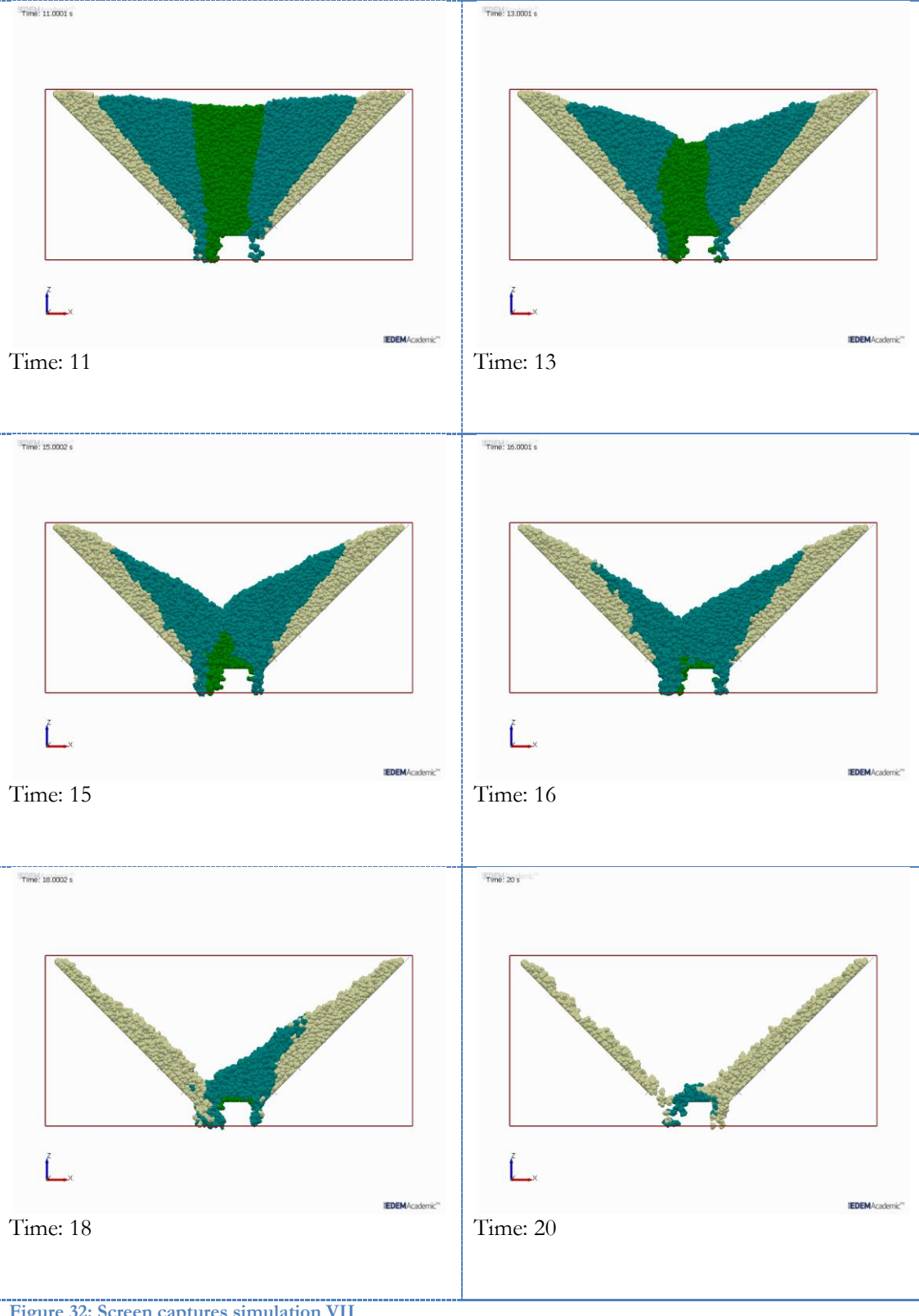
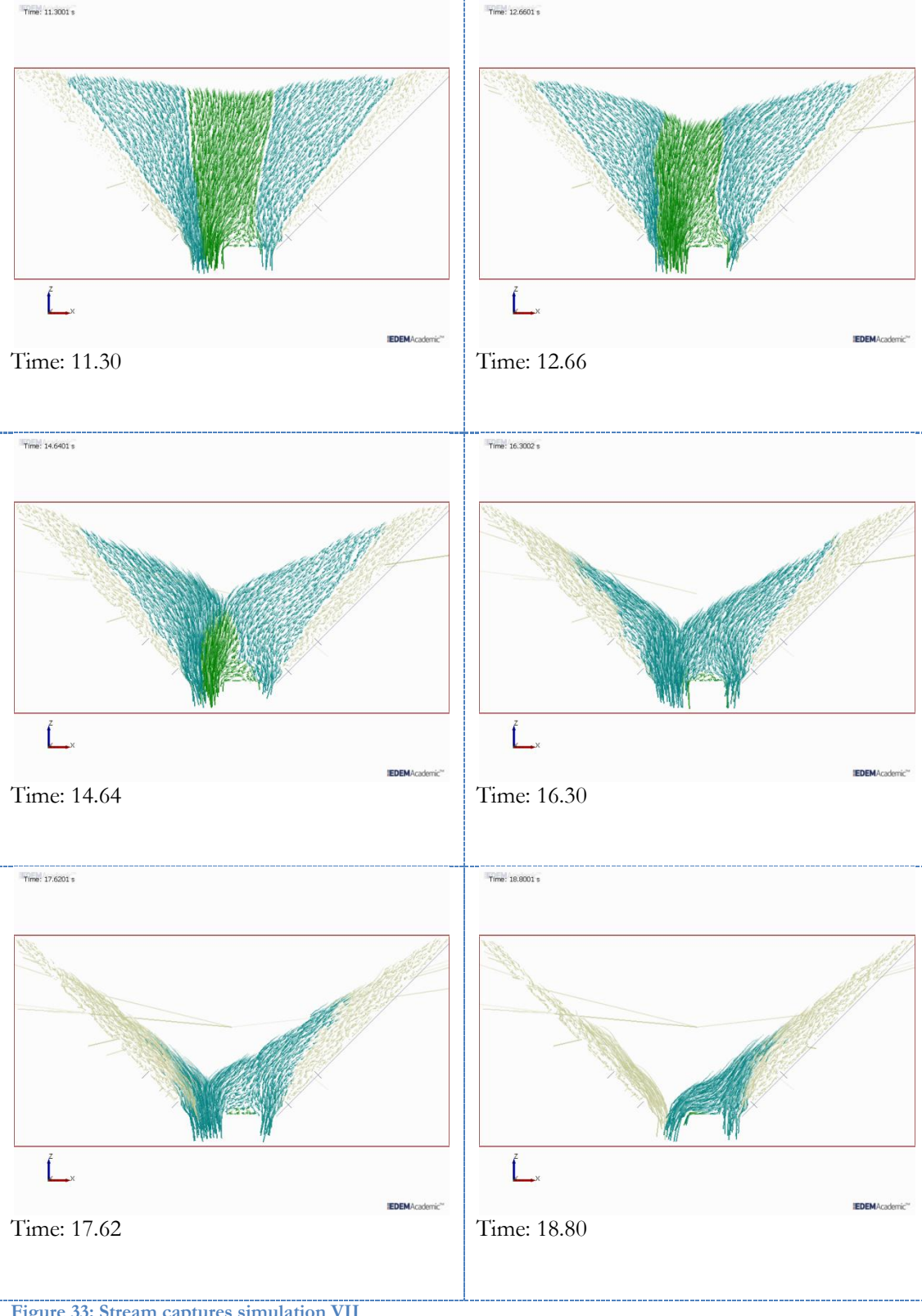


Figure 32: Screen captures simulation VII

Screen captures of stream



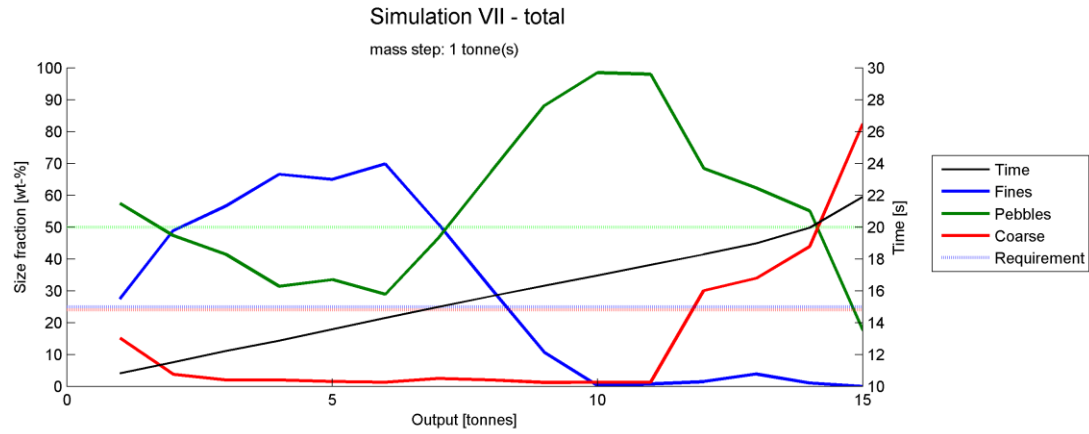


Figure 34: Size distribution graph of simulation VII; total

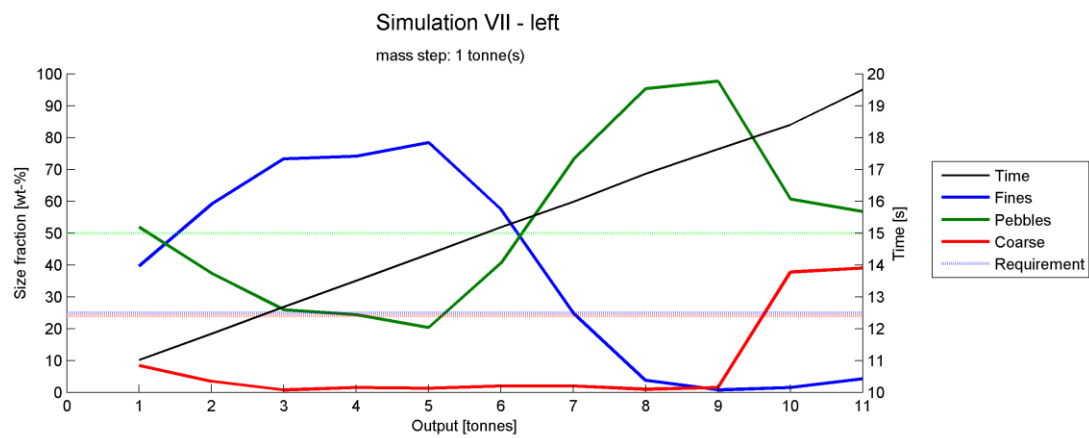


Figure 35: Size distribution graph of simulation VII; left outlet

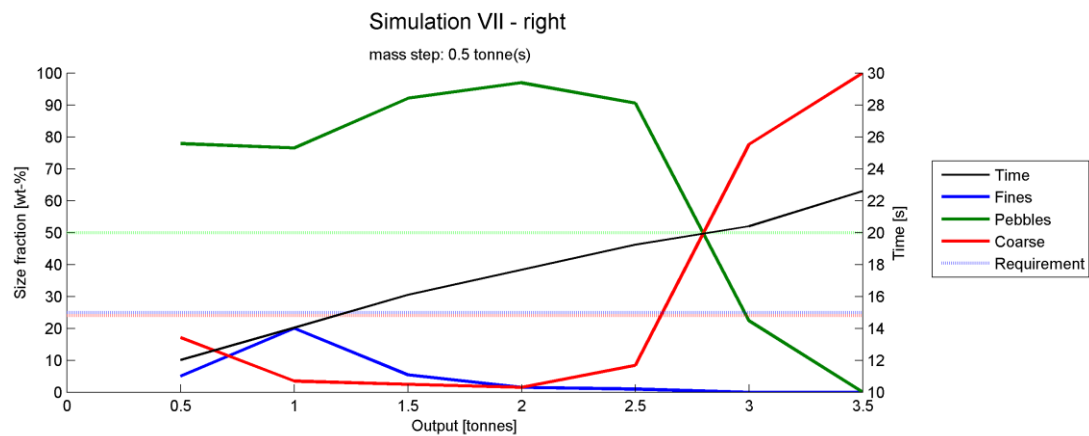


Figure 36: Size distribution graph of simulation VII; right outlet

The screen captures and the size distribution graphs are shown here. The contents are discussed in detail in *Section 5.4.1.b* and therefore not discussed further here.

Simulation A1

Screen captures

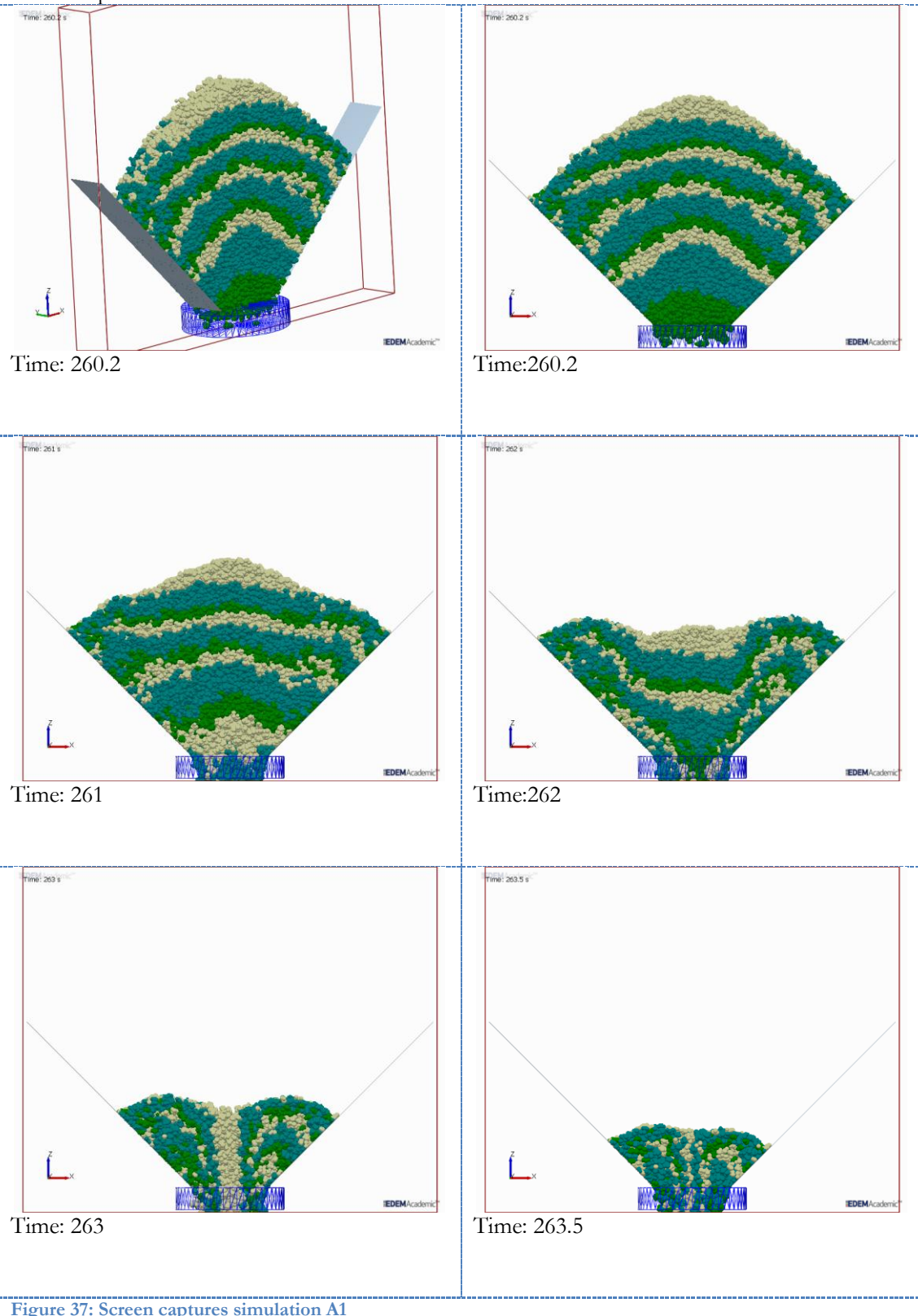


Figure 37: Screen captures simulation A1

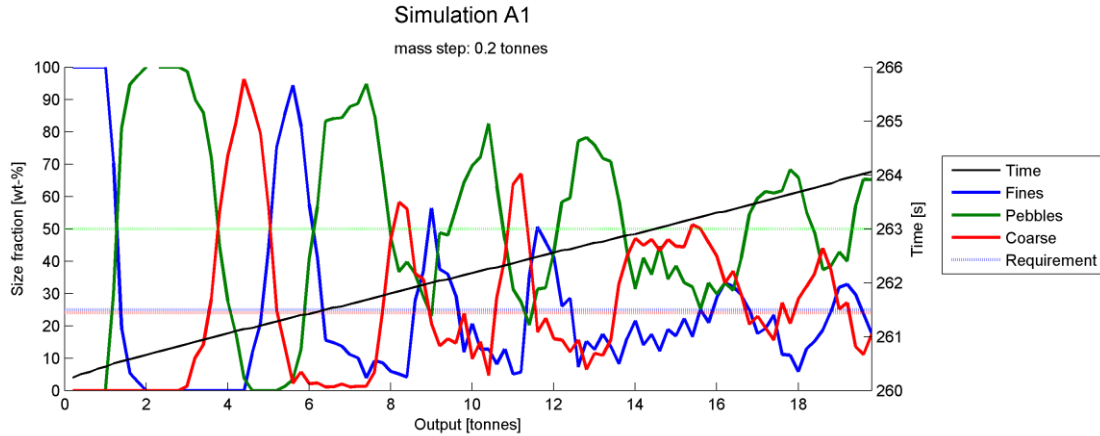


Figure 38: Size distribution graph of simulation A1

This section show the results of a model with high static friction and batch filling as input method. Although there is high static wall friction the models shows a combination of core and mass flow.

Opposite to *Simulation III.b* (with a wall angle of 60 degrees) the first part of the simulation is core flow, followed by mass flow. This is caused by the larger force on material to the side of the wall, due to the angles and higher filling level by the heap onto top of the filling. The screen captures show clearly the movement of core material at the start of discharge, where after the stagnant zones start moving downwards in a horizontal mass flow front.

The size distribution graph shows a repetition of fines, pebbles and coarse; caused by the batch layering. When these layers are thin enough this produces a quite ideal mix to meet the AG mill requirement.

Simulation A2

Screen captures

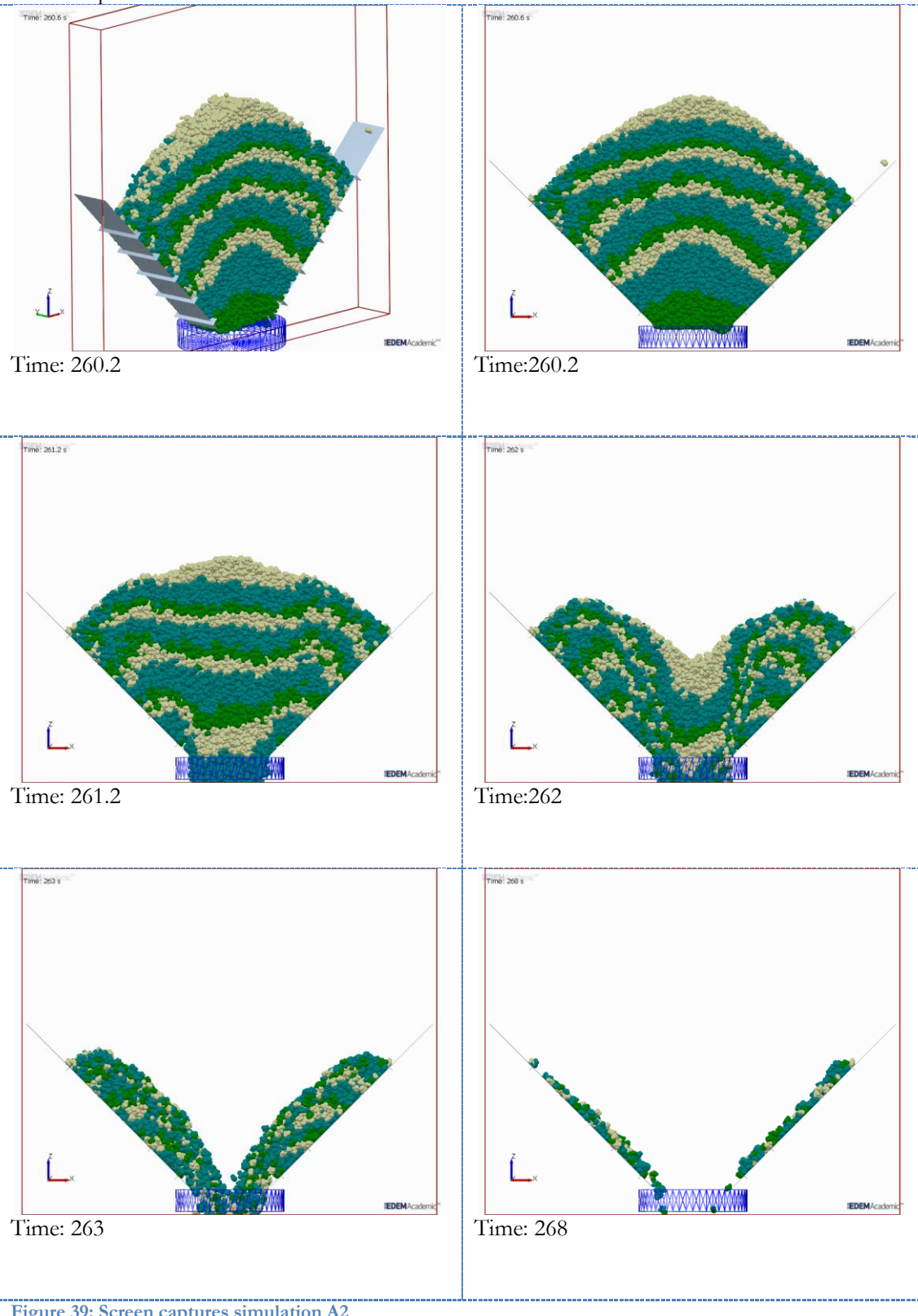


Figure 39: Screen captures simulation A2

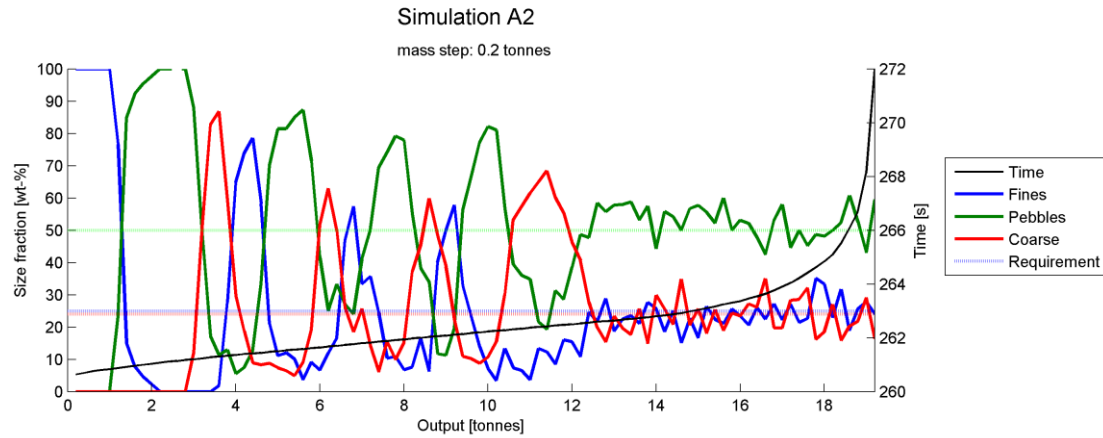


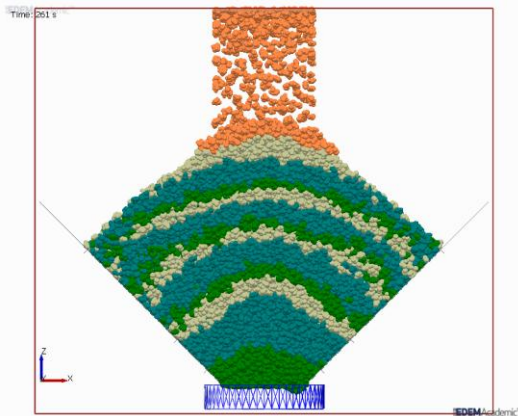
Figure 40: Size distribution graph of simulation A2

This simulation has a higher static friction applied, compared to the previous simulation. Hence, establishes a more obvious core flow, since the stagnant material remains at the side walls for a longer period. The mass flow period as seen in *Simulation A1* is not observed anymore.

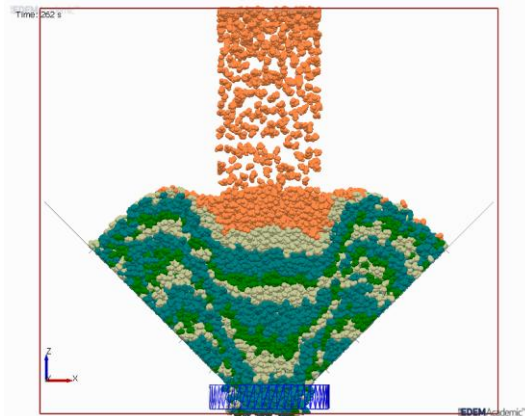
This simulation end with a period that produces the required AG mill size distribution. This is not seen for the identical simulation with low wall friction in *Simulation A1*, because there is no mass flow observed in this simulation. The ideal mix is produced during the period that the stagnant material starts moving inwards to the centre of the stockpile and there the layers are mixed.

Simulation C

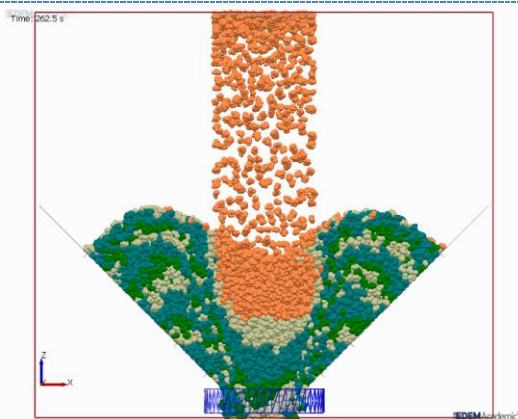
Screen captures



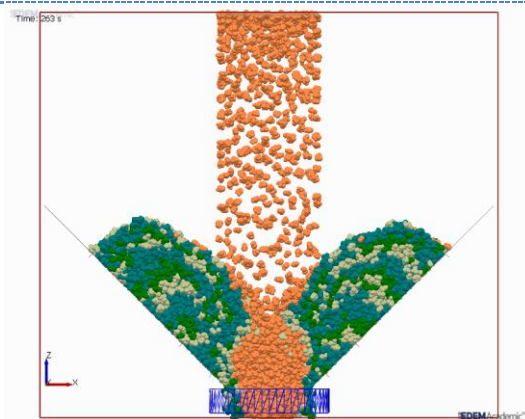
Time: 261



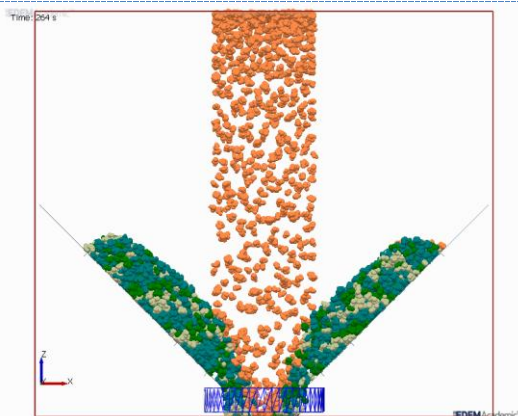
Time: 262



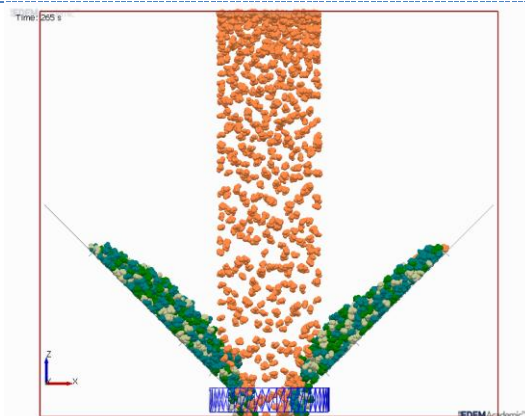
Time: 262.5



Time: 263



Time: 264



Time: 265

Figure 41: Screen captures simulation C

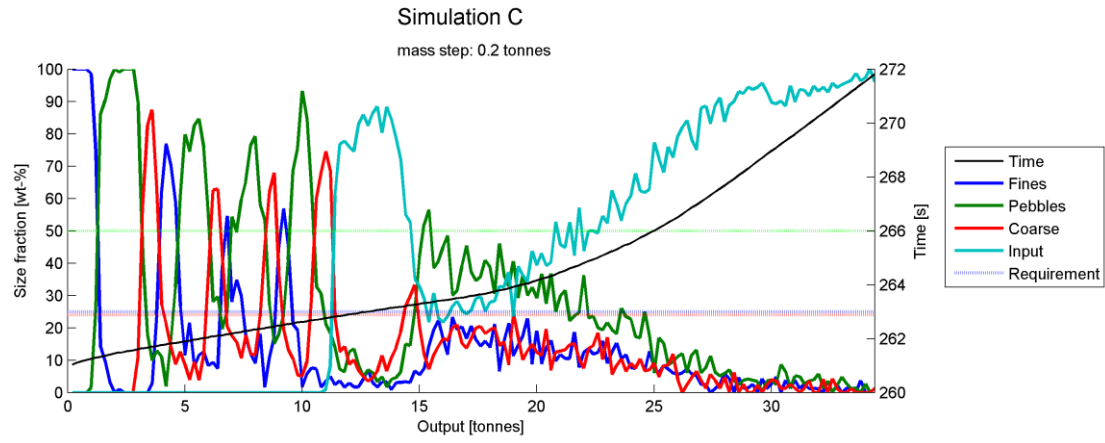


Figure 42: Size distribution graph of simulation C

This simulation is identical to *Simulation A2*, only there is also input of material in this simulation. The results of this simulation are discussed in *Section 5.3.1*.

Simulation D1

Screen captures

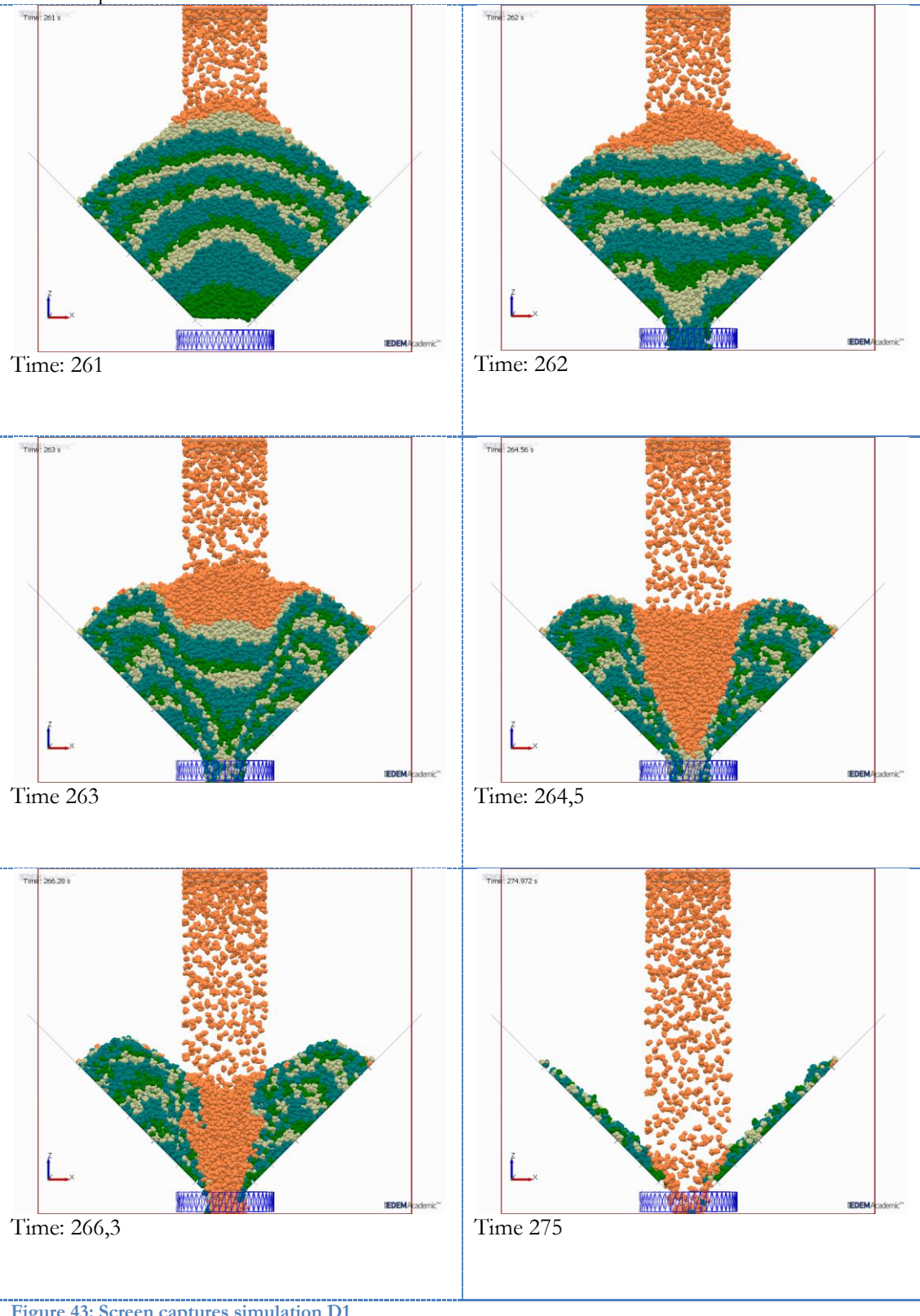
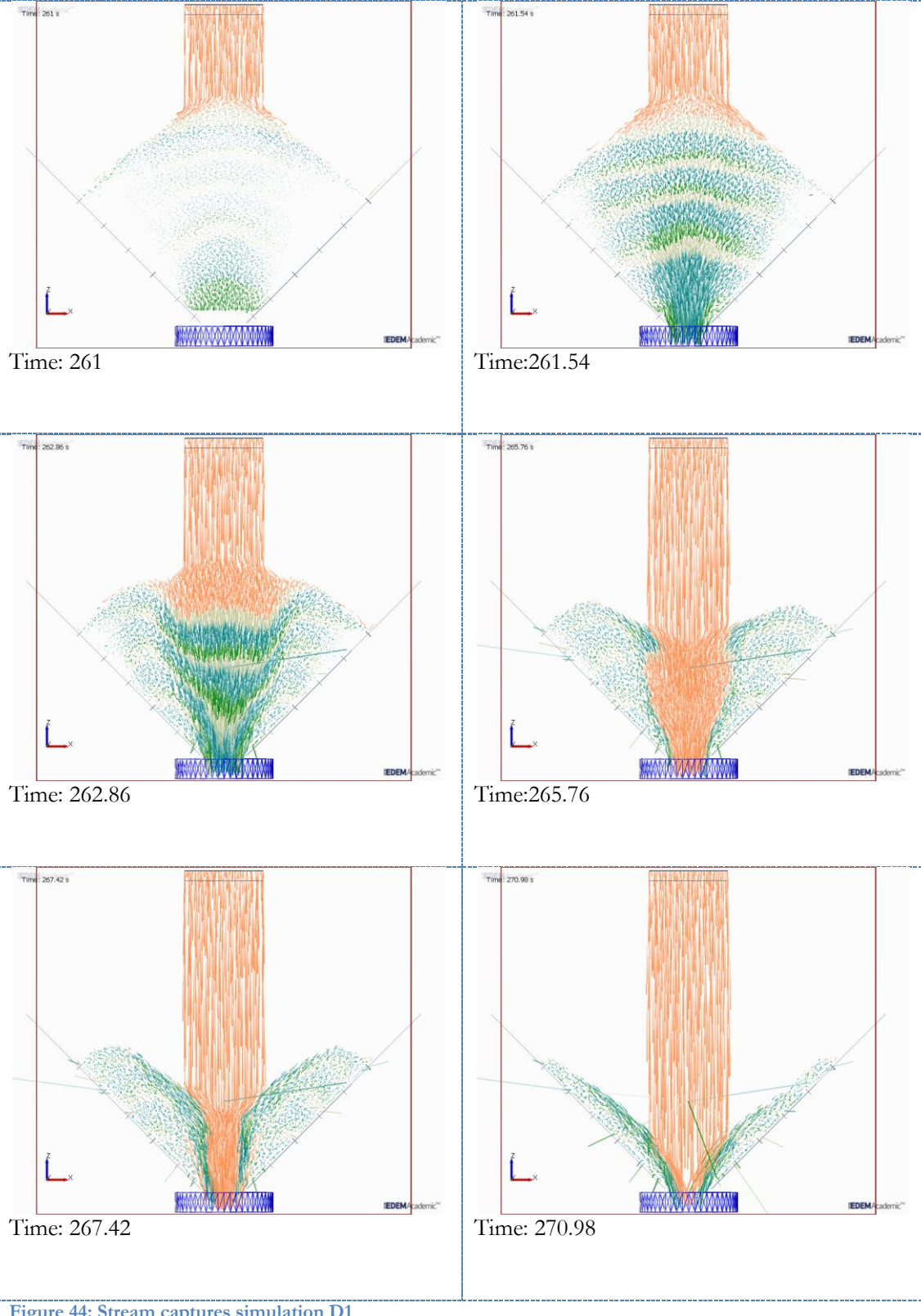


Figure 43: Screen captures simulation D1

Screen captures of stream



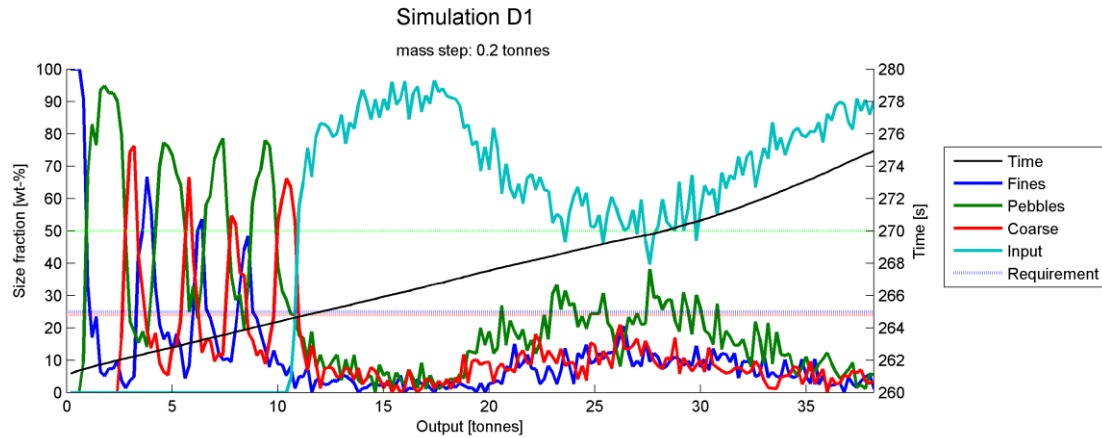


Figure 45: Size distribution graph of simulation D1

The results of this simulation are compared best to *Simulation C*, since this simulation is identical, except that the discharge rate is lower in this simulation.

Therefore, the size distribution shows similar behaviour, but the ‘*necking effect*’ is seen over a large amount of discharge tonnes. This is caused by the lower discharge rate.

Due to core flow, after 11 tonnes of discharge the size distribution is for more than 50% dependent on the size of the input material. This input material is dominant due to the ‘last-in, first-out’ effect.

The stream captures shown steep angles of withdrawal. Most likely, this is also caused by the low discharge rate.

Simulation D2

Screen captures

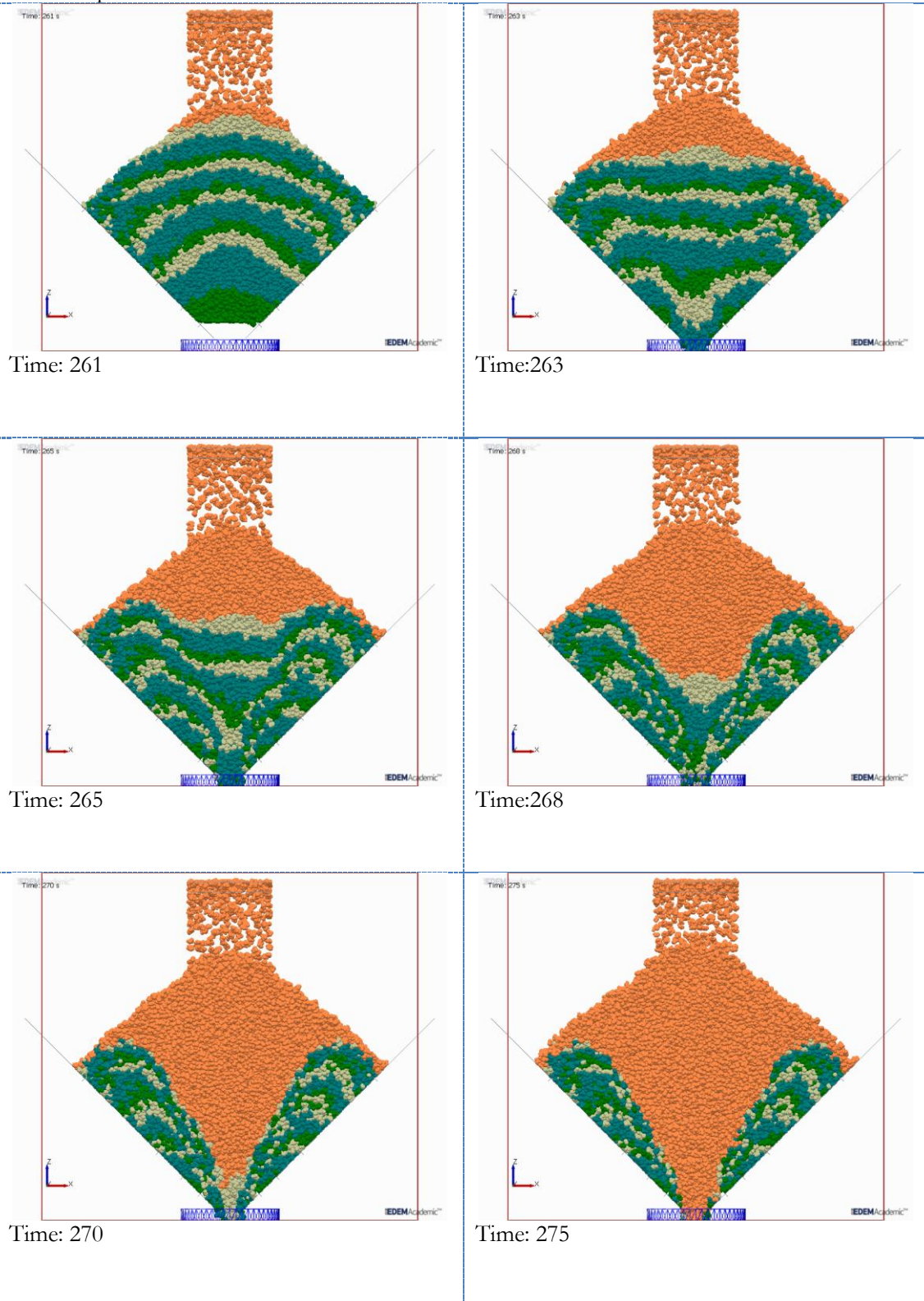


Figure 46: Screen captures simulation D2

Screen captures of stream

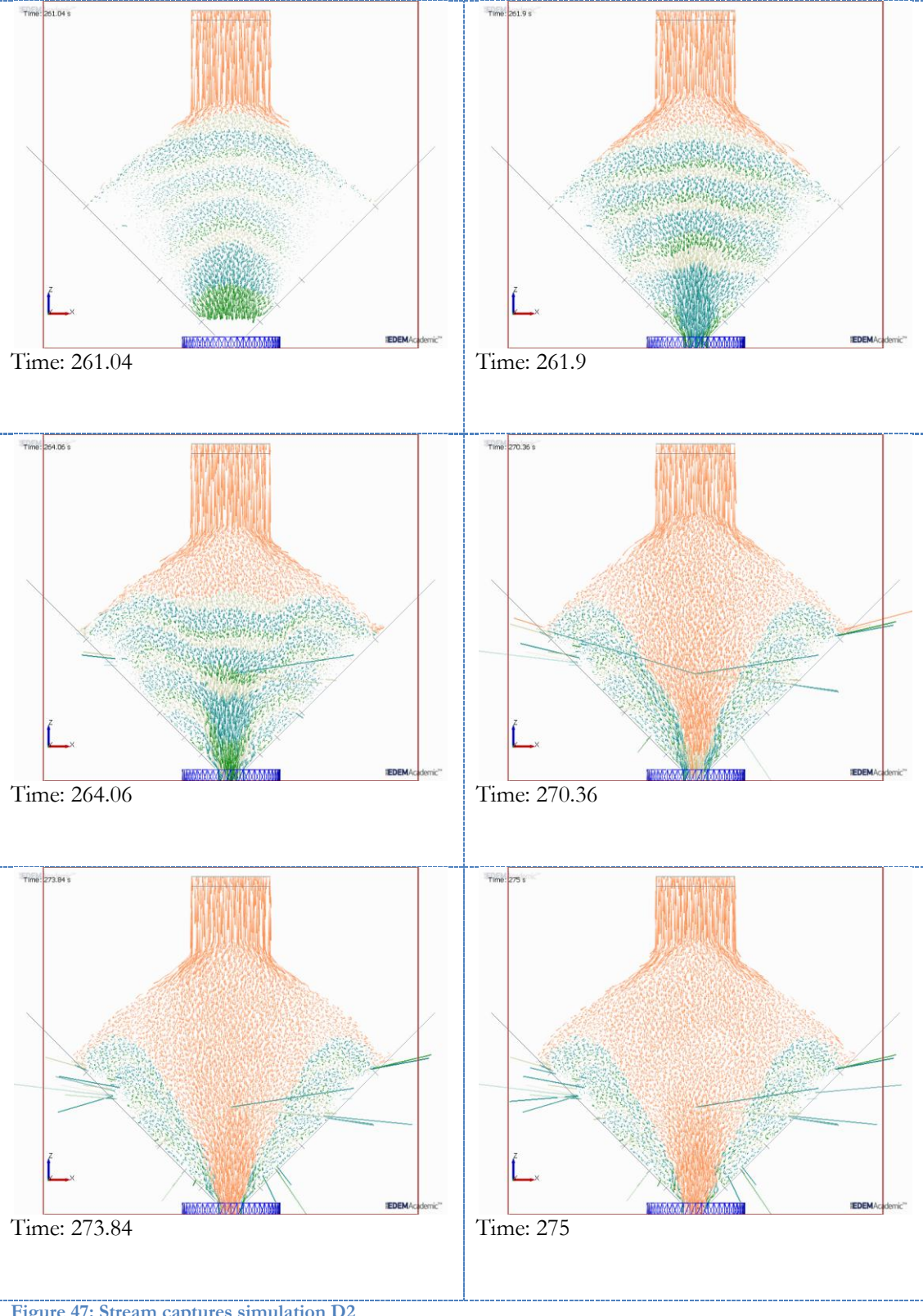


Figure 47: Stream captures simulation D2

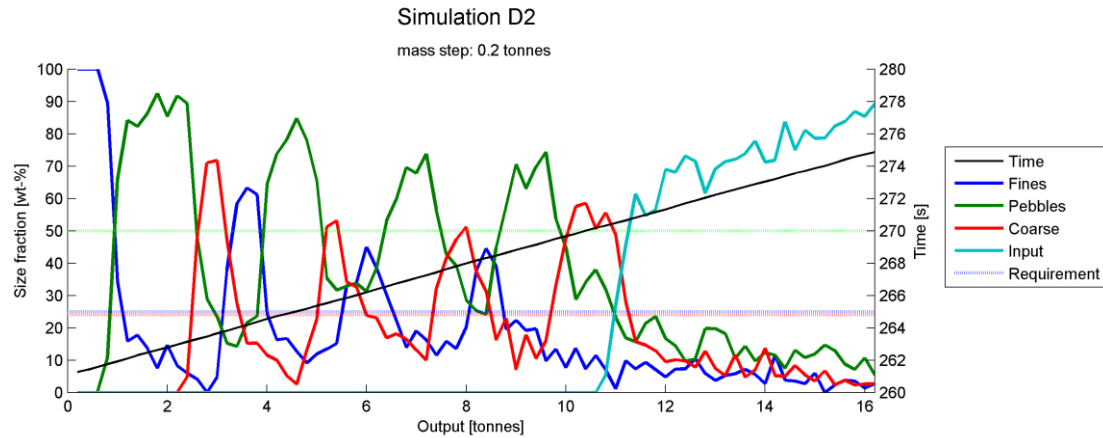


Figure 48: Size distribution graph of simulation D2

This simulation used the smallest outlet size; therefore the input rate is higher than the discharge rate. This is seen in the distribution graph, since there is no necking effect noticeable and the fine material keeps rising at the end of the simulation. This simulation is further discussed in *Section 5.3.2*.

A remark needs to be made when looking at the stream captures. Very long and straight lines are shown in the stream captures. These are also noticed in others stream. The long, straight lines are caused by the periodic boundaries in the simulation. Particles may reappear at the other side of the simulation, which results in this strange appearance of lines.

Simulation F

Screen captures

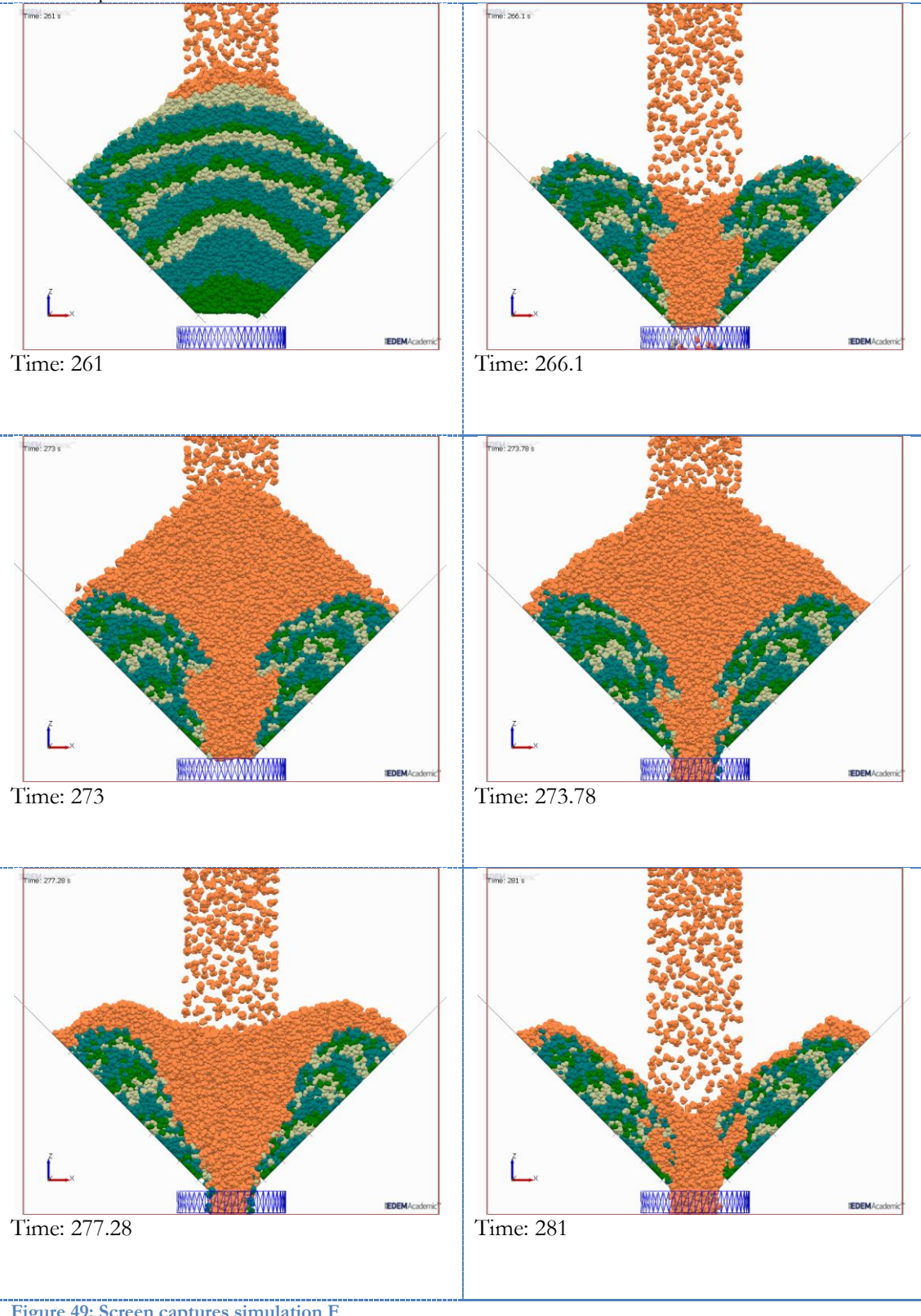


Figure 49: Screen captures simulation F

Screen captures of stream

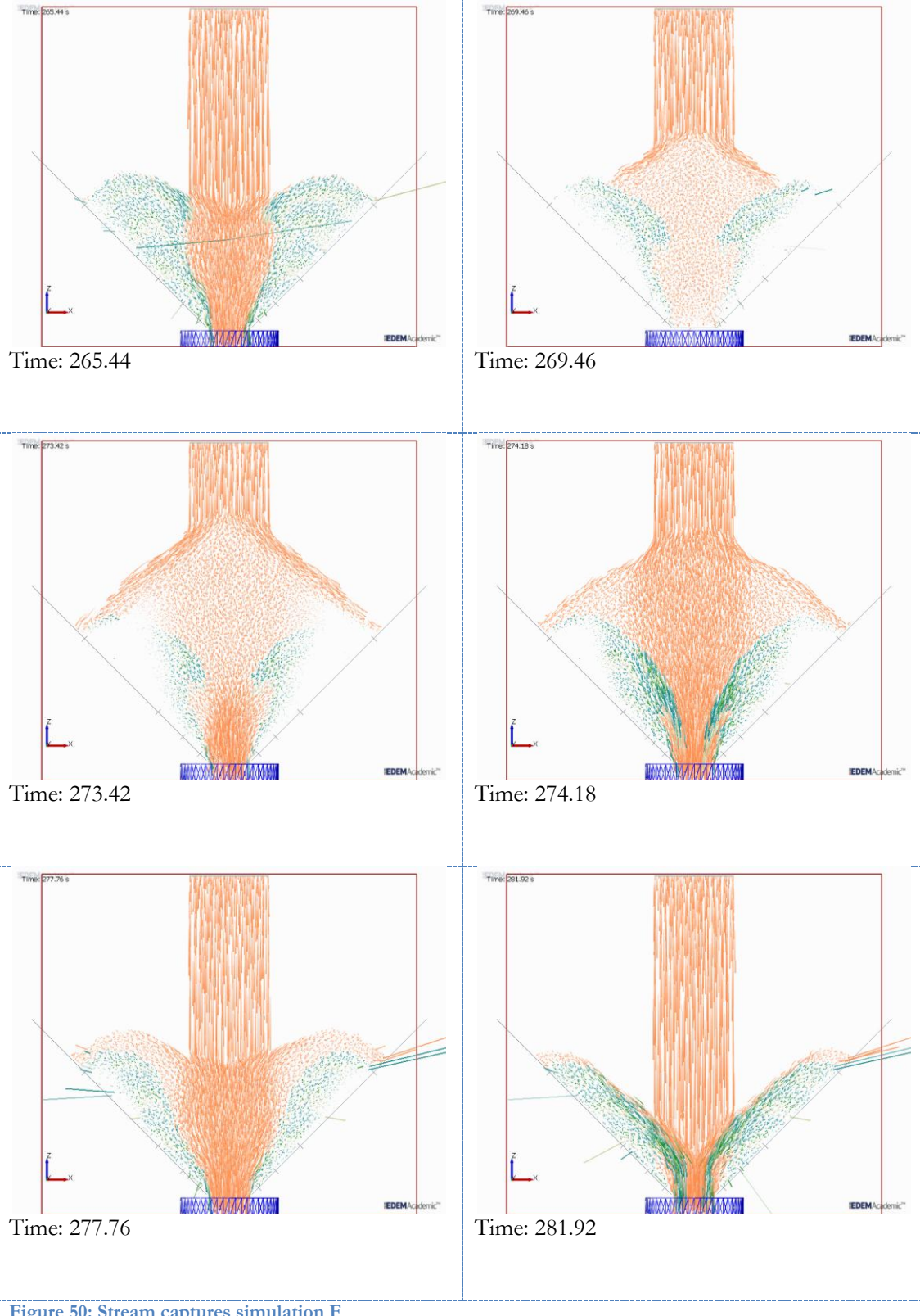


Figure 50: Stream captures simulation F

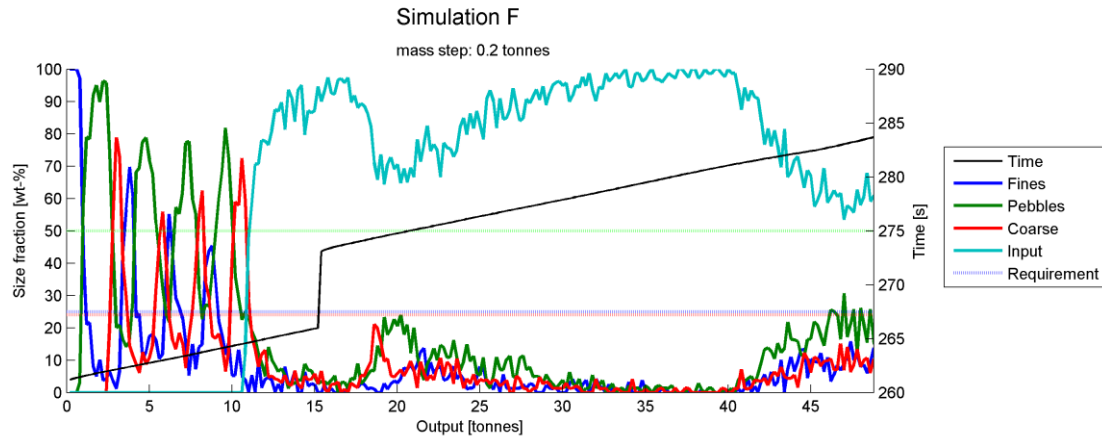


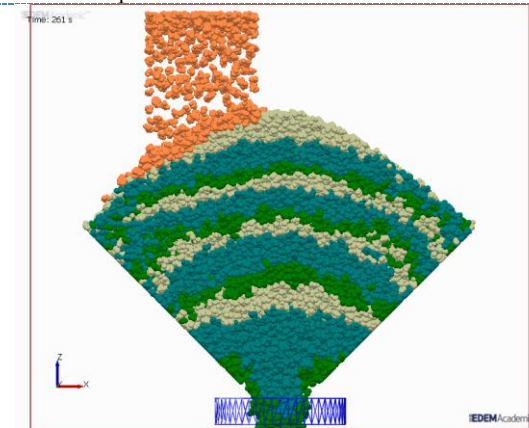
Figure 51: Size distribution graph of simulation F

In this simulation, the discharge was interrupted. The simulation is discussed in detail in *Section 5.4.3*.

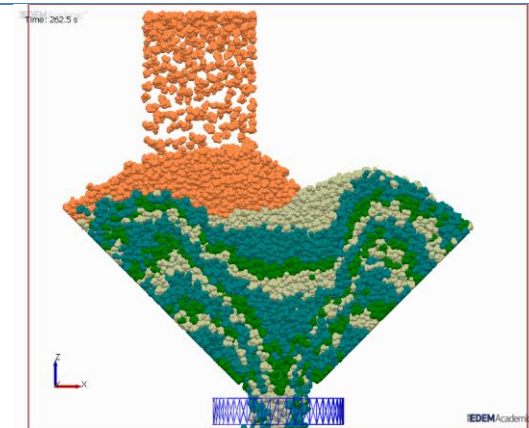
The captures taken from this simulation show the ‘*necking effect*’ several times very clearly. The flow mode is core flow and the flow is only stopped during the discharge interruption. When the outlet is opened again, the flow mode continues in a similar way.

Simulation G

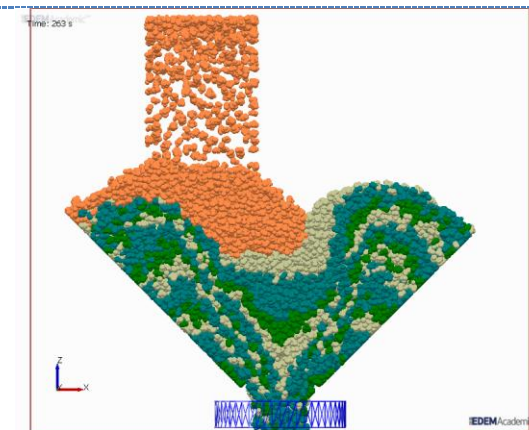
Screen captures



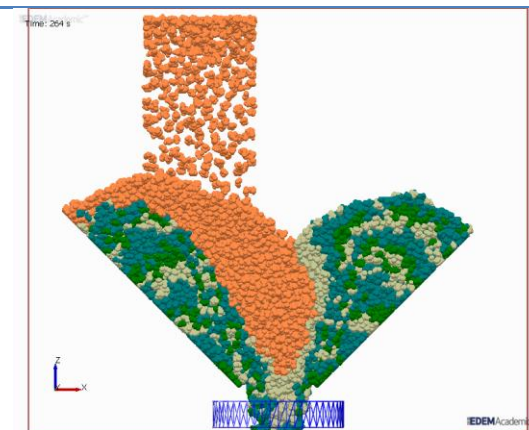
Time: 261



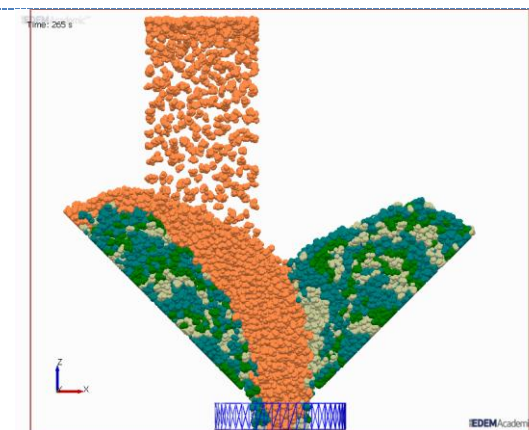
Time: 262.5



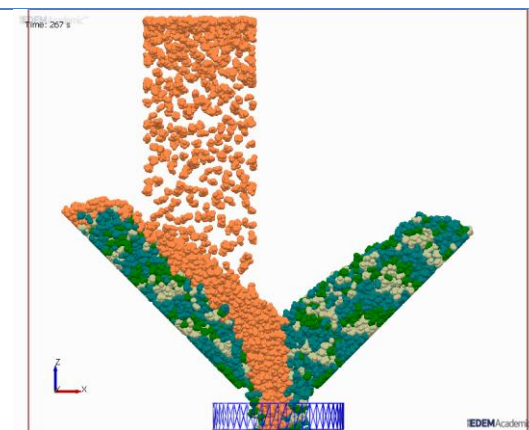
Time: 263



Time: 264



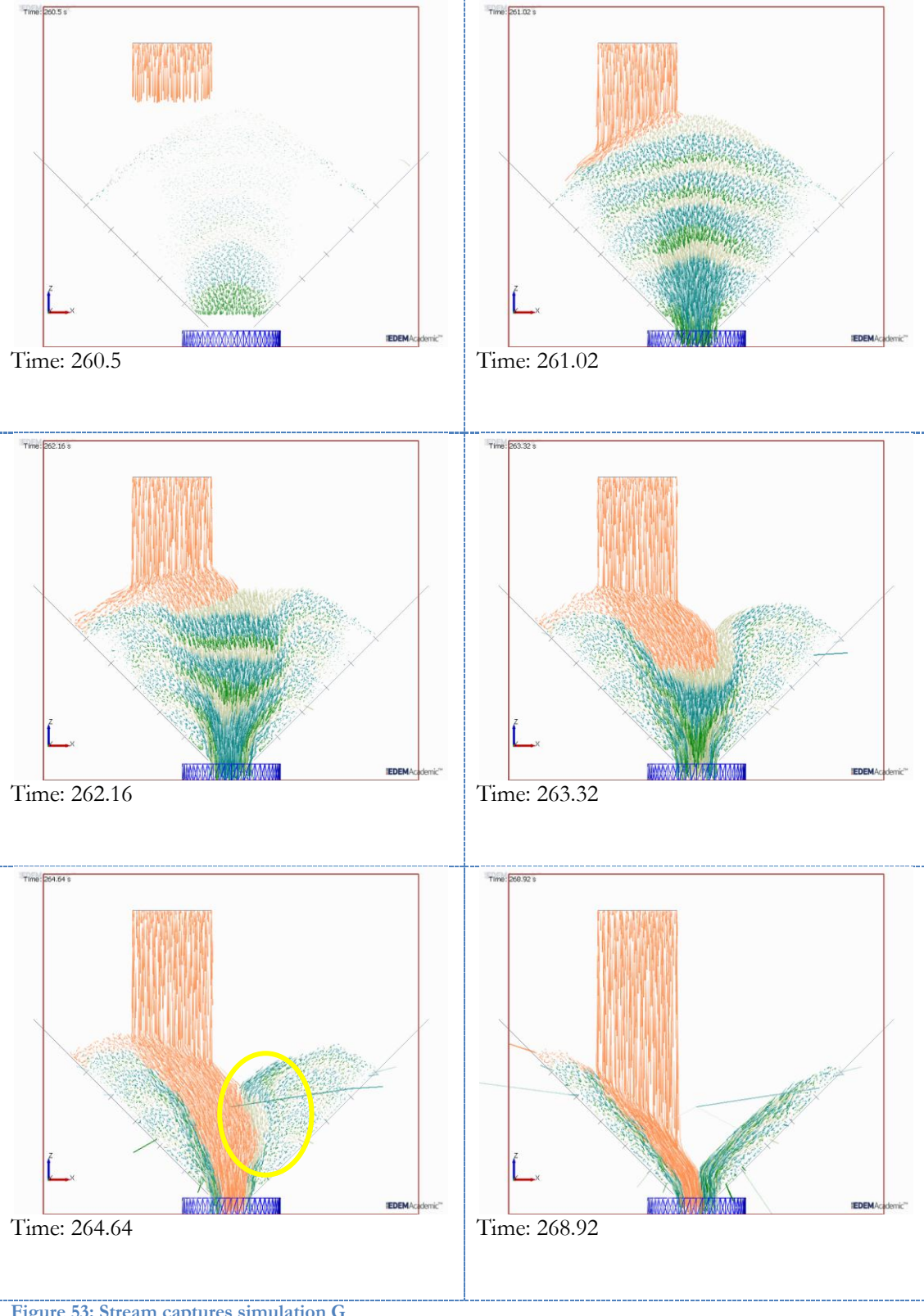
Time: 265



Time: 267

Figure 52: Screen captures simulation G

Screen captures of stream



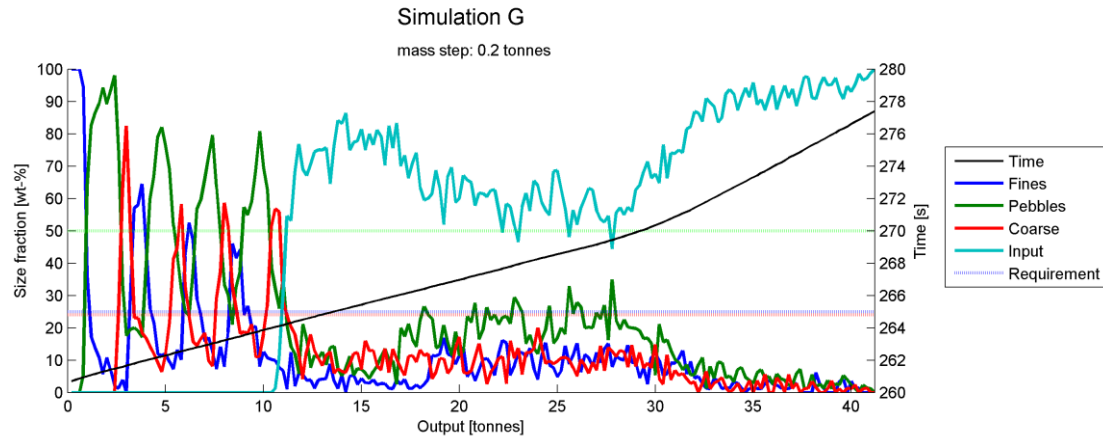


Figure 54: Size distribution graph of simulation G

In *Section 5.4.2* this simulation is also reviewed. The asymmetric input does not have significant impact on the size distribution shown in the graph. However, the flow is very different compared to the symmetric input *Simulation D1*.

The flow mode is core flow, since there are differences in the velocity of the material. The flow profile is however different, since it is not symmetric. The angles of withdrawal on the right side are different from the left side. The input material on the left side caused a push to the right side, where it holds the material on the right side longer in its initial place. This is seen clearly by the yellow-circled area; the material on the right side has almost no velocity due to the incoming material from the upper left side.

Simulation H

Screen captures

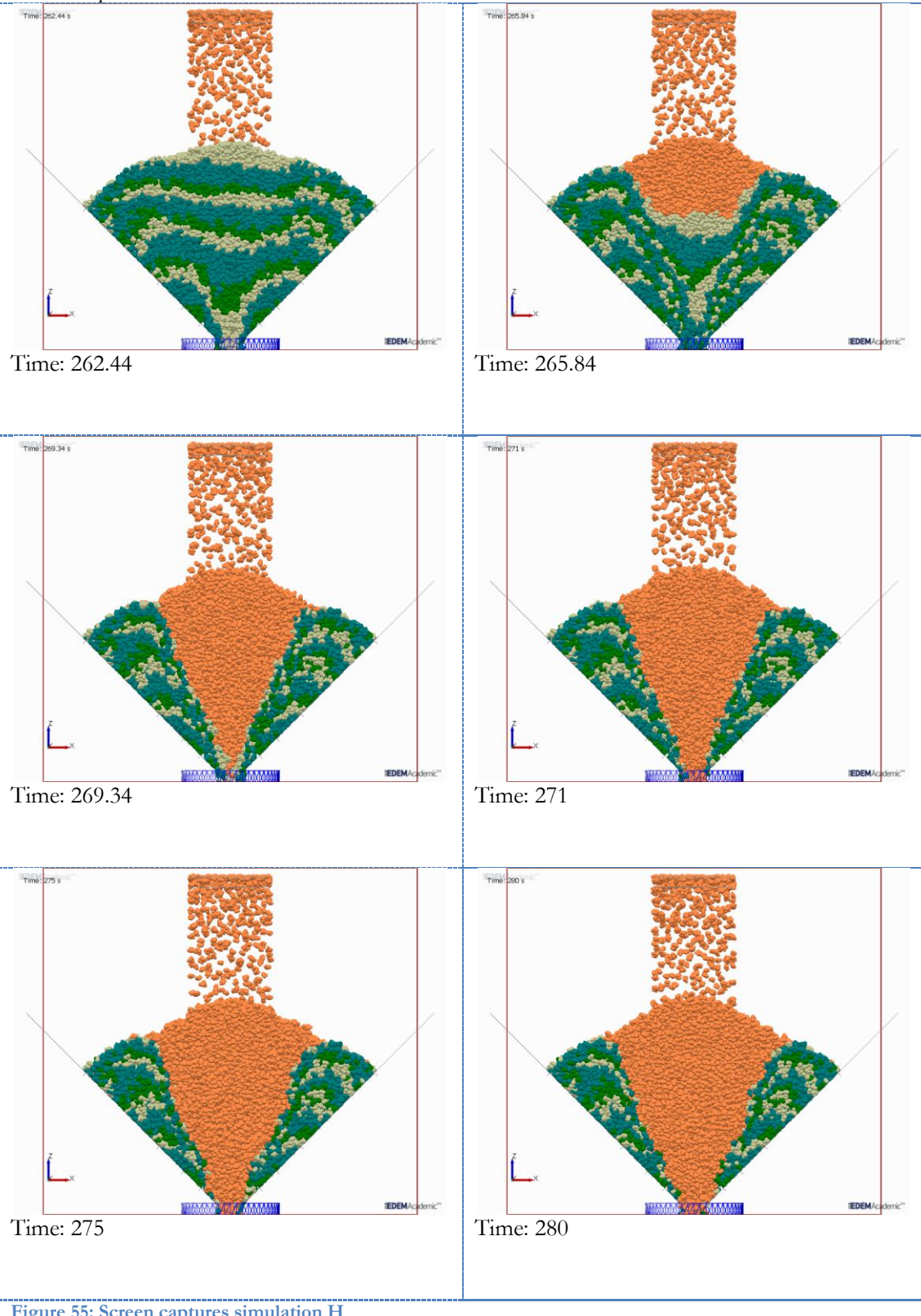


Figure 55: Screen captures simulation H

Screen captures of stream

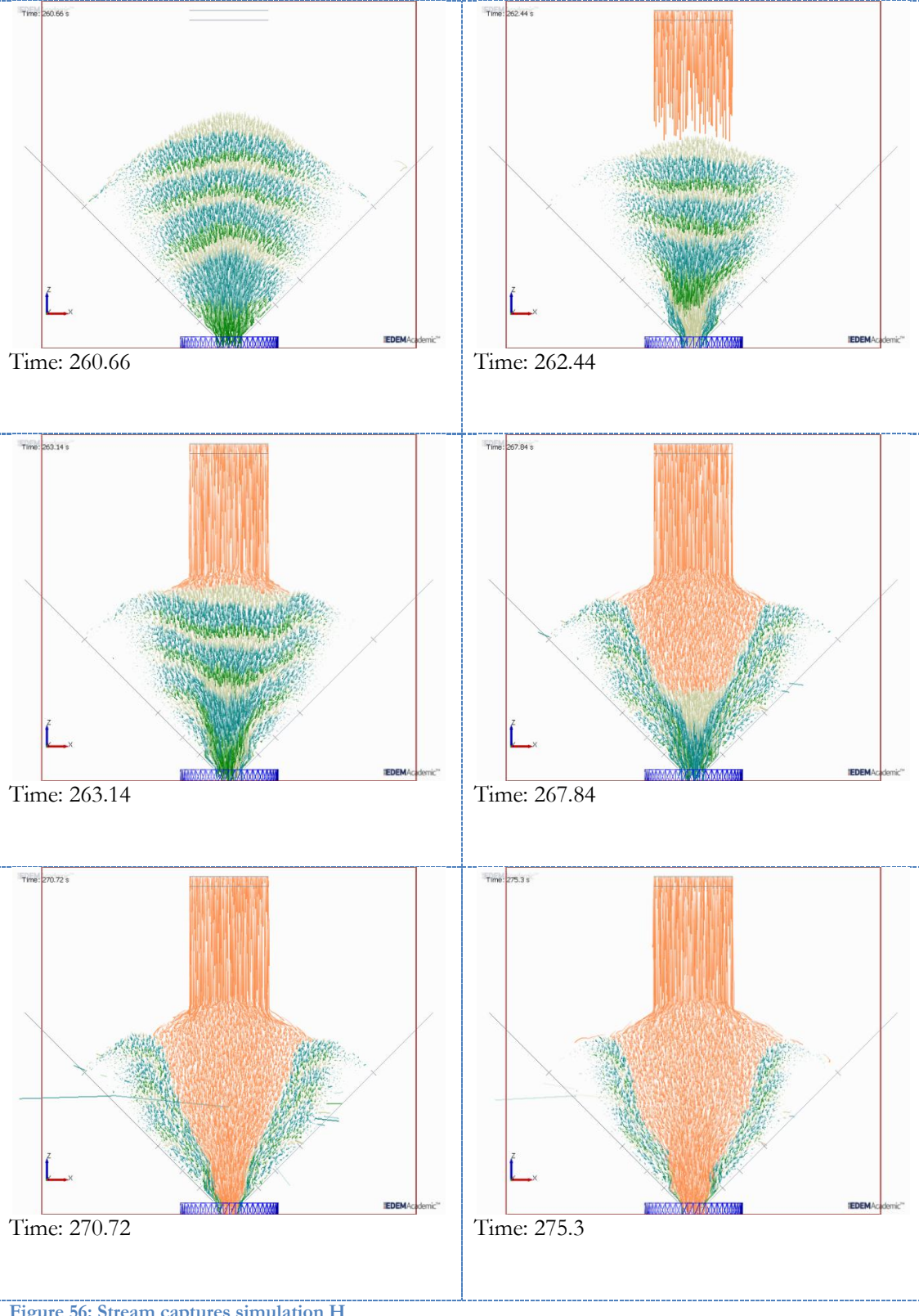


Figure 56: Stream captures simulation H

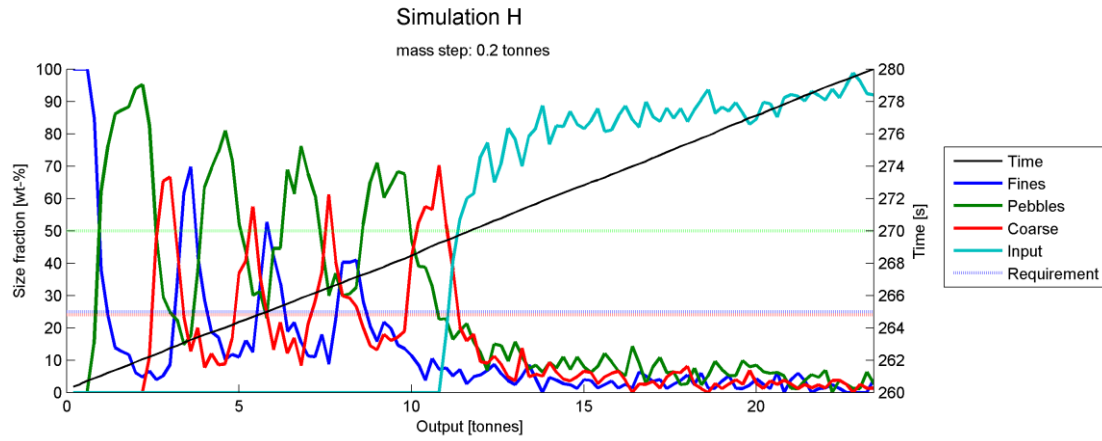


Figure 57: Size distribution graph of simulation H

The fill level in this simulation is kept at 70%, by equal input and discharge rate.

The angle of withdrawal as seen in the stream captures is roughly the same throughout the entire simulation. This is caused by the equal in and output, which keeps the pressure on the stagnant zones the same throughout the simulation.

This simulation is further reviewed in *Section 5.3.2*.